TRANSPORTATION RESEARCH RECORD 878

Soil-Structure Interaction of Subsurface Conduits

TRANSPORTATION RESEARCH BOARD

NATIONAL RESEARCH COUNCIL

NATIONAL ACADEMY OF SCIENCES
WASHINGTON, D.C. 1982

Transportation Research Record 878
Price $13.60
Edited for TRB by Naomi Kassabian

modes
1 highway transportation
2 public transit
3 rail transportation
4 air transportation

subject areas
25 structures design and performance
63 soil and rock mechanics

Library of Congress Cataloging in Publication Data
National Research Council. Transportation Research Board.
Soil-structure interaction of subsurface conduits.

(Transportation research record; 878)
Reports prepared for the 61st annual meeting of the Transportation Research Board.
1. Soil mechanics—Addresses, essays, lectures. 2. Culverts—Addresses, essays, lectures. I. National Research Council (U.S.). Transportation Research Board. II. Series.
TE7.H5 no. 878 [TA710] 380.5s [625.7'342] 83-4150
ISBN 0-309-03466-3 ISSN 0361-1981

Sponsorship of the Papers in This Transportation Research Record

GROUP 2—DESIGN AND CONSTRUCTION OF TRANSPORTATION FACILITIES
R. V. LeClerc, consultant, Olympia, Washington, chairman

Structures Section
LeRoy T. Oehler, Michigan Department of Transportation, chairman

Committee on Culverts and Hydraulic Structures
Richard A. Parmelee, Northwestern University, chairman
A. E. Bacher, Mike Bealey, Ray J. Behling, Thomas K. Breitfuss, Richey S. Dickson, W. B. Drake, Sam S. Gillespie, Frank J. Heger, John G. Hendrickson, Jr., L. R. Lawrence, A. P. Moser, M. G. Spangler, R. S. Standley, David C. Thomas, Corwin L. Tracy, Adrianus Vankampen, David C. Wyant

Soil Mechanics Section
Lyndon H. Moore, New York State Department of Transportation, chairman

Committee on Subsurface Soil-Structure Interaction
Raymond J. Krizek, Northwestern University, chairman
John F. Abel, Delon Hampton, Michael G. Katona, J. Neil Kay, G. A. Leonards, Don A. Linger, Russell B. Preuit, Jr., George W. Ring III, Ernest T. Selig, Corwin L. Tracy

Lawrence F. Spaine and John W. Guinnee, Transportation Research Board staff

Sponsorship is indicated by a footnote at the end of each report. The organizational units, officers, and members are as of December 31, 1981.

878

Contents

Authors of the Papers in This Record

Abdel-Sayed, George, Department of Civil Engineering, University of Windsor, Windsor, Ontario, Canada
Bacher, Alfred E., California Department of Transportation, 1120 N Street, Sacramento, CA 95814
Bakht, Baidar, Ministry of Transportation and Communications, 1201 Wilson Avenue, Downsview, Ontario M3M 1J8, Canada
Banke, Albert N., California Department of Transportation, 1120 N Street, Sacramento, CA 95814
Beal, David B., New York State Department of Transportation, 1220 Washington Avenue, State Campus, Albany, NY 12232
Chang, Ching S., Department of Civil Engineering, University of Massachusetts, Amherst, MA 01003
Davis, Raymond Eugene, California Department of Transportation, 1120 N Street, Sacramento, CA 95814
Duncan, J.M., Department of Civil Engineering, University of California, Berkeley, CA 94720
Flint, R.C.L., Department of Civil Engineering, University of Adelaide, GPO Box 498, Adelaide 5001, South Australia
Hain, Stephen J., Esso Australia, Ltd., Esso House, 127 Kent Street, Sydney 2000, Australia
Heger, Frank J., Simpson Gumpertz & Heger Inc., 1696 Massachusetts Avenue, Cambridge, MA 02138
Jeyapalan, J.K., Department of Civil Engineering, Texas A&M University, College Station, TX 77843
Katona, Michael G., Department of Civil Engineering, University of Notre Dame, Notre Dame, IN 46556
Kay, J. Neil, Department of Civil Engineering, University of Adelaide, GPO Box 498, Adelaide 5001, South Australia
Kirkland, Daniel E., California Department of Transportation, 1120 N Street, Sacramento, CA 95814
McVay, Michael C., Department of Civil Engineering, University of Florida, Gainesville, FL 32601
Moser, A.P., Department of Mechanical Engineering, Utah State University, Logan, UT 84322
Selig, Ernest T., Department of Civil Engineering, University of Massachusetts, Amherst, MA 01003
Semans, Frank M., California Department of Transportation, 1120 N Street, Sacramento, CA 95814
Vittes, Pedro D., Department of Civil Engineering, University of Notre Dame, Notre Dame, IN 46556

Soil-Structure Analysis and Evaluation of Buried Box-Culvert Designs

MICHAEL G. KATONA AND PEDRO D. VITTES

Precast reinforced-concrete box culverts are relatively new products in culvert technology. Currently, the most widely used design procedure is ASTM C789 (Specifications on Precast Reinforced Concrete Box Sections for Culverts, Storm Drains and Sewers). These ASTM design tables give maximum allowable earth-cover heights for standard box sizes and steel reinforcement, determined by a linear-elastic frame analysis of the box section with an assumed soil pressure loading. No consideration is given to soil stiffness or soil-structure interaction. In this study, the final objective is to evaluate the structural adequacy of the ASTM box designs by using the finite-element program Culvert Analysis and Design (CANDE), which includes nonlinear elements for reinforced concrete, incremental soil construction, and fully automated mesh-generation schemes for culvert applications. To this end, the CANDE reinforced-concrete box model is validated with experimental data from out-of-ground box culverts loaded to ultimate. Next, the CANDE box-soil model is validated with experimental data from an in-ground box-culvert test with incremented soil loading. After the CANDE box-soil model has been validated, it is used to evaluate the ASTM box designs with regard to the 0.01-in crack-width limitation and the load factor for ultimate failure. In general it is concluded that the ASTM box designs are conservative but not uniformly conservative and the effect of soil stiffness is significant.

Precast reinforced-concrete box culverts as opposed to cast-in-place box culverts are relatively recent additions in culvert technology; they have come into popular use within the last decade. Design guidelines for precast reinforced-concrete box culverts (hereafter called simply "box culverts") are provided by ASTM C789-79 and AASHTO M259-76I for earth covers more than 2 ft. Both the ASTM and the AASHTO box-culvert design tables, which are essentially identical, are based on linear-elastic frame analysis of the box cross section with an assumed soil-pressure distribution. Design heights of earth cover, box wall thicknesses, and reinforcing steel areas are determined by ultimate strength design criteria and 0.01-in crack-width limitations. Soil-structure interaction is not taken into account.

Although these design tables are commonly used in practice, the design and analysis method and assumptions have not been experimentally verified for in-ground conditions. Nor has the design been cross-checked with analytical procedures employing soil-structure interaction together with the nonlinear nature of reinforced concrete. The latter leads to the objective of this study.

By using a finite-element analysis procedure [Culvert Analysis and Design (CANDE)] for modeling the nonlinear behavior of box culverts along with the soil system, the objectives are (a) to validate the finite-element box-culvert model with experimental data from out-of-ground box tests loaded to failure in four-edge bearing, (b) to validate the combined box-soil finite-element model with experimental data from an in-ground box-culvert test with incremental soil loading, and (c) to evaluate the ASTM C789 buried box-culvert designs with the finite-element model, i.e., determine earth-cover heights that produce 0.01-in crack widths and cover heights that result in ultimate box failure in flexure or shear.

This box-culvert study is part of a larger buried-culvert research program that has been sponsored by the Federal Highway Administration and has been going on for several years. The major product of the research program is the finite-element program CANDE (1-4), which is used here for the objectives given above. Other applications of CANDE are cited in reports by Katona (5-9).

CANDE MODEL AND BOX-CULVERT CRITERIA

CANDE Program

CANDE is a special-purpose finite-element program primarily intended for the design and analysis of buried culverts. Because of the generality afforded by the finite-element solution methodology, a variety of other soil-structure interaction problems can also be analyzed, such as underground storage facilities, retaining walls, embankments, and tunnels.

Some useful features of the program include incremental construction to model the physical process of constructing soil structures in a progressive manner, linear and nonlinear soil models, nonlinear beam-rod elements to model yielding and cracking of structural components (e.g., reinforced concrete), and frictional interfaces (e.g., between soil and structure) to simulate frictional sliding, debonding, and rebonding during the loading schedule. Also, the program is equipped with completely automated mesh-generation schemes for culvert applications.

The scope of the program is limited to plane strain geometry and loading, real-time independence, and small-deformation theory. In particular for the case of a buried box culvert, a plane strain slice of the culvert cross section is modeled with a series of connected beam-rod elements, and the soil system is modeled with nonconforming, four-node quadrilateral elements in a plane strain formulation. Typically, the soil system contains three soil zones--in situ soil, bedding, and fill soil, where the fill soil is incremented into the system in a series of soil lifts that mimicks the actual construction process and provides a history of structural responses. For the purposes of this article, a brief overview of the reinforced-concrete beam-rod element is given along with the criteria used for predicting concrete crack widths and ultimate failure. Complete details, as well as details of other modeling assumptions (e.g., soil models, friction interfaces, and incremental construction), are given in CANDE documentation manuals (1-4).

Reinforced-Concrete Element

A reinforced-concrete element, whether it is part of a culvert or of any structural system, poses a difficult analysis problem due to the nonlinear material behavior of concrete in compression, cracking of concrete in tension, yielding of the reinforcement steel, and the composite interaction of concrete and reinforcement. Matters are complicated further when the internal moment, shear, and thrust at a particular cross section are not proportional (including load reversals) during the loading history. Such is the case for buried box culverts during the installation process.

To cope with these problems, the following geometric and kinematic assumptions are employed in the CANDE beam-rod element: (a) displacements and strains are small, (b) transverse planes remain plane and normal, and (c) the steel reinforcement

Figure 1. Idealized concrete stress-strain behavior.

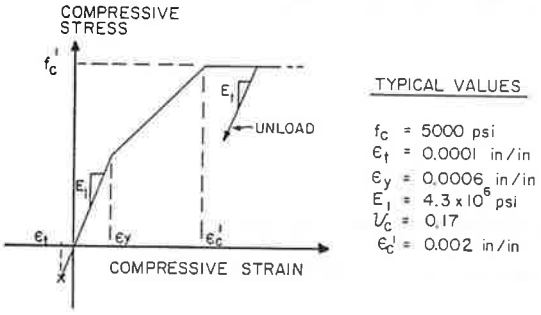

Figure 2. Steel reinforcement in concrete wall.

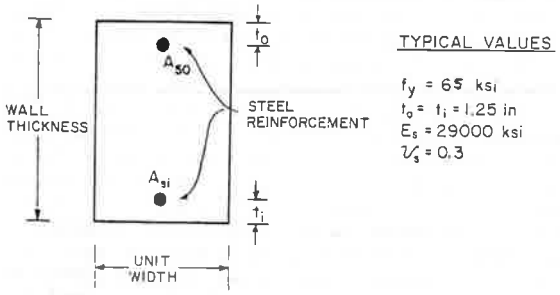

remains bonded to the concrete.

With regard to material behavior, the stress-strain behavior for concrete is represented by the trilinear curve shown in Figure 1 where the curve is defined (input) by the strain measures ϵ_t, ϵ_y, and ϵ_c' along with the initial modulus E_1 and strength f_c'. In compression, the concrete is linear elastic up to the initial yield strain ϵ_y. Between ϵ_y and ϵ_c' the response is plastic with hardening, and beyond ϵ_c' the response is perfectly plastic. Unloading from compression is elastic as shown. In tension, the concrete is linear up to ϵ_t (cracking strain). Cracked concrete is assumed stress-free so that precracked stresses are redistributed. Once a particular location in the beam cross section has cracked, the tensile strength of that location is set to zero; this infers that the cracks do not heal.

The stress-strain relation for reinforcing steel is assumed elastic and perfectly plastic, defined (input) by the elastic modulus E_s and yield stress f_y, taken identical in compression and tension, and unloading is elastic. Reinforcing steel is considered to be lumped near the top and bottom of the cross section located by concrete cover thicknesses (input) as indicated in Figure 2. Since the concrete cross section is of unit width (plane strain slice), the steel areas A_s are the bar areas divided by the spacing.

By using the above assumptions, the beam-rod element is developed from a displacement formulation based on incremental virtual work wherein standard two-point hermitian interpolation functions are used to approximate transverse displacement increments, and linear interpolation functions are used for axial-displacement increments. This results in a tangent element stiffness matrix corresponding to 6 degrees of freedom, two translations, and a rotation (increments) per node. Effective bending and axial stiffness terms in the element matrix are determined iteratively during each load step by using 11-point Simpson integration through the element cross section. That is, the strain profile at the end of the load step is used to recompute the stiffness terms, and the load step is repeated until convergence of all elements is observed.

Criteria for Crack Widths and Failure

Once a converged solution has been obtained for a reinforced-concrete culvert model under service loading, structural distress may be assessed by (a) maximum tensile steel stress, (b) maximum concrete compressive stress, (c) maximum concrete shear stress, and (d) maximum concrete crack width. The first three measures of distress are obtained directly from the structural response predictions of the CANDE model. Crack-width prediction, however, requires a semiempirical approach. An empirical formula relating crack widths to maximum tensile steel stress is given by Gergely and Lutz (10):

$$C_w = 0.000\,15(t_b^2 S)^{1/3}(f_s - 5.0) \quad (1)$$

where

C_w = crack width at tension steel (in),
t_b = concrete cover to steel center (in),
S = spacing of reinforcement (in), and
f_s = tensile steel stress (ksi).

The above formula was found to give good predictions for crack widths in this study and is further supported by other studies involving one-way slabs with deformed wire, deformed wire fabric, and deformed bars (11). For culvert installations, it is generally accepted that crack widths should be no larger than 0.01 in under service loading (ASTM C789-79 and AASHTO M259-76I).

When loading becomes excessive, failure of the reinforced-concrete beam-rod element occurs in either of two ways--flexure or shear. Flexure failure (actually flexure-thrust failure) occurs when the cross section cannot sustain any additional loading; i.e., all uncracked concrete is at maximum compressive strength f_c' and all steel reinforcement is yielding. Typically this infers flexural cracks, plastic hinging of steel reinforcement, and crushing of concrete.

Shear failure, characterized by diagonal cracking, is determined by a standard American Concrete Institute (ACI) strength definition (12). Specifically, shear failure of an element is said to occur when the predicted nominal shear stress is equal to the concrete shear strength; i.e.,

$$V/A_c = 2(f_c')^{1/2} \quad (2)$$

where V is the predicted shear force, A_c is the concrete area between the steel reinforcement, and 2 $(f_c')^{1/2}$ is the shear strength (f_c' is in psi units).

For a reinforced-concrete culvert (e.g., box or pipe) composed of an assemblage of elements, ultimate flexural failure (including thrust interaction) occurs when a sufficient number of elements fail in flexure (plastic hinges), which produces a collapse mechanism. However, ultimate shear failure of the culvert structure is said to occur when any single element fails in shear. These ultimate failure criteria were found to correlate well with experimental data for box and pipe culverts loaded in bearing.

VERIFICATION OF CANDE MODEL WITH EXPERIMENTAL DATA

To demonstrate the validity of the CANDE culvert model, comparisons are made with experimental data for (a) out-of-ground box culverts loaded in four-

edge bearing and (b) an in-ground box culvert with incremented soil loading.

Out-of-Ground Box Tests

These experimental data were obtained from a testing program (13,14) for reinforced-concrete box culverts with welded wire fabric reinforcement loaded to failure in four-edge bearing as indicated in Figure 3. Three box sizes were tested, each with three amounts of steel reinforcement--low, medium, and high. Thus, nine separate box designs were tested; there were two repeated tests per box design (18 tests). Table 1 (13,14) lists these boxes along with measured values for concrete strength (including repeated box tests), steel areas (corresponding to those in Figure 3), and measured steel strength. Experimental data from the test program include the load at which 0.01-in cracking occurs and the ultimate load in shear or flexure, to be compared subsequently with the CANDE model predictions (load-deformation curves were not measured during the experiments).

Figure 4 shows the finite-element model for a typical box-culvert test where, because of symmetry, only half the box is modeled by using 14 elements. Each element cross section is assigned the concrete thickness, steel area, steel location, and steel strength as actually reported from the experimental tests. For the concrete material properties, f'_c is taken as given in Table 1 so that repeated tests are also analyzed. The other concrete model parameters are assigned the standard values noted in Figure 1.

Figure 5 shows the comparison between test data and CANDE predictions for the load P per foot length of box that produces the first occurrence of an 0.01-in crack. These cracks occur on the inside surfaces of the top and/or bottom slabs near the centerline. Overall, a reasonably good correlation is observed; predicted load values average 10 percent lower than test results.

When the test boxes were loaded to ultimate, 10 tests failed in flexure and 8 tests failed in shear. Figure 6 shows the comparison between the ultimate load test data and CANDE predictions. In each case the predicted failure mode agrees with the observed failure mode. Good correlation is observed overall; predicted values average 1 percent lower than test results. Note that shear failures show slightly more scatter than flexure failures, as should be expected.

Additional out-of-ground experimental verification of the CANDE reinforced-concrete model has been made with circular pipes in three-edge bearing. Good correlation was observed for load-deformation curves as well as 0.01-in cracking loads and ultimate loads (4).

In-Ground Box Culvert

Test data for buried box culverts are very limited. However, recent research projects by the Kentucky Department of Transportation have provided some instrumented data for buried boxes. In particular, measured soil pressures on a buried box culvert (4x4--10) supported on a dense granular bedding within a bedrock formation are used for this study (15). A schematic idealization of the box-soil system is shown in Figure 7 along with box steel rein-

Figure 3. Box culvert in four-edge bearing.

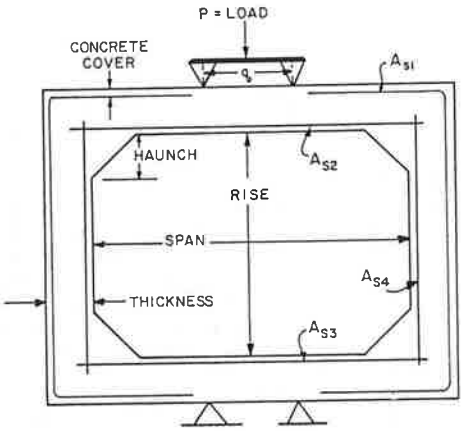

Table 1. Measured properties of test box design.

ASTM Box Size[a]	Concrete Strength f'_c (psi)	Ultimate Steel Strength f_y (ksi)	Load Spacing q (in)	Steel Area[b] (in^2/in)			Load at 0.01-in Crack (kips/ft)	Ultimate Load[c] (kips/ft)
				A_{S1}	A_{S2}	A_{S3}		
8x4–8	4930	84	12	0.025	0.025	0.025	9.3	17.9 (F)
	5510						11.3	17.2 (F)
8x4–8	4470	90	12	0.043	0.036	0.036	14.0	29.7 (F)
	5420						12.3	22.5 (S)
8x4–8	5280	95	12	0.043	0.043	0.043	13.0	20.9 (S)
	5850						13.5	24.5 (S)
6x4–7	7060	94	9	0.015	0.021	0.021	9.5	16.1 (F)
	7460						9.5	15.0 (F)
6x4–7	6680	99	9	0.036	0.035	0.027	14.5	19.4 (S)
	6960						10.5	25.3 (S)
6x4–7	5960	95	9	0.024	0.034	0.034	15.0	21.6 (S)
	7190						12.5	23.4 (S)
4x4–5	6030	96	6	0.011	0.011	0.011	6.7	9.0 (F)
	6670						6.0	8.4 (F)
4x4–5	7000	91	6	0.011	0.020	0.020	7.0	13.2 (F)
	6630						8.0	13.2 (F)
4x4–5	5710	93	6	0.016	0.027	0.027	7.8	13.2 (S)
	6430						8.5	19.3 (F)

[a] Box size given as span (ft) x rise (ft)–wall thickness (in); haunch = wall thickness.
[b] Note A_{S4} steel was not used; spacing of steel wires is 2.0 in; and nominal concrete cover to steel centroids is 1.25 in.
[c] (F) = flexure failure, (S) = shear failure.

Figure 4. CANDE model of box culvert in four-edge bearing.

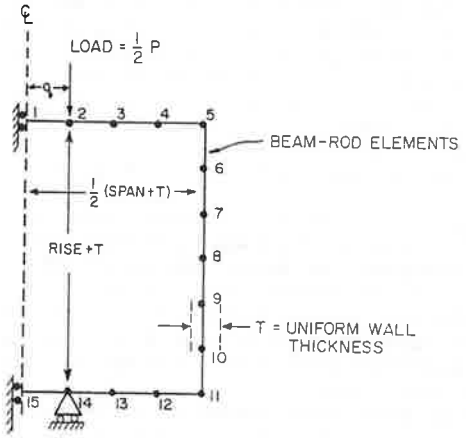

Figure 5. Prediction versus test for load at 0.01-in cracking.

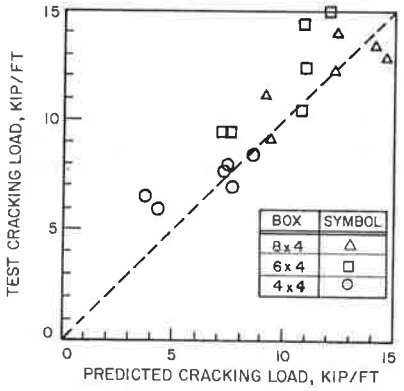

Figure 6. Predictions versus tests for ultimate load.

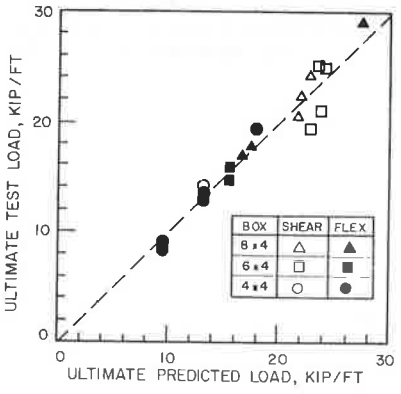

forcement and the location of eight Carlson earth-pressure cells mounted on the box [station 123 + 95 in the report by Russ (15)]. Soil pressure was recorded during the installation process as the fill soil, unified classification MH, was raised to the final cover height of 77 ft.

For the CANDE box-soil model, quadrilateral elements are used to represent the bedrock, bedding, and fill soil, which takes advantage of symmetry about the vertical centerline. Elastic soil properties are assumed as shown in Figure 7. The reinforced-concrete box is modeled similarly to the previous out-of-ground box tests by using the reported material properties. The initial configuration includes bedrock, bedding, and box loaded by its own weight. A total of 20 construction increments are used to simulate the construction process, in which the fill-soil weight density is 138 pcf.

Figure 7. Schematic view of box-soil system.

REINFORCEMENT AND CONCRETE PROPERTIES	f_c' psi	f_y ksi	STEEL AREAS IN^2/IN A_{s1}	A_{s2}	A_{s3}	A_{s4}
	4500	60	0.037	0.050	0.050	0.017

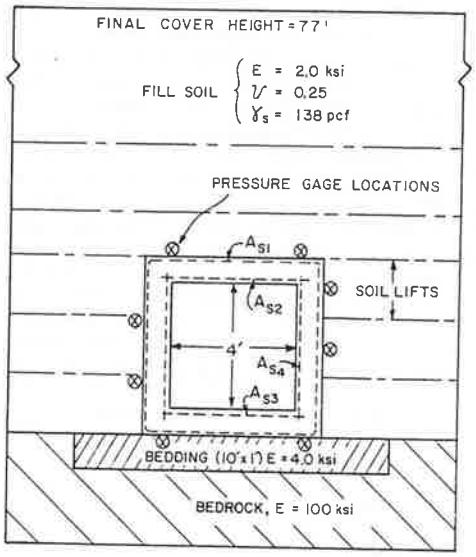

Figure 8 shows the predicted soil-pressure distributions around the box at an intermediate fill height and at the final fill height and corresponding test data points. Good correlation is observed on the top and bottom slabs. Measured pressures on the side walls are not symmetric as assumed in the CANDE model; better agreement is observed for the right wall than for the left wall.

Note that the predicted vertical pressure on the top slab is not uniform as is often assumed in traditional design procedures. This is to be expected due to the stiffness interaction of the fill soil with the slab bending stiffness. As slab cracking develops, a greater portion of the soil load is shifted to the stiffer corners, which are supported by the side walls.

Further experimental verification of CANDE soil-structure models for buried reinforced-concrete pipes is reported elsewhere (1,5). Good correlations are observed for pipe deformations and crack-width predictions during the soil-loading schedule.

EVALUATION OF ASTM C789 BURIED BOX-CULVERT DESIGNS

In the previous sections, the CANDE predictions were shown to correlate well with experimental data for both out-of-ground and in-ground box culverts, including crack widths, ultimate loads, and soil pressures on the box. Thus, a measure of confidence and validity having been established, the CANDE box-soil model is now used to evaluate the ASTM C789 designs that have not been validated with soil-structure analysis for buried conditions prior to this study.

ASTM Box-Culvert Designs

Table 2 shows the 32 standard box dimensions (rise, span, and wall thickness) used in the ASTM C789 design tables. For each box size, there are five or more selections for the amount of steel reinforce-

Figure 8. Prediction versus test data for soil pressure around box culvert.

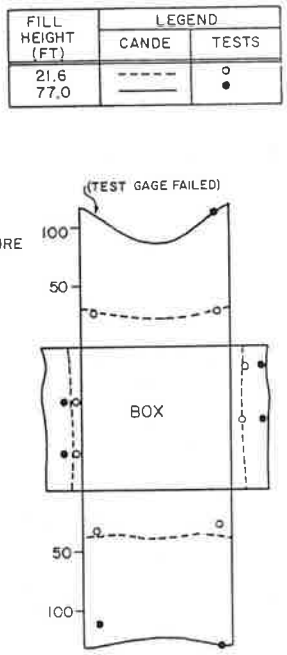

Table 2. Standard box sizes, ASTM C789.

Span (ft)	Rise (ft)									Wall Thickness (in)
	2	3	4	5	6	7	8	9	10	
3	X	X								4
4	X	X	X[a]							5
5		X	X	X						6
6		X	X	X	X					7
7			X	X	X	X				8
8			X[a]	X	X[a]	X	X[a]			8
9				X	X	X	X	X		9
10				X	X[a]	X	X	X	X	10

[a]Box sizes analyzed with CANDE.

ment, which in turn increases the structural capacity and permits a greater allowable earth-cover height. Shown in Table 3 is a subset of the box-culvert designs in Table 3 of ASTM C789 to be evaluated with CANDE. The sample subset contains five box sizes whose span lengths and rise-span ratios cover the range of standard sizes shown in Table 2. Three amounts of steel reinforcement, listed with each box size, represent low, medium, and high steel percentages from the available choices. Thus, Table 3 contains 15 different reinforced-concrete box-culvert designs whose dimensions and steel percentages represent a reasonable sampling of the larger ASTM design table. For each box-culvert design, ASTM specifies maximum allowable design earth cover, which in this case is the only source of loading (live loads are not considered in Table 3 of ASTM C789).

The ASTM box-culvert designs are based on a computerized design and analysis program (16) that operates with the following steps:

1. Soil pressure distributions are assumed around the culvert in proportion to the design earth-cover height and soil density. Soil pressure on the top and the bottom of the box is assumed uniform, while a linear variation is assumed along the side walls. No shear traction is considered.
2. Moment, shear, and thrust distributions around the culvert are determined by standard matrix

Table 3. Sample set of box-culvert designs from Table 3 in ASTM C789.

ASTM Box Size	Design Earth Cover (ft)	Steel Amount	Steel Area[a] (in^2/in)			
			A_{S1}	A_{S2}	A_{S3}	A_{S4}
4x3–5	10	Low	0.0100	0.0108	0.0108	0.0100
	14	Medium	0.0100	0.0142	0.0100	0.0100
	18	High	0.0117	0.0183	0.0183	0.0100
8x4–8	6	Low	0.0158	0.0158	0.0158	0.0158
	10	Medium	0.0200	0.0217	0.0255	0.0158
	14	High	0.0283	0.0292	0.0300	0.0158
8x6–8	6	Low	0.0158	0.0158	0.0167	0.0158
	10	Medium	0.0167	0.0242	0.0258	0.0158
	14	High	0.0233	0.0333	0.0350	0.0158
8x8–8	5	Low	0.0158	0.0158	0.0167	0.0158
	8	Medium	0.0158	0.0217	0.0233	0.0158
	12	High	0.0175	0.0308	0.0333	0.0158
10x6–10	6	Low	0.0200	0.0200	0.0200	0.0200
	10	Medium	0.0233	0.0283	0.0300	0.0200
	14	High	0.0325	0.0383	0.0400	0.0200

[a]Steel areas are converted to square inches per inch instead of square feet per inch.

methods by using elastic, uncracked reinforced-concrete section properties together with the loading assumptions in step 1.

3. For design, steel areas are determined by an ultimate-strength theory for bending and thrust, where ultimate moments and thrusts are obtained from step 2 multiplied by a load factor of 1.5.
4. Crack width (0.01 in allowable) is checked by using a semiempirical formula that is a function of tensile steel stress at service loads determined in step 2.
5. Ultimate shear stress is checked against the nominal shear stress obtained in step 2 multiplied by a load factor of 1.5.

Although the relative simplicity of the above design-and-analysis approach may be attractive, the resulting box designs have not been verified with in-ground experimental tests nor have they been cross-checked with soil-structure interaction analysis prior to this study. Indeed, the assumptions of linear-elastic behavior of concrete, uniform soil-pressure distributions, and the lack of soil-stiffness considerations are but a few of the concerns in assessing the adequacy of the ASTM box designs.

Evaluation Objectives and CANDE Model

For each ASTM box section shown in Table 3, the CANDE box-soil model is used to determine the fill-soil height at which 0.01-in cracking occurs and the fill-soil height at which failure (either shear or flexure) occurs. These fill-soil heights are compared with the corresponding ASTM design earth covers, thereby providing an evaluation of the conservativeness (or unconservativeness) of the box designs.

For the CANDE box-culvert model, the reinforced-concrete parameters listed in Figures 1 and 2 are used, which are consistent with the ASTM specifications. Box dimensions and steel areas are taken directly from Table 3 and haunch dimensions are taken equal to wall thicknesses. Since the ASTM approach does not consider soil stiffness, the CANDE predictions assume two soil conditions--soft and stiff--for the analysis of each box, thereby bracketing the practical range of soil stiffness. Figure 9 shows the box-soil model along with the elastic-modulus values for the soft and stiff soil conditions. The initial configuration consists of in situ soil, bedding, and the box loaded by its own

Figure 9. Box-soil model to evaluate ASTM designs.

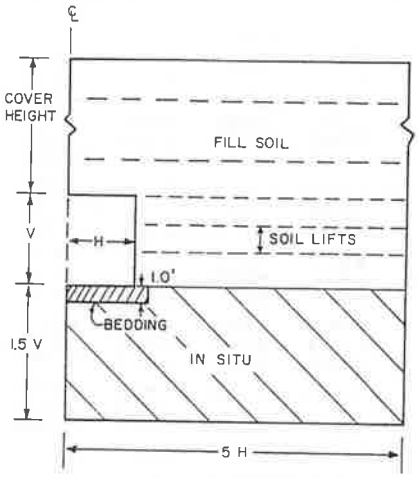

$H = \frac{1}{2}$ (SPAN + WALL THICKNESS)
V = RISE + WALL THICKNESS

SOIL CONDITION		YOUNG'S MOD. psi	POISSON'S RATIO —
SOFT	FILL	333.	0.33
	BEDDING	666.	0.33
STIFF	FILL	3333.	0.33
	BEDDING	6666.	0.33

* IN SITU = FILL

Figure 10. Evaluation of ASTM box designs of cracking fill cover.

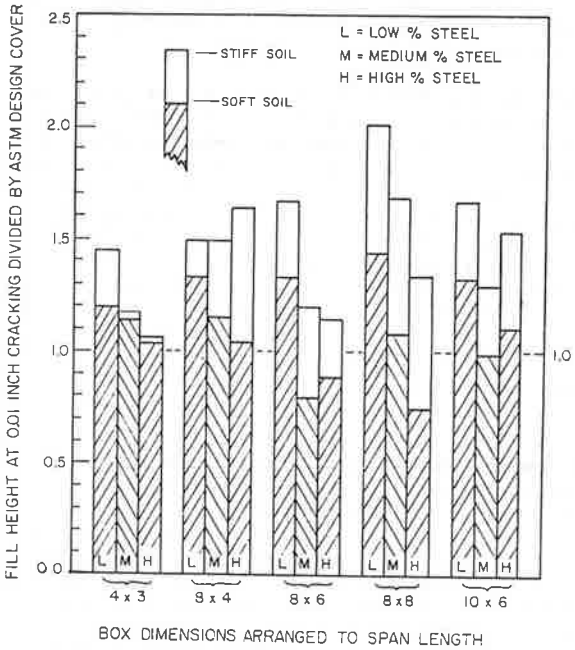

weight. Next, nine construction increments of fill soil (weight density = 120 pcf) are sequentially added to the system to raise the fill soil to the ASTM design cover height. Thereafter, additional fill-soil layers are added until a flexural failure mechanism occurs. During this loading sequence, the predicted cover height that causes initial 0.01-in cracking is determined along with the cover height that causes shear failure, providing that shear failure occurs prior to flexure failure (see previous discussion for cracking and failure criteria).

Figure 11. Evaluation of ASTM box design at ultimate fill cover.

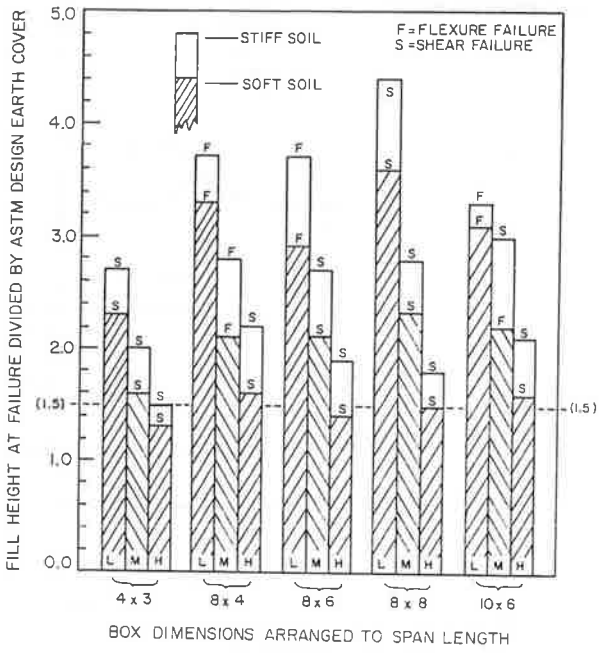

Results of ASTM versus CANDE Cover

Figure 10 shows a bar chart of fill-height ratios formed by dividing the CANDE cover-height prediction for 0.01-in cracking by the corresponding ASTM design earth cover. Here the five boxes, arranged to span size, are grouped into three bar graphs that represent the three levels of steel reinforcement. For each individual bar graph, two fill-height ratios are shown, which result from the soft and stiff soil conditions assumed in the CANDE model.

If the ASTM designs are conservative (safe) with regard to an allowable 0.01-in cracking, these fill-height ratios should be greater than or equal to 1.0. For the stiff soil condition, the ratio ranges from 1.06 to 2.02, which implies conservative designs. However, for the soft soil condition, the ratio ranges from 0.75 to 1.44, which indicates that some designs may not be conservative. As a general conclusion, the ASTM boxes are moderately conservative with respect to 0.01-in cracking at design earth cover providing good quality soil is used.

Figure 11 shows a similar bar chart for fill-height ratios formed by dividing the CANDE cover-height prediction at failure (flexure or shear) by the corresponding ASTM design earth cover. In this case, an ideal design should have a ratio of 1.5 since the ASTM design procedure assumes an ultimate soil loading of 1.5 times the design earth-cover loading. For stiff soils, the ratio varies from 1.5 to 4.4, whereas for soft soils, the ratio varies from 1.3 to 3.6. Thus, in general, the ASTM designs are conservative, perhaps overly conservative when good quality soil is employed.

It is interesting to observe (Figure 11) that for a given box size and soil condition, the ratios are higher for low reinforcement than for high reinforcement. In other words, the ASTM design earth cover specified for a box with low reinforcement is more conservative than the specified earth cover for the identical box with high reinforcement. Another observation indicated in Figure 11 is that shear failure is the predominant failure mode. The likelihood of flexural failure is increased when the span-rise ratio is high, the soil stiffness is low, and/or the steel reinforcement is low.

An observation not made here but reported elsewhere (4) is that the vertical soil-pressure distribution on the top and bottom slabs is not uniform (as in the ASTM loading assumption) but increases monotonically from the box centerline to the corners. Furthermore, the curvature of the pressure distributions becomes more pronounced as the soil-cover height increases due to flexural cracking and weakening of the slabs. Also, the shear traction on the side walls produces a significant downward force that must be equilibrated by an upward pressure on the bottom slab, an effect not taken into account in the ASTM loading assumption.

SUMMARY AND CONCLUSIONS

The CANDE box-culvert model correlates well with experimental data for boxes in four-edge bearing. Predicted loads for 0.01-in cracking averaged 10 percent lower than measured, and predicted ultimate loads averaged 1 percent lower than measured. Measured soil pressures from an in-ground box-culvert installation are in good agreement with CANDE box-soil model predictions at both intermediate and final earth-cover depths.

After the CANDE model has been verified, the ASTM C789 buried box designs are evaluated with CANDE, which results in the following conclusions:

1. Soil stiffness, which is not accounted for in the ASTM design and analysis procedure, has a significant influence on the crack width and structural capacity of buried box culverts. Stiff soils allow as much as 50 percent greater fill heights than do soft soils.
2. Soil shear traction on the side walls, also not accounted for in the ASTM procedure, produces a significant downward force that must be equilibrated by increased pressure on the bottom slab.
3. Specified earth covers for ASTM box designs are safe against exceeding the 0.01-in crack-width limitation if good quality soil and compaction are used.
4. Ultimate earth-cover loading for ASTM box designs is usually significantly greater than 1.5 times the design earth cover, which infers that ASTM designs are conservative. However, designs that require heavily reinforced boxes are less conservative than those for lightly reinforced boxes.
5. Shear failure is the predominant failure mode. The likelihood of flexural failure increases with increased ratio of box span to rise, decrease of soil stiffness, and decrease of steel reinforcement.

Further results and discussion of these findings are given elsewhere (6).

ACKNOWLEDGMENT

Deep appreciation is extended to the Federal Highway Administration and to George W. Ring III, Project Technical Manager, for supporting this work effort and providing helpful guidance. Thanks are extended to Frank J. Heger of Simpson Gumpertz and Heger, Inc., who, along with representatives of the American Concrete Pipe Association, supplied experimental data for out-of-ground culvert tests.

REFERENCES

1. M.G. Katona and others. CANDE--A Modern Approach for the Structural Design and Analysis of Buried Culverts. FHWA, Rept. FHWA-RD-77-5, Oct. 1976.
2. M.G. Katona and J.M. Smith. CANDE User Manual. FHWA, Rept. FHWA-RD-77-6, Oct. 1976.
3. M.G. Katona and J.M. Smith. CANDE System Manual. FHWA, Rept. FHWA-RD-77-7, Oct. 1976.
4. M.G. Katona and others. CANDE-1980: Box Culverts and Soil Models. FHWA, Oct. 1980.
5. M.G. Katona. CANDE: A Versatile Soil-Structure Design and Analysis Computer Program. Journal of Advances in Engineering Software, Vol. 1, No. 1, 1978, pp. 3-9.
6. M.G. Katona. Discussion and Application of CANDE Computer Program to Design Reinforced Concrete Culverts. In Concrete Pipe and the Soil-Structure System, ASTM Symposium Vol. STP-630, Aug. 1977, pp. 17-40.
7. M.G. Katona. Analysis of Long-Span Culverts by the Finite Element Method. TRB, Transportation Research Record 678, 1978, pp. 59-66.
8. M.G. Katona. A Modern Approach for the Structural Design of Pipe Culverts. Second International Conference on Computers in Engineering and Building Design (CAD76), IPC Science and Technology Press Limited, Guildford, Surrey, England, 1976, pp. 138-140.
9. M.G. Katona. Structural Evaluation of New Concepts for Long-Span Culverts. FHWA, Rept. FHWA-RD-79-115, Dec. 1979.
10. P. Gergely and L.A. Lutz. Maximum Crack Width in Reinforced Concrete Flexural Members. American Concrete Institute, Detroit, MI, 1968, SP-20, pp. 87-117.
11. J.P. Lloyd, H.M. Rejali, and C.E. Kesler. Crack Control in One-Way Slabs Reinforced with Deformed Welded Wire Fabric. American Concrete Institute Journal, May 1969, pp. 366-376.
12. Commentary on Building Code Requirements for Reinforced Concrete. American Concrete Institute, Detroit, MI, ACI 318-77, 1966.
13. M.R. Boring, F.J. Heger, and M. Bealey. Test Program for Evaluating Design Method and Standard Designs for Precast Concrete Box Culverts with Welded Wire Fabric Reinforcing. TRB, Transportation Research Record 518, 1974, pp. 49-63.
14. Simpson Gumpertz and Heger, Inc. Report of Test Programs for Evaluation of Design Method and Standard Designs for Precast Concrete Box Culverts with Welded Wire Fabric Reinforcing. American Concrete Pipe Association, Chicago, IL, July 1973.
15. R.L. Russ. Loads on Box Culverts Under High Embankments: Positive Projection, Without Imperfect Trench. Division of Research, Department of Transportation, Lexington, KY, Res. Rept. 431, Aug. 1975.
16. R.W. LaTona and F.J. Heger. Computerized Design of Precast Reinforced Concrete Box Culverts. HRB, Highway Research Record 443, 1973, pp. 40-51.

Publication of this paper sponsored by Committee on Subsurface Soil-Structure Interaction.

Abridgment

Effects of Frictional Slippage of Soil-Structure Interfaces of Buried Culverts

MICHAEL G. KATONA

A simple friction-contact interface element is used to simulate frictional slippage, separation, and rebonding along a soil-structure interface. The application is to a long-span buried culvert with incremental soil layering and it is solved by the finite-element method. It is concluded that interface elements, which permit relative slippage between soil and structure, are necessary in order that the predicted structure deformations conform with experimental data.

Although the ever-popular finite-element method (FEM) has been used extensively for the structural analysis and design of buried pipe culverts as well as for other soil-structure interaction problems, it is, of course, simply a numerical-solution methodology. The real challenge is to construct mechanistic models that behave something like the real world while at the same time to strike a balance between rigorous mechanics and engineering simplicity. For the buried-culvert problem, this challenge extends to almost every aspect of the soil-structure system, e.g., soil constitutive model, structural constitutive model, simulation of incremental soil layers, boundary conditions, and geometrical nonlinearities. One aspect of particular interest is the treatment of the culvert-soil interface. Typically, FEM models assume that the soil is bonded to the culvert during deformation.

Katona has introduced (1) a simple friction-contact interface element that simulates frictional slippage, separation, and rebonding of two bodies that initially mate at a common interface and subsequently deform with an arbitrary static loading schedule. Constraint equations between initially mating node pairs and the general principle of virtual work are used to formulate the interface element for an FEM solution procedure. This interface element is operational in the FEM program Culvert Analysis and Design (CANDE) (2,3).

CANDE is a special-purpose design and analysis program for buried culverts and includes capabilities for incremental construction and nonlinear material representations for structural and soil elements as well as the above-mentioned interface element. Plane strain geometry and small deformations are assumed. The culvert structure is modeled with a sequence of beam-column elements, and the soil is modeled with continuum quadrilateral or triangular elements.

With the aid of the CANDE program, the objective of this paper is to illustrate that the inclusion of interface elements helps to simulate the observed structural responses of long-span culverts during field installations.

LONG-SPAN CULVERT MODEL

Long-span arch culverts, which infers spans that range from 5 to 15 m, are constructed by bolting together curved structural plates of corrugated metal into the shape of an arch with the ends anchored into concrete footings. Backfill soil is compacted in a sequence of symmetrical layers on both sides of the arch. During this process, lateral soil pressure moves the arch sides inward and the crown upward (peaking). Subsequent soil layers placed above the crown reverse this trend by pushing the crown downward and the sides outward, which mobilizes passive soil resistance. Field experience indicates that the relative crown movement is a major performance criterion for assessing the structural integrity of the soil-structure system (4). Generally, it is considered desirable to maintain the relative crown movement (peaking and flattening) within 2 percent of the total arch rise.

The following example demonstrates that the soil-structure interface assumption significantly influences the crown movement prediction during the backfilling process. Moreover, a frictional slipping interface appears to be a better representation of observed behavior than a completely bonded interface.

Figure 1 is an FEM representation of a high-profile, long-span arch in which symmetry is assumed about the vertical centerline. Top rise is 3.4 m; half-span is 4.8 m. Sixteen beam-column elements (line segments) form half of the arch periphery; an additional element composed of four quadrilateral elements is embedded in the concrete footing. Interface elements connect the culvert nodes above the footing to corresponding soil nodes. Three separate interface conditions are to be considered: bonded ($\mu = \infty$), frictional slip ($\mu = 0.5$), and frictionless slip ($\mu = 0.0$), where μ is the coefficient of Coulomb friction. In all cases, the initial reference system includes the concrete footing, the metal arch, and the soil raised to the level of the springline. Loading consists of seven incremental layers of soil and includes body weight plus temporary compaction pressures (5 psi), which squeeze each soil layer to simulate the effects of the compaction equipment (5). For the purposes of this study, linear constitutive properties are assumed for all material as noted in Figure 1; effects of nonlinear material models are presented elsewhere (5).

DISCUSSION OF RESULTS

Figure 2 shows the resulting crown-displacement histories as a function of fill height for the three interface conditions. We observe that maximum crown peaking increases by nearly a factor of 3 for the frictionless case as compared with the bonded case. Moreover, for the slipping cases ($\mu = 0.0$ and 0.5), the crown does not return to the zero reference until the fill height is greater than 2.0 top-rise units above the springline, whereas the return to the zero reference occurs at a fill height of 1.3 top-rise units for the bonded case. The term "peaking range" will be used to refer to the fill-height level at which the crown returns to zero reference.

Also shown in Figure 2 is a typically observed crown-deflection history based on averaging experimental data from four different long-span arch installations (5), none of which conforms exactly to the model represented in Figure 1. Although not shown, the individual experimental curves exhibit a rather wide variation in the magnitude of crown peaking that ranges from 0.5 to 3.0 percent deflection of the total rise. However, one common trait is that the peaking range of the individual experi-

mental curves is fairly consistent; it measures slightly more than 2.0 top-rise units, as illustrated by the averaged-data curve.

In comparing the analytical deflection histories with the averaged experimental curve, it is apparent that the slipping conditions (μ = 0.0 and 0.5) provide a more reasonable representation of the averaged data than does the completely bonded condition. This conclusion is based on the observation that peaking ranges are in good agreement, not the

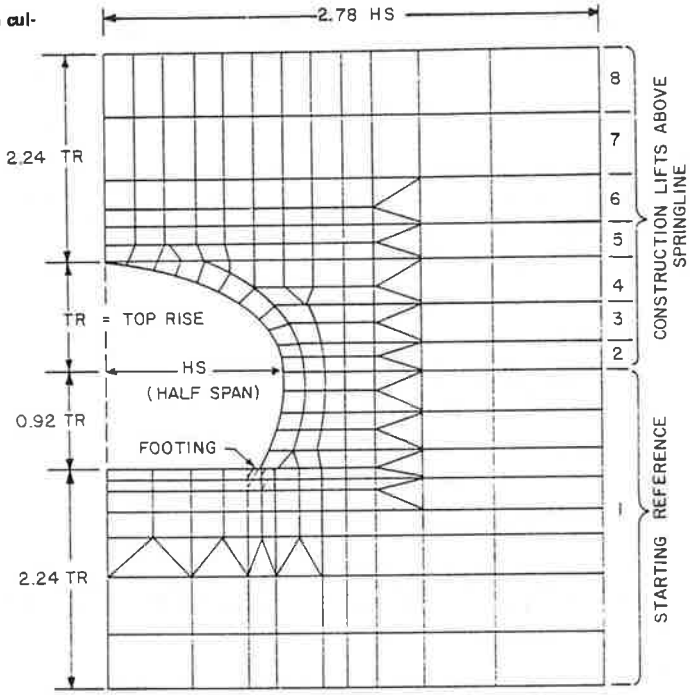

Figure 1. Dimensions of FEM model of arch culvert and soil system.

MATERIAL	YOUNG'S MOD. kPa	POISSON RATIO
SOIL	13.8×10^3	0.35
FOOTING	20.7×10^6	0.20
STEEL ARCH 5 GAGE, 6x2-INCH	20.7×10^7	0.30

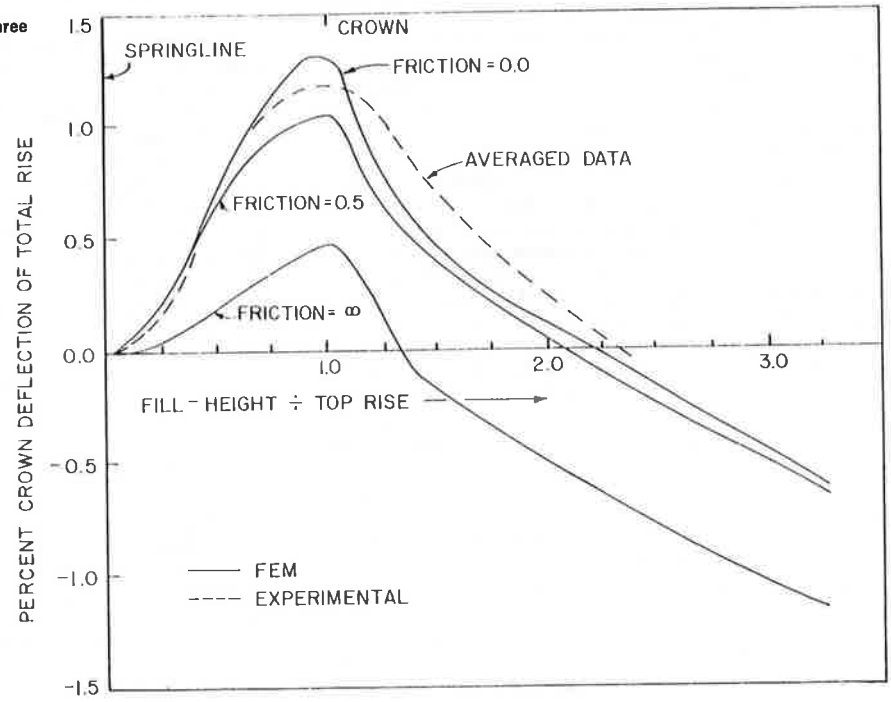

Figure 2. Crown-displacement histories for three friction values and averaged experimental observations.

observation that the peaking amplitudes also happen to be in good agreement. The observation that the peaking amplitude of the averaged data is bracketed by the two slipping conditions is incidental because amplitudes are easily changed by the assumed soil stiffness. However, the peaking range is unaffected by soil stiffness (5).

In summary, it is concluded that FEM models of long-span culvert installations should incorporate slipping interface conditions in order to properly predict deformation histories.

ACKNOWLEDGMENT

I wish to express my appreciation to the Federal Highway Administration and to the technical monitor, George W. Ring III, for sponsoring this effort. Thanks are extended to Rene Orillac, research assistant at the University of Notre Dame, for his energetic help in this study.

REFERENCES

1. M.G. Katona. Simple Contact-Friction Interface Element with Application to Buried Culverts. International Journal for Numerical and Analytical Methods in Geomechanics (in preparation).
2. M.G. Katona. CANDE: A Versatile Soil-Structure Design and Analysis Computer Program. Journal of Advances in Engineering Software, Vol. 1, No. 1, 1978, pp. 3-9.
3. M.G. Katona. Analysis of Long-Span Culverts by the Finite Element Method. TRB, Transportation Research Record 678, 1978, pp. 59-66.
4. E.T. Selig, J.F. Abel, F.H. Kulhawy, and W.E. Falby. Review of the Design and Construction of Long-Span, Corrugated-Metal Buried Conduits. FHWA, Tech. Rept. HRS-14, Oct. 1977.
5. M.G. Katona. Structural Evaluation of New Concepts for Long-Span Culverts and Culvert Installations. FHWA, Rept. FHWA-RD-79-115, Dec. 1979.

Publication of this paper sponsored by Committee on Subsurface Soil-Structure Interaction.

Deflection of Flexible Culverts due to Backfill Compaction

J.M. DUNCAN AND J.K. JEYAPALAN

A detailed study was made of the effects of compaction on the long-span aluminum culvert structure in Tice Valley, California. Finite-element analyses were performed to simulate field behavior. Measurements showed that the deflections due to compaction were very significant. The analysis procedure appeared to model the effects of compaction reasonably accurately.

Experience with flexible metal culverts has shown that the loads applied by rollers and other heavy construction equipment during compaction of the backfill can cause considerable deflection of a culvert. If heavy construction equipment is permitted to operate close to the sides of a flexible culvert, considerably more "peaking," or upward movement of the crown, may occur than if heavy equipment is kept away from the structure.

In an analytical study of these effects, Katona (1) performed finite-element analyses in which the application of temporary compaction loads was simulated. He found that temporary loads applied to the surface of each new layer of backfill resulted in additional amounts of peaking, and his results were therefore in agreement with field experience.

Thus it is clear from both field experience and analytical studies that compaction loads can induce appreciable deflections in flexible metal culverts. Although the experience and the analytical studies are in qualitative agreement, no data have been available that could serve as a basis for quantitative comparisons of field measurements with analytical results in any particular case.

The purpose of the study described in this paper is to make a detailed evaluation of the effects of compaction for the long-span aluminum culvert structure in Tice Valley, California. Deflections of the haunch, the crown, and the quarter point were measured before and after compaction of each new layer of backfill, and analyses were performed to simulate the field behavior. It was thus possible to determine the magnitude of the compaction load appropriate for the equipment used on the job, and it was also possible to determine the effect of the compaction loads on the bending moments in the culvert.

TICE VALLEY CULVERT STRUCTURE

The Tice Valley culvert structure is located in Walnut Creek, California, about 20 miles east of San Francisco. A cross section through the structure is shown in Figure 1. It is a horizontal ellipse with a span of 25 ft 1 in and a rise of 12 ft 11 in. The culvert is constructed of aluminum structural plate 0.15 in thick and has aluminum bulb angle stiffener ribs spaced at 2 ft 3 in across the crown.

The backfill is a sandy clay classified CL by the Unified Soil Classification System. It was compacted to a minimum of 95 percent of the maximum dry density determined by the standard compaction test of the American Association of State Highway and Transportation Officials (AASHTO) (AASHTO 799, ASTM D698). The final depth of cover over the crown of the structure was 4.0 ft. The backfill was spread in layers about 1.0 ft thick and was compacted by using a 16 500-lb bulldozer and a 3500-lb vibratory roller.

INSTRUMENTATION

Deflection gages were installed at two sections in the culvert located 6 ft 9 in apart. Four measurements were made at each section. As shown in Figure 2, these were (a) change in span, (b) change in rise, (c) deflection of quarter points relative to invert, and (d) vertical movement of quarter points relative to haunch.

The vertical movements of the quarter points were

observation that the peaking amplitudes also happen to be in good agreement. The observation that the peaking amplitude of the averaged data is bracketed by the two slipping conditions is incidental because amplitudes are easily changed by the assumed soil stiffness. However, the peaking range is unaffected by soil stiffness (5).

In summary, it is concluded that FEM models of long-span culvert installations should incorporate slipping interface conditions in order to properly predict deformation histories.

ACKNOWLEDGMENT

I wish to express my appreciation to the Federal Highway Administration and to the technical monitor, George W. Ring III, for sponsoring this effort. Thanks are extended to Rene Orillac, research assistant at the University of Notre Dame, for his energetic help in this study.

REFERENCES

1. M.G. Katona. Simple Contact-Friction Interface Element with Application to Buried Culverts. International Journal for Numerical and Analytical Methods in Geomechanics (in preparation).
2. M.G. Katona. CANDE: A Versatile Soil-Structure Design and Analysis Computer Program. Journal of Advances in Engineering Software, Vol. 1, No. 1, 1978, pp. 3-9.
3. M.G. Katona. Analysis of Long-Span Culverts by the Finite Element Method. TRB, Transportation Research Record 678, 1978, pp. 59-66.
4. E.T. Selig, J.F. Abel, F.H. Kulhawy, and W.E. Falby. Review of the Design and Construction of Long-Span, Corrugated-Metal Buried Conduits. FHWA, Tech. Rept. HRS-14, Oct. 1977.
5. M.G. Katona. Structural Evaluation of New Concepts for Long-Span Culverts and Culvert Installations. FHWA, Rept. FHWA-RD-79-115, Dec. 1979.

Publication of this paper sponsored by Committee on Subsurface Soil-Structure Interaction.

Deflection of Flexible Culverts due to Backfill Compaction

J.M. DUNCAN AND J.K. JEYAPALAN

A detailed study was made of the effects of compaction on the long-span aluminum culvert structure in Tice Valley, California. Finite-element analyses were performed to simulate field behavior. Measurements showed that the deflections due to compaction were very significant. The analysis procedure appeared to model the effects of compaction reasonably accurately.

Experience with flexible metal culverts has shown that the loads applied by rollers and other heavy construction equipment during compaction of the backfill can cause considerable deflection of a culvert. If heavy construction equipment is permitted to operate close to the sides of a flexible culvert, considerably more "peaking," or upward movement of the crown, may occur than if heavy equipment is kept away from the structure.

In an analytical study of these effects, Katona (1) performed finite-element analyses in which the application of temporary compaction loads was simulated. He found that temporary loads applied to the surface of each new layer of backfill resulted in additional amounts of peaking, and his results were therefore in agreement with field experience.

Thus it is clear from both field experience and analytical studies that compaction loads can induce appreciable deflections in flexible metal culverts. Although the experience and the analytical studies are in qualitative agreement, no data have been available that could serve as a basis for quantitative comparisons of field measurements with analytical results in any particular case.

The purpose of the study described in this paper is to make a detailed evaluation of the effects of compaction for the long-span aluminum culvert structure in Tice Valley, California. Deflections of the haunch, the crown, and the quarter point were measured before and after compaction of each new layer of backfill, and analyses were performed to simulate the field behavior. It was thus possible to determine the magnitude of the compaction load appropriate for the equipment used on the job, and it was also possible to determine the effect of the compaction loads on the bending moments in the culvert.

TICE VALLEY CULVERT STRUCTURE

The Tice Valley culvert structure is located in Walnut Creek, California, about 20 miles east of San Francisco. A cross section through the structure is shown in Figure 1. It is a horizontal ellipse with a span of 25 ft 1 in and a rise of 12 ft 11 in. The culvert is constructed of aluminum structural plate 0.15 in thick and has aluminum bulb angle stiffener ribs spaced at 2 ft 3 in across the crown.

The backfill is a sandy clay classified CL by the Unified Soil Classification System. It was compacted to a minimum of 95 percent of the maximum dry density determined by the standard compaction test of the American Association of State Highway and Transportation Officials (AASHTO) (AASHTO 799, ASTM D698). The final depth of cover over the crown of the structure was 4.0 ft. The backfill was spread in layers about 1.0 ft thick and was compacted by using a 16 500-lb bulldozer and a 3500-lb vibratory roller.

INSTRUMENTATION

Deflection gages were installed at two sections in the culvert located 6 ft 9 in apart. Four measurements were made at each section. As shown in Figure 2, these were (a) change in span, (b) change in rise, (c) deflection of quarter points relative to invert, and (d) vertical movement of quarter points relative to haunch.

The vertical movements of the quarter points were

Figure 1. Cross section of Tice Valley culvert.

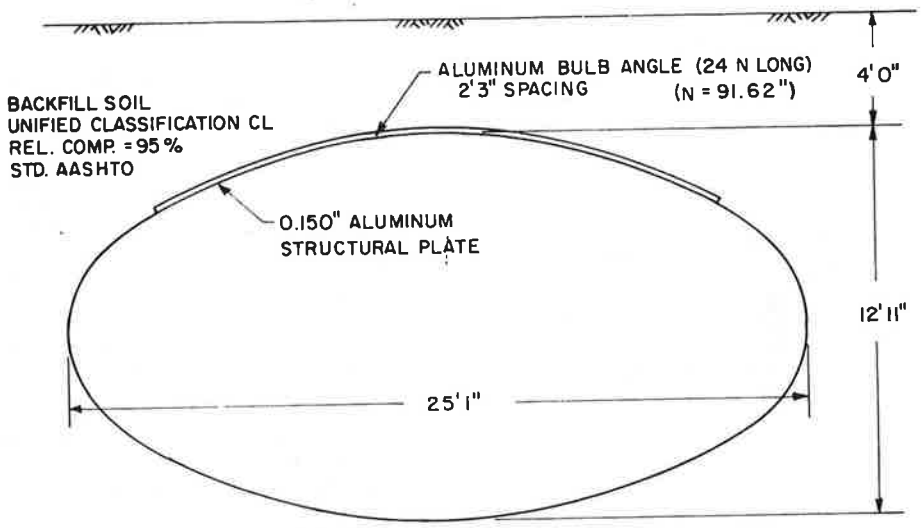

Figure 2. Location of instruments.

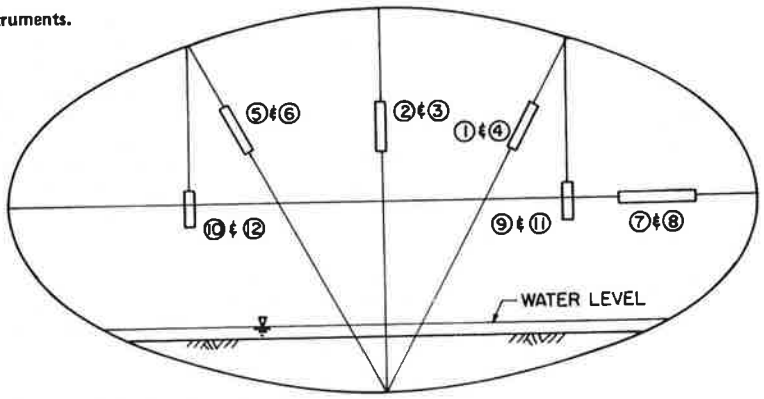

NOTE: GAGES WERE INSTALLED AT TWO SECTIONS (A and B) LOCATED 6'9" APART

measured by using steel weights with scales attached that were suspended from the quarter points on bead chains (instruments 9-12 in Figure 2). All other deflections (1-8 in Figure 2) were measured by using deflection gages of the type shown in Figure 3. These consist of a looped cable with a spring to maintain tension as the length changed. A block attached to one side of the loop slid within a tube attached to the other side of the loop, and a scale was attached to the outside of the tube. Changes in length between the ends of the deflection gage produced twice as great a change in the scale reading.

The accuracy of the deflection gages was checked under laboratory conditions and was found to be about ±0.03 in. The hanging plumb bobs used to measure vertical movements of the quarter points could be read with an accuracy of about ±0.05 in. However, to prevent damage by vandalism, it was necessary to remove the instruments from the culvert at the end of each day, and this reduced the accuracy of the readings. All things considered, it is estimated that the accuracy of the readings is within ±0.1 in, and the tolerance is probably less in most cases.

MEASURED DEFLECTIONS

The measured movement of the haunches and the crown is plotted against the level of the fill in Figures 4 and 5. In these figures the fill height is measured from the crown of the structure, so that H = 0 corresponds to the condition in which the top of the fill is level with the crown. The value of H is negative for fill levels below the crown and positive for fill levels above the crown. Measurements were begun with H = -5.5 ft, or fill level about 1 ft above the haunch of the structure.

Haunch movement is shown in Figure 4. Those points labeled "before compaction" are the sum of the incremental movements due to placement of each layer of fill. Those labeled "after compaction" represent the movement due to both the weight of fill and the compaction effects. It may be seen that by the time the fill had reached a level 2 ft below the crown (H = -2 ft) the decrease in span due to compaction effects was about twice as great as that due to the weight of the fill. The span increased slightly (more so at section B than at section A) as the fill was raised above the crown.

Crown movement is shown in Figure 5 by using the same convention as that for haunch movement. It may be seen that the movement of the crown due to compaction was about 1 1/3 times as large as that due to the weight of the fill.

Thus it is evident that compaction of the clay backfill around the Tice Valley culvert to 95 percent of the standard AASHTO maximum dry density with a 16 500-lb bulldozer and a 3500-lb vibratory roller caused considerable deflection of the culvert structure. This was true even though the roller was not

operated closer than about 2 ft from the side of the culvert and the fill immediately adjacent to the culvert was compacted with a light hand tamper. At both the haunch and the crown, the movement due to the effects of compaction exceeded that due to the weight of the fill.

Figure 3. Looped-cable displacement gages.

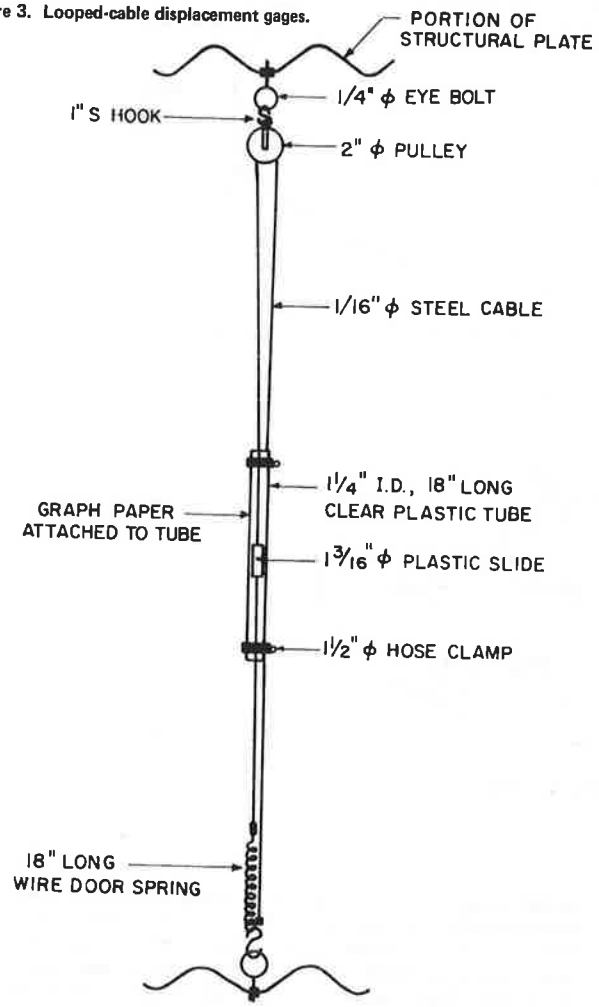

FINITE-ELEMENT ANALYSES

A number of finite-element analyses of the Tice Valley culvert were performed to calculate deflections of the culvert before and after compaction. Previous experience with finite-element analyses of flexible metal culverts has shown that it is essential in such analyses to model the nonlinear and stress-dependent stress-strain behavior of the backfill soil and to simulate the actual sequence of events during construction in order to achieve correspondence with the behavior of actual structures. Accordingly, the analyses of the Tice Valley culvert were performed in a series of increments by using hyperbolic stress-strain relationships for the backfill soil. These relationships, which have been described in detail by Duncan and Chang (2) and by Duncan and others (3), model the nonlinear stress-strain behavior of soils incrementally by varying the values of Young's modulus and bulk modulus in each element in accordance with the calculated stresses.

The analyses were performed incrementally, which simulated the placement of backfill around and over the culvert one layer at a time and the application of compaction loads to each layer of fill. The computer program used in these analyses (SSTIPN) models the culvert as a number of straight beam elements connected at common nodes. The backfill is modeled by two-dimensional isoparametric elements with compatible and incompatible deformation modes. The soil elements can be firmly attached to the beam elements at their common nodes or interface elements can be used to allow slip at the culvert-backfill interface.

The first analyses were performed to calculate deflections due to the weight of the backfill, with no compaction loads. The results showed that the best correspondence between the measured and the calculated deflections was achieved when interface elements were used to permit slip between the bottom half of the culvert and the underlying soil. This same condition was used in all subsequent analyses. A number of different procedures were employed to simulate the effects of compaction. These are discussed below.

Procedure 1

The first procedure was the same as that used by Katona (1). After the placement of each new layer

Figure 4. Changes in span.

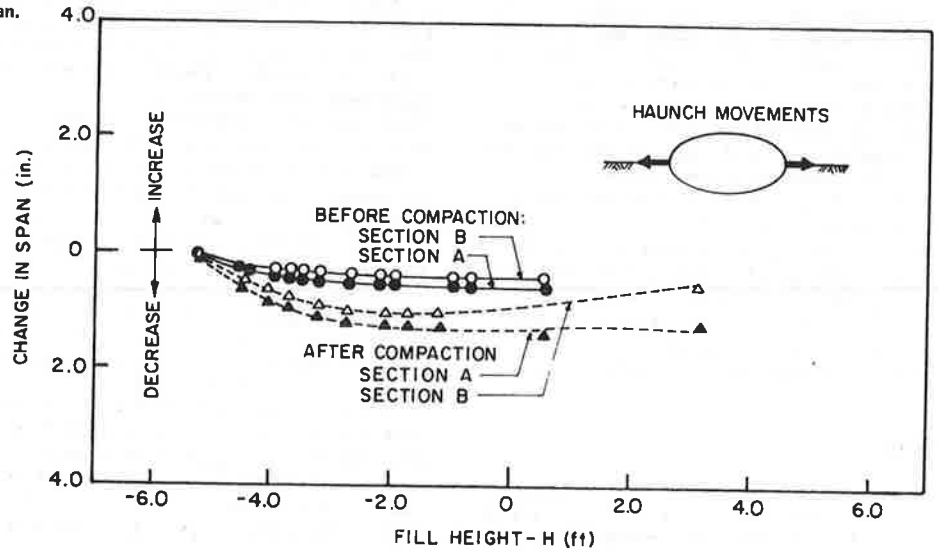

of backfill, a uniform pressure was applied on the upper surface of the layer to simulate the pressure imposed by the compaction equipment. Subsequently, when the next layer of fill was added, this pressure was removed and a pressure of equal magnitude was applied at the upper surface of the newly placed layer. This process was repeated up to the last layer, where the compaction pressure was applied and then removed. It was found that compaction pressure of 1 lbf•ft (7 psi) produced very little net deflection because the deflections induced when the pressure was applied were diminished to much smaller values when the pressure was removed.

Procedure 2

The next procedure was the same except that the compaction pressure was not removed when the next layer was added. This procedure produced very large deflections with a compaction pressure of 1 lbf•ft, and the variations of the deflections with fill height did not conform well with the measured values. Furthermore, this procedure does not satisfy equilibrium because the extra compaction load is not removed, and it thus does not constitute a rational means of simulating compaction effects.

Procedure 3

A complete analysis was performed, which included the placement of all layers of fill on the structure with no compaction load. The results calculated after addition of each new layer were punched onto cards. Then the conditions after placement of the first layer were used as the initial conditions for analysis of deflections due to compaction of the first layer, and these deflections were punched onto cards. Then these deflections together with the stresses and structural forces calculated previously with no compaction loads were used as the initial conditions for analysis of deflections due to compaction of the second layer. Subsequent stages were analyzed in the same way, up to H = 0.

This process may be described as follows: It is assumed that the deflections due to compaction are completely inelastic until the fill reaches crown level and completely elastic thereafter. Although the actual field behavior would not be expected to be quite so clear-cut, these assumptions do conform reasonably with expected field behavior. Before the crown of a culvert is covered, the wedging action of the fill at the sides of the structure tends to push the crown up and hold it there because soils rebound when unloaded by a fairly small percentage of the amount they deform on first loading. After the culvert has been completely surrounded by fill, the downward compaction loads on the crown tend to force the haunches out. However, the soil at the sides of the structure has been previously loaded in the same mode, and so it responds much more nearly elastically than during its first load-unload cycle. Therefore, when the compaction load is removed from the fill over the crown of the structure, the soil alongside the structure pushes the haunches back in, and the structure rebounds to nearly its original shape.

Procedure 3, though perhaps a somewhat oversimplified representation of the actual behavior, does satisfy equilibrium, and it results in deflections that agree well with those measured in the field. By using a compaction pressure of 0.8 lbf•ft, this procedure produced calculated deflections in substantial agreement with those measured in the Tice Valley culvert.

The calculated variation of crown deflection with fill height is shown in Figure 6. Each increment of deflection due to fill placement is followed by an increment of deflection due to compaction up to crown level. Subsequently, the compaction loads cause no permanent deflection of the structure.

COMPARISON OF CALCULATED AND MEASURED DEFLECTIONS

The measured and the calculated deflections before and after compaction are shown in Figures 7 and 8.

The measured and calculated haunch movements are shown in Figure 7. It may be seen that the calculated values agree quite well with those measured up to H = -2.0 ft. Subsequently, the calculations indicate a considerable increase in span (about 2.0 in), whereas very little occurred in the field. This lack of agreement indicates that the soil alongside the structure was probably considerably stiffer on reloading than was assumed in the analyses. It may be seen that the difference between the measured and the calculated changes in span is as great for conditions before compaction as for conditions after, which indicates that the calculated deflections due to compaction are approximately equal to those measured.

The measured and the calculated crown movements are shown in Figure 8. It may be seen that they are

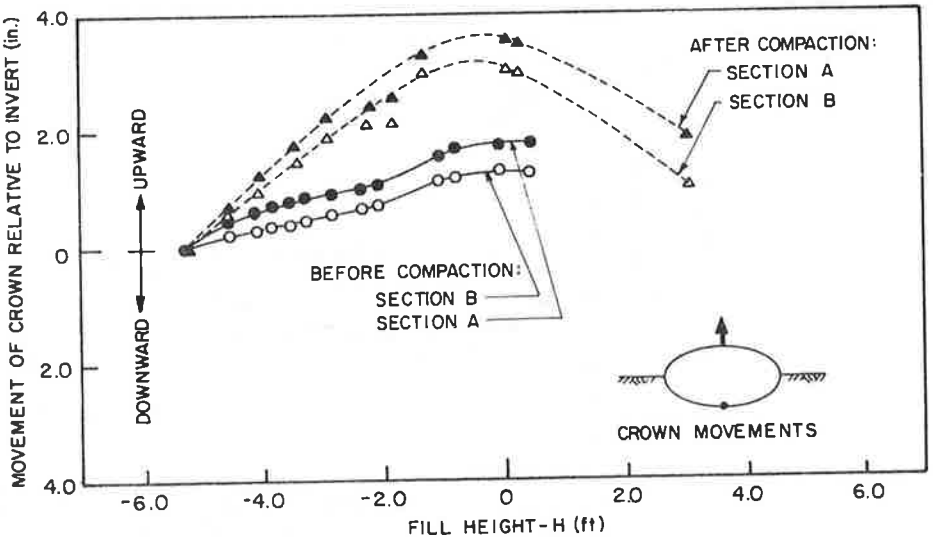

Figure 5. Movement of crown relative to invert.

in good agreement up to the stage when the crown begins to move down. Subsequently, the calculated downward movements are larger than those measured. It seems likely that the discrepancy is due to the fact that the soil adjacent to the haunches of the structure was actually stiffer than assumed for the analyses, as mentioned previously; restricting outward movement of the haunches, the soil in this zone also inhibits downward movement of the crown. The differences between the measured and the calculated deflections are about equal before and after compaction, which indicates that the calculated deflections due to compaction are reasonably accurate.

BENDING MOMENTS

Calculated distributions of bending moments around the Tice Valley culvert are shown in Figure 9 (for H = 0) and Figure 10 (for H = 4 ft). The dashed lines in these figures represent the distributions of calculated bending moments due to the weight of fill only. The solid lines indicate the range of values calculated assuming two values of percentage rebound on removal of the compaction loads. The actual amount of rebound is unknown; it is considered likely, however, that this value would fall between zero and 30 percent, probably closer to 30 percent. Thus it would be expected that the bending moments would fall somewhere within the shaded bands shown in Figures 9 and 10, most likely near the lower limit of these ranges.

It can be seen that the calculated moment values are very strongly affected by the compaction loads. Values at the crown (point A) and the quarter point (point B) are summarized in Table 1. At H = 0, the calculated bending moments due to both backfill weight and compaction effects are about three to four times as large as those due only to the weight of backfill. At H = 4 ft, the calculated moments at the crown with and without compaction loads are of

Figure 6. Scheme of compaction analyses.

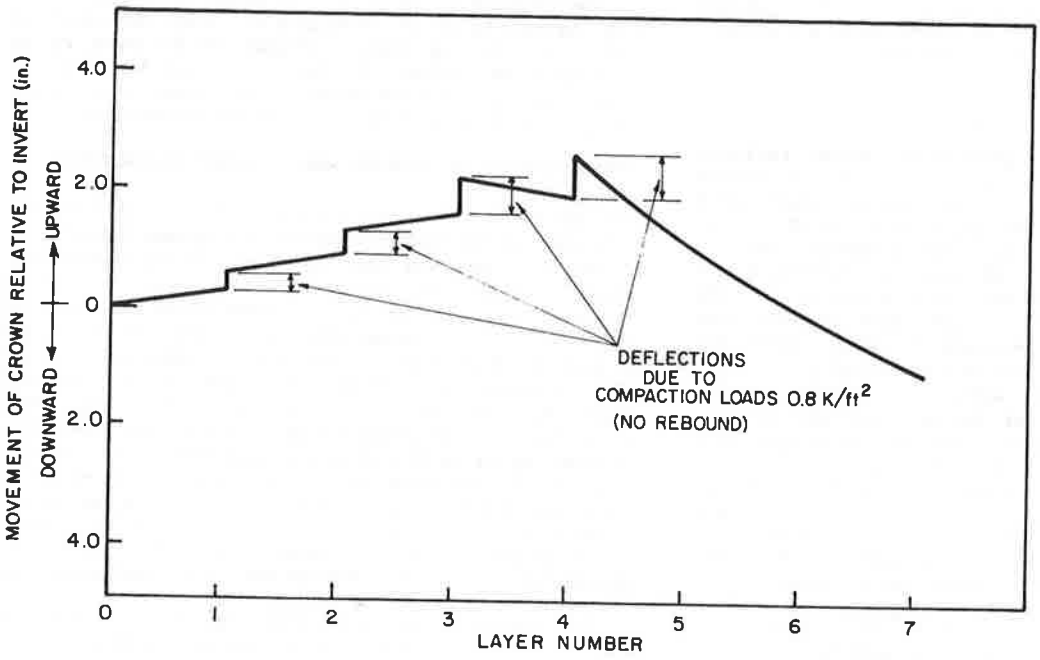

Figure 7. Comparison of measured and calculated haunch movements.

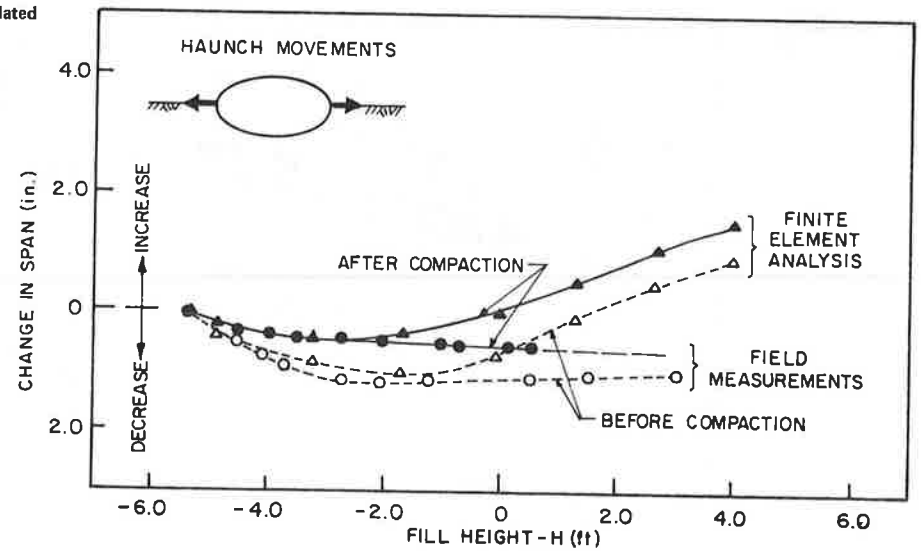

opposite sign: The calculations indicated that the crown would bend down without compaction loads and up with compaction loads. At the quarter point, the calculated moments with compaction loads are about three times as large as those due only to the backfill.

These values of bending moment determined from the finite-element analyses compare reasonably well with values calculated by using the simple soil-culvert interaction (SCI) method of structural design described by Duncan (4). The SCI design procedure can be used to estimate the bending moment at the quarter point (point B). At H = 0 the SCI method indicates a bending moment at B equal to -1.97 lbf•ft. At H = 4 ft, the SCI method indicates a bending moment at B equal to -0.88 lbf•ft. Thus at H = 0, the bending moment from the SCI procedure is 91 percent of the value calculated from finite-element analyses by assuming no rebound and 115 percent of the value calculated by assuming 30 percent rebound. At H = 4 ft, the bending moment from the SCI procedure is 41 percent of the value calculated by assuming no rebound and 51 percent of the value calculated by assuming 30 percent rebound.

The greatest moment in the structure will occur under the H-20 (design load) vehicle. The SCI procedure indicates that this vehicle will induce a bending moment of -1.53 lbf•ft at the quarter point, with tension on the inside of the culvert. Superimposing this moment with the quarter-point moments calculated by the finite-element method (Table 1) results in maximum bending moments from 3.24 lbf•ft to 3.69 lbf•ft. The maximum moment determined from the SCI method is 2.41 lbf•ft, or 66 to 74 percent of the values determined by adding the live load moment to the finite-element values.

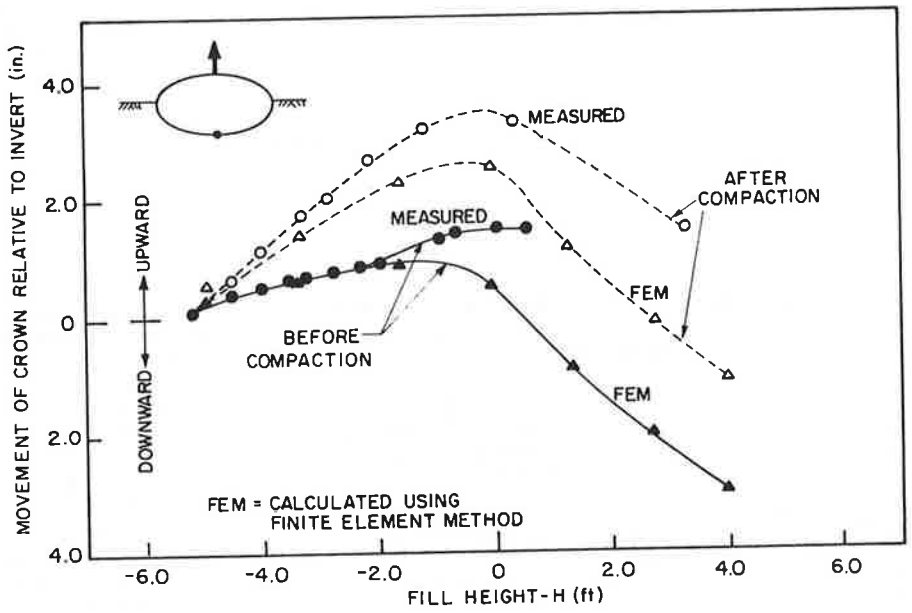

Figure 8. Comparison of measured and calculated crown movements.

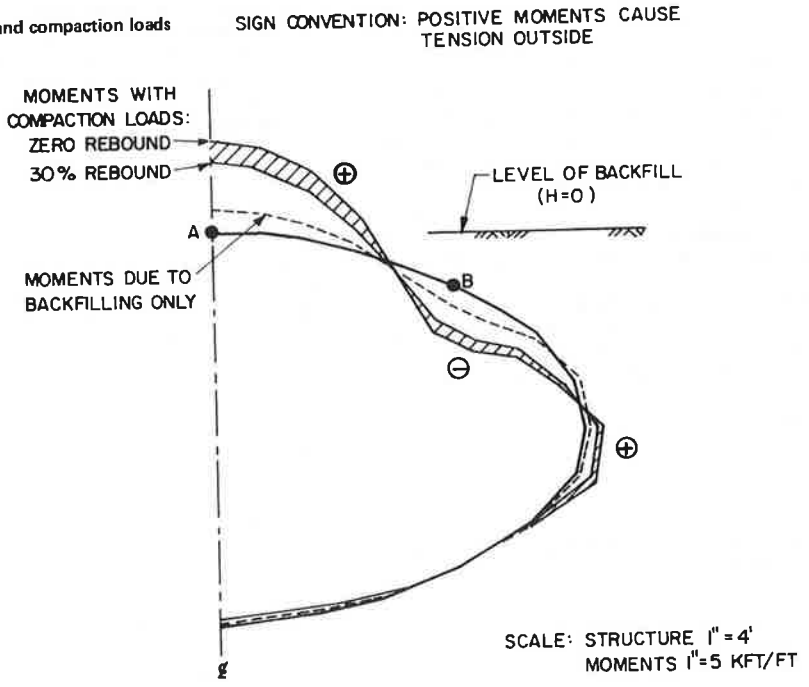

Figure 9. Moments due to backfilling and compaction loads (H = 0).

Figure 10. Moments due to backfilling and compaction loads (H = 4 ft).

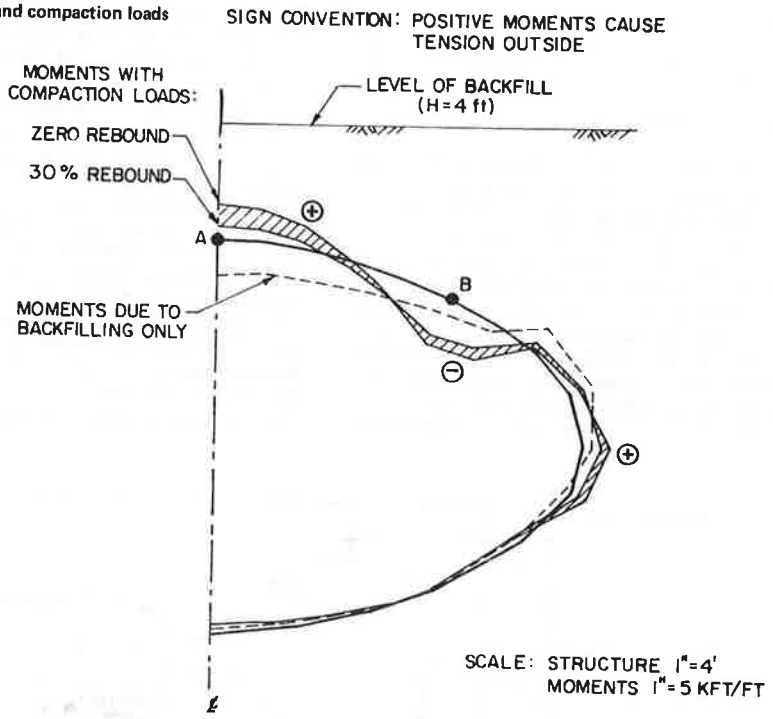

Table 1. Moments in structure due to backfilling and compaction loads.

Fill Level (ft)	Location	Moment (lbf·ft)		
			With Compaction	
		Backfill Only	Zero Rebound	30 Percent Rebound
H = 0	A	+1.04	+3.97	+3.09
	B	−0.67	−2.16	−1.71
H = 4	A	−1.42	+1.51	+0.63
	B	−0.67	−2.16	−1.71

Note: Positive moments cause tension outside the structure; negative moments cause tension inside the structure.

The plastic moment capacity of the Tice Valley culvert at the quarter point is 7.5 lbf•ft and the factor of safety against formation of a plastic hinge is thus about 1.9 as compared with the minimum value of 1.65 conventionally used for design. Thus, although the finite-element analyses including compaction effects indicate moments about 30 percent higher than the simplified SCI procedure, the Tice Valley culvert has more than adequate capacity to withstand these moments.

It should be emphasized that these considerations of the effects of compaction on bending moments are approximate and should be considered speculative until confirmed by more-detailed field studies. More-exact evaluation of bending moments will require strain-gage instrumentation.

CONCLUSIONS

This study of the movement of the Tice Valley long-span aluminum culvert structure during construction shows that the deflections due to compaction were very significant. The upward movement of the crown relative to the invert caused by compaction was about 2.0 in as compared with 1.5 in due to the weight of the fill.

The procedure used to analyze the effects of compaction by the 16 500-lb bulldozer and the 3500-lb vibratory roller appears to model the effects of compaction reasonably accurately. This procedure involved application of a uniform compaction pressure of 0.8 lbf•ft to the surface of each new layer of fill. It was assumed that the backfill behaved completely inelastically during the period when the fill level was below the crown of the culvert (i.e., it was assumed that no rebound occurred during this stage of backfill and compaction) and that the backfill behaved completely elastically when the fill level was above the crown. Although these assumptions are approximations of the actual field behavior, they appear to model the field behavior with a reasonable degree of accuracy.

The bending moments calculated in these finite-element analyses are somewhat larger than values calculated by using the simplified SCI design procedure. Accurate evaluation of the actual moments would require strain-gage instrumentation.

ACKNOWLEDGMENT

We are grateful for the assistance provided by Ron Drawsky, Tim D'Orazio, and John Duncan in making the field measurements. This study was conducted under the sponsorship of Kaiser Aluminum and Chemical Sales, Inc.

Joy Taylor, Nancy Hoes, and Rosalind Iiams typed the manuscript.

REFERENCES

1. M.G. Katona, D.F. Meinheit, R. Orillac, and C.H. Lee. Structural Evaluation of New Concepts for Long-Span Culverts and Culvert Installations. FHWA, 1979.
2. J.M. Duncan and C.-Y. Chang. Nonlinear Analysis of Stress and Strain in Soils. Journal of the Soil Mechanics and Foundations Division of ASCE, Vol. 96, No. SM5, 1970, pp. 1629-1653.

3. J.M. Duncan, P.M. Byrne, K.S. Wong, and P.N. Mabry. Hyperbolic Volume Change Parameters for Nonlinear Finite Element Analyses of Stresses and Movements in Soil Masses. Univ. of California, Berkeley, Geotechnical Engineering Rept., 1979.

4. J.M. Duncan. Soil-Culvert Interaction Method for Design of Metal Culverts. TRB, Transportation Research Record 678, 1978, pp. 53-59.

Publication of this paper sponsored by Committee on Subsurface Soil-Structure Interaction.

Finite-Element Modeling of Buried Concrete Pipe Installations

ERNEST T. SELIG, MICHAEL C. McVAY, AND CHING S. CHANG

A finite-element computer program, Soil-Pipe Interaction Design and Analysis (SPIDA), was developed for buried concrete pipe. The purpose of the program is to update the current concrete pipe design methods based on the Marston-Spangler approach with the expectation of reducing the cost of the installations and providing a more accurate representation of field conditions. Separate computer models were prepared for a positive-projecting embankment installation and a vertical-sided trench installation to optimize the representation of these two different cases. A wide range of bedding and soil conditions can be simulated. Experience with SPIDA indicates that it gives reasonable results. The program has advanced to the stage where it is ready for trial applications in pipe design.

Research was undertaken to develop a finite-element computer program for design and analysis of buried concrete pipe. The resulting program, Soil-Pipe Interaction Design and Analysis (SPIDA), is described and some examples are given of results obtained with it. Some of the details of the supporting research have been given elsewhere (1).

The purpose of the program is to update the current concrete pipe design methods based on the Marston-Spangler approach. This effort is expected both to reduce the cost of the installations and to provide a more accurate representation of the wide range of conditions experienced in the field.

The guidelines for the development of the computer program were to

1. Achieve low computer cost,
2. Be able to adapt to a wide range of field conditions,
3. Accurately represent characteristics of both trench and embankment installations,
4. Accurately model behavior of reinforced concrete pipe,
5. Permit easy extension to new conditions as experience develops, and
6. Provide simplicity of use by pipe designers.

In spite of the many past efforts to develop finite-element models for soil-structure interaction of buried pipe and conduits, none of the available programs were able to adequately satisfy all of the above guidelines. For example, neither the Northwestern University nor the Culvert Analysis and Design (CANDE) program had incorporated the desired soil models or a suitable reinforced concrete pipe model. These inadequacies together with mesh deficiencies and high computer cost that also exist with NUPIPE precluded the use or modification of that program to achieve the desired objectives. Recent changes in CANDE have improved the suitability of that program, but CANDE was not so easy to modify to meet the specific objectives of this study as the development of SPIDA, and it costs more to run. Only after a careful consideration of all other options was the decision made to begin with a new approach.

GENERAL MODEL FEATURES

The problem was divided into two subgroups, one for embankment installations and one for trench installations. This independent treatment permitted the development of the optimum computer model for each subgroup.

The basic features of the trench model are shown in Figure 1. The sides of the trench are vertical, and no slip is permitted between the backfill soil and the sides of the trench. The backfill is placed in layers to simulate construction. Bedding conditions are represented by the choice of properties of the material under the pipe and the geometry of the bedding zone. The trench depth and width are each variable independent of the pipe diameter. Tight sheeting for trench support is not considered.

The basic features of the embankment model are shown in Figure 2. The soil above the existing ground represents an embankment constructed of placed backfill. The main emphasis in the embankment model development was devoted to the positive-projecting conduit case (Figure 2a). However, the induced-trench condition produced by a compressible zone above the pipe can be simulated by placing soft material in the designated zone in the computer model (Figure 2b). The negative-projecting case (Figure 2c) can be simulated by changing the location of preexisting ground from that in the positive-projecting case.

The following general features apply to both the trench and the embankment models:

1. Two-dimensional plane strain representation of the installation,
2. Symmetry about the vertical pipe centerline,
3. Circular reinforced-concrete pipe,
4. No slip between the soil and the pipe and between the placed backfill and the existing ground,
5. Incremental placement of the soil in layers,
6. Bedding conditions variable to fit actual field conditions, and
7. Representation of any soil type and compaction state in any location.

Time-dependent properties of the soil and pipe have not yet been incorporated nor has a procedure for handling live loads been developed.

3. J.M. Duncan, P.M. Byrne, K.S. Wong, and P.N. Mabry. Hyperbolic Volume Change Parameters for Nonlinear Finite Element Analyses of Stresses and Movements in Soil Masses. Univ. of California, Berkeley, Geotechnical Engineering Rept., 1979.

4. J.M. Duncan. Soil-Culvert Interaction Method for Design of Metal Culverts. TRB, Transportation Research Record 678, 1978, pp. 53-59.

Publication of this paper sponsored by Committee on Subsurface Soil-Structure Interaction.

Finite-Element Modeling of Buried Concrete Pipe Installations

ERNEST T. SELIG, MICHAEL C. McVAY, AND CHING S. CHANG

A finite-element computer program, Soil-Pipe Interaction Design and Analysis (SPIDA), was developed for buried concrete pipe. The purpose of the program is to update the current concrete pipe design methods based on the Marston-Spangler approach with the expectation of reducing the cost of the installations and providing a more accurate representation of field conditions. Separate computer models were prepared for a positive-projecting embankment installation and a vertical-sided trench installation to optimize the representation of these two different cases. A wide range of bedding and soil conditions can be simulated. Experience with SPIDA indicates that it gives reasonable results. The program has advanced to the stage where it is ready for trial applications in pipe design.

Research was undertaken to develop a finite-element computer program for design and analysis of buried concrete pipe. The resulting program, Soil-Pipe Interaction Design and Analysis (SPIDA), is described and some examples are given of results obtained with it. Some of the details of the supporting research have been given elsewhere (1).

The purpose of the program is to update the current concrete pipe design methods based on the Marston-Spangler approach. This effort is expected both to reduce the cost of the installations and to provide a more accurate representation of the wide range of conditions experienced in the field.

The guidelines for the development of the computer program were to

1. Achieve low computer cost,
2. Be able to adapt to a wide range of field conditions,
3. Accurately represent characteristics of both trench and embankment installations,
4. Accurately model behavior of reinforced concrete pipe,
5. Permit easy extension to new conditions as experience develops, and
6. Provide simplicity of use by pipe designers.

In spite of the many past efforts to develop finite-element models for soil-structure interaction of buried pipe and conduits, none of the available programs were able to adequately satisfy all of the above guidelines. For example, neither the Northwestern University nor the Culvert Analysis and Design (CANDE) program had incorporated the desired soil models or a suitable reinforced concrete pipe model. These inadequacies together with mesh deficiencies and high computer cost that also exist with NUPIPE precluded the use or modification of that program to achieve the desired objectives. Recent changes in CANDE have improved the suitability of that program, but CANDE was not so easy to modify to meet the specific objectives of this study as the development of SPIDA, and it costs more to run. Only after a careful consideration of all other options was the decision made to begin with a new approach.

GENERAL MODEL FEATURES

The problem was divided into two subgroups, one for embankment installations and one for trench installations. This independent treatment permitted the development of the optimum computer model for each subgroup.

The basic features of the trench model are shown in Figure 1. The sides of the trench are vertical, and no slip is permitted between the backfill soil and the sides of the trench. The backfill is placed in layers to simulate construction. Bedding conditions are represented by the choice of properties of the material under the pipe and the geometry of the bedding zone. The trench depth and width are each variable independent of the pipe diameter. Tight sheeting for trench support is not considered.

The basic features of the embankment model are shown in Figure 2. The soil above the existing ground represents an embankment constructed of placed backfill. The main emphasis in the embankment model development was devoted to the positive-projecting conduit case (Figure 2a). However, the induced-trench condition produced by a compressible zone above the pipe can be simulated by placing soft material in the designated zone in the computer model (Figure 2b). The negative-projecting case (Figure 2c) can be simulated by changing the location of preexisting ground from that in the positive-projecting case.

The following general features apply to both the trench and the embankment models:

1. Two-dimensional plane strain representation of the installation,
2. Symmetry about the vertical pipe centerline,
3. Circular reinforced-concrete pipe,
4. No slip between the soil and the pipe and between the placed backfill and the existing ground,
5. Incremental placement of the soil in layers,
6. Bedding conditions variable to fit actual field conditions, and
7. Representation of any soil type and compaction state in any location.

Time-dependent properties of the soil and pipe have not yet been incorporated nor has a procedure for handling live loads been developed.

Figure 1. Basic features of trench model.

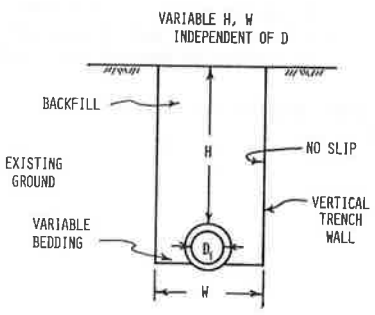

Figure 2. Basic features of embankment model.

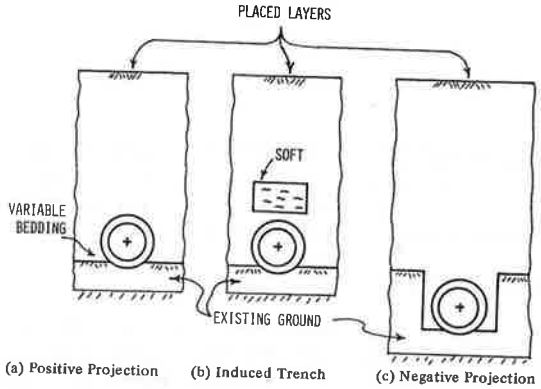

CONCRETE PIPE MODEL

The concrete pipe model was developed by Simpson Gumpertz and Heger, Inc. It consists of a half ring with 17 finite elements. Each element is a straight line between nodes located at the mid-thickness of the pipe wall. The element lengths are sufficiently short so that the beam properties may be taken constant with distance along the element. When the wall has cracked, the moment of inertia of the beam element that represents the portion of the wall with the crack is reduced according to an expression for effective moment of inertia similar to an equation given in an American Concrete Institute publication (2) but with coefficients determined as described below.

The model represents a circular pipe with two circular cages of reinforcing steel. The variables that define the reinforcement cages are the wire diameters of the inside and outside steel, the inside and outside concrete cover depths, the number of wires per foot of pipe length, and the type of bond between the steel and concrete. The concrete is described by its compressive strength (f_c') and a bilinear stress-strain relation; the knee in the stress-strain curve is at $f_c = 0.5f_c'$. The remaining pipe variables are the inside diameter and wall thickness.

The pipe model is capable of simulating the nonlinear load-deflection relation observed in three-edge bearing tests. Three conditions of the pipe wall are included in the model: an uncracked wall, a cracked wall in which the maximum compressive stress of the concrete is less than $0.5f_c'$, and a cracked wall in which the maximum compressive stress exceeds $0.5f_c'$.

The coefficients in the equations for cracked section moment of inertia were obtained by using three-edge bearing load-deflection plots. They vary with type of reinforcement: (a) smooth wires or rods, (b) welded smooth wire fabric with cross wires spaced at 6 or 8 in, and (c) deformed wire, wire fabric, or bar reinforcements or any reinforcement type with radial ties (transverse stirrups). The latter types provide better crack control and thus greater stiffness than the reinforcement with poorer bond characteristics.

The following assumptions were used:

1. The displacements in the pipe are small compared with its wall thickness and the strains are small compared with unity;
2. Shear deformation is negligible so that longitudinal planes before deformation remain plane after deformation in cracked or uncracked sections;
3. The stress-strain relation for steel is linear up to the yield point;
4. The stress-strain relation for concrete is bilinear up to f_c' with a knee at $0.5\ f_c'$, as described above; and
5. The effect of the dead weight of the pipe can be included as an initial elastic stress.

The pipe model is valid for stresses in steel that are below the yield stress and for stresses in concrete that are below f_c'.

SOIL MODEL

Considerable research effort was devoted to determining the requirements for properly representing the soil behavior in the finite-element model (1). The research indicated that the following soil-model features were the most appropriate for the placed backfill soil:

1. Nonlinear relationship of stress to strain relevant to the stress conditions in culvert installations,
2. Parameters dependent on both shear-stress and confining-stress states,
3. Parameters that can be related to compaction or density state,
4. Yielding as stress state approaches strength limits, and
5. Parameters that can be estimated for design purposes without individual tests.

The most suitable model currently available that incorporates these features is the model that combines a hyperbolic Young's modulus with bulk modulus (3). This will be termed the E-B model. The basic features of this model are illustrated in Figure 3. For a given confining stress (σ_3), the relationship between deviator stress and axial strain up to failure is represented by a hyperbolic function in which the tangent soil stiffness decreases with increasing deviator stress. This stiffness increases with increasing confining stress and degree of compaction. Bulk modulus is assumed to be dependent only on σ_3. Thus volumetric strain also increases hyperbolically with axial strain up to failure. Increases in amount of compaction or decreases in σ_3 decrease the volumetric strain. At failure, the soil is given a very small constant stiffness.

Generally, the initial stress state of existing ground is unknown, particularly after trench excavation, and its stress-strain properties during backfilling cannot be accurately estimated from available information. Thus the existing ground is represented in the finite-element model only as a linear elastic material with constant Young's modulus and constant Poisson's ratio. However, a more precise model can be used for this material if conditions warrant it.

TRENCH MESH

The geometry of the finite-element mesh for the trench case is shown in Figure 4. The soil elements are all of the four-node, isoparametric type.

The trench wall can be located at either of the vertical lines shown. In addition, the distances C and H can be varied independently of the pipe average diameter D. These features permit flexibility in establishing the trench width. Values assigned to dimensions A and B establish the height of soil cover above the pipe.

The bottom of the trench may be located at the top of any of the elements directly beneath the pipe invert. The dimensions E, F, and G also can be independently varied to obtain the proper thickness of layers beneath the pipe. By the choice of these dimensions and the soil properties assigned to the elements directly beneath the pipe, a wide range of bedding conditions can be represented.

The investigations showed that the trench mesh must be extended to the full height of soil above the pipe, and hence surcharge pressure should not be substituted for finite elements, regardless of the height of soil cover. Computer costs are less if the mesh is stopped at one to two diameters of soil cover over the crown and the remaining soil is represented by surcharge pressure. However, the arching action of the backfill in the trench is lost in the zones where surcharge is used instead of elements. The number and heights of the elements above the pipe are selected by the computer program based on the value of dimension A and constraints on the element-aspect ratios. Also, as A increases, the dimension I automatically increases, so that the right boundary of the mesh remains far enough from the pipe to avoid influencing the response.

Any soil type and compaction condition can be assigned to any of the elements in the backfill zone and any values for the linear elastic properties to any of the existing ground elements. For convenience in computer input, a variety of element combinations have been designated as standard zones that each require only one set of soil properties. Elements within a zone can have different properties by an override feature.

The backfill soil is added in sequential layers in the computer analysis to simulate the placement of backfill in the field. The research showed that the layers must be kept small and begin below the pipe as shown, for example, in Figure 5.

The mesh in Figure 4 is designed primarily for cover heights of more than two to three times the pipe diameter. For cover heights less than this, a

Figure 3. Soil-model characteristics.

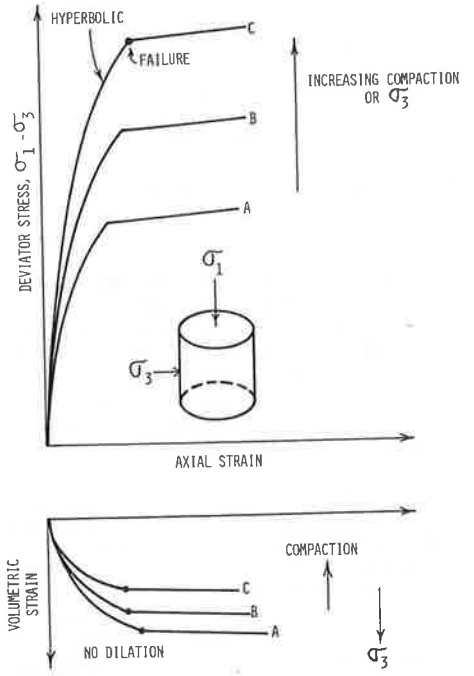

Figure 4. Trench finite-element mesh.

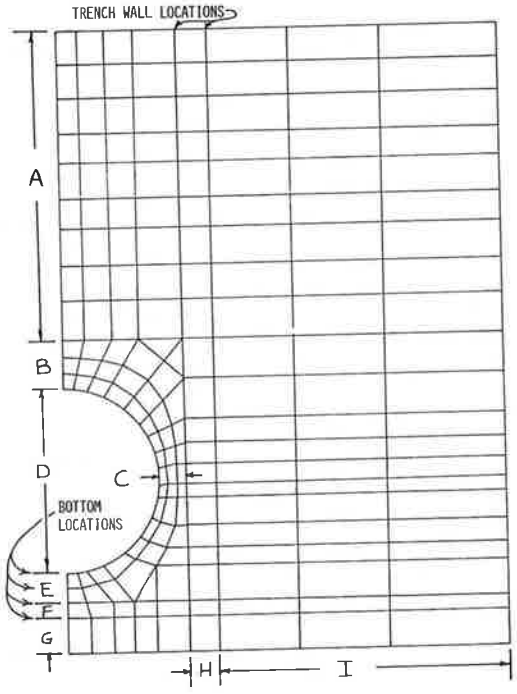

Figure 5. Backfill layers used in trench model.

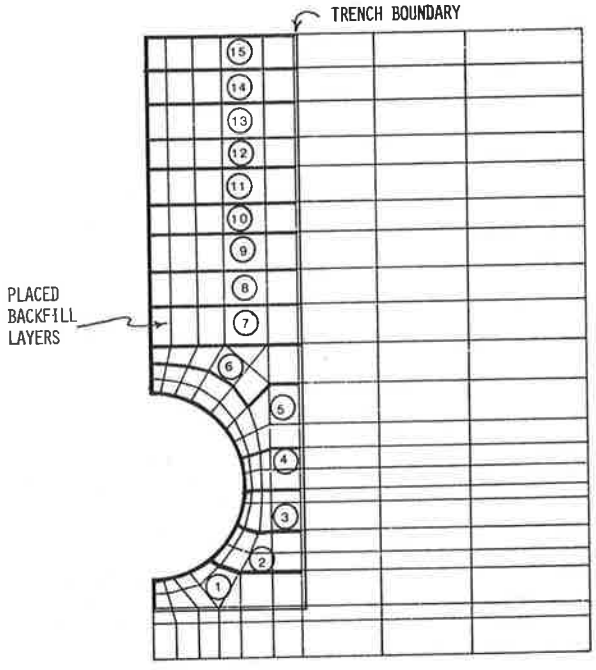

Figure 6. Embankment finite-element mesh.

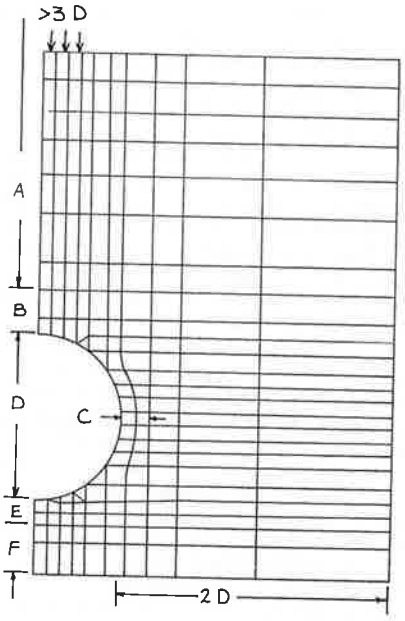

Figure 7. Bedding conditions for trench installation in East Liberty, Ohio.

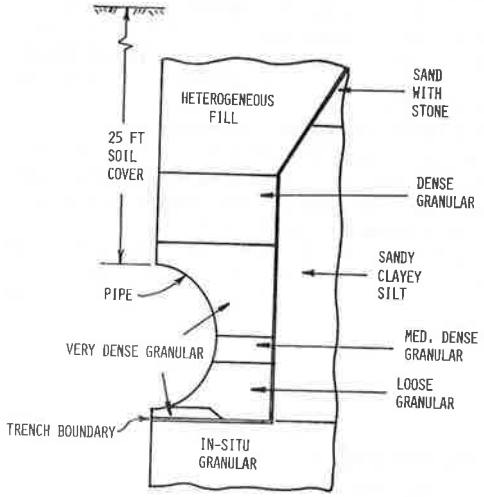

mesh with fewer elements was developed to provide a lower computer cost. This mesh is similar to the one in Figure 4; the primary difference is the elimination of the outer vertical column of existing ground soil elements.

EMBANKMENT MESH

The geometry of the finite-element mesh for the embankment case is shown in Figure 6. The soil elements are the same as those in the trench case.

The average pipe diameter is D. The width of soil adjacent to the pipe springline is set at twice the pipe diameter. The existing ground can be specified anywhere below and beside the pipe to establish the proper projection ratio. All the soil above the existing ground is placed in horizontal layers.

Dimensions B, C, E, and F are selected to represent the geometry of the zone immediately around the pipe. The choice of soil properties for these completes the bedding definition.

The height of soil cover over the crown defines dimensions A and B. However, above a soil cover equal to three pipe diameters, the elements are replaced with surcharge pressure to reduce computer cost. This is possible with the embankment case, because above the pipe crown the full width of the layer is placed simultaneously and no existing ground is present to develop arching.

The assignment of soil properties by zone is the same in the embankment mesh as that described for the trench mesh.

COMPUTER OUTPUT

The computer program SPIDA permits a detailed output after each layer of the pipe and soil response, which includes the following:

1. Deflections at all node points in the soil and on the structure;
2. Stresses and strains in the center of all soil elements; and
3. Moment, thrust, and shear at all pipe nodes.

From this information, the following were obtained:

1. Distribution of normal stress and shear stress around the pipe from the surrounding soil;
2. Pipe vertical and horizontal diameter change;
3. Weight of prism of soil above crown of pipe and above springline of pipe;
4. Vertical soil geostatic stress at crown; and
5. Arching factor, defined as ratio of springline thrust to one-half the soil prism weight.

The first step of the computer program generates the finite-element mesh from the input dimensions. This mesh can be plotted automatically for inspection at the option of the user. This provides the opportunity to ensure that the geometry of the installation is being satisfactorily represented by the mesh.

An output table is also generated that indicates the occurrence of cracking on the inside or outside of the pipe at any node after each layer of backfill has been placed.

For the convenience of the analyst, a program has been prepared that can plot distributions around the pipe of the computed pipe moment and thrust and the soil normal stress and shear stress on the surface of the pipe.

TRENCH IN EAST LIBERTY, OHIO

To illustrate the SPIDA trench model, results will be shown for the computer simulation of an installation in East Liberty, Ohio. The details of this analysis are available elsewhere (1). This case involved a 60-in inside diameter, Class IV, B wall, reinforced-concrete pipe placed in a trench with 25 ft of backfill cover (4). The bedding conditions for the pipe are shown in Figure 7. Although the trench side wall sloped back beginning a few feet above the pipe, the vertical trench model was used as an approximation. The zones selected for the trench mesh are shown in Figure 8, but the individual elements, as in Figure 4, have been omitted for clarity.

The computer simulation began with the trench empty. The existing soil was assigned a constant Young's modulus and Poisson's ratio based on values suggested by Krizek and McQuade (4). The first layer of backfill shown in Figure 5 was placed, followed by the pipe, and then the remaining layers. The E-B model was used to represent all the backfill zones. The parameters were selected from values

Figure 8. Finite-element mesh zones of trench installation in East Liberty.

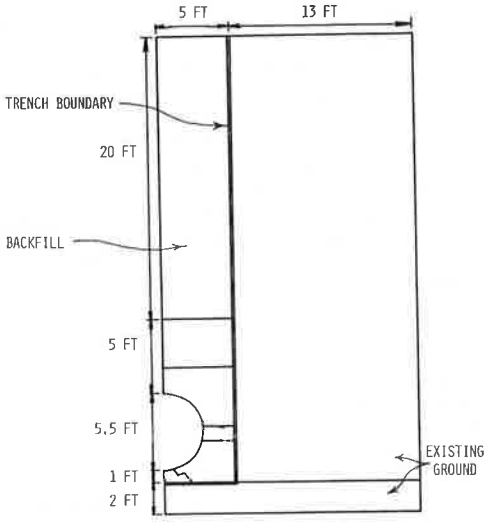

Figure 9. Predicted response for trench installation in East Liberty with vertical-side trench approximation.

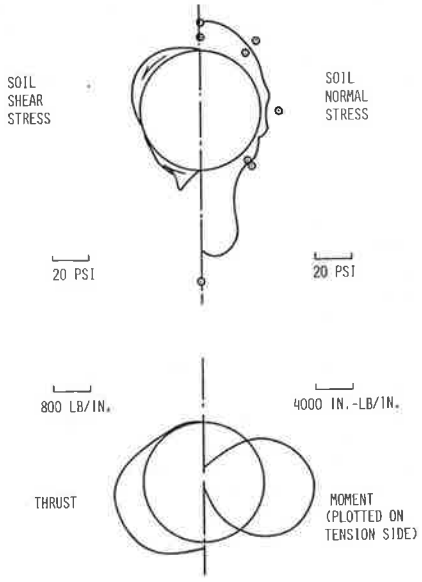

Figure 10. Pipe diameter change for trench installation in East Liberty.

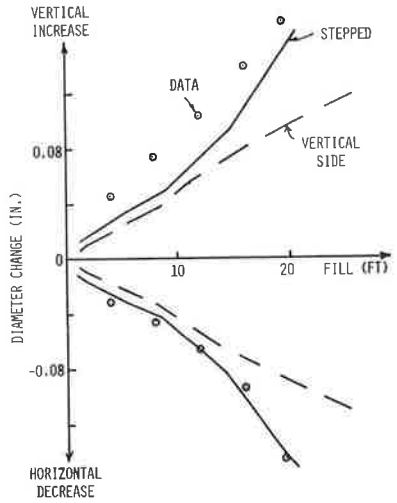

recommended by Duncan and others (3) based on information on material type and compaction state from reports by Krizek and others (4-6). The specific values are given by McVay (1).

The distributions of predicted soil-pipe interface stresses and pipe moment and thrust are shown in Figure 9. The soil pressures on the pipe are in reasonable agreement with the measured values, although the predicted invert pressure is low. However, the predicted pipe deflections (dashed curves, Figure 10) were lower than those measured, and the computer output did not indicate the cracking observed in the field.

Inadequate representation of the pipe bedding and the sloped trench were considered to be possible reasons for the low deflection predictions. Thus the analysis was rerun with a more concentrated support at the invert and with the top four layers of existing soil elements placed as backfill along with the corresponding trench layers 12 through 15 (Figure 5). The resulting distributions are shown in Figure 11. The pipe thrust and moment have increased. The soil pressure on the pipe has also increased, particularly at the invert. However, only the invert pressure is clearly inconsistent with the measured values. Thus the pipe support was too concentrated. However, the pipe-deflection predictions were improved (Figure 10), and cracking was indicated as observed in the field.

MOUNTAINHOUSE CREEK EMBANKMENT

To illustrate the SPIDA embankment model, results will be given for the computer simulation of an installation at Mountainhouse Creek in California. The details of this analysis are available elsewhere (1). In this case, an 84-in inside diameter reinforced-concrete pipe was installed in an induced-trench condition with 78 ft of soil cover (7). The installation configuration is shown in Figure 12. The site was prepared by excavating unsuitable material for 5-10 ft below the original ground level for a width of about 29 ft at the pipe location. This excavated zone was backfilled with compacted embankment soil to an elevation of about 5 ft above the bottom of the culvert. An 11-ft-wide trench was then excavated in this material to a depth of 5 ft to form the existing ground for the start of the pipe installation. The zones assigned to the mesh

Figure 11. Predicted response for trench installation in East Liberty with sloped-trench approximation and stiff support.

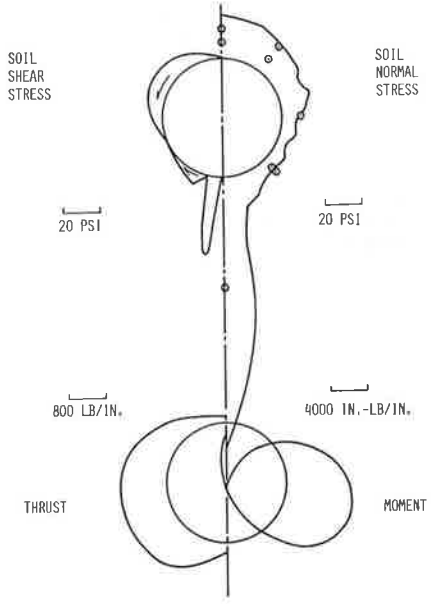

in Figure 6 are shown in Figure 13. The existing ground was added in layers simultaneously with the embankment and bedding-material layers for convenience in modeling, on the basis that the site conditions and the method of establishing the existing ground around the pipe would make this approach reasonable. However, the existing ground may be placed before the embankment and bedding layers.

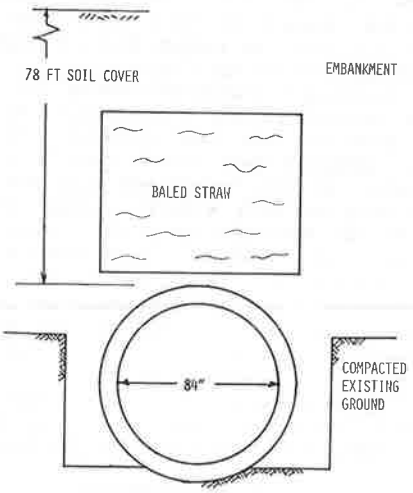

Figure 12. Configuration of Mountainhouse Creek embankment installation.

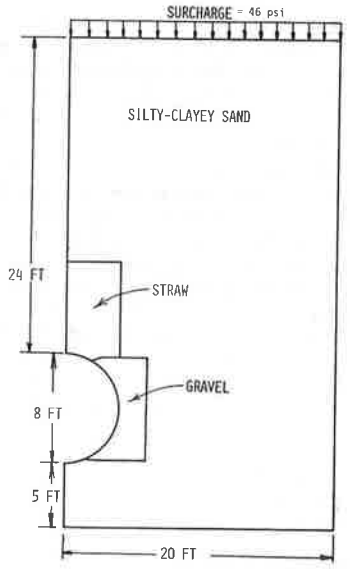

Figure 13. Finite-element mesh zones for Mountainhouse Creek embankment installation.

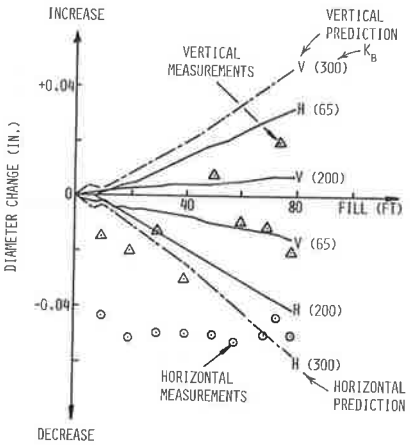

Figure 14. Pipe diameter change for Mountainhouse Creek embankment installation.

One-dimensional compression-test data for the baled straw from a report by Davis (8) were used to establish appropriate parameters for the E-B soil model for this zone. The gravel-zone E-B model properties were obtained from a report by Duncan and others (3) based on compaction and classification descriptions. The Young's modulus parameters for the E-B model for the remainder of the embankment were derived from triaxial test results (7), and the bulk-modulus values were initially estimated (3) based on compaction and classification descriptions. The specific values are given by McVay (1).

The bulk-modulus (B) formulation for the E-B model is as follows:

$$B = K_b P_a (\sigma_3/P_a)^m \quad (1)$$

where P_a is atmospheric pressure, σ_3 is the minimum principal stress, and K_b and m are dimensionless parameters. K_b was estimated to be 65 (3,7).

The field observations (7) showed that for the induced-trench test sections, the pipe horizontal diameter decreased and the vertical diameter increased slightly or at least decreased less than the horizontal diameter. For the initially selected K_b of 65, the predicted results show an increase in horizontal diameter and a smaller decrease in vertical diameter (Figure 14). A parameter-sensitivity study with SPIDA indicated that the most likely cause of these contradicting trends between predicted and measured pipe deflections was the value of bulk modulus.

Increasing the bulk modulus causes an increase in pipe lateral confinement, which increases the springline (horizontal) pressure on the pipe, and at the same time a decreasing soil pressure on the pipe crown. This will cause the predicted pipe deflections to change in a manner consistent with the field observations. As shown in Figure 14, a K_b of 300 makes too large a change, but a K_b of 200 gives reasonable results. Further adjustments in all the soil parameters could apparently improve the agreement.

The resulting distributions of soil normal and shear stress and pipe thrust and moment are shown in Figure 15 for K_b = 200. The moment distribution is consistent with an increase in vertical pipe diameter and decrease in horizontal diameter. The soil pressure on the pipe is lowest at the crown as a result of positive arching induced by the straw zone.

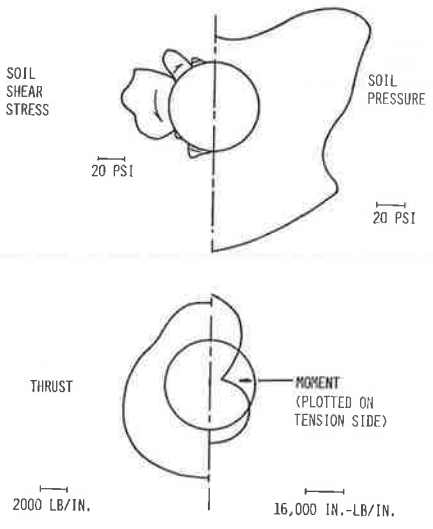

Figure 15. Predicted response for Mountainhouse Creek pipe with K_b = 200.

SUMMARY

The research leading to the SPIDA program has indicated that the choice of soil model and values of soil parameters are important for accurately modeling the soil-pipe interaction. The overburden-dependent soil model often used in the past is not satisfactory because the model assumptions are inconsistent with the stress states at many locations in the soil. The hyperbolic model using Young's modulus and bulk modulus was found to be suitable. The value of bulk modulus had a great influence on the computed pipe deflections because it affects the compressibility of the soil adjacent to the pipe and hence the lateral support. Because of its importance, bulk modulus deserves more attention in the future.

The installation geometry must also be properly represented. To achieve this, the SPIDA model has two basic subgroups, one for trench installations and one for embankment installations. This permits optimization of the model for each of these two different situations. Considerable flexibility in representing bedding conditions has been incorporated into the models. In addition, a wide variety of soil types and compaction conditions can be designated. Thus a broad range of field conditions can be simulated.

Experience with SPIDA indicates that it gives reasonable results. The program has advanced to the stage where the basic trench and embankment models are ready for trial applications in pipe design. It is through such applications that the benefits of the program will be proved to the profession. Compared with current design methods, the successful use of SPIDA is expected to reduce the cost of the pipe or reduce the risk of failure or some combination of both.

ACKNOWLEDGMENT

This research was sponsored by the American Concrete Pipe Association. The concrete pipe computer model was developed by Frank J. Heger and Atis A. Liepins of Simpson Gumpertz and Heger, Inc.

REFERENCES

1. M.C. McVay. Evaluation of Numerical Modeling of Buried Conduits. Department of Civil Engineering, Univ. of Massachusetts, Amherst, Ph.D. dissertation, Feb. 1982.
2. ACI Standard Building Code Requirements for Reinforced Concrete. American Concrete Institute, Detroit, MI, ACI-318-77, 1977.
3. J.M. Duncan, P. Byrne, K.S. Wong, and P. Mabry. Strength, Stress-Strain, and Bulk Modulus Parameters for Finite Element Analysis of Stresses and Movements in Soil Masses. Univ. of California, Berkeley, Rept. UCB/GT/80-01, Aug. 1980.
4. R.J. Krizek and P.V. McQuade. Behavior of Buried Concrete Pipe. Journal of the Geotechnical Engineering Division of ASCE, Vol. 99, No. GT7, July 1978, pp. 815-836.
5. R.J. Krizek, R.B. Corotis, and T.H. Wenzel. Soil-Structure Interaction of Concrete Pipe Systems. Proc., National Structural Engineering Conference on Methods of Structural Analysis, Madison, WI, ASCE, Vol. 2, Aug. 1976, pp. 607-643.
6. R.J. Krizek and R.B. Corotis. Synthesis of Soil Moduli Determined from Different Types of Laboratory and Field Tests. Proc., Specialty Conference on In Situ Measurements of Soil Properties, Raleigh, NC, ASTM, Vol. 1, June 1975, pp. 225-240.
7. R.E. Davis and A.E. Bacher. Structural Behavior of Concrete Pipe Culvert--Mountainhouse Creek (Part 2). California Department of Transportation, Sacramento, Rept. FHWA-CA-ST-4121-75-8, Sept. 1975.
8. R.E. Davis. Structural Behavior of a Reinforced Concrete Arch Culvert. Bridge Department, California Division of Highways, Sacramento, Rept. SSR3-66, Sept. 1966.

Publication of this paper sponsored by Committee on Subsurface Soil-Structure Interaction.

Performance and Analysis of a Long-Span Culvert

MICHAEL C. McVAY AND ERNEST T. SELIG

A low-profile-arch long-span corrugated-steel culvert was installed in Pennsylvania as a bridge-replacement structure. The Republic Steel Company maxispan design was used. Instrumentation was installed in the soil and on the structure to monitor performance during construction. Field and laboratory soil property tests were conducted to characterize the soil behavior. Predictions from finite-element computer analyses were compared with the field results. From this and previous research, a number of conclusions were drawn. The choice of soil model had its most significant influence on the culvert deformation and bending-stress predictions. Overburden-dependent and linear-elastic soil models were shown to be unsatisfactory. Effects of construction procedures are difficult to predict accurately. Further study is needed to evaluate the importance of factors such as compaction-induced deformation, soil-culvert interface conditions, culvert wall yielding, and wall buckling. Seam slip rather than bending flexibility is needed to develop positive arching and hence further study is warranted. A particularly important observation was that special features like compaction wings appear to be both unnecessary and undesirable.

A long-span flexible corrugated-steel low-profile-arch culvert was constructed in Bucks County, Pennsylvania, as a bridge-replacement structure. The owner was the Pennsylvania Department of Transportation (PennDOT). The design used was a Republic Steel Company maxispan with compaction wings. The structure and soil backfill were instrumented to monitor performance during construction. Field and laboratory tests were conducted on the backfill soil to characterize the soil behavior. In addition, a series of finite-element computer analyses were carried out to help evaluate the performance of the structure and to assess the validity of the computer model.

This paper summarizes the field installation and the measurements made. The computer model is then described. This is followed by comparisons between some of the important calculated and measured results. Finally, the computer model is assessed and the culvert design concepts are evaluated.

SUMMARY

The research leading to the SPIDA program has indicated that the choice of soil model and values of soil parameters are important for accurately modeling the soil-pipe interaction. The overburden-dependent soil model often used in the past is not satisfactory because the model assumptions are inconsistent with the stress states at many locations in the soil. The hyperbolic model using Young's modulus and bulk modulus was found to be suitable. The value of bulk modulus had a great influence on the computed pipe deflections because it affects the compressibility of the soil adjacent to the pipe and hence the lateral support. Because of its importance, bulk modulus deserves more attention in the future.

The installation geometry must also be properly represented. To achieve this, the SPIDA model has two basic subgroups, one for trench installations and one for embankment installations. This permits optimization of the model for each of these two different situations. Considerable flexibility in representing bedding conditions has been incorporated into the models. In addition, a wide variety of soil types and compaction conditions can be designated. Thus a broad range of field conditions can be simulated.

Experience with SPIDA indicates that it gives reasonable results. The program has advanced to the stage where the basic trench and embankment models are ready for trial applications in pipe design. It is through such applications that the benefits of the program will be proved to the profession. Compared with current design methods, the successful use of SPIDA is expected to reduce the cost of the pipe or reduce the risk of failure or some combination of both.

ACKNOWLEDGMENT

This research was sponsored by the American Concrete Pipe Association. The concrete pipe computer model was developed by Frank J. Heger and Atis A. Liepins of Simpson Gumpertz and Heger, Inc.

REFERENCES

1. M.C. McVay. Evaluation of Numerical Modeling of Buried Conduits. Department of Civil Engineering, Univ. of Massachusetts, Amherst, Ph.D. dissertation, Feb. 1982.
2. ACI Standard Building Code Requirements for Reinforced Concrete. American Concrete Institute, Detroit, MI, ACI-318-77, 1977.
3. J.M. Duncan, P. Byrne, K.S. Wong, and P. Mabry. Strength, Stress-Strain, and Bulk Modulus Parameters for Finite Element Analysis of Stresses and Movements in Soil Masses. Univ. of California, Berkeley, Rept. UCB/GT/80-01, Aug. 1980.
4. R.J. Krizek and P.V. McQuade. Behavior of Buried Concrete Pipe. Journal of the Geotechnical Engineering Division of ASCE, Vol. 99, No. GT7, July 1978, pp. 815-836.
5. R.J. Krizek, R.B. Corotis, and T.H. Wenzel. Soil-Structure Interaction of Concrete Pipe Systems. Proc., National Structural Engineering Conference on Methods of Structural Analysis, Madison, WI, ASCE, Vol. 2, Aug. 1976, pp. 607-643.
6. R.J. Krizek and R.B. Corotis. Synthesis of Soil Moduli Determined from Different Types of Laboratory and Field Tests. Proc., Specialty Conference on In Situ Measurements of Soil Properties, Raleigh, NC, ASTM, Vol. 1, June 1975, pp. 225-240.
7. R.E. Davis and A.E. Bacher. Structural Behavior of Concrete Pipe Culvert--Mountainhouse Creek (Part 2). California Department of Transportation, Sacramento, Rept. FHWA-CA-ST-4121-75-8, Sept. 1975.
8. R.E. Davis. Structural Behavior of a Reinforced Concrete Arch Culvert. Bridge Department, California Division of Highways, Sacramento, Rept. SSR3-66, Sept. 1966.

Publication of this paper sponsored by Committee on Subsurface Soil-Structure Interaction.

Performance and Analysis of a Long-Span Culvert

MICHAEL C. McVAY AND ERNEST T. SELIG

A low-profile-arch long-span corrugated-steel culvert was installed in Pennsylvania as a bridge-replacement structure. The Republic Steel Company maxispan design was used. Instrumentation was installed in the soil and on the structure to monitor performance during construction. Field and laboratory soil property tests were conducted to characterize the soil behavior. Predictions from finite-element computer analyses were compared with the field results. From this and previous research, a number of conclusions were drawn. The choice of soil model had its most significant influence on the culvert deformation and bending-stress predictions. Overburden-dependent and linear-elastic soil models were shown to be unsatisfactory. Effects of construction procedures are difficult to predict accurately. Further study is needed to evaluate the importance of factors such as compaction-induced deformation, soil-culvert interface conditions, culvert wall yielding, and wall buckling. Seam slip rather than bending flexibility is needed to develop positive arching and hence further study is warranted. A particularly important observation was that special features like compaction wings appear to be both unnecessary and undesirable.

A long-span flexible corrugated-steel low-profile-arch culvert was constructed in Bucks County, Pennsylvania, as a bridge-replacement structure. The owner was the Pennsylvania Department of Transportation (PennDOT). The design used was a Republic Steel Company maxispan with compaction wings. The structure and soil backfill were instrumented to monitor performance during construction. Field and laboratory tests were conducted on the backfill soil to characterize the soil behavior. In addition, a series of finite-element computer analyses were carried out to help evaluate the performance of the structure and to assess the validity of the computer model.

This paper summarizes the field installation and the measurements made. The computer model is then described. This is followed by comparisons between some of the important calculated and measured results. Finally, the computer model is assessed and the culvert design concepts are evaluated.

Figure 1. Approximate geometry of culvert installation.

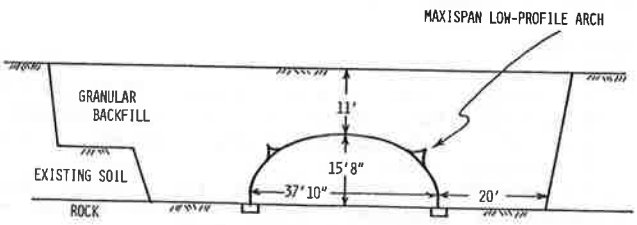

FIELD INSTALLATION

The size and shape of the culvert were based on the estimated flow in the creek, the presence of underlying rock, and the desired grade elevation of the roadway. The strength of the culvert wall was based on ring-compression theory, handling criteria, and buckling considerations.

The culvert had approximately a 16-ft rise, a 38-ft span (Figure 1), and 11 ft of backfill cover above the structure when completed. The conduit wall was assembled from 5-gauge structural steel plates that had 2x6-in corrugations. The structure was 88 ft 4 in long and had concrete end walls to protect the backfill against erosion from creek flooding and provide stability to the soil mass adjacent to the culvert opening.

The preexisting embankment soil was classified as a silty loam from visual inspections. The backfill material was all granular, primarily PennDOT 2A material, which is classified GW in the Unified Soil Classification System.

The backfill was placed in horizontal lifts of approximately 4 in or greater thickness. Compaction was supplied by several passes of a 10-ton smooth-wheel roller away from the culvert and a hand-operated vibratory plate compactor near the culvert. Tests of nuclear field density and moisture content were conducted by PennDOT at various elevations throughout the backfill as part of construction control to check the adequacy of compaction. An average field density of 121 pcf and moisture content of 7.6 percent were measured. The difference in fill elevations on the two sides of the culvert was maintained within 1.5 ft during the backfilling process.

The construction began in September 1978 and was completed by January 1979. To evaluate the performance of the structure during construction and provide information for future design and analysis of long-span structures, the culvert and surrounding soil mass were extensively instrumented.

A pair of weldable strain gages was installed at many locations on the structure to determine both bending and thrust stresses in the steel. Displacements of the culvert during backfilling were monitored by using survey targets located around the inside of the structure. In addition, structural extensometers were used to measure displacements of the springline and crown of the structure at three longitudinal cross sections.

Instrumentation was installed in the soil at the springline, compaction wing, and crown elevations. Included were inductance-type soil stress gages, hydraulic soil stress gages, horizontal soil extensometers, vertical soil extensometers, and 11-in-diameter inductance soil strain gages. The extensometers, the inductance stress gages, and the soil strain gages have been described elsewhere (1). The stress gages were laboratory calibrated in soil as described by Selig (2) and placement conditions intended to simulate those in the field were used.

Both laboratory and field tests were performed to document the backfill conditions and obtain soil stress-strain relationships, physical state identification, and strength properties of the soil for the analysis. During the backfilling phase of construction, soil samples were collected from various locations throughout the backfill. Laboratory sieve tests were performed on each of the samples for classification purposes. Laboratory uniaxial strain compression tests and constant confining pressure triaxial compression tests were then conducted at densities and moisture contents representative of field conditions to determine the stress-strain properties of the placed backfill. In addition, during construction six plate-load tests were performed to provide field data representative of the backfill stiffness.

FINITE-ELEMENT APPROACH

The discretization, geometric boundaries, and restraints employed to represent the field installation by a finite-element analysis are shown in Figure 2. Only half the installation was considered on the assumption that the constructed structure and backfill were symmetrical. The soil nodes on the two vertical boundaries were restrained to vertical movements only. The soil nodes on the bottom horizontal boundary were restrained against both horizontal and vertical movement, which allowed in situ shearing stresses to develop between the soil and the rock. The right vertical boundary was placed three culvert spans from the centerline of the soil-culvert system, based on past experience of other researchers (3). The structural nodes were constrained to permit no horizontal or rotational movements at the crown and no horizontal or vertical movements at the footings. The culvert was modeled with straight beam elements and the adjacent soil as either triangular or quadrilateral isoparametric elements. Because no information was available on the initial stress state and stress-strain behavior of the preexisting soil, the soil was modeled in the same manner as the backfill. All soil was given a density of 0.075 lb/in^3.

The finite-element modeling of the installation began at the stage where the soil excavation and construction of the structure were completed, but no backfill was placed. Thus the height of fill is referenced to the top of the footings.

Soil Models

Four different models were considered for simulation of the constitutive relationships of the soil in the finite-element analysis: the constant-modulus linear-elastic model, the stress-dependent bulk-modulus and hyperbolic Young's-modulus model, the bilinear modulus model with constant Poisson's ratio, and the overburden stress-dependent modulus model with constant Poisson's ratio. The soil parameters required by each model were determined from laboratory and field tests performed on the backfill material.

The characterization of soil as a linear-elastic material uses a constant Young's modulus (E) and a constant Poisson's ratio (ν). Based on a synthesis of the results of the field plate-load tests, one-dimensional compression tests, and triaxial compression laboratory tests, a lower-bound estimate of 3000 psi was selected for the Young's modulus of the backfill. The Poisson's ratio value was assumed to be 0.25 based on the measured value of angle of internal friction for the backfill soil. This model does not incorporate a failure condition.

The model represented by a stress-dependent hyperbolic Young's modulus and a bulk modulus was

Figure 2. Finite-element mesh used in computer analysis.

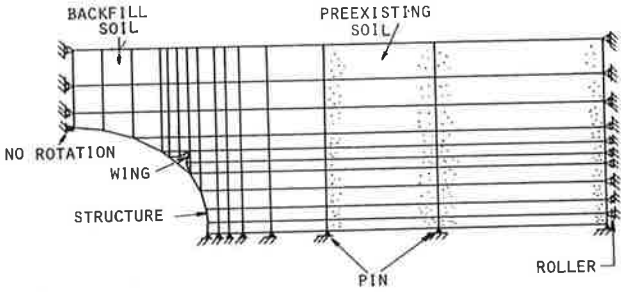

Figure 3. Hyperbolic E-B soil model.

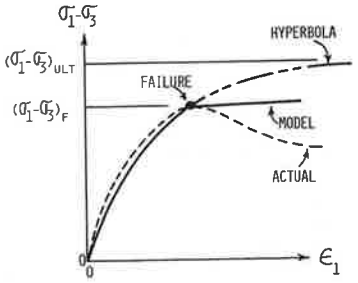

Figure 4. Bilinear soil model.

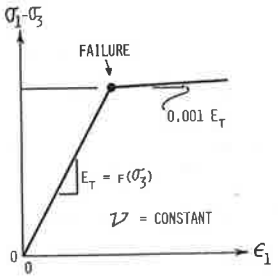

proposed by Duncan and others (4). This model, which will be designated the E-B model, assumes that the triaxial stress-strain curve up to the failure point can be represented by a hyperbola (see Figure 3). Beyond failure a small constant stiffness is assumed for the model instead of the reduction in stress usually exhibited by actual soils. The tangent Young's modulus (E_t) is the tangent to the hyperbola below failure. It is expressed by (4) the following:

$$E_t = [1 - R_f(1 - \sin\phi)(\sigma_1 - \sigma_3)/(2c\cos\phi + 2\sigma_3 \sin\phi)]\, KP_a(\sigma_3/P_a)^n \quad (1)$$

where

R_f = failure ratio = $(\sigma_1 - \sigma_3)_f/(\sigma_1 - \sigma_3)_{ult}$,
σ_1 = axial stress,
σ_3 = confining pressure,
c = cohesion,
ϕ = angle of internal friction,
P_a = atmospheric pressure, and
K,n = experimentally determined parameters defining stress dependency of soil stiffness.

The variation of ϕ with confining pressure is represented by the following:

$$\phi = \phi_0 - \Delta\phi \log_{10}(\sigma_3/P_a) \quad (2)$$

The bulk modulus (B) is assumed dependent only on the confining pressure (σ_3) as represented by the following:

Figure 5. Overburden-dependent soil model.

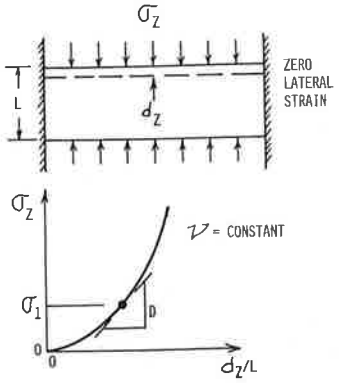

$$B = K_b P_a(\sigma_3/P_a)^m \quad (3)$$

where K_b and m are experimentally determined parameters. The predicted volumetric strains will always be compressive because dilation is not represented by the model.

The values of the parameters for the Republic Steel culvert installation were determined from triaxial and one-dimensional compression tests. The results are listed below. The one-dimensional compression tests were particularly useful in estimating the bulk modulus.

Parameter	Value
K	660
n	0.81
R_f	0.45
K_b	240
m	0.56
c	0
ϕ_0	52 degrees
$\Delta\phi$	18 degrees

The observed stress-strain behavior of the backfill up to failure in the triaxial tests was almost linear; thus a bilinear soil model was established by using a Young's modulus that increases with confining pressure, a failure criterion, and a constant Poisson's ratio (Figure 4). Above failure the modulus is assumed to be a very low value equal to 0.001 of the value (E_t) below failure for the same σ_3.

The relationship between the constant average slope (E_t) and the confining pressure (σ_3) employed in the model is of the following form:

$$E_t = K_1 P_a(\sigma_3/P_a)^{n_1} \quad (4)$$

where

E_t = tangent modulus,
σ_3 = minor principal stress,
P_a = atmospheric pressure expressed in same pressure units as E_t and σ_3, and
K_1, n_1 = experimentally determined constants.

From triaxial tests on the backfill soil in the Republic Steel culvert installation, the values of the parameters were $K_1 = 392$ and $n_1 = 0.567$. Poisson's ratio was assumed to be 0.25 as for the linear-elastic model. The strength parameters c, ϕ, and $\Delta\phi$ defining failure were taken to be the same as those given above for the E-B model.

The overburden-dependent soil model assumes that the soil elements are confined in a state of uniaxial strain, and hence the stiffness increases with stress as indicated in Figure 5. The slope of the

curve in Figure 5 at any axial stress is the constrained modulus D. Since σ_z is the major principal stress, it is designated σ_1. Poisson's ratio is assumed to be constant.

The finite-element program uses Young's modulus as the stiffness parameter. To represent the overburden-dependent model, Young's modulus (E) corresponding to the constrained modulus (D) is obtained from elasticity theory by the following:

$$E = \{[(1 + \nu)(1 - 2\nu)]/(1 - \nu)\}D \quad (5)$$

where ν is Poisson's ratio. The confined compression test gives values of D as a function of maximum principal stress σ_1. Then Equation 5 gives E as a function of σ_1. Since D increases with σ_1, it is obvious that E will increase with σ_1. This is quite different than indicated by the E-B and bilinear models. The values of E used in the Republic Steel culvert analysis are given below. These are based on one-dimensional compression tests performed in the laboratory on backfill soil samples. (The model incorporates a constant Poisson's ratio of 0.25.)

Vertical Stress (psi)	Young's Modulus (psi)
0.0	44
0.5	623
1.0	840
3.0	1100
5.0	1170
10.0	1720
15.0	2200
20.0	2700
25.0	3200
30.0	3600
40.0	4600

For all the soil models the initial stresses from placement of the soil layers were defined as geostatic. Thus the vertical stress in the center of a placed element was set equal to the product of the soil unit weight and one-half the element height. The corresponding horizontal stress was set equal to K_0 times the vertical. The selected value of K_0 was 0.35 based on a ϕ of 44 degrees. However, the results are not very sensitive to this value.

Structural Plate Representation

The corrugated-steel culvert was represented by 13 plane strain linear-elastic beam elements (Figure 2). The properties of the corrugated steel plates are listed below (plates are 5-gauge steel with 2x6-in corrugations):

Parameter	Value
Actual area	0.267 in²/in
Reduced area (A)	0.0444 in²/in
Modulus of elasticity (E)	30 x 10⁶ psi
Poisson's ratio (ν)	0.33
Moment of inertia (I)	0.127 in⁴/in
Section modulus (S)	0.115 in²/in
Plate thickness (t)	0.218 in

However, the bolted seams in the structure cause the circumferential stiffness (EA) of the culvert wall under compressive loads to be lower than that of a continuous corrugated-steel plate. To model the reduction in this thrust stiffness (EA) and maintain the same bending stiffness (EI) of the bolted joints, the cross-sectional area of the beam element (A) was artificially lowered for all the beam elements. An area reduction of six times the original value was selected based on previous research (4).

MEASURED RESPONSE AND PREDICTIONS

Culvert Displacements

One of the most important but most difficult responses of the culvert installation to predict by finite-element analysis is the displacement of the culvert during the backfilling process. Accurate simulation of the resulting deflection pattern is needed to obtain the correct moment distribution in the culvert wall, but it is also important for evaluating the appropriateness of the soil model and the soil properties.

A comparison of the measured crown vertical displacement as a function of backfill height above the footings with predicted values for the four soil models investigated is shown in Figure 6. The measured crown displacements are combined for three different longitudinal cross sections of the culvert, based on results from the structural extensometers. From the measured response, the crown of the culvert appears to have risen approximately 3-5 in at its midsection from backfilling to the crown and then to have settled back about 2 in as a result of placing the backfilling cover above the crown.

Only the two confining stress-dependent models gave reasonable agreement with the measured values. Even though the linear-elastic and overburden-dependent models show the peaking of the structure at the same fill height as the other two models, both underpredict the crown vertical movements by a sizable amount. They also result in final crown movements that are much lower than the original position before backfilling.

Other finite-element studies of culvert crown vertical movements incorporating the overburden-dependent soil model show similar trends (3,5,6). This displacement discrepancy has suggested the need to include the modeling of the compaction process itself. However, Figure 6 suggests that the choice of soil model could be the problem instead.

Soil Stress

The measured and predicted horizontal stress (σ_H) at the springline elevation at the completion of backfilling are shown in Figure 7. Agreement is quite good for all the soil models studied and the computed stress is not very sensitive to the choice of soil model. The horizontal stress is greatest near the culvert and decreases rapidly with distance from the culvert wall. The stresses continue to decrease until the geostatic or free-field value is reached.

The measured vertical soil stresses (σ_V) above the crown for the final fill height are shown in Figure 8 together with the predicted vertical stresses. The stress is lowest above the crown and highest above the compaction wings. The free-field values lie between the crown and wing values. Measured values show a greater reduction directly over the crown than the predicted values but agree at their maximum values directly over the compaction wing-tip location.

Soil Strain

The measured and predicted average horizontal strain at the springline elevation is shown in Figure 9 as a function of fill height above the footings. The average strain was defined as the horizontal differential movement between the culvert and a position about 10 ft away from the culvert divided by this distance. Only the bilinear and E-B models agreed with the measured values. The other two models predicted strains that were much too small.

Figure 6. Measured and predicted crown vertical displacements with height of backfill above footings.

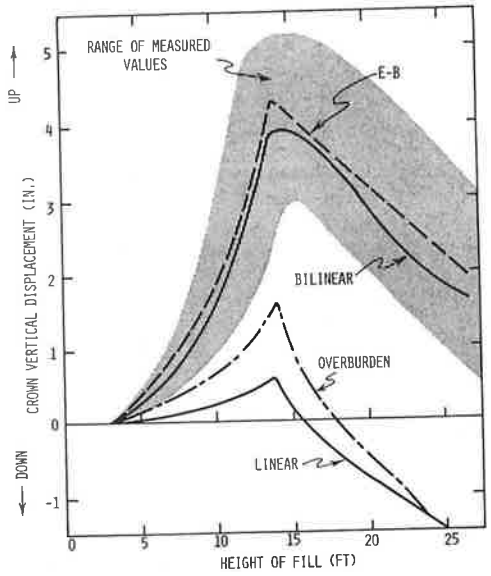

Figure 7. Measured and predicted horizontal stresses at springline elevation at final fill height.

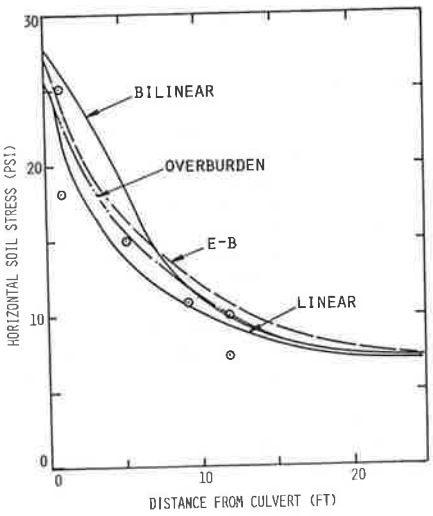

Figure 8. Measured and predicted vertical soil stresses over crown for final fill height.

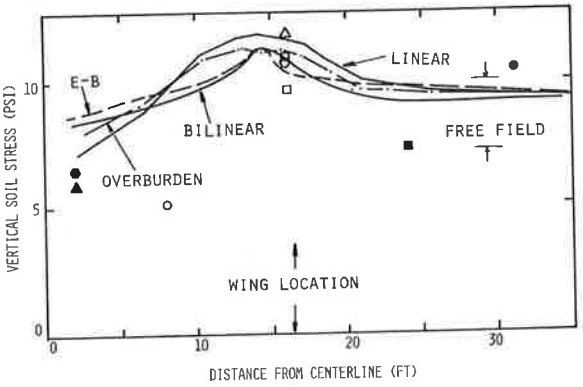

Figure 9. Measured and predicted average horizontal soil strain at springline elevation adjacent to culvert as function of backfill height above footing.

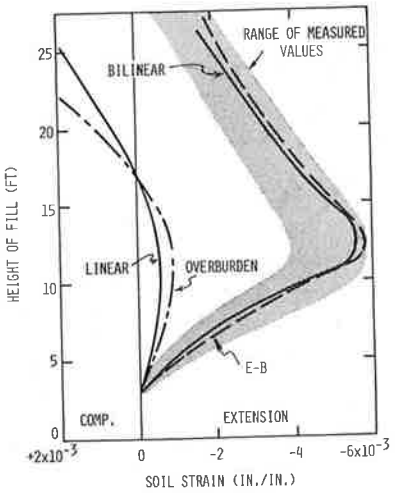

Culvert Thrust and Bending Stress

The measured and predicted thrust compression stresses around the barrel of the structure for the final fill height are compared in Figure 10. Both the measured and the predicted values gradually increase from the crown to the springline. This is due partly to soil-steel friction and partly to the keying action of the compaction wings. The keying action is illustrated by the step changes in thrust stress at the compaction-wing connections. The predicted thrust stresses are in general agreement with the measured values except for those from the linear-elastic model, which are lower by 40 percent at the crown location.

Although not shown in Figure 10, the measured thrust stresses were almost zero for the top wing plates and small in magnitude for the side wing plates. The extremely low thrust stress in the top plates suggests that little if any thrust load is being transferred from the barrel of the culvert to the surrounding backfill through the compaction wing. Both the measured and the predicted thrust stresses in the compaction wings were in close agreement for all the soil models investigated.

Also shown in Figure 10 is the thrust stress at the springline location calculated by the ring-compression theory. The magnitude of the measured springline thrust force in the culvert wall was found to be approximately equal to the overlying weight of backfill above the culvert half-span. However, the calculated ring-compression values considered only the soil weight above the crown, as is the conventional practice, and hence excluded the soil weight between the crown and springline of the culvert. This accounts for most of the difference between the ring-compression theory and measured thrust stresses.

A plot of the measured bending stresses in the culvert at the final fill elevation is shown in Figure 11. As a result of the final displacement patterns of the culvert, at the crown and springline the outer wall is in tension and the inner wall is in compression (positive moment). The maximum bending stresses were larger than the thrust compression stresses. Although not shown, the measured bending stresses in the compaction wing were of the same order of magnitude as those in the culvert barrel, which indicates that the surrounding soil is pushing the wing toward the barrel of the culvert.

Both the bilinear and E-B model results agree quite well with the measured bending stresses. However, the predicted linear-elastic and overburden-dependent bending stresses at the crown of the culvert disagree with the measured values as a result

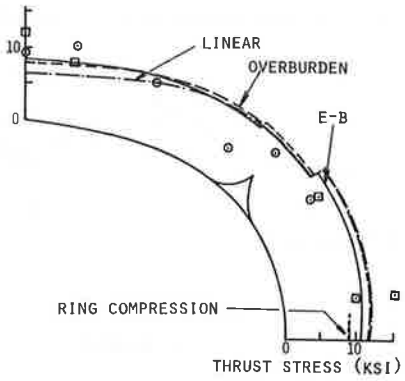

Figure 10. Measured and predicted thrust compression stresses at final fill height.

Figure 11. Bending stress in culvert at final fill height.

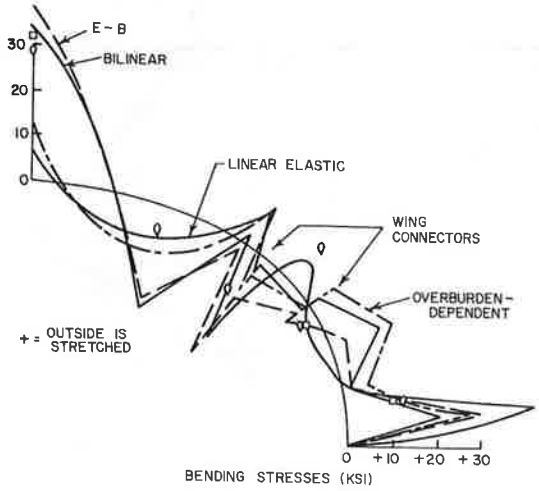

Figure 12. Culvert deflection change for fill increase above compaction wings based on survey target data.

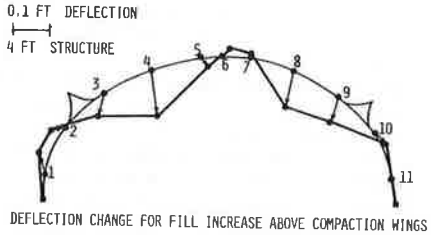

of the error in their predicted displacement patterns.

EFFECT OF COMPACTION WINGS

As part of this investigation of the soil-structure interaction of flexible conduits, the role of the compaction wings on the structure was evaluated. The response of the structure was analyzed with and without the compaction wings by use of the finite-element method, incorporating the E-B soil model. The field measurements with the maxispan structure were also examined.

The computer solution showed a larger upward crown movement during backfilling to the crown and smaller downward movement for backfilling from the crown elevation to the final elevation with no compaction wings. This may be attributed to the reduced barrel stiffness with the removal of the compaction wings. However, according to the survey target data, the compaction wings moved inward relative to the soil during backfilling from the compaction-wing elevation to the final fill elevation (Figure 12). Thus the wings did not serve as abutments or stabilize the top arch of the structure as frequently claimed. The same trend was indicated by a culvert with a thrust beam (7).

The predicted thrust stresses in the barrel of the culvert are slightly smaller without the compaction wings than with them. Thus the thrust in the side walls is not reduced but instead is increased by the presence of the compaction wings. This indicates that the compaction wings do not serve to transfer soil load on top of the structure to the adjacent soil as is sometimes claimed.

The compaction wings may provide stiffness to the barrel of the culvert. However, a more efficient approach would be either to supply the structure with struts during construction or to provide rib stiffeners on the structure.

CONCLUSIONS

The investigation of the Republic Steel structure in Pennsylvania described in this paper together with previous research have led to the following conclusions:

1. The choices of soil model and parameter values are critical to the prediction of culvert deformation and bending stress. They are not critical to the prediction of thrust stress, however.
2. The overburden-dependent soil model should not be used. A model that has stress-dependent soil moduli and a yield (failure) criterion is needed. Of those evaluated, the most suitable is the E-B model. Among its advantages is the ability to estimate parameter values from available data or to determine them from conventional soil-property tests.
3. Incremental placement of the backfill is essential for good predictions. The effects of other construction-related factors such as compaction, bolt tightening, and temporary supports are difficult to predict. This will limit the accuracy of the computed results, particularly deflection and bending stresses.
4. The need for simulation of compaction should be further evaluated. Simulation by surcharge pressure is not representative of the actual process and may partly be compensating for errors from other causes such as inadequate soil modeling.
5. Compaction wings appear to be unnecessary. They do not appear to perform the intended functions such as supporting the top arch. In addition, they have disadvantages, which include increasing cost and increasing springline thrust. Although evidence to support this conclusion already exists, some demonstration installations are desired for confirmation.
6. Satisfactory predictions have been obtained by using modeling techniques described in this paper. However, the finite-element models might be improved by better representing seam slip, soil-culvert interface slip, interface tension release, wall yielding, and wall buckling.
7. Rational criteria have not yet been established for the design of the structural backfill zone, particularly the size of the zone. A better understanding of the role of this zone should result in better economy and an extension of the range of conditions in which long-span structures can be constructed.
8. The bending flexibility of long-span structures does not lead to positive arching. Positive arching can come from seam slip, however. Thus

further study of the influence of seam yielding appears beneficial.

ACKNOWLEDGMENT

Partial support for this research was provided by the Republic Steel Corporation. Overall supervision of the field work was provided by Irvine G. Reinig. Responsibility for major portions of the field instrumentation study was assumed by John Black, Vincent Pascucci, and Brian Dorwart. Preliminary computer analyses were also carried out by John Black.

REFERENCES

1. E.T. Selig. Instrumentation of Large Buried Culverts. In Performance Monitoring for Geotechnical Construction. American Society for Testing and Materials, Philadelphia, PA, Special Tech. Publ. 584, Aug. 1975, pp. 159-181.
2. E.T. Selig. Soil Stress Gage Calibration. ASTM Geotechnical Testing Journal, Vol. 3, No. 4, Dec. 1980, pp. 153-158.
3. G.A. Leonards and T.H. Wu. Predicting Performance of Buried Conduits. Engineering Experiment Station, Purdue Univ., Lafayette, IN, March 1981.
4. J.M. Duncan, P. Byrne, K.S. Wong, and P. Mabry. Strength, Stress-Strain, and Bulk Modulus Parameters for Finite Element Analysis of Stresses and Movements in Soil Masses. Univ. of California at Berkeley, Rept. UCB/GT/80-01, Aug. 1980.
5. C.S. Chang, J.M. Espinoza, and E.T. Selig. Computer Analysis of Newton Creek Culvert. Journal of the Geotechnical Engineering Division of ASCE, Vol. 106, No. GT5, May 1980, pp. 531-556.
6. M.G. Katona, J.B. Forrest, R.J. Odello, and J.R. Allgood. Computer Design and Analysis of Pipe Culverts. Civil Engineering Laboratory, Port Hueneme, CA, Interim Tech. Rept. 51-040, Oct. 1974.
7. E.T. Selig, C.W. Lockhart, and R.W. Lautensleger. Measured Performance of Newtown Creek Culvert. Journal of the Geotechnical Engineering Division of ASCE, Vol. 105, No. GT9, Sept. 1979, pp. 1067-1087.

Publication of this paper sponsored by Committee on Subsurface Soil-Structure Interaction.

Design Method for Concrete Pipe Under High Fills

J. NEIL KAY AND STEPHEN J. HAIN

A method is proposed for design of reinforced concrete pipe installed in embankment conditions under high fills. At the current stage, the method is restricted to pipes bedded in the natural soil. The method widely used at this time has seen little change since its introduction more than 40 years ago, and recent research has indicated that it is highly conservative for present practice. A study of the complex soil-structure interaction system has been made by using the finite-element method. A simplified linear-elastic approach has enabled comparison of three-edge bearing test conditions with those encountered by a pipe in the field in such a way as to provide curves suitable for a rapid design procedure. Justification for such an approach can be obtained from review of field response data for such conditions. For a large-scale field study the method predicts the cover height to produce cracking within about 20 percent, whereas the conventional procedure provides a safety margin in the ratio of 4.6:1.

On the basis of his own work and that of his colleagues, Spangler (1) proposed a method for concrete pipe design. He recognized the interaction effects of the pipe, the underlying soil, the pipe bedding, and the compacted fill and suggested a parameter, the settlement ratio r_{sd}, defined as follows:

$$r_{sd} = [(S_m + S_g) - (S_f + d_c)]/S_m$$

where

S_m = compression of soil on either side of pipe,
S_g = settlement of natural ground adjacent to conduit,
S_f = settlement of conduit into its foundation, and
d_c = change in vertical height of conduit.

The settlement ratio was used in conjunction with the projection ratio, the lateral pressure coefficient, the soil friction coefficient, the soil unit weight, the height of soil cover, and the pipe diameter to obtain an equivalent total load on the pipe (W_c). On the basis of bedding type, a load factor L_c was estimated. The required class of pipe was then determined from the three-edge bearing strength (S_{eb}) as follows:

$$S_{eb} = W_c/L_f$$

The theory was based on the ultimate resistance to movement on boundaries of a rectangular prism of soil above the pipe. Crude guidelines for selection of r_{sd} were suggested by Spangler based on back-calculation from field tests (2), but the basis for proposals for appropriate values of lateral earth pressure coefficient, friction angle, and load factor, all extremely uncertain, is not so evident. Review of the field tests indicates that the proposed values for r_{sd} are questionable, particularly in the light of the other uncertainties.

Nearly five decades and many computer hours of concrete pipe studies later, the Spangler approach remains the conventional approach to the problem, in spite of the fact that capabilities for analysis are now many times greater than those that were available to Spangler. Some finite-element studies of the buried reinforced concrete pipe problem have been completed (3-5), but they either constitute a parametric study of particular aspects of the problem or offer a complex programming procedure for the system that is not usable for ordinary design purposes.

In this work certain simplifications have been made to enable presentation of results from a comprehensive finite-element study in a simple graphical form. Both the pipe and the soil are assumed to deform in a linear manner under load. Some nonlinearity is to be expected for both the pipe and the

further study of the influence of seam yielding appears beneficial.

ACKNOWLEDGMENT

Partial support for this research was provided by the Republic Steel Corporation. Overall supervision of the field work was provided by Irvine G. Reinig. Responsibility for major portions of the field instrumentation study was assumed by John Black, Vincent Pascucci, and Brian Dorwart. Preliminary computer analyses were also carried out by John Black.

REFERENCES

1. E.T. Selig. Instrumentation of Large Buried Culverts. In Performance Monitoring for Geotechnical Construction. American Society for Testing and Materials, Philadelphia, PA, Special Tech. Publ. 584, Aug. 1975, pp. 159-181.
2. E.T. Selig. Soil Stress Gage Calibration. ASTM Geotechnical Testing Journal, Vol. 3, No. 4, Dec. 1980, pp. 153-158.
3. G.A. Leonards and T.H. Wu. Predicting Performance of Buried Conduits. Engineering Experiment Station, Purdue Univ., Lafayette, IN, March 1981.
4. J.M. Duncan, P. Byrne, K.S. Wong, and P. Mabry. Strength, Stress-Strain, and Bulk Modulus Parameters for Finite Element Analysis of Stresses and Movements in Soil Masses. Univ. of California at Berkeley, Rept. UCB/GT/80-01, Aug. 1980.
5. C.S. Chang, J.M. Espinoza, and E.T. Selig. Computer Analysis of Newton Creek Culvert. Journal of the Geotechnical Engineering Division of ASCE, Vol. 106, No. GT5, May 1980, pp. 531-556.
6. M.G. Katona, J.B. Forrest, R.J. Odello, and J.R. Allgood. Computer Design and Analysis of Pipe Culverts. Civil Engineering Laboratory, Port Hueneme, CA, Interim Tech. Rept. 51-040, Oct. 1974.
7. E.T. Selig, C.W. Lockhart, and R.W. Lautensleger. Measured Performance of Newtown Creek Culvert. Journal of the Geotechnical Engineering Division of ASCE, Vol. 105, No. GT9, Sept. 1979, pp. 1067-1087.

Publication of this paper sponsored by Committee on Subsurface Soil-Structure Interaction.

Design Method for Concrete Pipe Under High Fills

J. NEIL KAY AND STEPHEN J. HAIN

A method is proposed for design of reinforced concrete pipe installed in embankment conditions under high fills. At the current stage, the method is restricted to pipes bedded in the natural soil. The method widely used at this time has seen little change since its introduction more than 40 years ago, and recent research has indicated that it is highly conservative for present practice. A study of the complex soil-structure interaction system has been made by using the finite-element method. A simplified linear-elastic approach has enabled comparison of three-edge bearing test conditions with those encountered by a pipe in the field in such a way as to provide curves suitable for a rapid design procedure. Justification for such an approach can be obtained from review of field response data for such conditions. For a large-scale field study the method predicts the cover height to produce cracking within about 20 percent, whereas the conventional procedure provides a safety margin in the ratio of 4.6:1.

On the basis of his own work and that of his colleagues, Spangler (1) proposed a method for concrete pipe design. He recognized the interaction effects of the pipe, the underlying soil, the pipe bedding, and the compacted fill and suggested a parameter, the settlement ratio r_{sd}, defined as follows:

$$r_{sd} = [(S_m + S_g) - (S_f + d_c)]/S_m$$

where

S_m = compression of soil on either side of pipe,
S_g = settlement of natural ground adjacent to conduit,
S_f = settlement of conduit into its foundation, and
d_c = change in vertical height of conduit.

The settlement ratio was used in conjunction with the projection ratio, the lateral pressure coefficient, the soil friction coefficient, the soil unit weight, the height of soil cover, and the pipe diameter to obtain an equivalent total load on the pipe (W_c). On the basis of bedding type, a load factor L_c was estimated. The required class of pipe was then determined from the three-edge bearing strength (S_{eb}) as follows:

$$S_{eb} = W_c/L_f$$

The theory was based on the ultimate resistance to movement on boundaries of a rectangular prism of soil above the pipe. Crude guidelines for selection of r_{sd} were suggested by Spangler based on back-calculation from field tests (2), but the basis for proposals for appropriate values of lateral earth pressure coefficient, friction angle, and load factor, all extremely uncertain, is not so evident. Review of the field tests indicates that the proposed values for r_{sd} are questionable, particularly in the light of the other uncertainties.

Nearly five decades and many computer hours of concrete pipe studies later, the Spangler approach remains the conventional approach to the problem, in spite of the fact that capabilities for analysis are now many times greater than those that were available to Spangler. Some finite-element studies of the buried reinforced concrete pipe problem have been completed (3-5), but they either constitute a parametric study of particular aspects of the problem or offer a complex programming procedure for the system that is not usable for ordinary design purposes.

In this work certain simplifications have been made to enable presentation of results from a comprehensive finite-element study in a simple graphical form. Both the pipe and the soil are assumed to deform in a linear manner under load. Some nonlinearity is to be expected for both the pipe and the

Figure 1. Details of pipe problem.

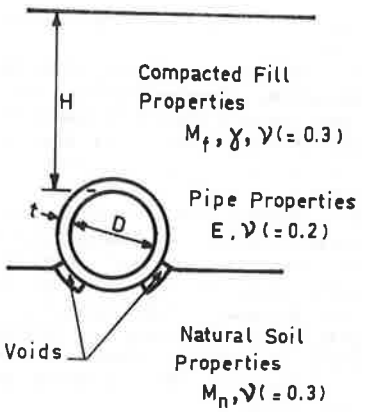

Figure 2. Arrangement of finite-element mesh.

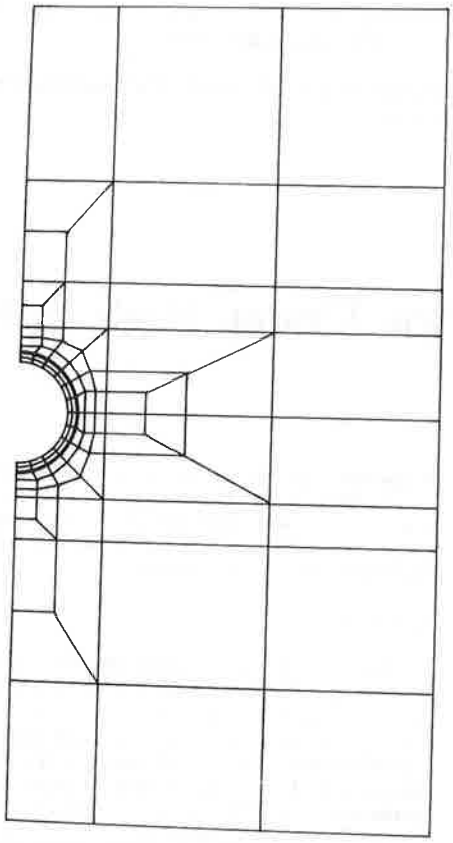

soil, but there is considerable justification for use of the linear model in this context. First, there is considerable uncertainty associated with selection of even average linear parameters. Second, evidence from field measurements of pipe deflections and stresses appears to indicate that a straight line is an equally acceptable fit to results from complex nonlinear models (3).

Only the first of a range of problems is considered in this work. Finite-element results indicated that for cover heights greater than about two pipe diameters, the pipe response associated with a given uniform load increment was constant. The graphs are based on response levels for cover heights beyond two pipe diameters and give conservative results for cases where the cover height is less. A separate study will be needed for cases of cover heights less than two diameters. In many of these cases concentrated vehicle loads rather than fill loads will dominate the design.

In addition, only one type of bedding is considered at this stage--a shaped bedding in the natural soil. The profile is illustrated in Figure 1. The area of shaped-bedding contact has an included angle of 60 degrees. For a further 30 degrees on either side, a void space is introduced to account for the practical difficulties of soil compaction in this area.

FINITE-ELEMENT MODEL

The model considered by the finite-element system was an elastic ring that represented the reinforced concrete pipe contained in a two-layer system of elastic soil as shown in Figure 1. The pipe is bedded over an angle of 60 degrees in the lower stratum and has void spaces on either side to simulate real voids or poor compaction at that location.

The vertical plane of symmetry at the center of the soil-pipe system was used in constructing the finite-element mesh indicated in Figure 2. The side and bottom boundaries both extended to 4.125 diameters' distance from the pipe centerline. The upper boundary was varied from a cover height of 0.75 to 9.5 diameters above the pipe. Eight-node isoparametric elements were used for the soil and the pipe wall, and a quadratic shape function was incorporated to closely approximate the circular shape of the pipe. The pipe wall thickness was 1/16 of the pipe diameter.

It should be noted that it was not possible to vary the ratio of pipe diameter to wall thickness (d/t) for the various finite-element analyses. Such variation would have made the required computing effort prohibitive. However, similitude considerations indicate that independent control of d/t is not necessary in a general sense. Control of the flexibility parameter $[(M_f/E)(d/t)^3$, where M_f is the compacted-fill constrained modulus and E is the pipe Young's modulus] is sufficient. Appropriate variation of M_f and E provided the necessary data for the required range of flexibility parameter. This approach left some error associated with the geometric effects of wall thickness where d/t varied from 16; however, this error will be small. A similar but considerably greater error would have occurred if a thin ring had been used to represent the pipe.

A uniformly distributed load was applied at the upper boundary. This method was selected in preference to a material self-weight approach, because it permitted a simpler evaluation of the problem. The influence of compaction of the fill on either side of the pipe is neglected. This is conservative for a 0.01-in (25-mm) crack-width failure criterion and will have only a small influence at high cover heights. It was found that beyond a cover height of two pipe diameters the response was independent of cover height; that is, for a given change in uniformly distributed load at the upper boundary, there is similar change in pipe diameter or pipe stress level independent of the boundary location. Whether the load was a thin layer of finite thickness with some unit weight or an equal uniformly applied stress at the layer center made little difference.

The accuracy of the finite-element model was established by comparison of results with those obtained from an idealized theoretical model. Burns and Richard (6) have developed a closed-form solution for an elastic tube surrounded by a homogeneous isotropic linear-elastic infinite medium subject to an overpressure. Pipe and soil elements were given similar modulus values in the finite-element and the closed-form models and both were subjected to the

same overpressure. Results indicated very close agreement between the two methods, and data generated from the finite-element model should therefore be relatively free from numerical errors.

BASIS FOR CONSIDERATION OF REAL PIPE RESPONSE

An alternative to the traditional 0.01-in crack as the criterion for failure is to use the more conventional methods for general reinforced concrete design. However, the three-edge bearing test associated with this criterion is a widely accepted method of pipe quality control that provides the manufacturer with some flexibility in product design. It would therefore appear to be a desirable procedure and should be maintained. Field experience seems to indicate that crown or invert tension cracking precedes other possible failure modes such as compression or diagonal shear. Continued use of the 0.01-in crack criterion is proposed.

In order to use the linear-elastic ring approach and to equate failure conditions in a three-edge bearing test with failure conditions in the field, a hypothetical outer-fiber stress is used. The conventional approach is to equate failure in the field with failure in the three-edge bearing test in both cases in terms of the 0.01-in crack. The pipe in the three-edge bearing test at the failure condition has associated with it a bending moment at the pipe crown. The hypothetical outer-fiber stress is the outer-fiber stress exhibited by a homogeneous geometrically similar elastic pipe that exhibits the same deformation characteristics when subjected to the same bending moment in the three-edge bearing test. This hypothetical outer-fiber stress is then used to define failure in the elastic ring contained in the finite-element model. Of course, the hypothetical outer-fiber stress value will not exist, because the pipe will have cracked. However, it is postulated that equal hypothetical outer-fiber stresses will represent equal crack widths. This will not be precisely correct, since the differences between field and three-edge bearing test bending-moment distributions will lead to slightly different crack patterns, but the error from this source is likely to be small.

The outer-fiber stress (σ_m) for an elastic beam subject to combined axial force T and bending moment M is given by the following:

$$\sigma_m = (My/I) \pm (T/A) \tag{1}$$

where y is the beam half-depth, I is the beam moment of inertia, and A is the beam cross-sectional area. When the wall of a pipe is subject to combined axial force and bending moment, some modification is necessary owing to the curved-beam effect. This effect is relatively small except for very thick-walled pipes and might well have been neglected, but since very little additional computational effort was necessary, it was included. Curved-beam factors k and j are introduced (7, p. 624) to account for this effect at the inside of the pipe crown as follows:

$$\sigma_m = (kMy/I) - (jT/A) \tag{2}$$

where

$$k = [(1/3)/(d/t - 2/m)] \cdot [(1 - d/t + 2/m)/(d/t - 1)]$$

$$m = \ln[(d/t + 1)/(d/t - 1)]$$

$$j = t/d + 1$$

The symbols d and t refer to mean pipe diameter and pipe wall thickness, respectively.

In the three-edge bearing test a sufficiently accurate solution for the bending moment at the pipe crown (M_c) is given by the following:

$$M_c = (qd^2/2\pi) \tag{3}$$

where q is the three-edge bearing test load per unit length of pipe per unit of pipe mean diameter. The stress at the inside of the pipe crown (σ_i) is given by the following:

$$\sigma_i = kMy/I = (3/\pi)kq(d/t)^2 \tag{4}$$

For equal field and three-edge bearing test outer-fiber stresses, Equations 2 and 4 may be combined and rearranged to give the following:

$$q/\gamma H = 2\pi\{(M/\gamma Hd^2) - [(1/6)(j/k)(t/d)(T/\gamma Hd)]\} \tag{5}$$

The soil unit weight (γ) and the cover height (H) are introduced on both sides of the equation to produce convenient dimensionless parameters. The ratio $q/\gamma H$ becomes a key design parameter and $M/\gamma Hd^2$ and $T/\gamma Hd$ are the dimensionless forms of the data obtained from the finite-element analyses for solving Equation 5.

The three-edge bearing test load is not normally defined in terms of the pipe mean diameter (d) but rather the inside diameter (D). The conventional three-edge bearing test load (Q) is related to q by the following:

$$Q = q[(d/t)/(d/t - 1)] \tag{6}$$

Equation 5 now becomes

$$Q/\gamma H = 2\pi\left([(d/t)/(d/t - 1)]\{(M/\gamma Hd^2) - [(1/6)(j/k)(t/d)(T/\gamma Hd)]\}\right) \tag{7}$$

A careful study of previous theoretical work by Burns and Richard (6) together with other considerations of similitude indicated that determination of the moment and axial-force dimensionless parameters depended on variation of the dimensionless parameters $[(M_f/E)(d/t)^3]$ and (M_f/M_n) for a given value of Poisson's ratio ν. M_f is the constrained modulus of the compacted fill, E is the elastic modulus for the concrete pipe, and M_n is the constrained modulus of the underlying soil. Subject to the slight error associated with the location of the pipe-soil interface in the model discussed previously, this enabled solution of the problem over a wide range of d/t values without actual variance of this parameter in the finite-element model. Substitution in Equation 7 of the moment and axial-force parameters from the finite-element analyses gave the numerical data for the general relationship:

$$Q/\gamma H = f[(M_f/E)(M_f/M_n)(d/t)] \tag{8}$$

For practical purposes, design curves are more desirable in terms of the pipe inside diameter (D) than the mean diameter (d). The d/t values are converted on the basis of D/t = d/t - 1, and the curves of Figure 3 were plotted in the following form:

$$Q/\gamma H = g[(M_f/E)(M_f/M_k)(D/t)] \tag{9}$$

VALIDITY OF ELASTIC MODEL

Although the approach taken is very much more sophisticated than was possible in the 1930s, the extent of idealization that remains is considerable. Both to achieve a successful analysis and to present

Figure 3. Design graphs.

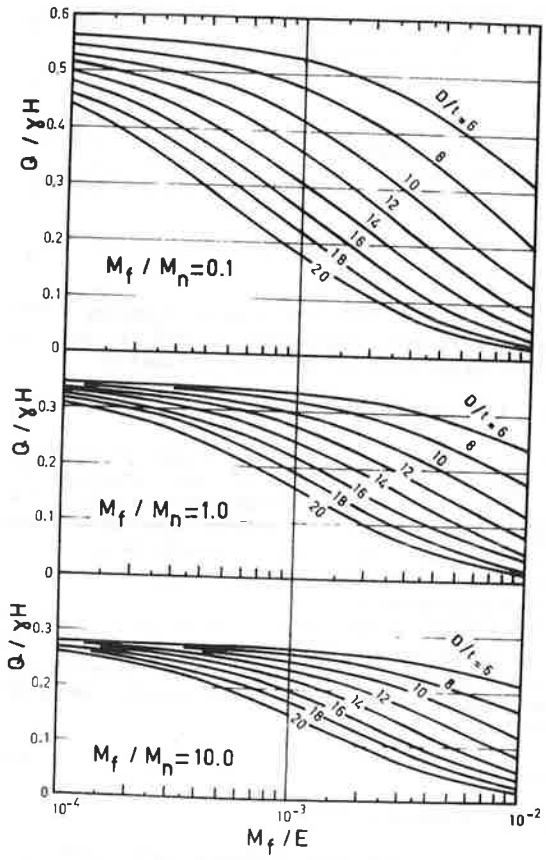

a practical design method, numerous simplifications to material properties are necessary. Many of the difficulties are itemized in the following:

1. Soil uniformity: In the compacted fill, the soil in close proximity to the pipe is likely to exhibit different compressibility characteristics from that further from the pipe. Also, stratum changes and thus compressibility changes may occur in the underlying soil.
2. Anisotropy: Both compacted fills and overconsolidated natural soil exhibit different compressibility properties parallel and perpendicular to the layering or bedding direction.
3. Soil compressibility: The compressibility of soil is nonlinear, stress-level dependent, and time dependent.
4. Pipe stiffness: The pipe exhibits a cracked modulus as well as an uncracked modulus that may differ by as much as a factor of 3 or more. Owing to variation in moment around the pipe, a nonuniform modulus will normally exist.
5. Poisson's ratio: The analyses are based on a Poisson's-ratio value of 0.3 for the soil. Although this is an average value for natural soils, little information is available on appropriate values for compacted soils. It is also likely to vary.
6. Interface slip conditions: Results are based on a no-slip condition at the concrete-soil interface. Fortunately, this error should be small; consideration of stress and strength levels from appropriate theory (8, p. 158) indicates that little slip is likely.

Obviously, the model used has shortcomings, particularly in relation to soil compressibility. Unfortunately, at the present time, very little information is available on which even average soil compressibilities may be based. Present practice in relation to pipe installation does not involve sophisticated soil-property determination, and no change in this situation is likely. Therefore, a study based on an average isotropic linear modulus would seem acceptable for the present. It should be noted that, although similar problems exist for prediction of settlement of building foundations, similar simplifications are made (9).

COMPARISON BETWEEN PREDICTIONS AND FIELD-TEST RESULTS

An extensive program of loading of concrete pipe to failure has been conducted by Davis and others (10-12) of the California Division of Highways. In these studies a series of reinforced concrete pipes with 84-in (2130-mm) diameter and 8-in (200-mm) walls were subjected to loads from compacted fills up to 136 ft (41.5 m) in height. For identical pipes under a variety of bedding conditions, the detailed crack conditions have been recorded and carefully illustrated from the onset of cracking through various stages of further deterioration. These tests offer an excellent opportunity to evaluate the proposed method for a pipe installed under embankment conditions.

In the following, the data associated with a case covered by the design graphs are assembled. A prediction is first made from Figure 3 of the fill height required to cause a 0.01-in crack. Then the outcome of the field tests for this case is reported. Finally, an estimate of fill height is made from a modern concrete pipe users' handbook based on the Spangler approach.

Field-Test Conditions

One of the bedding types studied by Davis and others (10) at Mountainhouse Creek, California, is appropriate for the design graphs prepared at this stage. In Zone 9 the pipe was placed in a shaped bedding and the fill was brought up after placement of the pipe from approximately invert level.

The constrained modulus for the compacted fill (M_f) can be determined approximately from the reported data. Some large-diameter undrained triaxial tests indicated undrained deformation-modulus values in the range 4400-5800 psi (30-40 MPa), but both end-of-construction and long-term values would reasonably be lower than these values. Measured settlement data provide a means for back-calculation of constrained modulus and indicated 3000-4500 psi (20-30 MPa) at the end of construction and 1500-2000 psi (10-15 MPa) in the longer term. The last figures showed reasonable agreement with a prediction of 1500 psi (10 MPa) based on an empirical relationship proposed by Espinosa, Krizek, and Corotis (13). Even though the usual design should be based on the drained-modulus value, the end-of-construction figure is more appropriate for this case, since it corresponds with the time of the observations for comparison of results. A value of 3500 psi (24.2 MPa) is chosen on this basis. The average in-place unit weight of the compacted fill was 130 pcf (20.5 kN/m³) and the dry weight was 116.5 pcf (18.3 kN/m³).

Little information is available on which assessment of the modulus of the in situ soil (M_n) can be made. It is assumed that this determination is the same as that of the compacted fill.

For the pipe, the average 28-day concrete compressive strength was 5200 psi (36 MPa). This corresponds to a Young's modulus of about 3.5×10^6 psi (25.2 GPa). The pipe diameter was 84 in and the pipe wall thickness was 8 in. The three-

edge bearing test load (Q) for the pipe was specified as 1000 lbf•ft/ft of pipe diameter (48 kN•m/m), but the results of three tests indicated an average strength of 1500 lbf•ft/ft (72 kN•m/m). Again, since the object here is to predict the failure fill height, the latter value is used.

Data summary: M_f = 3500 psi, M_n = 3500 psi, $E = 3.5 \times 10^6$ psi, D = 84 in, t = 8 in, Q = 1500 lbf•ft/ft, γ = 130 pcf. M_f/M_n = 1; $M_f/E = 10^{-3}$; D/t = 10.5.

Predicted fill height at failure: From Figure 3 ($Q/\gamma H = 0.30$),

$$H = Q/0.30\gamma = 1500/0.30 \times 130 = 38.5 \text{ ft } (11.7 \text{ m}).$$

Field conditions at failure: From Davis and others (11), Zone 9:

1. Fill height 30 ft (9.1 m), intermittent hairline cracks;
2. Fill height 32 ft (9.8 m), intermittent crack at invert greater than 0.01 in;
3. Fill height 34 ft (10.4 m), intermittent crack at invert averages 0.035-0.55 in (0.9-1.4 mm) localized spall.

Predicted Failure Height: Spangler Approach

Handbooks have been developed by the concrete pipe industry for use in pipe selection. Certain conditions are presumed for the field installation and specific values of the uncertain "Spangler constants" are used to permit more direct selection of the appropriate class of pipe. One such handbook, the Concrete Pipe Guide (14), was published by the Concrete Pipe Association of Australia in 1980. The product of settlement ratio and projection ratio ($r_{sd}p$) is taken to be 0.5 and the product of lateral earth pressure coefficient and coefficient of friction $K\mu$ is taken as 0.1650 for "well compacted clayey sand". For each pipe diameter an allowable fill height is given in terms of trench width, bedding type, and pipe class.

For the case of interest, a type-C bedding and a pipe with an average three-edge bearing strength of 1500 lbf•ft/ft (72 kN•m/m), the allowable fill height is indicated as about 7 ft (2.1 m).

DISCUSSION OF RESULTS

Comparison of the prediction based on the proposed design method with field results shows very reasonable agreement. The predicted height to cause failure of 38.5 ft (11.7 m) versus the actual failure height of 32 ft (9.8 m) indicates that use of the allowable (1000 lbf•ft/ft) in place of the average (1500 lbf•ft/ft) three-edge bearing value may well have provided sufficient safety margin in a design context. However, more information from field tests is required with better information on field-modulus values. It may be for the case studied that the modulus of the natural soil was considerably more than for the fill rather than equal to it as assumed. If it were 35 000 psi rather than 3500 psi, for example, the ratio M_f/M_n is then 0.1 and the predicted fill height to cause failure is 27.3 ft (8.3 m).

The Spangler approach is very clearly grossly conservative for this particular case. The allowable fill height of 7 ft versus a measured failure at 32 ft implies a factor of safety of 4.6.

SUMMARY AND CONCLUSIONS

For the proposed approach to design of concrete pipe, comparisons of predictions based on the method with results measured in one extensive field-test program are very encouraging. However, the approach is based on an idealized model, and the uncertainties associated with the required parameters are not all negligible. Work is required to provide guidelines for selection of typical parameters for design purposes, and more field testing is needed for further evaluation of the method. In addition, extension of the method is required to cover a broader range of cases such as other bedding types and shallow cover conditions.

REFERENCES

1. M.G. Spangler. Supporting Strength of Rigid Pipe Culverts. Engineering Experiment Station, Ames, IA, Bull. 112, 1933.
2. M.G. Spangler. Field Measurements of the Settlement Ratios of Various Highway Culverts. Engineering Experiment Station, Ames, IA, Bull. 170, 1950.
3. R.J. Krizek and P.V. McQuade. Behavior of Buried Concrete Pipe. Journal of the Geotechnical Division of ASCE, Proc. Vol. 104, No. GT7, July 1978, pp. 815-836.
4. G.C. Nayak, S. Prakash, and R. Gupta. Finite-Element Analyses of Ditch Conduits. Proc., International Symposium of Soil-Structure Interaction, Roorkee, India, 1977, pp. 51-59.
5. T.H. Wenzel and R.A. Parmalee. Computer-Aided Structural Analysis and Design of Concrete Pipe. In Concrete Pipe and the Soil-Structure System, American Society for Testing and Materials, Philadelphia, PA, Special Tech. Publ. 630, 1977.
6. J.Q. Burns and R.M. Richard. Attenuation of Stresses for Buried Cylinders. Proc., Symposium on Soil-Structure Interaction, Univ. of Arizona, Tucson, 1964, pp. 378-392.
7. R.J. Roark and W.C. Young. Formulas for Stress and Strain. McGraw-Hill, New York, 1975.
8. R.J. Krizek, R.A. Parmalee, J.N. Kay, and H.A. Elnaggar. Structural Analysis and Design of Pipe Culverts. NCHRP, Rept. 116, 1971.
9. T.W. Lambe and R.V. Whitman. Soil Mechanics. Wiley, New York, 1969.
10. R.E. Davis, A.E. Bacher, and J.C. Obermuller. Structural Behavior of a Concrete Pipe Culvert--Mountainhouse Creek (Part 1). California Division of Highways, Sacramento, Rept. R&D 4-71, 1971.
11. R.E. Davis, A.E. Bacher, and J.C. Obermuller. Structural Behavior of a Concrete Pipe Culvert--Mountainhouse Creek (Part 1). Journal of the Structural Division of ASCE, Vol. 100, No. ST3, March 1974, pp. 599-614.
12. R.E. Davis, A.E. Bacher, and E.E. Evans. Structural Behavior of a Concrete Pipe Culvert--Mountainhouse Creek (Part 2). California Department of Transportation, Sacramento, Rept. FHWA-CA-ST-4121-75-8, 1975.
13. J.H.S. Espinosa, R.J. Krizek, and R.B. Corotis. Statistical Analysis of Constrained Modulus. TRB, Transportation Research Record 539, 1975, pp. 59-68.
14. Concrete Pipe Guide. Concrete Pipe Association of Australia, 1980.

Publication of this paper sponsored by Committee on Subsurface Soil-Structure Interaction.

Heavy-Vehicle Loading of Arch Structures of Corrugated Metal and Soil

J.N. KAY AND R.C.L. FLINT

Results of measurements of both the direct and the residual effects of heavy-vehicle loading of an arch with a 12-m (39-ft) span of corrugated metal and soil constructed as an overpass are presented. Both in-plane stress and vertical deflection of the arch are reported for 70-tonne (77-ton) and 290-tonne (319-ton) trucks positioned at various locations over the arch. The residual effects are shown in terms of a graph of cumulative deflection versus construction and service history. The heavy vehicles caused considerably more permanent deflection of the arch crown than did the 2.1 m (6.9 ft) of soil cover above crown level.

Overpasses and bridges associated with the mining industry are important applications for arch structures of corrugated metal and compacted soil. Low-cost fill materials are generally available and these, in conjunction with the low cost of supply and transportation for the metal components, make the economics extremely attractive. However, an unusual feature associated with the design for many mining applications is the heavy-vehicle loading. This was the case for a corrugated-steel overpass constructed at Leigh Creek, South Australia, in conjunction with an open-cut coal-mining operation for the Electricity Trust of South Australia.

The structure was designed by Coffey and Partners Proprietary, Ltd., for continuous use by 70-tonne (77-ton) and occasional use by 290-tonne (319-ton) coal haulage trucks (gross weights). Detailed measurements of stresses and deformations were taken by the University of Adelaide at two sections of the arch during the construction period and for some time after. In addition, measurements were taken of the static live-loading effects of both vehicles. The influence of the intermittent heavy-vehicle loading on the long-term deflection response appears to be considerable. The live-loading effects are the subject of this paper.

BRIEF REVIEW OF PROJECT DETAILS

Details of the construction, the instrumentation, and some results of measurements have been published previously (1). In brief, the structure as shown in Figure 1 had a span of 11.8 m (39 ft), a rise of 4.7 m (15.4 ft), and a fill height above the crown of 2.1 m (6.9 ft). The initial shape consisted of circular arcs that approximated an ellipse. The steel was supported on either side by retaining walls 3 m (9.8 ft) high tied back to anchorages in the side fills. The plate was 7 mm (0.28 in) thick and had 150x50-mm (6x2-in) corrugations. Steel strains and deflections relative to the retaining walls were measured at two sections (the one-third points) with 150x50-mm corrugations along the length of the 26.7-m (87.6-ft) long steel arch. The spacing of the retaining walls was measured, but no relative horizontal movements were detected.

Fill construction above the springline level began about November 1, 1978, and reached 1.9 m (6.2 ft) above the crown on November 25, 1978. However, completion of the road base to 2.1 m above the crown level was not accomplished until January 3, 1979. Use of the structure for haulage by the 70-tonne loaded haulage trucks began a few days prior to that time.

Measurements of live load response associated with the 70-tonne loaded trucks were conducted on January 3, 1979. After continuous use of the structure for haulage by these same vehicles, the first use of the structure by a 290-tonne loaded truck was monitored on July 25, 1979.

70-TONNE TRUCK LOADING

The relative locations of the 70-tonne loaded truck for the live-load tests are shown in plan in Figure 2. The truck facing west was stopped at four positions on a line such that one set of wheels was always immediately over the southernmost instrumented section. On each occasion strain readings were taken at seven locations around the steel arch. Strain values were converted to stress based on a Young's modulus value for steel of 200 GPa (29×10^6 psi) and results are plotted in Figure 3. Values shown represent average stress levels across the section in that gauges were located near the neutral axis on both sides of the steel and were connected in series. They are related to zero stress levels at all stations both before and after the truck movement on the bridge. No readings were registered on the gauges at the northern end of the structure.

Deflection measurement was attempted by the conventional level-surveying procedures, but no valuable readings were obtained. Deflections occurred but were apparently less than 1 mm (0.04 in). A second series of measurements was taken with the truck on the same line but in the opposite direction. The resulting stresses are plotted in Figure 4. No residual stresses were observed in either series.

290-TONNE TRUCK LOADING

Dimensions associated with the 290-tonne loaded-truck tests are indicated in Figure 5. In view of the earlier inadequacies of surveying methods, vertical deflections were measured in the later truckload tests by electrical displacement transducers fixed to vertically aligned telescopic rods. Steel stresses associated with the various positions are shown in Figure 6 and measured vertical deflections in Figure 7. A repeat test was done at one location only, with the truck facing the same direction (east), and these additional results are shown in Figure 6d and 7d, respectively. In the case of the first test a permanent deflection of 0.5 mm (0.02 in) remained at the crown. No residual deflection could be detected for the repeat test. Likewise no residual stresses were observed.

LONG-TERM DEFLECTION OBSERVATIONS

A summary of permanent deflections versus time is given in Figure 8. All permanent deflections measured after the fill reached the crown level, including effects of truck loading, are shown in a cumulative fashion.

Of major interest is the fact that only 30-40 percent of the total permanent deflection appears to have been associated with placement and compaction of the fill. The major part of the permanent deflection was caused by the heavy-vehicle loading of

Figure 1. Cross section through structure.

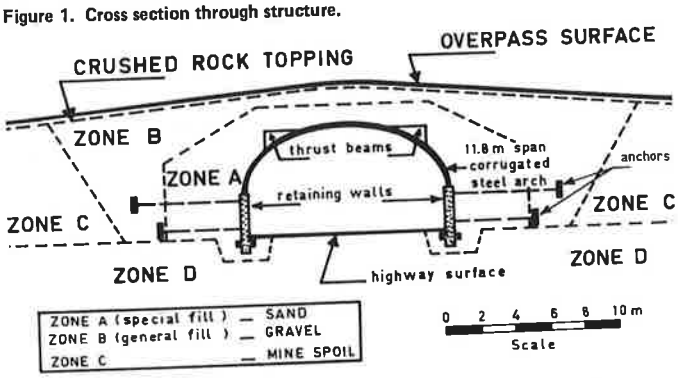

Figure 2. Relative locations of 70-tonne loaded truck.

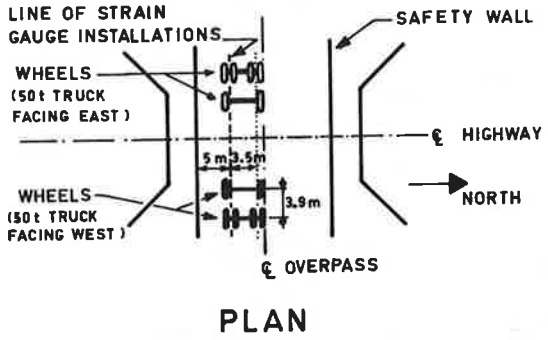

Figure 3. Compressive stresses in steel for 70-tonne truck facing west.

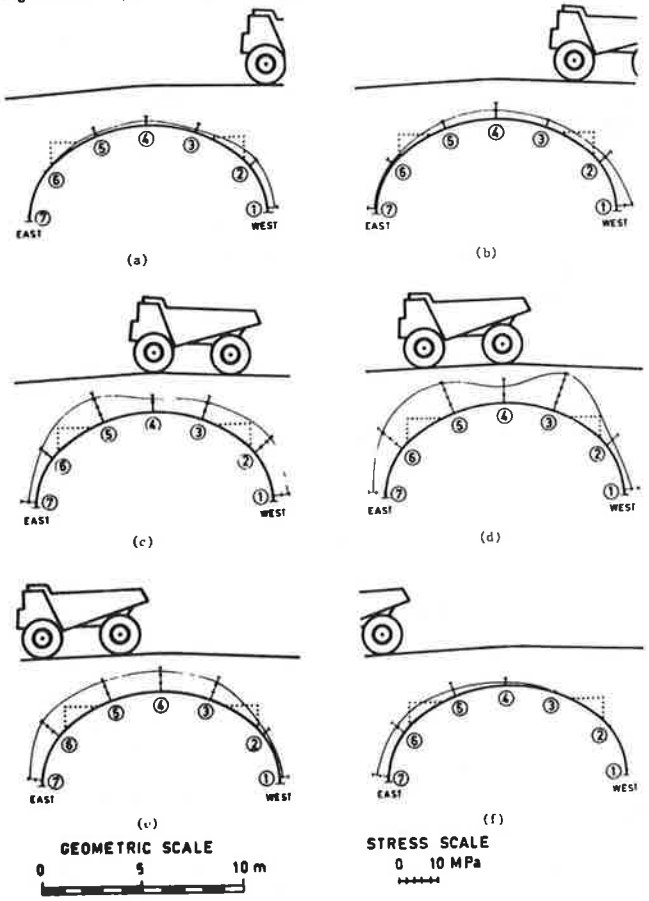

the 70-tonne trucks. Although it is possible that little further deflection may be caused by these vehicles, the effect of the first loading by the 290-tonne truck in producing a total deflection of 5 mm (0.2 in) and a residual deflection of 0.5 mm leaves little doubt that further permanent deflection would be caused by the bigger trucks.

When the weight of the vehicles that pass over the in-service structure is many times that of the equipment used in the compaction process, it is not surprising that additional settlement occurs. Further compaction of the soil in the upper meter is likely. However, the major cause of the additional permanent deflection of the steel arch is probably associated with the concentrated loading applied to the crown area. The profiles of stress shown in Figures 3, 4, and 6 and the deflections shown in Figure 7 appear to bear this out. When the vehicle rear wheels are over the crown, the stress levels at stations 3 and 5 are considerably higher than stress levels at stations 2 and 6. Also, the temporary vertical deflection at the crown is very much greater than that at the thrust-beam locations. The vertical load at the crown apparently causes primarily horizontal movement at the thrust beam and part of this movement associated with initial load

Figure 4. Compressive stresses in steel for 70-tonne truck facing east.

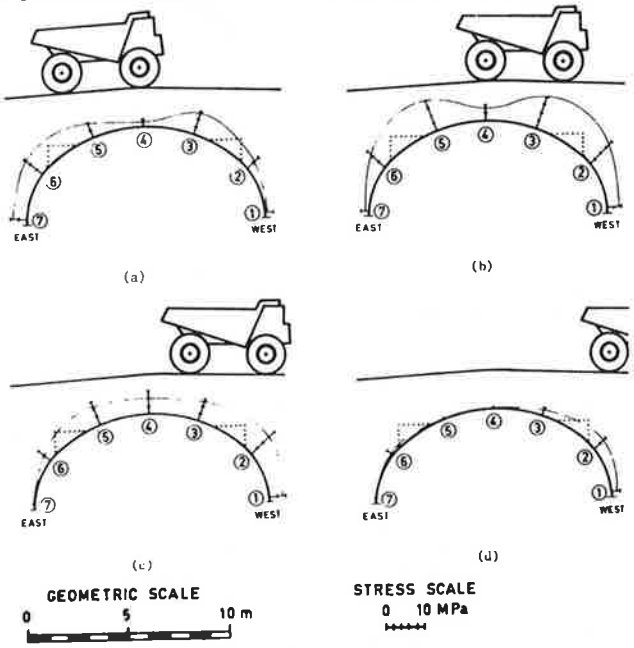

Figure 5. Relative location of 290-tonne loaded truck.

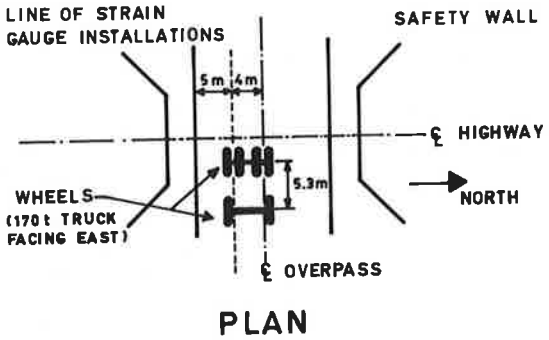

Figure 6. Compressive stresses in steel for 290-tonne loaded truck.

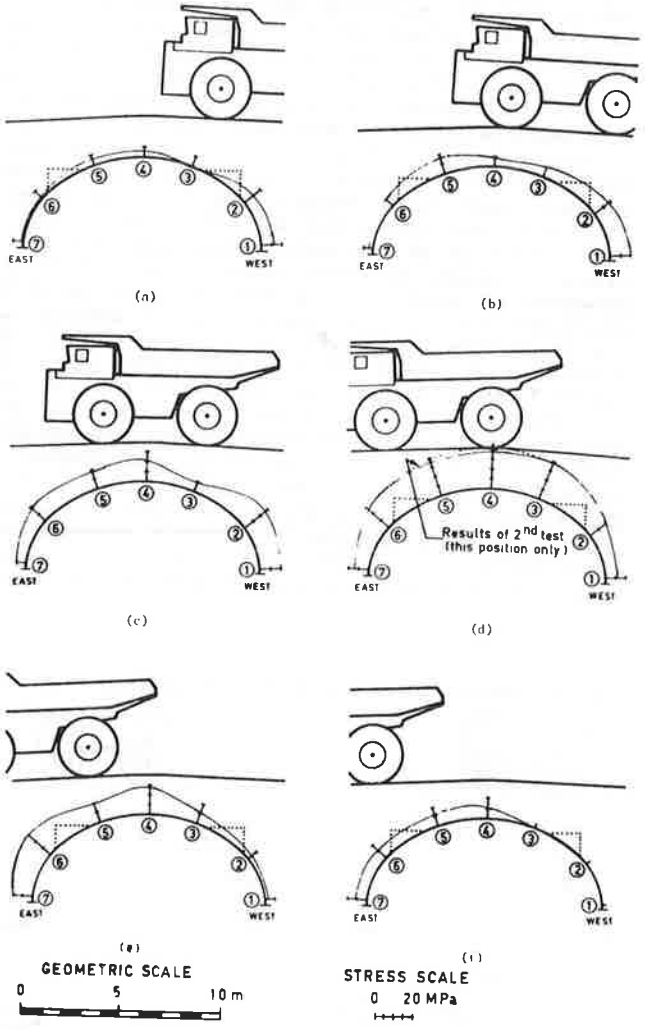

Figure 7. Vertical deflection of steel arch for 290-tonne loaded truck.

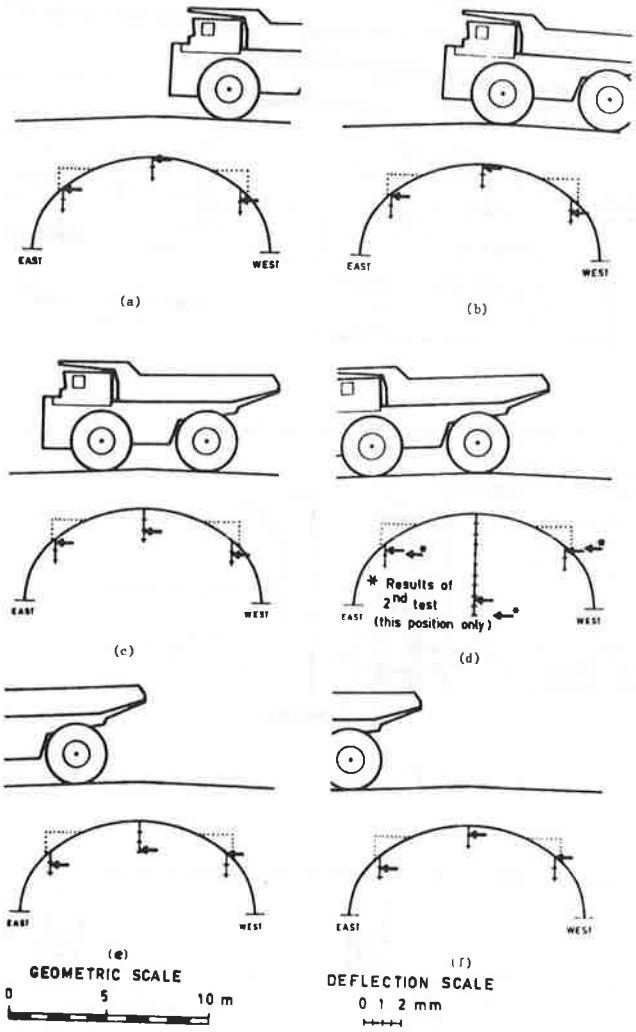

cycles remains. Two factors that contribute to the permanent horizontal movement component of the thrust beam are compaction-stress history and overburden pressure.

During the compaction process, recycling of stresses at a given level tends to produce a soil that will respond relatively elastically provided certain stress levels are not exceeded. It is possible that, locally, stress levels adjacent to the thrust beam exceed the compaction-stress levels when truck loads are applied. Also, the low overburden pressure on the soil adjacent to the thrust beam provides an unfavorable stress state compared with that for a uniform fill loading. Although the vertical stress above the crown increases, the vertical stress outside of the thrust beam is little affected. This condition leads to higher elastic deflection, higher plastic deflection, and a lower level of ultimate load capacity.

Many engineering structures undergo considerable deformation after they are placed in use. Frequently such deformation is unrecognized because it causes little difficulty and it remains unobserved because no measurements are taken. The additional deformation appears to have little significance as far as the Leigh Creek structure is concerned. However, it has important implications in relation to attempts to develop design procedures for such structures. Whereas it appears to be possible to predict the

Figure 8. Summary of permanent deflections versus time.

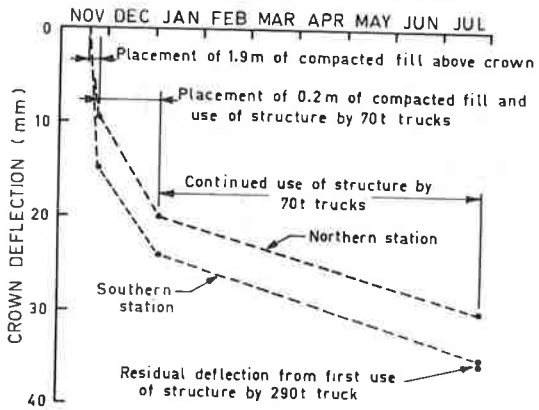

response of the structure to fill loads, as discussed by Flint and Kay in another paper in this Record, the problem becomes much more complex when live loads are considerably higher than those associated with compaction equipment. If some progress is to be made, it is extremely important to gather and report field data on such projects. Measurement of deflection is probably of greatest importance and

this is a relatively simple matter. Gathering of such data will assist with development of criteria for design.

CONCLUSIONS

Details of measured results of stresses and deflections associated with extremely heavy live loading of large-span corrugated-metal arches have been presented. In addition, the permanent effects of these loads on the deflection response have been demonstrated and discussed. Further research in this area will be necessary to enable proper consideration of heavy live loading in the design phase.

REFERENCE

1. J.N. Kay, D.L. Avalle, R.C.L. Flint, and C.F.R. Fitzhardinge. Instrumentation of a Corrugated Steel-Soil Arch Overpass at Leigh Creek, South Australia. Proc., 10th Conference of Australian Road Research Board, Vol. 10, No. 3, 1980, pp. 57-70.

Publication of this paper sponsored by Committee on Subsurface Soil-Structure Interaction.

Response of Corrugated-Metal Arches to Soil Loads

R.C.L. FLINT AND J.N. KAY

To enable prediction of the response of systems with corrugated-metal arches and compacted soil bridges to soil loading above crown level, graphs were developed from a large number of finite-element analyses. The graphs are based on analysis of a flexible arch in the form of a half ellipse supported on either side by typical footings. They facilitate prediction of response parameters as the fill is placed and compacted in layers above the crown level. The material surrounding the arch is considered homogenous in terms of elastic modulus and Poisson's ratio. Although the graphs are based on linear analysis, important nonlinear effects may be taken into account by application of the graphs in a stepwise manner. Comparison of predicted response with that from a specific finite-element analysis of a field structure suggests that the errors introduced by idealizations associated with the graphical approach may be insignificant for many projects. In addition, comparisons of predictions with field measurements show encouraging results.

Large-span corrugated-metal arch structures are becoming more common as an alternative to conventional bridges for rail or highway overpasses spanning minor roads or small waterways. Current installations use spans up to about 15 m (50 ft), and several with spans around 12 m (40 ft) have been constructed in Australia. The corrugated plate used is typically 3-7 mm (1/8 to 5/16 in) thick, depending on the size of the arch, with 150x50-mm (6x2-in) corrugations.

The response of these structures to loading is governed by an interaction between a flexible membrane (corrugated metal) and a relatively compressible surrounding medium (compacted soil fill). Analysis of such systems is difficult due to the complex interaction mechanisms involved. No closed-form solution can adequately approximate the true behavior. Most manufacturers use design methods based on formulas that assume a grossly simplified system but at the same time have the backing of considerable experience. Others have developed empirical methods based on small-scale model studies. Some discussion of these methods has been provided by Selig and others (1).

The finite-element method has now been developed to the extent where models for soil-structure interaction problems may be formulated to provide an adequate means for analysis of these structures under working loads. A number of large-span corrugated-metal arch systems have been individually analyzed by this method (2-4), and the results appear to show acceptable correlation with field measurements. However, the cost associated with such analysis is high, due largely to the time involved in formulating and checking the input data for finite-element programs as well as the actual computing costs. Access to a large computer is also required and is not always available to the design engineer.

This paper presents a method whereby the designer may reap the benefits of the finite-element method without the need to resort to the costly detailed analysis of individual structures. Design graphs based on numerous finite-element analyses are presented that may be used to predict the essential response parameters required for design of the wide range of structural configurations likely to be encountered in practice.

To demonstrate the validity and versatility of the graphs, response predictions based on the graphs are compared both with measured results from a field structure and with results obtained from a specific finite-element analysis of the field structure by using mesh data to more accurately fit the specific field conditions. Subject to the uncertainty associated with determination of the appropriate soil modulus, the results are promising.

CONFIGURATION AND CONSTRUCTION CONSIDERATIONS

Although many full-ellipse structures have been completed, the trend in Australia in recent years has been toward construction of half-ellipse and low-profile arch structures. These appear to be more practical and more economical, particularly for overpass applications. Consequently, the half-ellipse profile has been selected as the basic geometry around which the graphs are developed.

The arch is constructed from curved corrugated-plate sections approximately 2x1 m (6x3 ft), which are bolted together on site. Profiles close to elliptical are formed from circles of two different radii for the top and side arch sections. The junction of the two circles occurs at the point where the two radii have a common angle of 50 degrees to the horizontal.

It is convenient to subdivide the construction operation into two stages--stage 1, where the arch is erected and the fill is placed and compacted to crown level, and stage 2, where the fill above the crown is placed and compacted to finished level. The response of the structure to loading during stage 1 is largely dependent on the construction techniques employed. Up to this time, engineering

this is a relatively simple matter. Gathering of such data will assist with development of criteria for design.

CONCLUSIONS

Details of measured results of stresses and deflections associated with extremely heavy live loading of large-span corrugated-metal arches have been presented. In addition, the permanent effects of these loads on the deflection response have been demonstrated and discussed. Further research in this area will be necessary to enable proper consideration of heavy live loading in the design phase.

REFERENCE

1. J.N. Kay, D.L. Avalle, R.C.L. Flint, and C.F.R. Fitzhardinge. Instrumentation of a Corrugated Steel-Soil Arch Overpass at Leigh Creek, South Australia. Proc., 10th Conference of Australian Road Research Board, Vol. 10, No. 3, 1980, pp. 57-70.

Publication of this paper sponsored by Committee on Subsurface Soil-Structure Interaction.

Response of Corrugated-Metal Arches to Soil Loads

R.C.L. FLINT AND J.N. KAY

To enable prediction of the response of systems with corrugated-metal arches and compacted soil bridges to soil loading above crown level, graphs were developed from a large number of finite-element analyses. The graphs are based on analysis of a flexible arch in the form of a half ellipse supported on either side by typical footings. They facilitate prediction of response parameters as the fill is placed and compacted in layers above the crown level. The material surrounding the arch is considered homogenous in terms of elastic modulus and Poisson's ratio. Although the graphs are based on linear analysis, important nonlinear effects may be taken into account by application of the graphs in a stepwise manner. Comparison of predicted response with that from a specific finite-element analysis of a field structure suggests that the errors introduced by idealizations associated with the graphical approach may be insignificant for many projects. In addition, comparisons of predictions with field measurements show encouraging results.

Large-span corrugated-metal arch structures are becoming more common as an alternative to conventional bridges for rail or highway overpasses spanning minor roads or small waterways. Current installations use spans up to about 15 m (50 ft), and several with spans around 12 m (40 ft) have been constructed in Australia. The corrugated plate used is typically 3-7 mm (1/8 to 5/16 in) thick, depending on the size of the arch, with 150x50-mm (6x2-in) corrugations.

The response of these structures to loading is governed by an interaction between a flexible membrane (corrugated metal) and a relatively compressible surrounding medium (compacted soil fill). Analysis of such systems is difficult due to the complex interaction mechanisms involved. No closed-form solution can adequately approximate the true behavior. Most manufacturers use design methods based on formulas that assume a grossly simplified system but at the same time have the backing of considerable experience. Others have developed empirical methods based on small-scale model studies. Some discussion of these methods has been provided by Selig and others (1).

The finite-element method has now been developed to the extent where models for soil-structure interaction problems may be formulated to provide an adequate means for analysis of these structures under working loads. A number of large-span corrugated-metal arch systems have been individually analyzed by this method (2-4), and the results appear to show acceptable correlation with field measurements. However, the cost associated with such analysis is high, due largely to the time involved in formulating and checking the input data for finite-element programs as well as the actual computing costs. Access to a large computer is also required and is not always available to the design engineer.

This paper presents a method whereby the designer may reap the benefits of the finite-element method without the need to resort to the costly detailed analysis of individual structures. Design graphs based on numerous finite-element analyses are presented that may be used to predict the essential response parameters required for design of the wide range of structural configurations likely to be encountered in practice.

To demonstrate the validity and versatility of the graphs, response predictions based on the graphs are compared both with measured results from a field structure and with results obtained from a specific finite-element analysis of the field structure by using mesh data to more accurately fit the specific field conditions. Subject to the uncertainty associated with determination of the appropriate soil modulus, the results are promising.

CONFIGURATION AND CONSTRUCTION CONSIDERATIONS

Although many full-ellipse structures have been completed, the trend in Australia in recent years has been toward construction of half-ellipse and low-profile arch structures. These appear to be more practical and more economical, particularly for overpass applications. Consequently, the half-ellipse profile has been selected as the basic geometry around which the graphs are developed.

The arch is constructed from curved corrugated-plate sections approximately 2x1 m (6x3 ft), which are bolted together on site. Profiles close to elliptical are formed from circles of two different radii for the top and side arch sections. The junction of the two circles occurs at the point where the two radii have a common angle of 50 degrees to the horizontal.

It is convenient to subdivide the construction operation into two stages--stage 1, where the arch is erected and the fill is placed and compacted to crown level, and stage 2, where the fill above the crown is placed and compacted to finished level. The response of the structure to loading during stage 1 is largely dependent on the construction techniques employed. Up to this time, engineering

Figure 1. Diagram of notation.

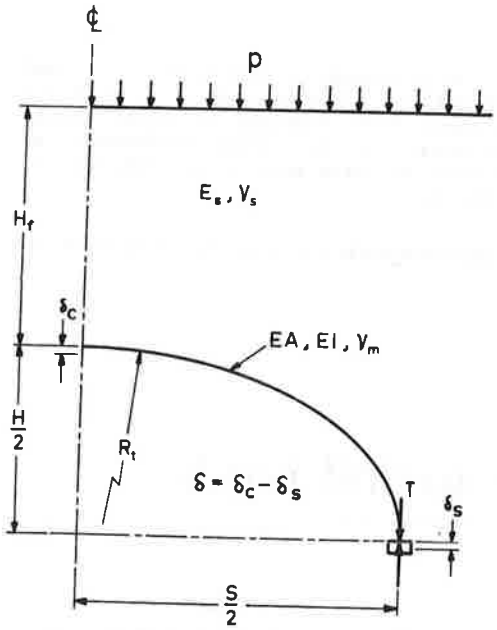

computation has provided little assistance, and an on-site trial-and-error approach in accordance with specified tolerances appears to be the best approach.

For the second stage (placement and compaction of fill above the crown level), the response of the system is considerably less dependent on construction effects and can be treated in terms of fundamental engineering mechanics. Fortunately, provided the specifications on system geometry are achieved in stage 1, the loading and the response during the second stage and after govern the in-service safety of the structure.

Widespread practice in corrugated-metal arch construction is to incorporate thrust beams. These are concrete beams running longitudinally along the shoulder of the arch on either side near the change in plate radius. The beams are cast in situ directly on the corrugated metal and are fixed to the arch by shear connectors. It is widely accepted that thrust beams serve to provide a nearly vertical wall against which the side fills may be compacted to a high standard without severely distorting the arch. They constitute an easily placed comparatively rigid material in this critical region where it is difficult to obtain satisfactory soil compaction.

Based on these considerations, the procedure presented in this paper covers prediction of response due to loading imposed during stage-2 construction for a semielliptical structure that incorporates thrust beams.

FAILURE CRITERIA

Failure of large-span corrugated-metal arch structures has been observed to occur by either of two modes. The first involves a snap-through type buckling failure of the top section of the corrugated-metal arch and is obviously of a catastrophic nature. The second involves seam failure of the corrugated-metal arch wall and is most likely to occur at the springline where the tangential thrust is greatest. In some cases, seam failure may be repairable, but in others it may be associated with catastrophic collapse.

For a design to be satisfactory, the system must exhibit an acceptable factor of safety against both modes of failure. The proposed procedure entails prediction of structural response under working load. This may be compared with acceptable limits derived from consideration of the failure mechanisms. The seam-failure mode is a relatively simple matter associated with the tangential thrust in the arch wall. However, the snap-through buckling mode is much more complex. For small circular pipes, Spangler (5) considered excessive deflection to be the logical criterion for such failure and suggested a maximum safe change in diameter of 5 percent. This is based on laboratory tests that indicated a collapse condition when deflection reached about 20 percent of the diameter. No comprehensive study of this collapse mechanism has yet been made for large-span corrugated-metal arch systems, and no limits for safe deflections based on rational analysis of the problem are available (6). However, control of deflection would appear to be the most promising approach.

METHODS OF ANALYSIS

The method presented enables calculation of the structural response associated with a uniformly distributed load applied on a level surface at any height above crown level. Nonlinear effects may be taken into account by analyzing any given problem in a stepwise fashion that simulates fill placement in the field. For analysis, the fill to be placed above crown level is divided into a number of layers. The load equal to the overburden pressure imposed by the layer is applied to the system with the upper boundary level at the layer mid-height. The structural response resulting from this load is then determined from the graphs.

By summing the contributions from successive layers, the total structural response as fill is placed above crown level is determined.

The parameters used to describe the behavior of the system are illustrated in Figure 1. The top radius (R_t) associated with the circle approximations to the ellipse is uniquely related to the major and minor diameters (S and H, respectively) by the following:

$$R_t = 0.937S - 0.437H.$$

The two key response parameters--the relative crown deflection (δ) and the springline thrust (T)--are some function of the input parameters:

$$\delta = f_\delta(E_s, \nu_s, EA, EI, \nu_m, H, S, R_t, H_f, p) \quad (1)$$

$$T = f_t(E_s, \nu_s, EA, EI, \nu_m, H, S, R_t, H_f, p) \quad (2)$$

where

A = cross-sectional area of arch-wall material per unit length,
E = elastic modulus of material in arch wall,
E_s = elastic modulus of compacted fill,
H_f = height of fill above crown level,
I = moment of inertia of arch-wall material per unit length,
p = uniform soil load per unit area,
ν_s = Poisson's ratio of compacted fill, and
ν_m = Poisson's ratio of arch-wall material.

It has been demonstrated elsewhere (6) that these equations may be written efficiently in dimensionless form as follows:

$$\delta E_s/pR_t = f'_\delta[(H_f/R_t), (E_sR_t/EA), (E_sR_t^3/EI), (S/H), \nu_s, \nu_m] \quad (3)$$

Figure 2. Typical finite-element mesh used for development of graphs.

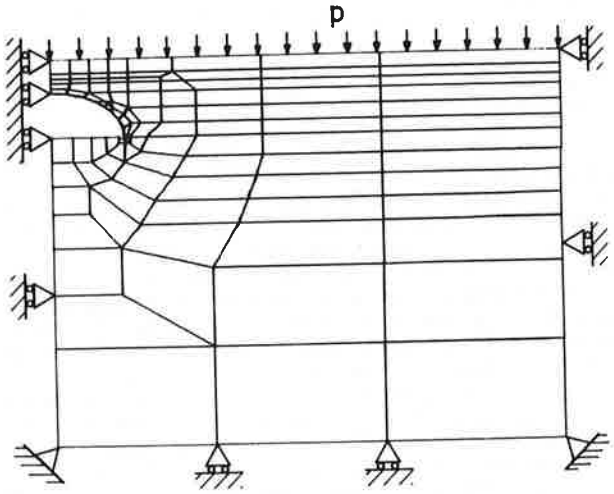

Figure 3. Range of standard arch dimensions available from major supplier.

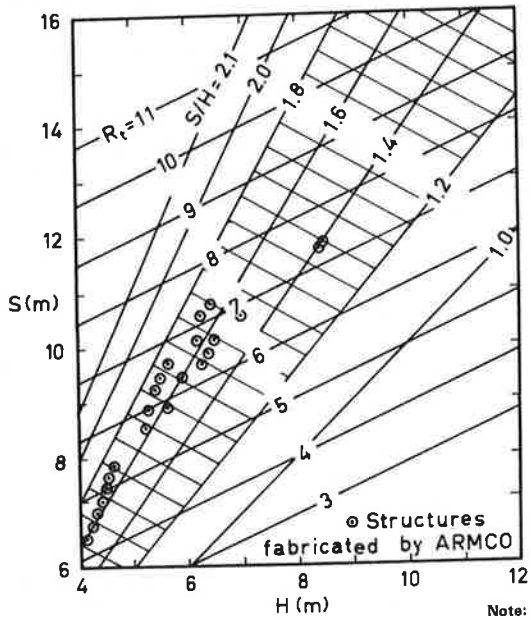

$$T/pR_t = f_f[(H_f/R_t), (E_sR_t/EA), (E_sR_t^3/EI), (S/H), \nu_s, \nu_m] \quad (4)$$

The realistic range for values of each of these dimensionless parameters has been determined, and finite-element analyses of specific structures exhibiting values over the entire range of possible combinations have been performed. The results of these analyses have been used to prepare curves that then provide a graphical solution to Equations 3 and 4.

Once the dimensionless response parameters $\delta E_s/pR_t$ and T/pR_t have been determined from the charts, substitution of the original values of E_s, p, and R_t yields the values of the actual response parameters δ and T.

FINITE-ELEMENT ANALYSIS

The two-dimensional finite-element program Elaspipe (2) was used for the parameter studies. The program employs rectangular, quadrilateral, and triangular elements to represent the soil. The formulations

Figure 4. Range of flexibility parameter combinations corresponding to current practice.

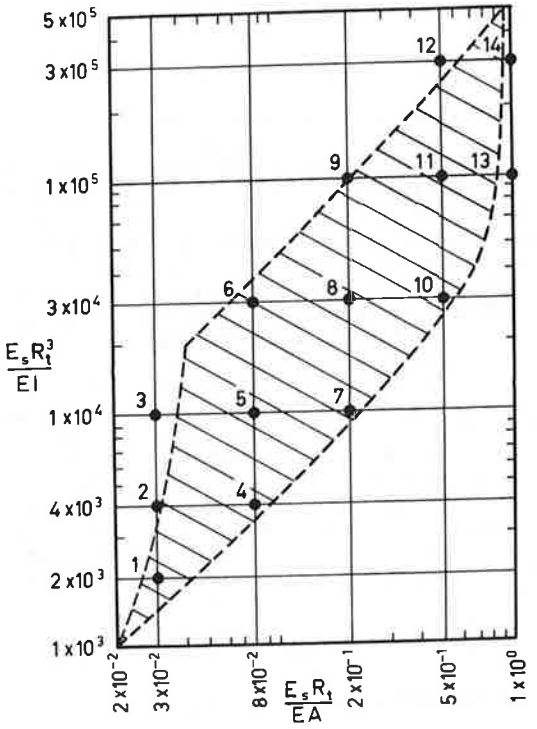

for these types of elements are, respectively, the Q6, Q4, and CST formulations. The pipe is represented by a series of elliptical, cubic-displacement bending and stretching elements with independently specified flexural and axial stiffnesses. All analyses assume linear-elastic, plane-strain conditions.

Figure 2 shows a typical element mesh. The problem is symmetrical about the vertical centerline, and the boundaries as shown are clear of the influence of the arch. Top layers of elements are added or removed as appropriate for different cover heights. Note that the only load applied is the uniformly distributed load on the top surface. The elements are weightless.

Bounds on values for the dimensionless parameters have been determined from consideration of the possible combinations of arches and soil properties. Where considered appropriate, values have been extended beyond present practice to allow for larger future spans.

Poisson's ratio for steel (ν_m) was assumed to be 0.3. Poisson's ratio for soil (ν_s) appears to vary for structural fills from approximately 0.25 to 0.4, but since this is essentially a second-order variable compared with the other parameters, it was taken to be constant at 0.3. The sensitivity of the response parameters to variation in ν_s is discussed subsequently.

Fill height was considered in terms of the H_f/R_t ratio. Results were obtained over the range 0.1-1.0 for this ratio. As a guide to the desirable ranges for S/H, E_sR_t/EA, and $E_sR_t^3/EI$, data for readily available standard geometries were obtained from catalog LMSS-1976 of ARMCO Inc., Middletown, Ohio. Specifically available spans (S) and heights (H) are plotted in Figure 3 and corresponding ranges for $E_sR_t^3/EI$ and E_sR_t/EA associated with E_s values from 10 to 100 MPa (1450-14 500 psi) are hatched in Figure 4. The specific

points covered by the subsequently developed graphs are indicated by the black dots in Figure 4.

SOURCES OF ERROR

Soil-Metal Slip and Thrust-Beam Effects

Two factors that have potentially significant effects on the response of the structure are the conditions of slip at the soil-metal interface and the presence of thrust beams. A specific study was made to evaluate the relative effects of these factors. The program capabilities permitted a comparison of results for these four cases: (a) no slip and no thrust beams, (b) full slip and no thrust beams, (c) no slip and thrust beams, and (d) full slip and thrust beams. As might be expected, the presence of thrust beams decreased the deflection and increased the thrust (in both cases by about 5 percent). The no-slip condition produced less deflection (by about 6 percent) than the full-slip case. However, greater thrust was associated with no slip only at greater cover heights. At lower cover heights the no-slip condition resulted in less thrust (maximum difference about 5 percent). Most large-span arches constructed to date have incorporated thrust beams, and consequently they were incorporated in the model. The true slip condition lies between full and no slip; the full-slip case was chosen for the model as the more conservative one.

Effect of Variations in Soil Poisson's Ratio

The effect of variations in Poisson's ratio of the soil (ν_s) from the value of 0.3 used in the analysis for the design charts has been investigated. Both the deflection and thrust decrease roughly linearly with increasing ν_s, and vice versa. The increase in deflection is between 7 and 10 percent at $\nu_s = 0.25$. The decrease is from 9 to 13 percent at $\nu_s = 0.35$ and 17 to 25 percent at $\nu_s = 0.40$. Thrust is increased by about 6 percent at $\nu_s = 0.2$ and decreased by about 8 percent at $\nu_s = 0.40$.

The value of 0.3 selected for the design charts is on the low side of values likely to be encountered for good-quality structural fills, and so predicted responses will generally be conservative. Further provision of details for exact determination of the effect of variations in ν_s is considered unwarranted due to the unknown nature of its value in most practical situations.

Nonlinearities

Three basic sources of nonlinearity exist in the large-span corrugated-metal arch problem. They are as follows:

1. Incremental construction nonlinearity--the nature of the construction process produces a progressively changing upper boundary and hence a progressively changing system geometry,
2. Material nonlinearity--the strain for a given stress increment changes depending on the prevailing stress conditions, and
3. Geometric nonlinearity--the deformation of the arch under load produces a progressively changing arch shape.

The approach taken whereby the system response is determined for a series of independent incremental uniform load additions permits consideration of the significant aspects of these effects. The crown deformation and springline thrust are determined separately for each discrete layer. In association with each layer, separate values may be assigned for the system upper boundary and the soil modulus. Summation of the layer responses provides a total response that effectively accounts for the nonlinearities. It has been shown (7) that up to working-load levels the influence of geometric nonlinearity is small.

This approach does not allow for variations in soil modulus arising from differential stress conditions throughout the soil mass. In addition there are potential locations of tensile strains, and the assigned modulus would be inappropriate at these locations. Nevertheless, correlations with results from field studies to date (discussed subsequently) appear to indicate that these factors are of little significance for fill loads up to working-load level. In fact, it appears likely that in most instances a discrete-layer approach that accounts for the changing boundary conditions alone will be sufficient for response prediction. Current methods for prediction of soil modulus provide extremely uncertain parameter values, and until these methods are improved, the higher levels of sophistication appear to be unwarranted.

Effect of Footing Width

Footing widths for these structures are generally determined from consideration of the bearing capacity of the foundation soils. Katona and others (7) have investigated the effect of variations in footing width over the range 0.6-1.3 m (2-4 ft) on the structural response and have found it to be negligible. Displacements vary by about 3 percent and thrusts by about 1 percent.

DESIGN GRAPHS

The design graphs are plotted in Figures 5-16 as a series of pairs indicating the dimensionless deflection parameter ($\delta E_s/pR_t$) and the dimensionless thrust parameter (T/pR_t) versus the fill height ratio (H_f/R_t). There are four groups of 12 graphs at respective S/H ratios of 1.2, 1.4, 1.6, and 1.8. Within each group there are six pairs of graphs corresponding to various values of $E_sR_t^3/EI$, and on each graph is one, two, or three curves for values of E_sR_t/EA.

Analysis of a typical large-span corrugated-metal arch structure is presented to illustrate the procedure for use of the graphs (Figure 17). The fill above crown level is divided into five layers. The deformation and thrust response resulting from the placement of each layer of fill above crown level is determined from the graphs as shown in Table 1.

Consider layer 1 (row 1 in Table 1). Placement of this 1.2-m (4-ft) thick layer brings the fill level to 1.2 m above crown level. The total overburden stress applied to the system by this layer is 23.5 kN/m² (490 psf). Approximate the effect of placement of this layer to that of a uniformly distributed load, equivalent to this overburden stress, applied to the system when the fill level is at the mid-height of the layer. That is, 23.5 kN/m² applied with the fill height (H_f) 0.6 m (2 ft) above crown level. The response under this loading is then determined from the design graphs.

For this configuration, $H_f/R_t = 0.10$, $E_sR_t/EA = 7.9 \times 10^{-2}$, $E_sR_t^3/EI = 9.9 \times 10^3$, and S/H = 1.40. From Figures 9e and 9f, $\delta E_s/pR_t = 2.52$ and $T/pR_t = 1.051$; substituting the known values of E_s, p and R_t, δ = 15.9 mm (0.6 in), and T = 152.1 kN/m (867 lbf·in) [or 17.4 MPa (2522 psi) in terms of plate stress].

The procedure is repeated for successive layers and the response due to each layer is added to that

Figure 5. Deflection and thrust parameters for S/H = 1.2(a-d).

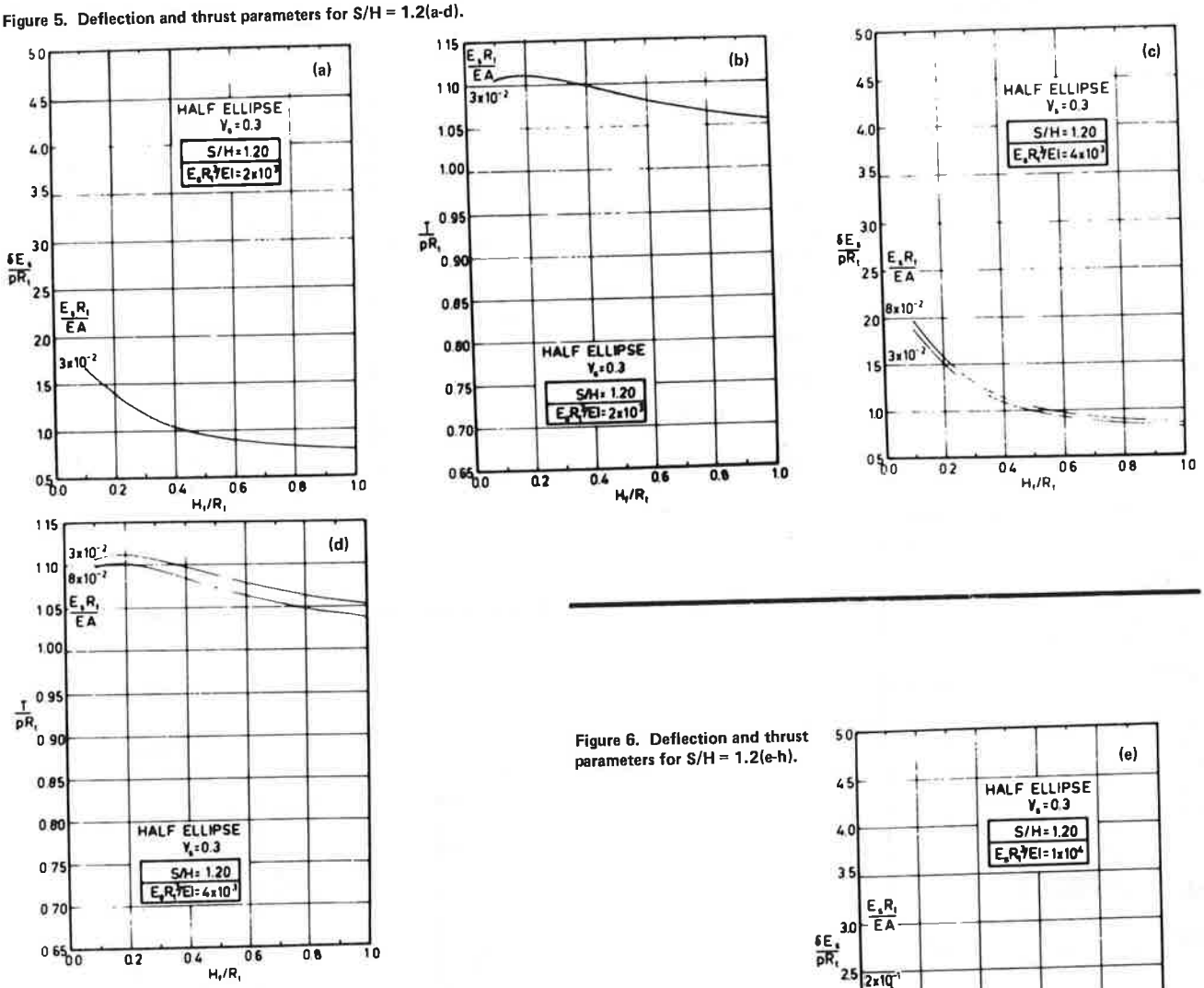

Figure 6. Deflection and thrust parameters for S/H = 1.2(e-h).

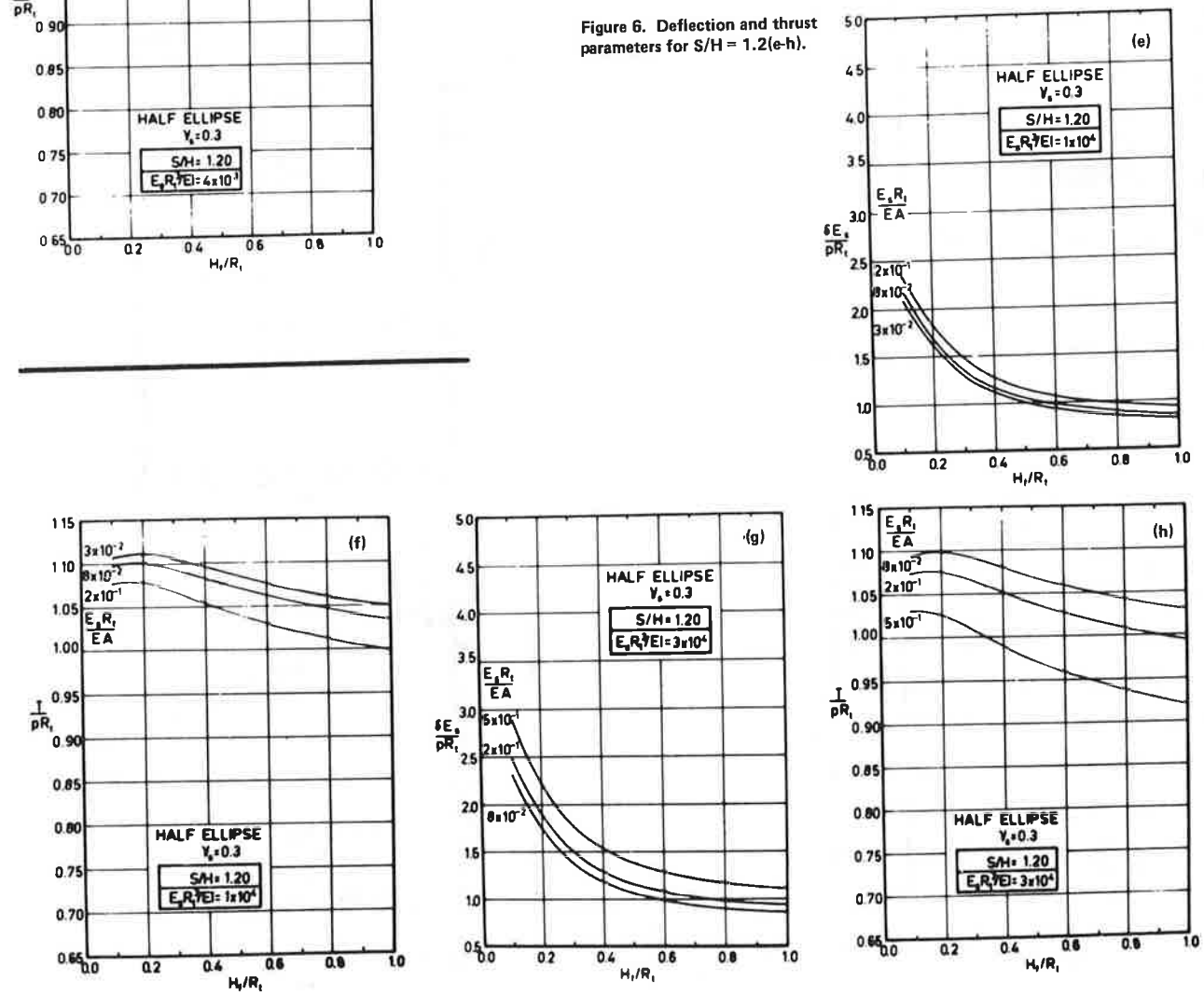

Figure 7. Deflection and thrust parameters for S/H = 1.2 (i-l).

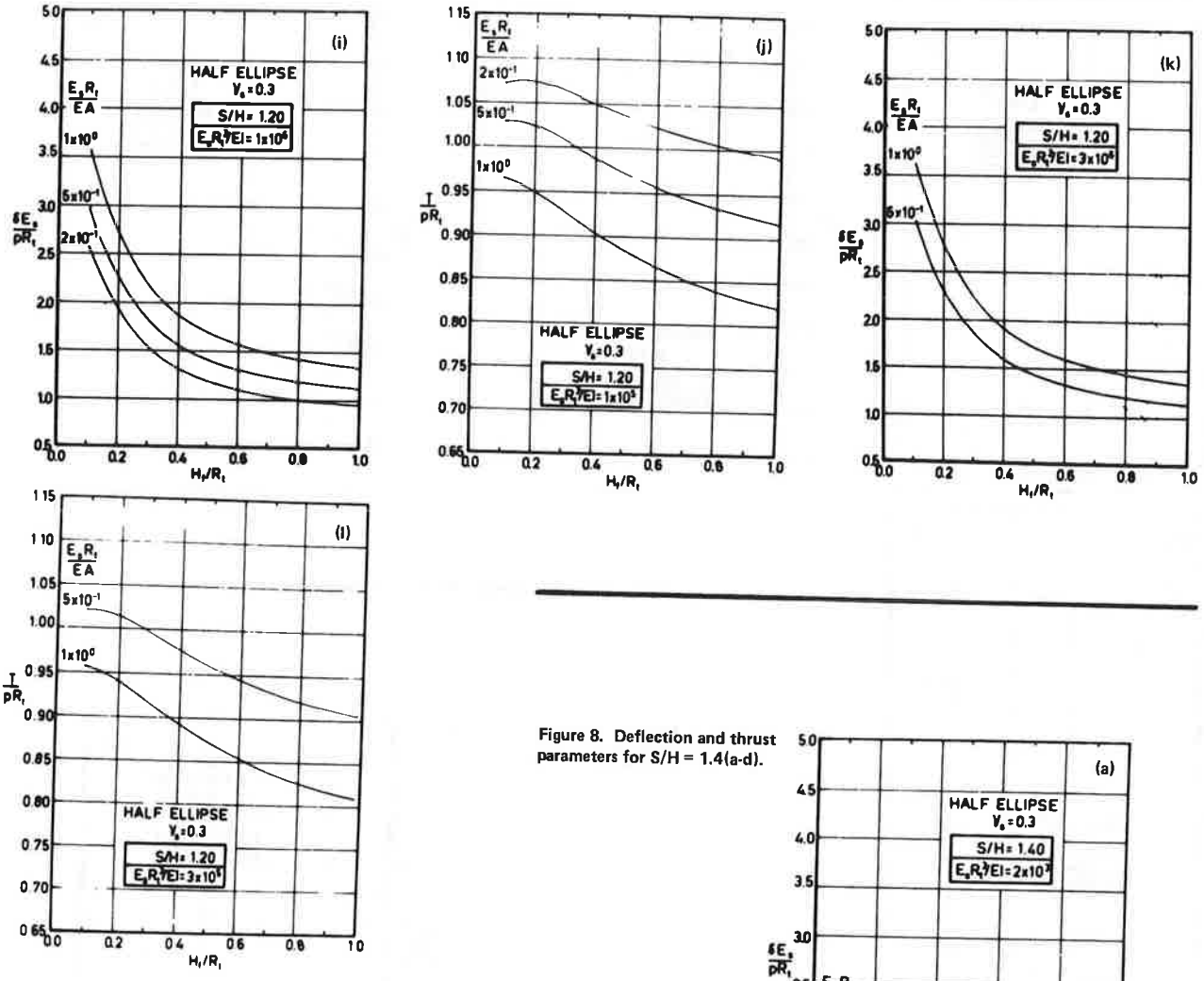

Figure 8. Deflection and thrust parameters for S/H = 1.4(a-d).

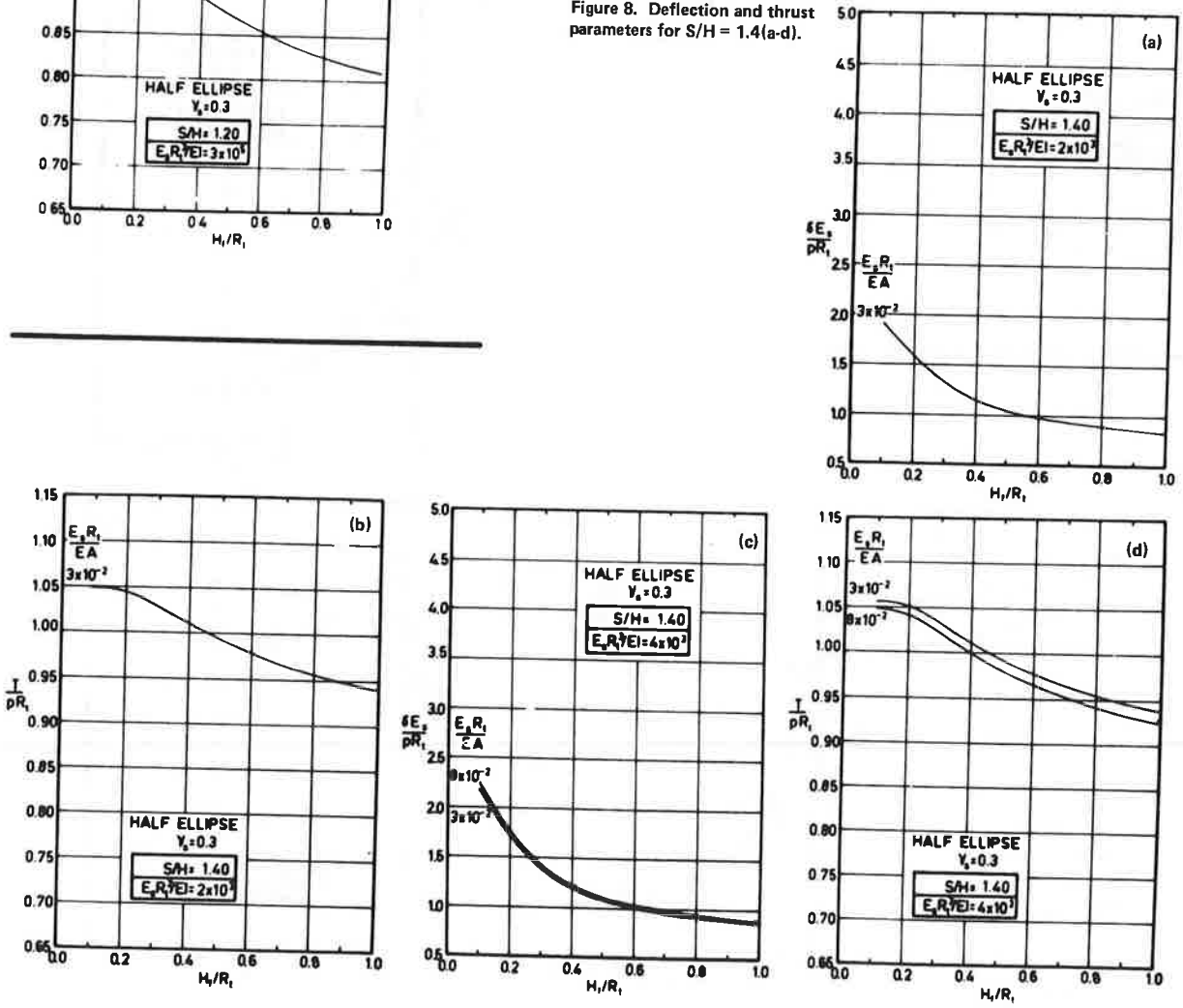

Figure 9. Deflection and thrust parameters for S/H = 1.4(e-h).

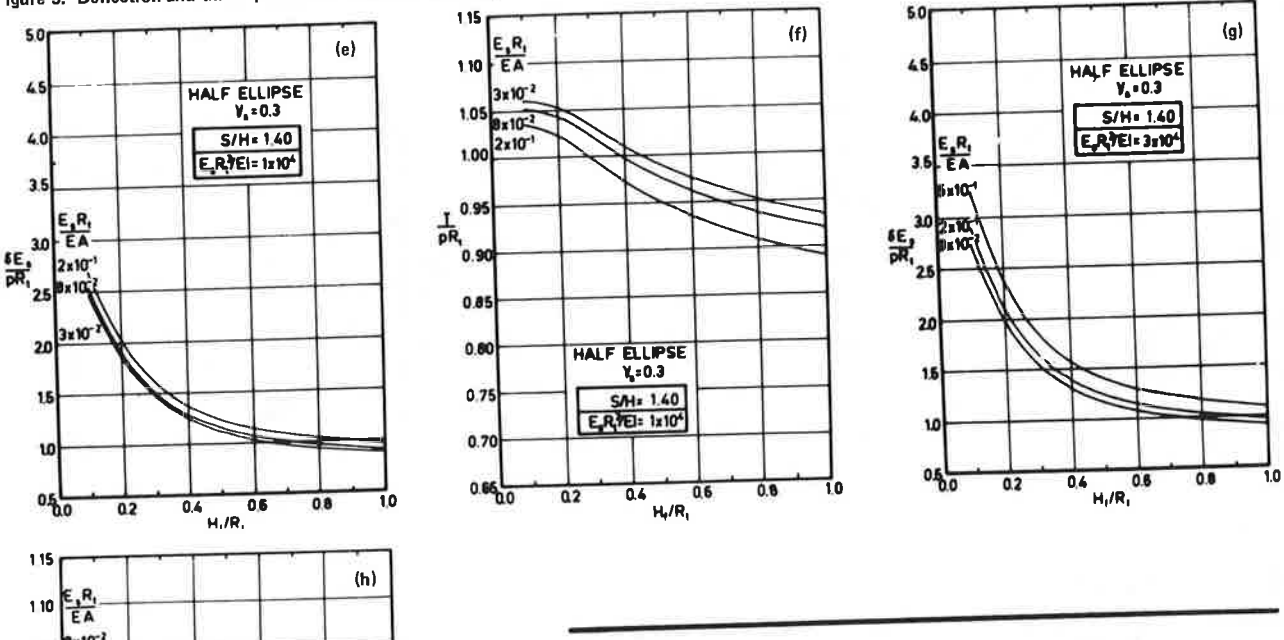

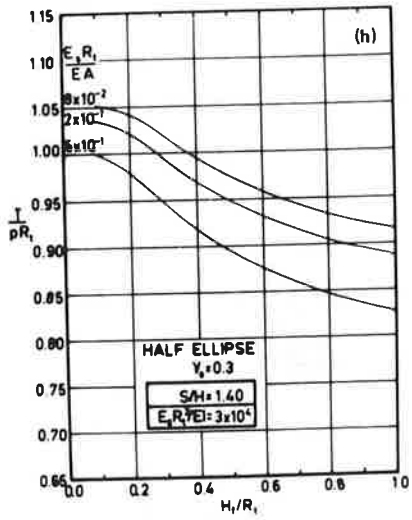

Figure 10. Deflection and thrust parameters for S/H = 1.4(i-l).

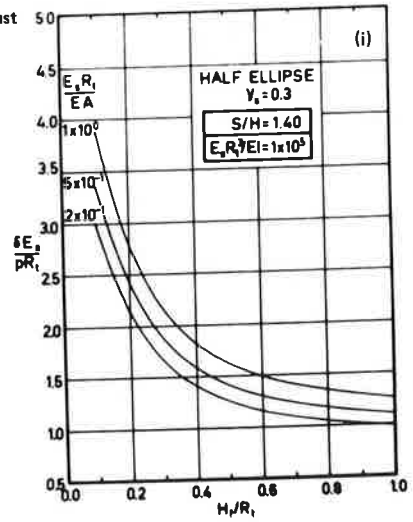

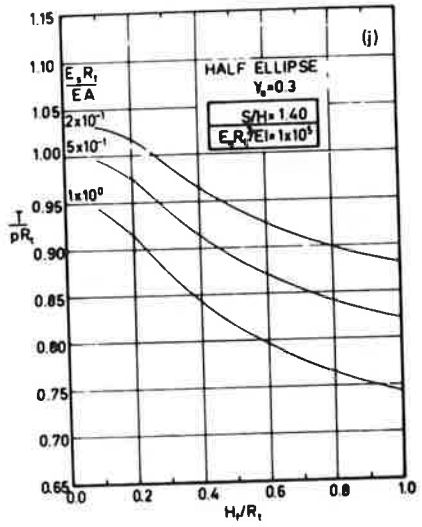

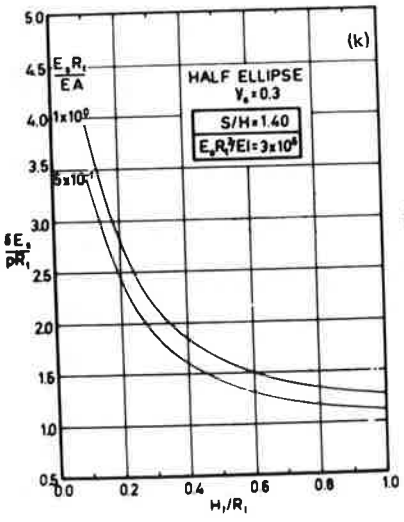

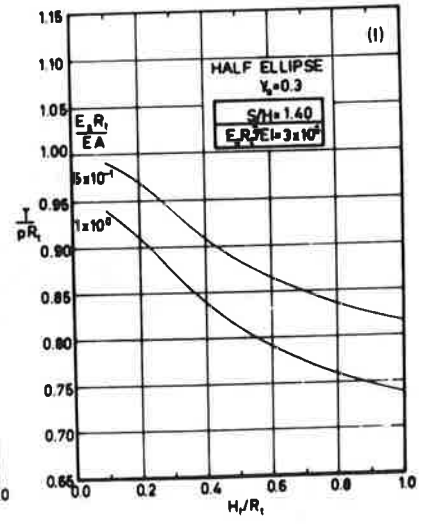

Figure 11. Deflection and thrust parameters for S/H = 1.6(a-d).

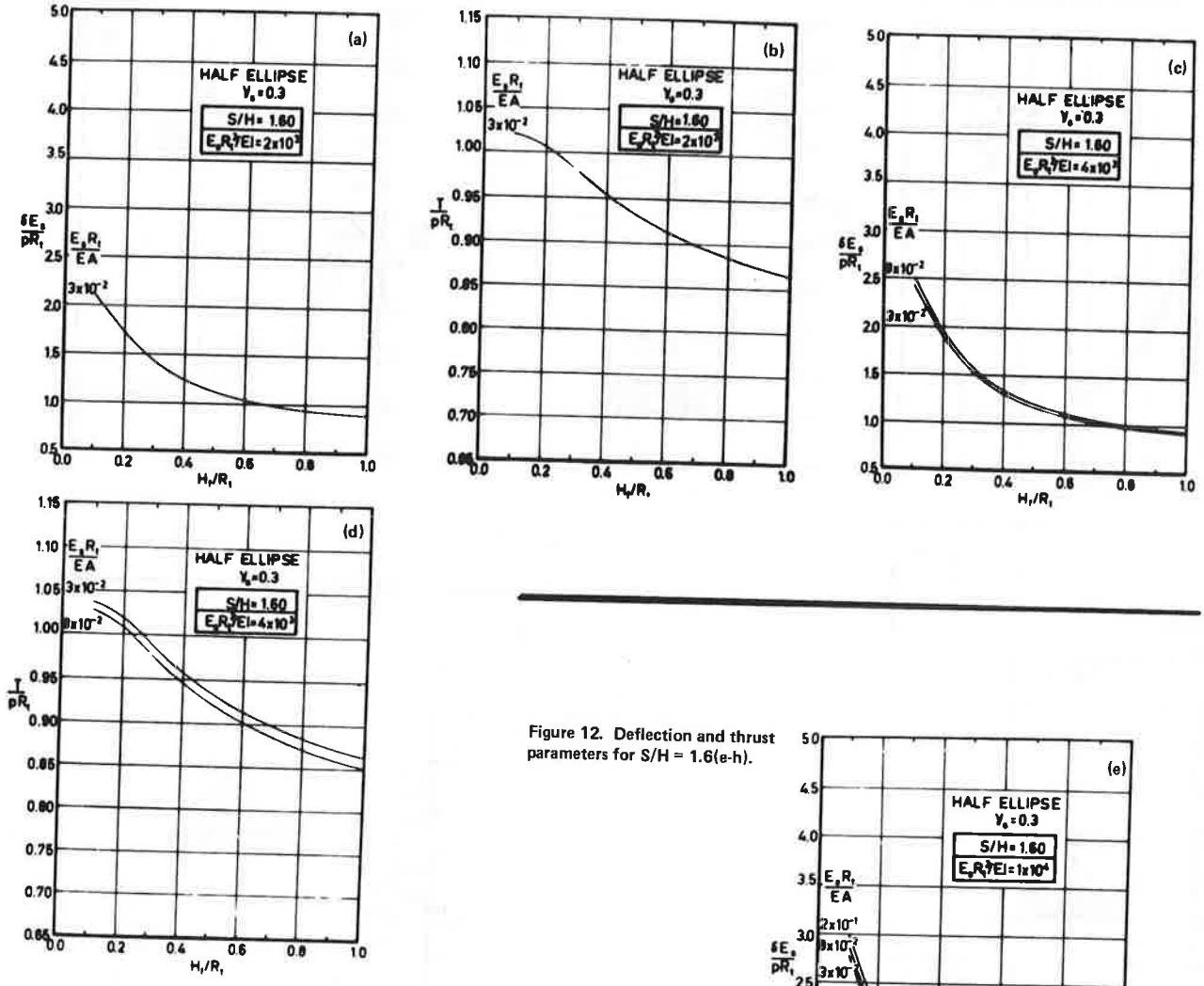

Figure 12. Deflection and thrust parameters for S/H = 1.6(e-h).

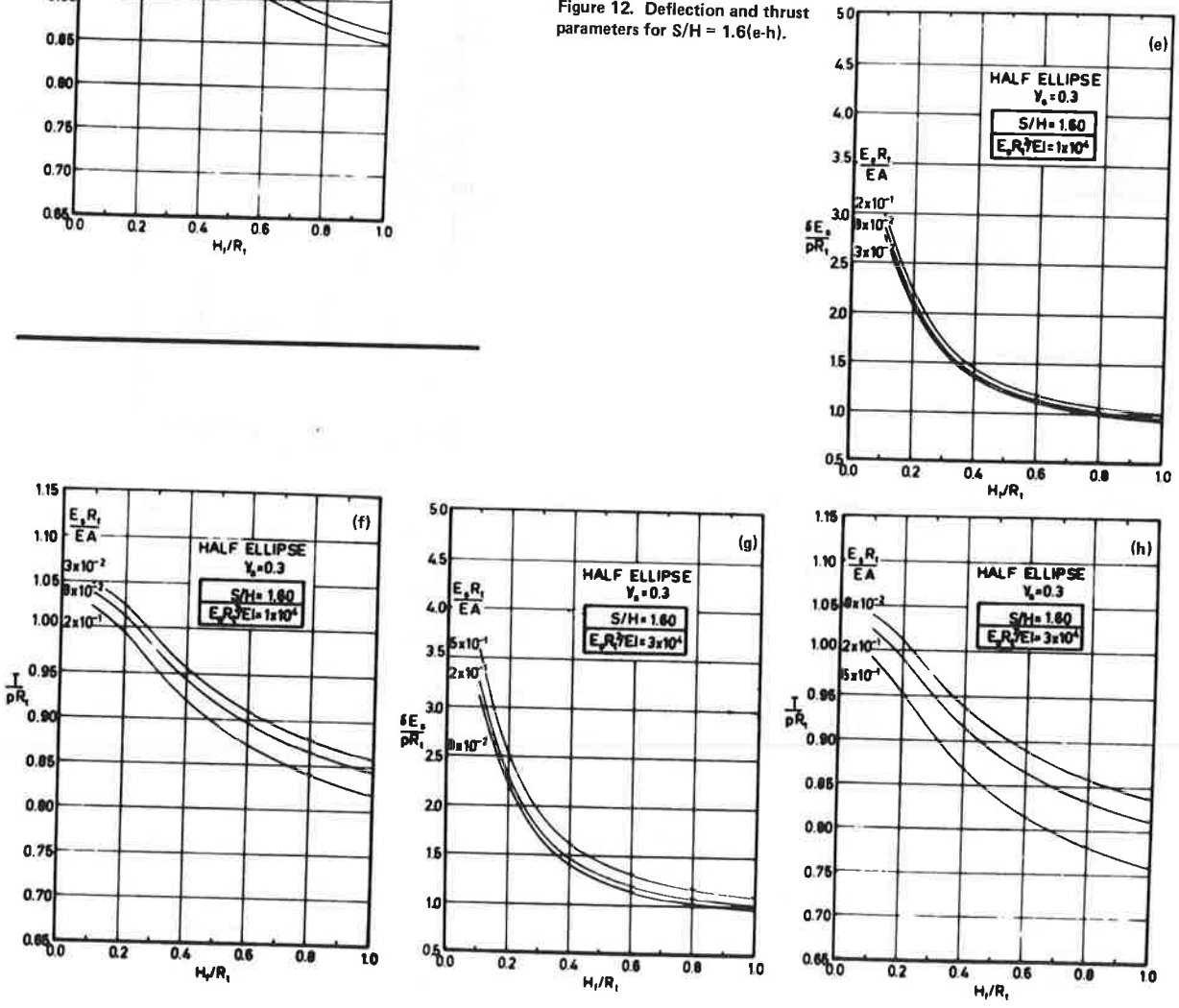

Figure 13. Deflection and thrust parameters for S/H = 1.6(i-l).

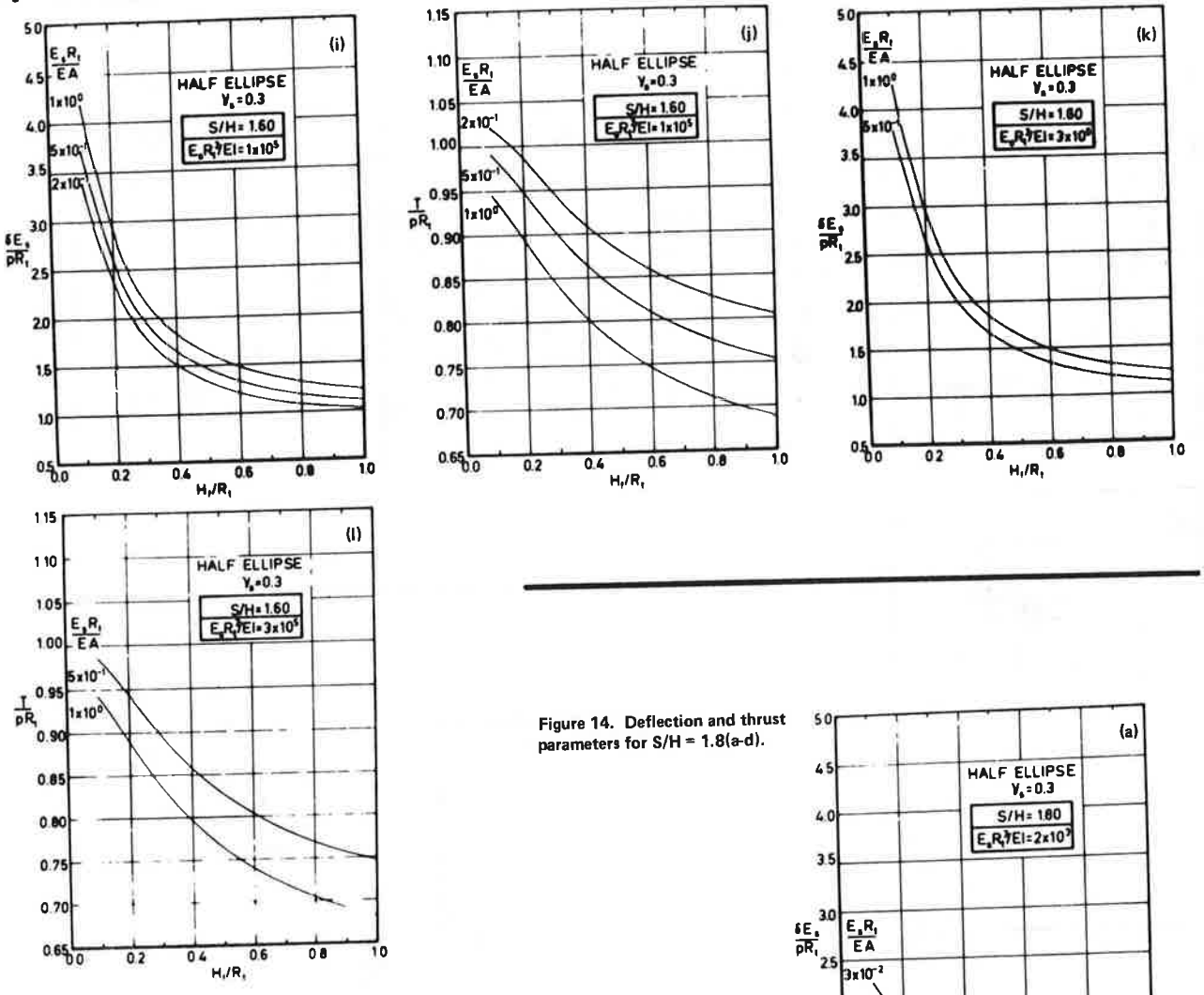

Figure 14. Deflection and thrust parameters for S/H = 1.8(a-d).

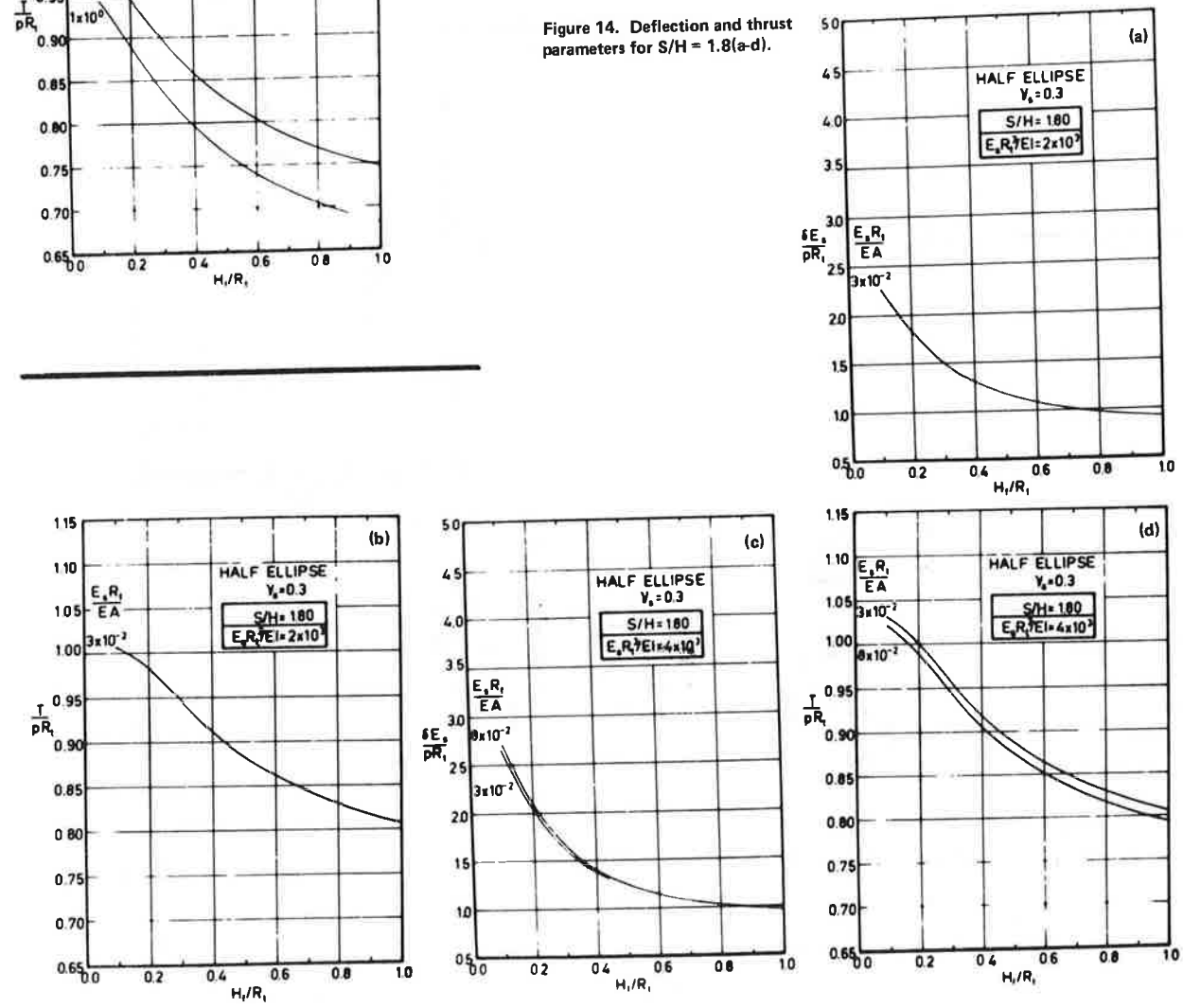

Figure 15. Deflection and thrust parameters for S/H = 1.8(e-h).

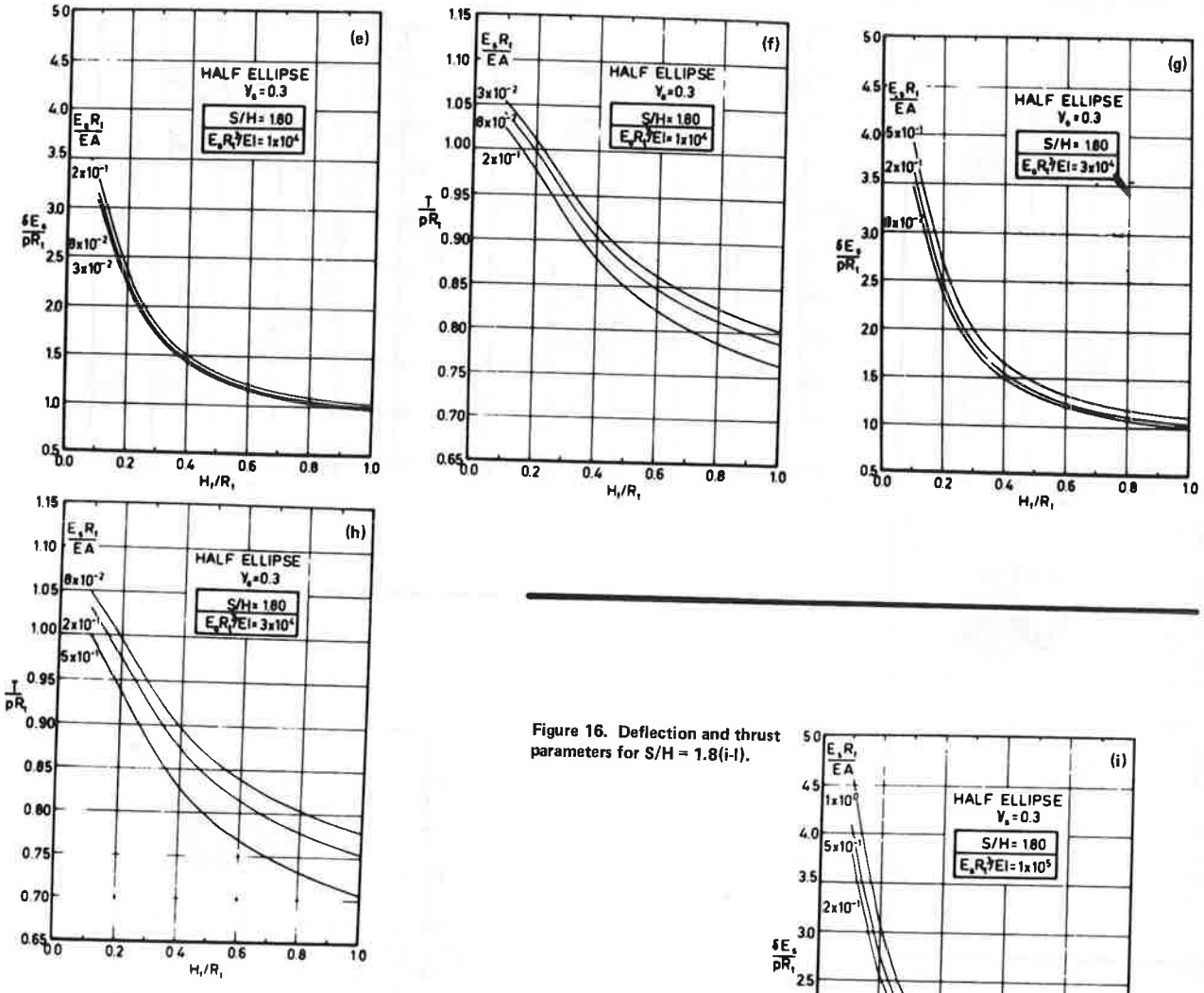

Figure 16. Deflection and thrust parameters for S/H = 1.8(i-l).

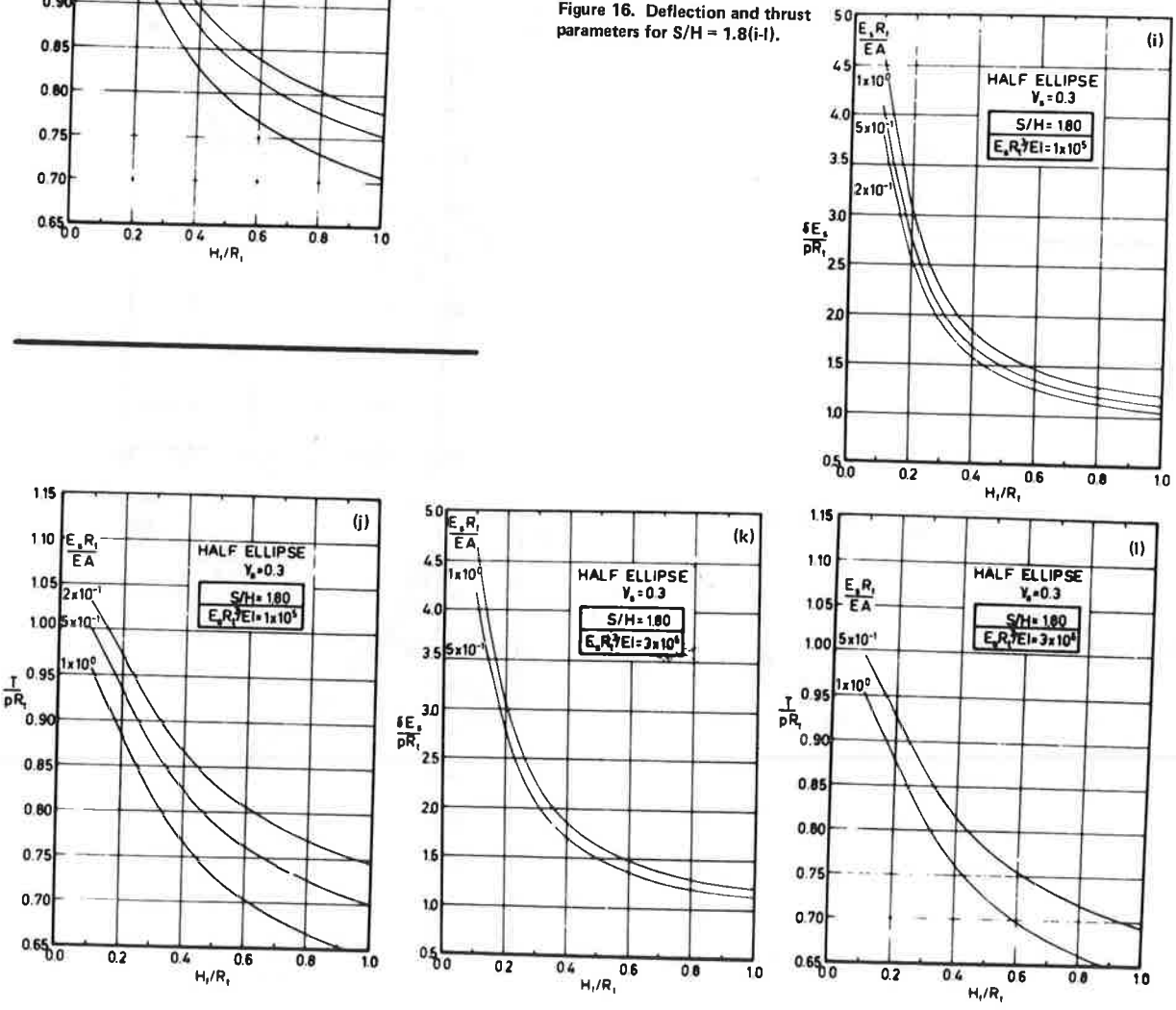

for previous layers to yield the total response for the fill height at the top of each layer. For this typical structure, the predicted total downward crown deflection due to placement of fill above crown level is 45 mm (1.8 in), and the predicted increase in thrust in the steel arch wall at the springline is 715 kN/m (4080 lbf•in).

Figures 18 and 19 show the progressive deflection and thrust, respectively, versus height of fill. It is seen that the deflection response is noticeably nonlinear with respect to fill height, whereas the thrust response is essentially linear. This indicates that deflection is sensitive to the effects of incremental construction, whereas thrust is relatively independent.

Over the linear section of the curves, fewer layers could be used in the analysis to achieve the same result. For example, if the last three layers are combined, the response predictions are altered by less than 1 percent. However, incremental construction nonlinearities are significant in the overall picture. If only a single layer is used, the deflection prediction is almost 20 percent lower than that for five layers.

COMPARISON OF PREDICTIONS WITH FIELD MEASUREMENTS

The validity of this form of analysis as applied to large-span corrugated-metal arch structures is investigated by comparison of predicted and measured performance for a full-scale structure.

Extensive field measurements of the response parameters were taken for a large-span corrugated-metal arch structure built at Leigh Creek, South Australia. Details have been reported by Kay and others (8). The structure consisted of a 12-m (39-ft) span semielliptical arch constructed from 7-mm (5/16-in) corrugated plate, rising 4.7 m (15.4 ft) above tied-back reinforced concrete retaining walls 2.3 m (7.5 ft) high as shown in Figure 20.

The vertical deflection of the crown relative to the footings of the retaining walls and the vertical thrust in the steel arch at the springline on either side were monitored during construction at two sections located at the one-third points along the 26.7-m (87.6-ft) length of the structure. Deflections were measured directly by conventional level surveying, and thrusts were measured indirectly through strain measurements from electrical resistance strain gauges. Continued measurements were only obtained from three of the four relevant strain-gauge stations due to damage at one station during the early stages of construction.

The time for placement of fill above crown level was six days up to a fill height of 1.9 m (6.2 ft). Then there was a break of six weeks before the final 0.2 m (0.7 ft) of fill was placed. During the intervening period, dump trucks of loaded weight about 70 tonnes (77 tons) began crossing the structure.

The soil surrounding the arch consisted of four zones as shown in Figure 20; zone D was the natural foundation soil; zone C, the approach embankments, was constructed from mine spoil with minimal compaction; zones A and B were both constructed with higher-quality material and good compaction. The material used in zone A, closest to the arch, was sand, and in zone B a sandy gravel. The modulus of the zone-A material was determined to be 30 MPa (4350 psi) on the basis of tests on the soil recompacted in the laboratory to the field density. The modulus of the material in zone B was estimated at 30 MPa; that in zone C, 10 MPa (1450 psi); and that in zone D, 40 MPa (5800 psi).

The measured deflection and thrust response are plotted in Figures 21 and 22, respectively, together with response obtained through use of the graphs. Additional data are plotted based on results from a specific finite-element analysis that accounted for the details of the Leigh Creek site such as the tied-back retaining wall, the curved shape of the upper fill boundary, and zones of differing compressibility away from the arch area.

DISCUSSION OF RESULTS

The plotted results in Figures 21 and 22 show much better agreement for prediction of springline thrust

Figure 17. Profile for sample problem.

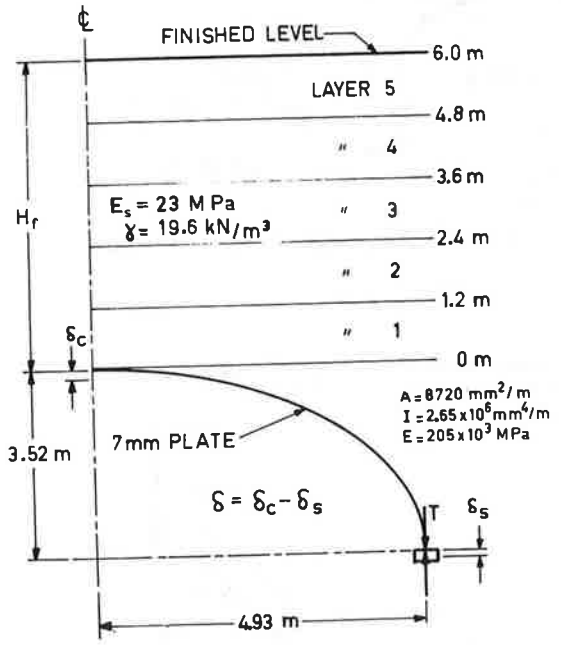

Note: 1 m = 3.3 ft, 1 mm = 0.04 in, 1 MPa = 145 psi, and 1 kN/m³ = 224.8 lbf/ft³.

Table 1. Illustration of procedure.

Layer	Thickness (m)	Fill Level at Top of Layer (m)	Overburden Stress p (kN/m²)	Fill Level at Mid-Height of Layer H_f (m)	H_f/R_t	Data from Graphs		Layer Response	
						$\delta E_s/pR_t$	T/pR_t	δ (mm)	T(kN/m)
1	1.2	1.2	23.5	0.6	0.10	2.52	1.05	15.9	152
2	1.2	2.4	23.5	1.8	0.29	1.50	1.02	9.4	148
3	1.2	3.6	23.5	3.0	0.49	1.15	0.98	7.2	141
4	1.2	4.8	23.5	4.2	0.68	1.01	0.95	6.3	138
5	1.2	6.0	23.5	5.4	0.88	0.93	0.93	5.8	134
Total								44.6	713

Notes: $E_s R_t/EA = 7.9 \times 10^{-2}$; $E_s R_t^3/EI = 9.9 \times 10^3$; S/H = 1.4.
1 m = 3.3 ft; 1 kN/m² = 20 psf; 1 mm = 0.04 in; 1 MPa = 145 psi.

Figure 18. Crown deflection versus fill height for sample problem.

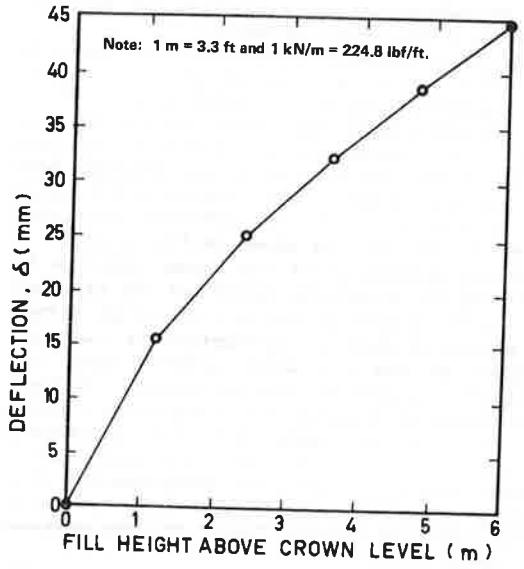

Figure 19. Springline thrust versus fill height for sample problem.

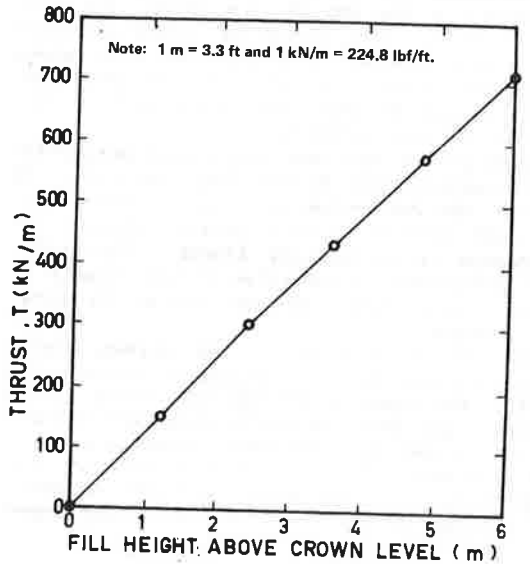

Figure 20. Cross section of instrumented structure at Leigh Creek, South Australia.

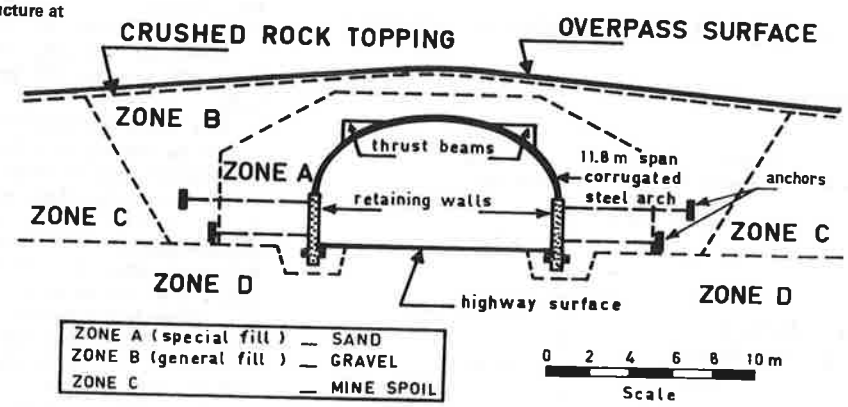

Figure 21. Comparison of results from graphs, specific finite-element program, and field measurements: deflection.

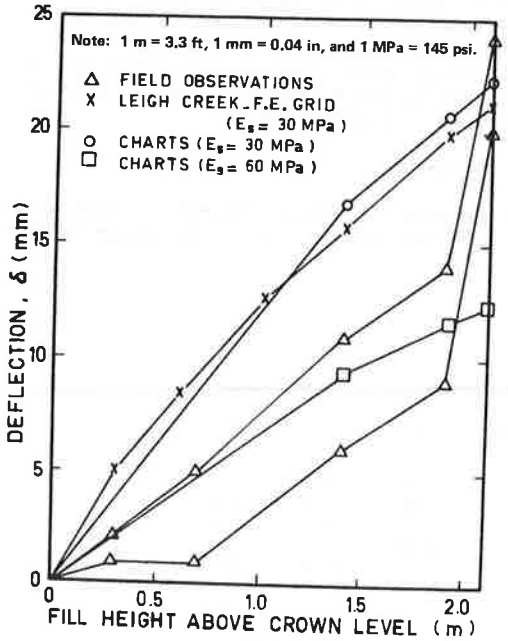

Figure 22. Comparison of results from graphs, specific finite-element program, and field measurements: springline wall stress.

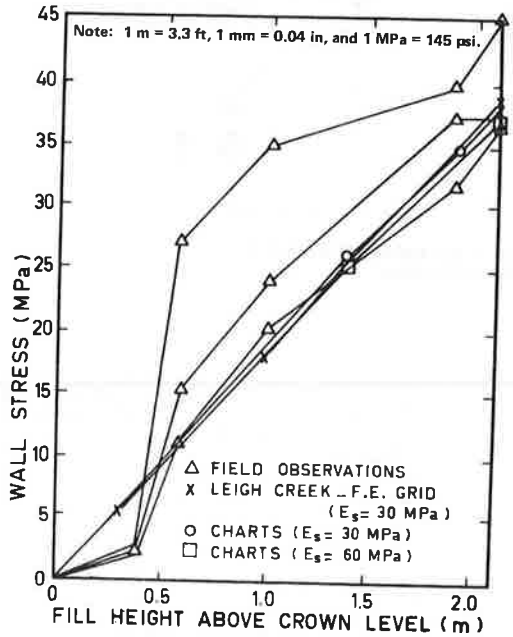

than for prediction of crown deflection. The comparison between results obtained through use of the graphs and those from the specific finite-element analysis was encouraging. For similar values of E_s = 30 MPa the difference in deflection results was 5 percent, whereas the difference in thrust was negligible. This would suggest that the graphs based on the idealized system geometry can be applied to cases where details are somewhat different from the ideal system. Agreement is also demonstrated between predictions of springline thrust and field measurements. Two of the three pertinent strain-gauge results show agreement with predictions within a few percentage points. (It is notable that, for this case, a computation based on the ring compression theory gives a springline thrust that is about 25 percent too low.)

Crown deflection is not predicted with the same level of reliability. Total deflection associated with fill load up to 1.9 m of fill was predicted approximately 70 percent higher than the average measured deflection. (Deflection due to the final 0.2 m of fill could not be separated from that due to heavy-truck loading, according to a paper in this Record by Kay and Flint.) Calculations were based on soil modulus of 30 MPa determined from laboratory triaxial test measurements on the reconstituted granular soil. As demonstrated in Figure 22, a value of E_s = 60 MPa would have given a better estimate. However, it is notable that during the initial fill period over the crown, the measured deflection was small and, in the later stages, the slopes of the as-measured graphs are similar to those of the graphs based on predictions. This performance suggests an explanation in terms of construction procedure. The initial layers of fill placed over the crown do not receive the full compactive effort but are compacted by hand-held equipment. The effect of reduced compaction is considerably greater compressibility of the fill in this zone than the general compressibility, and as the general soil system moves downward with compression of the sidefills, the crown area of the arch, instead of moving downward in a similar fashion, penetrates the zone of more compressible soils. It is likely that improvement to prediction of crown deflection would result if zero deflection were assumed to occur to the level where mechanical compaction has begun. However, further observation of field installations is necessary to justify such an approach.

The effect of the heavy-vehicle live loading on crown deflection is considerable. This is the subject of the paper in this Record by Kay and Flint.

SUMMARY AND CONCLUSION

Graphs have been presented that enable prediction of crown deflection and springline thrust for systems of soil and corrugated-metal arches subject to loads from compacted fills placed above the crown level. Stepwise application of the graphs can minimize errors associated with nonlinear effects for conditions within the working-load range. Comparisons made between predictions based on the graphs and results of field measurements show reasonable agreement.

No recommendations are made concerning criteria for safe design in terms of these aspects of response. Insufficient research on the collapse of such structures has been completed to date to enable suggestions along these lines. Both large-scale testing and analytical work are in progress at the University of Adelaide through which it is hoped to contribute to some preliminary guidelines to a more complete design procedure in the future.

REFERENCES

1. E.T. Selig, J.F. Abel, F.H. Fulhawy, and W.E. Falby. Review of the Design and Construction of Long-Span, Corrugated-Metal, Buried Conduits. FHWA, Interim Rept. FHWA-RD-77-131, 1977.
2. J.G. Abel, G.A. Nasir, and R. Mark. Stresses and Deflections in Soil Structure Systems Formed by Long-Span Flexible Pipe. Department of Civil Engineering, Princeton Univ., Princeton, NJ, Res. Rept. 77-SM-13, 1977.
3. J.M. Duncan. Finite-Element Analysis of Buried Flexible Metal Culvert Structures. Laurits Bjerrum Memorial Volume, March 1975.
4. C.S. Chang, J.M. Espinoza, and E.T. Selig. Computer Analysis of Newtown Creek Culvert. Journal of the Geotechnical Engineering Division of ASCE, Vol. 106, No. GT5, 1980, p. 531.
5. M.G. Spangler. Culverts and Conduits. In Foundation Engineering (G.A. Leonards, ed.), McGraw-Hill, New York, 1962.
6. J.N. Kay and R.C.L. Flint. Design Charts for Large-Span Metal Arch Culverts. Department of Civil Engineering, Adelaide Univ., Australian Road Res. Board, Interim Rept., 1978.
7. M.G. Katona, D.F. Meinhart, T. Orillac, and C.H. Lee. Structural Evaluation of New Concepts for Long-Span Culverts and Culvert Installations. FHWA, Interim Rept. FHWA-RD-79-115, 1979.
8. J.N. Kay, D.L. Avalle, R.C.L. Flint, and C.F.R. Fitzhardinge. Instrumentation of a Corrugated Steel-Soil Arch Overpass at Leigh Creek, South Australia. Proc., 10th Conference of Australian Road Res. Board, Vol. 10, No. 3, 1980, pp. 57-70.

Publication of this paper sponsored by Committee on Subsurface Soil-Structure Interaction.

Analysis of Live-Load Effects in Soil-Steel Structures

GEORGE ABDEL-SAYED AND BAIDAR BAKHT

This paper is based on an analytical study undertaken to complement a previously reported experimental study on live-load effects in the metallic shell of a soil-steel structure. An account of load dispersion above the conduit cannot be made by neglecting the presence of the conduit. The plane-strain approach of analyzing a soil-steel structure is found to be a defensible one even for concentrated loads. It is found that the manner of load dispersion in the longitudinal direction of the conduit is distinctly different from that in the transverse direction. This observation confirms previously reported experimental results. A simplified method, which at best is a crude approximation, can only pick up the maximum thrust values in the conduit wall and is dependent on the con-

than for prediction of crown deflection. The comparison between results obtained through use of the graphs and those from the specific finite-element analysis was encouraging. For similar values of E_s = 30 MPa the difference in deflection results was 5 percent, whereas the difference in thrust was negligible. This would suggest that the graphs based on the idealized system geometry can be applied to cases where details are somewhat different from the ideal system. Agreement is also demonstrated between predictions of springline thrust and field measurements. Two of the three pertinent strain-gauge results show agreement with predictions within a few percentage points. (It is notable that, for this case, a computation based on the ring compression theory gives a springline thrust that is about 25 percent too low.)

Crown deflection is not predicted with the same level of reliability. Total deflection associated with fill load up to 1.9 m of fill was predicted approximately 70 percent higher than the average measured deflection. (Deflection due to the final 0.2 m of fill could not be separated from that due to heavy-truck loading, according to a paper in this Record by Kay and Flint.) Calculations were based on soil modulus of 30 MPa determined from laboratory triaxial test measurements on the reconstituted granular soil. As demonstrated in Figure 22, a value of E_s = 60 MPa would have given a better estimate. However, it is notable that during the initial fill period over the crown, the measured deflection was small and, in the later stages, the slopes of the as-measured graphs are similar to those of the graphs based on predictions. This performance suggests an explanation in terms of construction procedure. The initial layers of fill placed over the crown do not receive the full compactive effort but are compacted by hand-held equipment. The effect of reduced compaction is considerably greater compressibility of the fill in this zone than the general compressibility, and as the general soil system moves downward with compression of the sidefills, the crown area of the arch, instead of moving downward in a similar fashion, penetrates the zone of more compressible soils. It is likely that improvement to prediction of crown deflection would result if zero deflection were assumed to occur to the level where mechanical compaction has begun. However, further observation of field installations is necessary to justify such an approach.

The effect of the heavy-vehicle live loading on crown deflection is considerable. This is the subject of the paper in this Record by Kay and Flint.

SUMMARY AND CONCLUSION

Graphs have been presented that enable prediction of crown deflection and springline thrust for systems of soil and corrugated-metal arches subject to loads from compacted fills placed above the crown level. Stepwise application of the graphs can minimize errors associated with nonlinear effects for conditions within the working-load range. Comparisons made between predictions based on the graphs and results of field measurements show reasonable agreement.

No recommendations are made concerning criteria for safe design in terms of these aspects of response. Insufficient research on the collapse of such structures has been completed to date to enable suggestions along these lines. Both large-scale testing and analytical work are in progress at the University of Adelaide through which it is hoped to contribute to some preliminary guidelines to a more complete design procedure in the future.

REFERENCES

1. E.T. Selig, J.F. Abel, F.H. Fulhawy, and W.E. Falby. Review of the Design and Construction of Long-Span, Corrugated-Metal, Buried Conduits. FHWA, Interim Rept. FHWA-RD-77-131, 1977.
2. J.G. Abel, G.A. Nasir, and R. Mark. Stresses and Deflections in Soil Structure Systems Formed by Long-Span Flexible Pipe. Department of Civil Engineering, Princeton Univ., Princeton, NJ, Res. Rept. 77-SM-13, 1977.
3. J.M. Duncan. Finite-Element Analysis of Buried Flexible Metal Culvert Structures. Laurits Bjerrum Memorial Volume, March 1975.
4. C.S. Chang, J.M. Espinoza, and E.T. Selig. Computer Analysis of Newtown Creek Culvert. Journal of the Geotechnical Engineering Division of ASCE, Vol. 106, No. GT5, 1980, p. 531.
5. M.G. Spangler. Culverts and Conduits. In Foundation Engineering (G.A. Leonards, ed.), McGraw-Hill, New York, 1962.
6. J.N. Kay and R.C.L. Flint. Design Charts for Large-Span Metal Arch Culverts. Department of Civil Engineering, Adelaide Univ., Australian Road Res. Board, Interim Rept., 1978.
7. M.G. Katona, D.F. Meinhart, T. Orillac, and C.H. Lee. Structural Evaluation of New Concepts for Long-Span Culverts and Culvert Installations. FHWA, Interim Rept. FHWA-RD-79-115, 1979.
8. J.N. Kay, D.L. Avalle, R.C.L. Flint, and C.F.R. Fitzhardinge. Instrumentation of a Corrugated Steel-Soil Arch Overpass at Leigh Creek, South Australia. Proc., 10th Conference of Australian Road Res. Board, Vol. 10, No. 3, 1980, pp. 57-70.

Publication of this paper sponsored by Committee on Subsurface Soil-Structure Interaction.

Analysis of Live-Load Effects in Soil-Steel Structures

GEORGE ABDEL-SAYED AND BAIDAR BAKHT

This paper is based on an analytical study undertaken to complement a previously reported experimental study on live-load effects in the metallic shell of a soil-steel structure. An account of load dispersion above the conduit cannot be made by neglecting the presence of the conduit. The plane-strain approach of analyzing a soil-steel structure is found to be a defensible one even for concentrated loads. It is found that the manner of load dispersion in the longitudinal direction of the conduit is distinctly different from that in the transverse direction. This observation confirms previously reported experimental results. A simplified method, which at best is a crude approximation, can only pick up the maximum thrust values in the conduit wall and is dependent on the con-

figuration of the design vehicle. The Ontario Highway Bridge Design Code method is found to be applicable only when there is a pair of closely spaced axles on the embankment. When the governing load is made up of a single axle, another simplified method is proposed.

Underground conduits of relatively large spans [up to 55 ft (16.75 m)] are being built in increasing number for use as culverts, bridges, and tunnels. It has been usual in the past to idealize these structures for analysis by plane-strain transverse slices of the metallic shell and the surrounding soil envelope. The inherent assumption in this kind of idealization is that load effects due to both dead and live loads do not vary along the conduit. This assumption may be axiomatic for dead loads but needs a rational scrutiny for live loads, especially because of the trend for larger spans and shallow depths of cover, which together tend to make live-load effects a fairly large proportion of the total load effects in the metallic shell.

This paper is based on the results of an analytical study of the distribution of concentrated live loads in soil-steel structures. The study, which was undertaken at the University of Windsor in cooperation with the Ministry of Transportation and Communications of Ontario, complements the experimental work reported elsewhere (1). In this study the dispersion of concentrated loads through the soil is examined by taking into account the different geometric conditions along the conduit axis and in the transverse direction. A simple analysis procedure, similar to those currently employed, is developed to realistically assess live-load effects in the metallic shell.

LIVE-LOAD DISPERSION IN SOIL

Several solutions are available in published literature to calculate the stress distribution (or load dispersion) in soil due to concentrated point or line loads. Some of the various assumed soil characteristics and boundary conditions relevant to the different solutions can be summarized as follows (2,3):

1. Homogeneous isotropic half-space: The soil is assumed to be of semiinfinite extent, and its modulus of elasticity (E_s) is considered to be constant.

2. Homogeneous isotropic finite layer: The soil is assumed to have finite depth and to be supported by a rigid subsurface.

3. Nonhomogeneous half-space: The soil is again assumed to be of semiinfinite extent, but its modulus of elasticity varies with depth according to the following relationship:

$$E_s = E_0 \cdot (z/z_0)^{\lambda} \quad (1)$$

where E_0 is the modulus of elasticity at a depth $z = z_0$, z is the depth of soil under consideration, and λ is a constant ≥ 0.

4. Cross-anisotropic half-space: The soil is assumed to be of infinite extent and its degree of anisotropy is expressed by the ratio of the moduli of elasticity in the horizontal and vertical directions (E_h/E_v), the ratio of the shear modulus to the vertical modulus of elasticity (G/E_v), and the Poisson's ratios μ_h and μ_{hv}.

Solutions based on the above assumed conditions give widely differing patterns of stress distribution in the soil, as shown in Figure 1, which shows the variation of $I_{\sigma z}$ corresponding to a point load (P). Vertical stress (σ_v) is given by the following relationship:

$$\sigma_v = I_{\sigma z} P/z^2 \quad (2)$$

where z is the depth at which the stress is investigated. Figure 1 is instructive in studying the various factors that have a significant influence on load dispersion in soil.

A comparison of the $I_{\sigma z}$ values corresponding to the assumptions of "isotropic half-space" and "isotropic finite layer" (in which the stresses are calculated at the level of the supporting surface) shows that the peak vertical stress in the former case is considerably less than that in the latter case; thus the significance of the relative stiffness of the underlying layer on load dispersion is emphasized. It can be readily concluded that the insertion of a conduit in a half-space would have the effect of changing the soil stiffness, and therefore the load dispersion above the conduit cannot be justifiably obtained by neglecting the presence of the conduit, i.e., by assuming the soil to be homogeneous.

Figure 1. Pressure distribution under concentrated load.

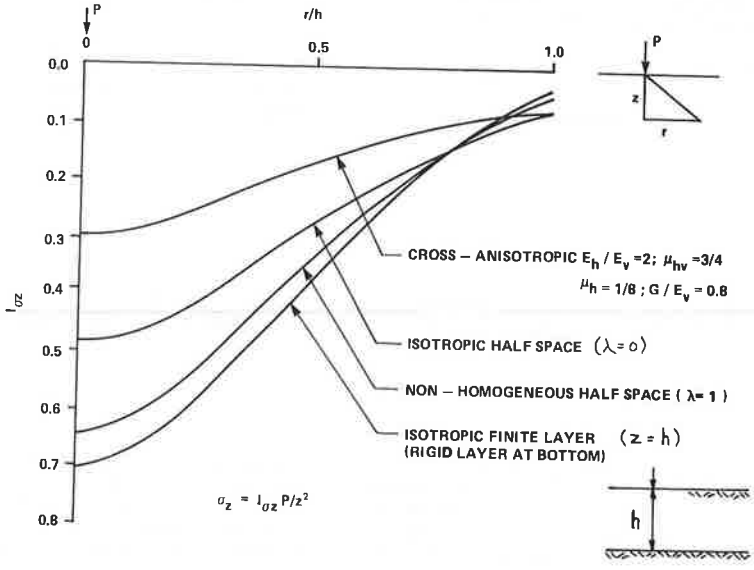

Figure 2. Load dispersion through soil.

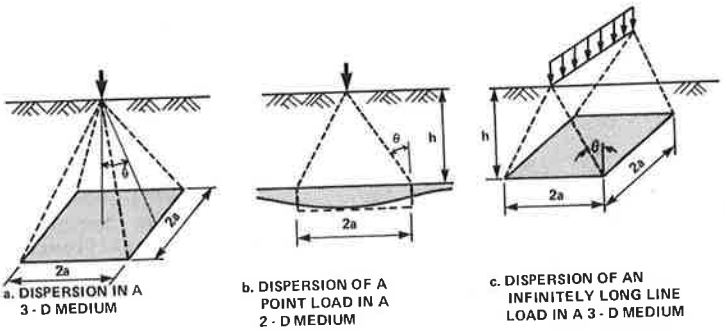

Table 1. Comparison of different approaches for obtaining equivalent areas.

Soil Idealization and Boundary Condition	$\alpha = h/a$			$\theta°$		
	Approach 1	Approach 2	Difference (%)	Approach 1	Approach 2	Difference (%)
Isotropic half-space	1.37	1.27	7.4	35.9	38.1	5.6
Isotropic finite layer	1.66	1.87	1.6	31.0	31.4	1.3
Nonhomogeneous half-space						
$\lambda = 1$	1.60	1.50	6.2	32.0	33.6	4.8
$\lambda = 2$	1.79	1.69	5.1	29.3	30.5	3.9
$\lambda = 3$	1.96	1.87	4.6	27.0	28.1	4.1

Note: Approach 1 corresponds to the three-dimensional analysis and Approach 2 to the two-plane method.

Figure 3. Load dispersion above conduit.

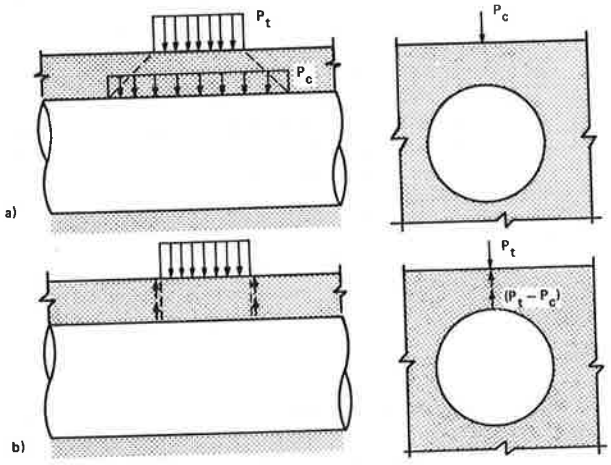

From Figure 1 it can also be observed that the vertical stress concentration in the homogeneous soil is lower than that in the nonhomogeneous soil in which the modulus of elasticity increases linearly with depth. The decrease in the stress concentration is also caused by the increase of the shear modulus of the soil.

LOAD DISPERSION IN SOIL BY PLANE STRAIN

When an elastic half-space is subjected to a concentrated load P at the boundary, the vertical stress under the load at a plane parallel to the boundary can, for the sake of convenience, be assumed to be uniformly distributed over an effective 2ax2a area. This equivalent area is such that its product with the peak vertical stress is equal to the load P. Let the depth of the level at which the equivalent area is sought be denoted by h and the angle of dispersion to the vertical by θ (Figure 2).

The equivalent area under a point load can be obtained by considering dispersion in the three-dimensional medium, as shown in Figure 2a. Alternatively, the load can first be dispersed in only one plane (Figure 2b) and then the resulting maximum load per unit width acting at the depth h is reapplied as a line load to the boundary and dispersed in the perpendicular plane (Figure 2c). The latter approach has often been applied for establishing equivalent live loads on the plane-strain slice of the soil-steel structures, and the former approach has often been the basis of simplified methods of analyzing live-load effects in the metallic shell (1). The following exercise was undertaken to establish the degree of error involved if the latter approach were adopted.

Equivalent distributed areas corresponding to a single concentrated load were obtained for various idealized soil media and different boundary conditions according to the two above-mentioned procedures. Values of $\alpha = h/a$ and θ obtained by the two procedures are compared in Table 1 for different cases. It can be seen that the procedure of distributing the load first in one plane and then in another produces results that are not significantly different from those obtained by the corresponding three-dimensional analysis; thus the use of the two-plane analysis approach in the analysis of soil-steel structures is justified.

As observed by Bakht (1), the dispersion of a concentrated load in the longitudinal direction of a conduit is significantly different from that in the transverse direction. An account of this different dispersion pattern can be made by first distributing the load in the longitudinal direction and then applying the dispersed load on the transverse slice as shown in Figure 3a; alternatively, as shown in Figure 3b, the full concentrated load can be applied directly at the top of the soil along with subsurface negative upward forces accounting for the load dispersed to the adjacent slices in the longitudinal direction. The two methods were used to analyze two soil-steel structures described by Bakht (1) by the plane-strain finite-element method. As shown in Table 2, the difference between the thrust and moment predictions by the two methods does not amount to more than 5 percent. This comparison

further justifies the use of the two plane-strain approaches to live-load analysis of soil-steel structures.

LOAD DISPERSION ALONG CONDUIT

It is assumed that the problem of load dispersion along the conduit can be independently solved by isolating a longitudinal unit-width slice of soil above the crown. As shown in Figure 4, the support provided by the metallic shell is simulated by uniformly spaced linear springs. The spring stiffness K, which represents the ratio of pressure to deflection at the crown, was found by analysis of soil-steel structures to be of the order of 60 psi/in. It was decided to scan values of K between 30 and 300 psi/in for the study discussed below.

The plane-strain finite-element method (4) was used to analyze the longitudinal slice for the two load cases of direct wheel pressure as shown in Figure 4. The analyses are based on a nonlinear soil model developed by Wong and Duncan (5). Three types of soil are considered for which the properties are given in Figure 5a. Figure 5a also shows the distribution of σ_v corresponding to load case 1 (Figure 4) for the three types of soil. As expected, the peak value of σ_v increases with the decrease of soil stiffness. Also, as shown in Figure 5b, the peak value of σ_v increases with the increase of the spring stiffness.

The load dispersion in the longitudinal direction can be approximately represented by an equivalent length that, as shown in Figure 6, has a projection of length (a) beyond the extremity of the surface load. For the two load cases mentioned earlier and considering soil type B (Figure 5a), the relationship between $\alpha = h/a$ and K is plotted in Figure 6. It can be seen that the depth of cover has relatively little influence on this relationship. It is noted that the current simplified methods of the American Association of State Highway and Transportation Officials (AASHTO) (6) and the Ontario Highway Bridge Design Code (OHBDC) (7) do not account for the stiffness of the metallic shell. For the former, the value of α is 1.14 and for the latter, 2.0. These two values of α are compared in Figure 6 with those obtained by the finite-element analysis. It can be observed that both methods give results that are distinctly different from those of the finite-element analysis. However, for values of K that are usually encountered in practice, the OHBDC method is in error on the safe side. It is noted that the effect of error in estimation of α is reduced in practice because of the finite length of the concentrated load.

The relationship between α and K can be represented in hyperbolic form:

$$\alpha = K/(c + bK) \tag{3}$$

where c and b are constants depending on the properties of soil. Equation 3 can be rewritten in the form of a linear relationship between K and (K/α):

$$(K/\alpha) = C + bK \tag{4}$$

This linear relationship is confirmed in Figure 7, which shows that although the relationship between α and (K/α) is independent of the depth of cover, it still depends on the configuration of applied loading. For given soil properties and load cases, it is possible to determine values of constants b and c from graphs such as that shown in Figure 7. From values obtained of b and c, charts could be prepared to readily provide the values of constants and thence the value of α from Equation 3. However, for everyday designs the process would still be too tedious and not worth the effort, and it is recommended that a value of α equal to 2.0 be used for all practical purposes.

Table 2. Comparison between analytical results by using methods a and b, Figure 3, for live load.

Beam Element No.	Thrust (lbf/in)				Moment (lbf·in/in)	
	White Ash Creek Structure[a]		Adelaide Creek Structure[a]		Adelaide Creek Structure[a]	
	Loading a	Loading b	Loading a	Loading b	Loading a	Loading b
1	-16.6	-11.5	10.8	14.5	5.9	6.0
3	-19.0	-16.2	-19.9	-19.0	1.0	1.3
5	-41.2	-41.1	-59.0	-59.8	-26.0	-26.6
7	-87.5	-89.7	-77.5	-79.0	6.5	5.2
9	-156.7	-161.1	-84.8	-86.6	1.8	0.6
11	-239.3	-246.0	-235.3	-242.3	-60.3	-65.5
13	-239.3	-246.0	-235.2	-242.2	4.9	3.9
15	-298.9	-307.8	-321.6	-332.1	69.4	72.9
17	-299.0	-307.8	-321.7	-332.2	84.1	87.1
19	-337.2	-350.1	-385.9	-400.6	97.3	100.0
21	-337.2	-350.2	-385.9	-400.6	90.0	93.6
23	-289.7	-307.0	-399.9	-420.5	82.4	86.9
25	-289.6	-307.0	-399.8	-420.3	41.6	45.0
27	-150.7	-167.1	-201.2	-218.6	4.6	7.1
29	-149.7	-166.1	-200.5	-217.8	-67.2	-70.4

[a]For details of structure, see report by Bakht (1).

LOAD DISPERSION IN SPAN DIRECTION

After the approximate equivalent live load on the plane-strain slice of a soil-steel structure had been established, the slice was analyzed by a special-purpose plane-strain finite-element program incorporating high-order nonlinear elements to model the soil, beam elements to simulate the metallic shell, and nonlinear interface elements to represent the bond between the soil and the metallic shell (4). Effects of the construction procedure were taken into account by an iterative process in which the equivalent of compaction loads was applied at various backfill levels. Structures tested by Bakht

Figure 4. Idealization for load dispersion along conduit axis.

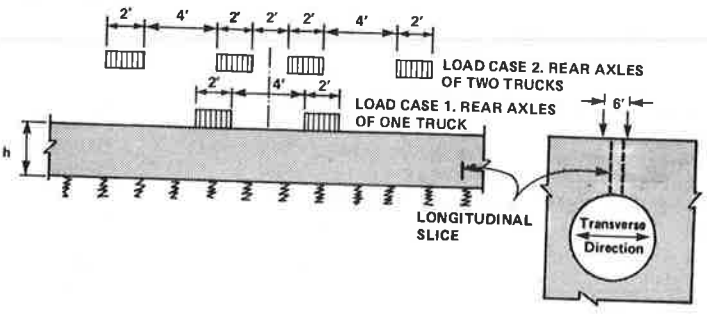

Figure 5. Effect of soil type and spring constants on load dispersion through soil along conduit.

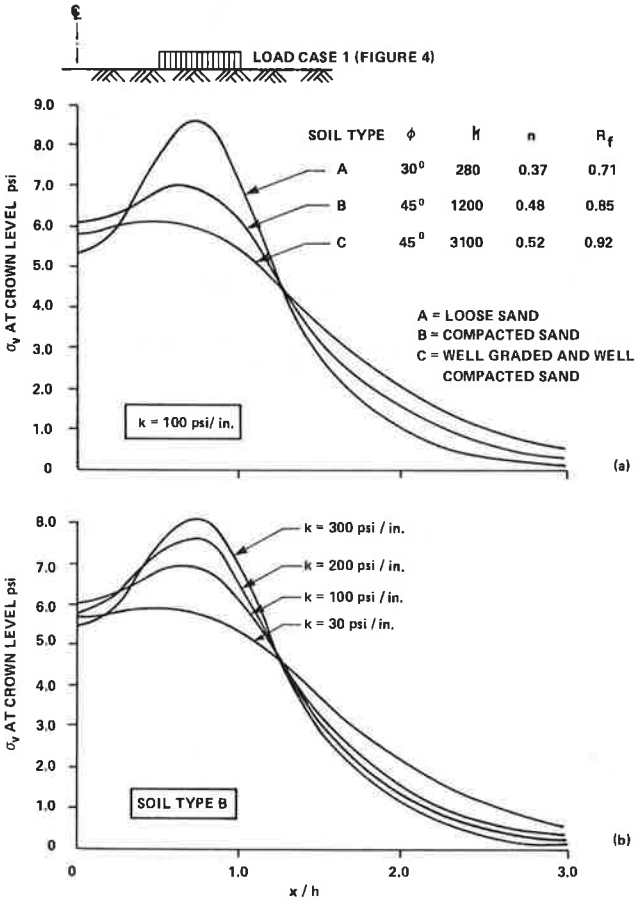

Figure 6. Comparison of various methods accounting for load dispersion along conduit.

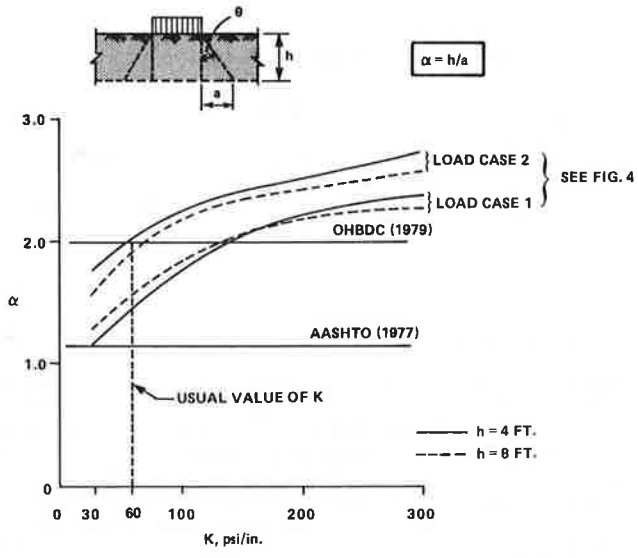

(1) were analyzed for live-load effects by the above procedure. The correlation between the analytically obtained and observed values of conduit wall thrust and moments, although not quite perfect, was reasonably good. Comparisons between the analytical and

Figure 7. Relationship between K and (K/α).

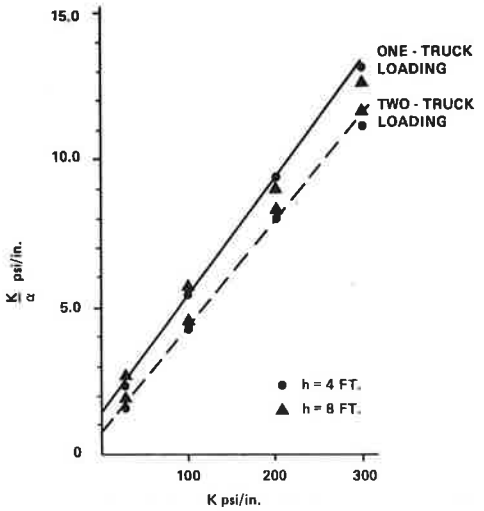

observed values of the conduit wall thrust are shown in Figure 8 for two load cases on one structure. It can be seen that with the analytical approach it is possible to reasonably predict the peak values of thrust and also the pattern of thrust around the conduit.

From the tests and analyses it was observed that the peak value of thrust due to live load takes place at the shoulders and that this value is maximum when the loads are placed symmetrically to the crown. The study described later was therefore limited to only symmetrical load cases.

Analytical results showed that the vertical soil pressures at crown level due to concentrated loads at the embankment level were fairly widely distributed across the span, as shown in Figure 9. This observation confirms the experimental findings of Bakht (1), which indicated that a concentrated load disperses over a greater length in the transverse direction of the conduit than it does along the conduit.

An insight into the composite action between the soil and the metallic shell can be obtained by studying the conduit wall thrust and soil stresses as obtained from the finite-element analysis and shown in Figure 10. It can be seen that with the exception of soil above the conduit, the maximum soil stresses are more or less tangential to the conduit wall. The variation in conduit wall thrust can be attributed to the bending action of the composite arch made out of the metallic shell and the surrounding soil envelope.

SIMPLIFIED METHOD

Although the finite-element method has been shown above to be capable of realistically predicting live-load thrust in the conduit wall, its use for everyday design is not recommended because of its complexity. A more appropriate role for the finite-element method would be in studying the behavior of the structure and in establishing the validity of existing simplified methods, such as those described by Bakht (1).

The nonlinear finite-element method, discussed above and described by Hafez (4), was used to validate the AASHTO (6) and the revised OHBDC methods described by Bakht (1). According to the AASHTO method, conduit wall thrust (T_L) due to live load is given by the following:

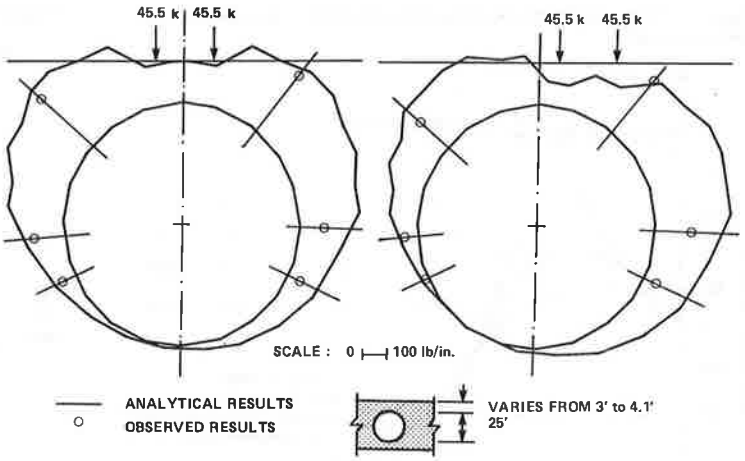

Figure 8. Comparison of observed and analytical thrust in conduit wall of soil-steel structure.

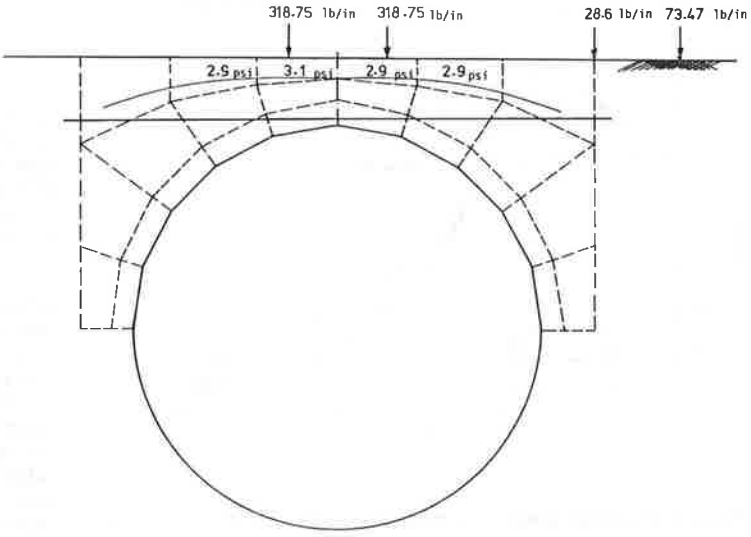

Figure 9. Vertical pressure in soil at crown level due to live loading.

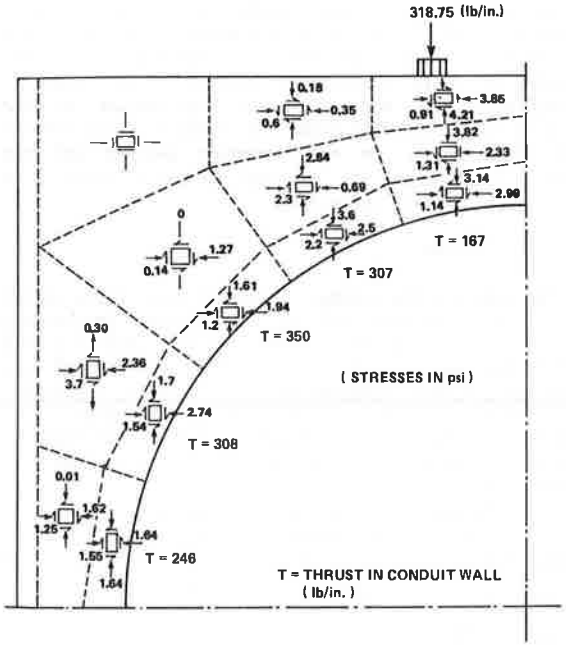

Figure 10. Analytical soil stresses around conduit due to live loading.

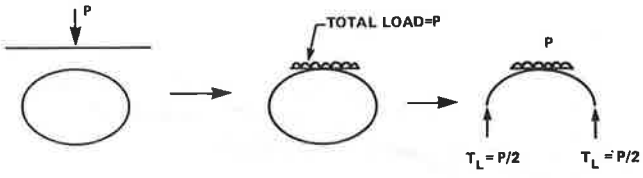

Figure 11. Thrust from equivalent load on transverse slice.

$$T_L = 0.5\sigma_L (1 + I) D_h \quad (5)$$

where D_h is the conduit span, I is the impact factor, and σ_L is the equivalent distributed load at crown level, obtained by assuming that the dispersed load is uniformly distributed over a square the sides of which are equal to 1.75h.

According to the revised OHBDC method, σ_L is obtained by assuming that the live load disperses at a 1:1 slope in the direction of the conduit span and at an angle of two vertical to one horizontal along the conduit length. The live-load thrust is then obtained by multiplying σ_L with the smaller of half the conduit span and half the length of the distributed load along the span (Figure 11).

A comparison of the AASHTO and OHBDC live-load thrust values with those obtained by the finite-ele-

Table 3. Comparison of maximum thrust values given by various methods.

Conduit Shape	Loading	Assumed Loading on Plane-Strain Slice (lbf/in)	h (in)	D_h (in)	D_h/D_v	Maximum Thrust (lbf/in)			
						Finite Element	OHBDC	AASHTO	Proposed for AASHTO
Circular	↓	306	48	300	1.0	192	153	390	227
	↓	302	96	300	1.0	127	153	176	116
	↓ ↓ ←72 in→	2 x 153	48	300	1.0	168	153	210	173
	↓ ↓ 48 in ←→	2 x 437	96	300	1.0	392	437	606	297
	↓ ↓ ←72 in→	2 x 153	48	150	1.0	100	128	147	87
Vertical ellipse	↓	306	46	300	0.625	180	153	250	227
	↓ ↓ ←72 in→	2 x 153	48	300	0.625	142	153	135	168
	↓ ↓ ←72 in→	2 x 153	48	150	0.625	99	86	70	84
Horizontal ellipse	↓	306	48	300	1.6	224	153	530	227
	↓ ↓ 48 in ←→	2 x 163	96	300	1.6	163	163	310	111
	↓ ↓ ←72 in→	2 x 153	48	300	1.6	168	153	285	168
	↓ ↓ ←72 in→	2 x 153	48	150	1.6	99	153	143	84

ment method (by using the properties of soil C, Figure 5a) for various cases is given in Table 3. It can be seen that the AASHTO method grossly overestimates live-load thrust in most cases. The revised OHBDC method gives closer answers to the finite-element method; however, it tends to underestimate the thrust corresponding to the single-axle loading case. It is noted that the combined weight of the dual axles (consisting of axles 4 ft apart) of the OHBDC design vehicle is 40 percent higher than the weight of the heaviest single axle. In this case the governing loading for conduit wall design is always made up of the dual axles. Therefore, it can be concluded that the revised OHBDC method gives adequate results corresponding to the OHBDC vehicle.

For governing single axles, as is the case for AASHTO design loadings, it is proposed to calculate the live-load conduit wall thrust according to Equation 5 after considering the axle load to be dispersed in the span direction at one vertical to two horizontal. Results obtained from this proposed simplified method are also given in Table 3. It can be seen that for single-axle loads, this approach yields safe and yet fairly accurate values of maximum live-load thrust.

OBSERVATIONS

A scrutiny of live-load thrust values obtained by the finite-element method will readily show that some of the basic assumptions on which the simplified methods are based are not entirely correct. For example, in the OHBDC method it is assumed that the equivalent distributed load within the span is entirely supported by the conduit wall thrust as shown in Figure 11. If this assumption were correct, then for loads that have an equivalent distributed load well within this span, the thrust would be in the same proportions as the loads. This is not true, as can be seen by comparing finite-element thrusts in rows 1 and 3 of Table 3, which show values of 192 and 168 lbf/in for the same total applied loads. It is observed that a simplified method at best is a crude approximation for solving an extremely complex problem.

CONCLUSIONS

It has been shown that live-load effects in the metallic shell of a soil-steel structure can be realistically calculated by first considering load distribution in the longitudinal direction of the conduit and then analyzing a transverse plane-strain slice of the structure. A concentrated load disperses more rapidly in the transverse direction than in the longitudinal direction.

In spite of the complexity of the problem and the inability of simplified methods to account for all the factors responsible for load dispersion, the use of a simplified method for everyday design-office use is attractive. The revised OHBDC method was found to be adequate only when the governing loading consists of a pair of closely spaced axles, as is the case for the OHBDC design loading. A new method is proposed for isolated single axles such as those of the AASHTO design vehicles.

REFERENCES

1. B. Bakht. Soil-Steel Structure Response to Live Loads. Journal of the Geotechnical Division of ASCE, June 1981, pp. 779-798.
2. D.M. Burmister. General Theory of Stresses and Displacements in Layered Soil Systems. Journal of Applied Physics, Vol. 16, No. 2, 1945, pp. 89-96; No. 3, pp. 126-127; No. 5, pp. 296-302.
3. H.G. Poulos and E.H. Davis. Elastic Solutions for Soil and Rock Mechanics. Wiley, New York, 1974.
4. H. Hafez. Soil-Steel Structures Under Shallow Covers. Univ. of Windsor, Windsor, Ontario, Ph.D. thesis, 1981.
5. K.S. Wong and J.M. Duncan. Hyperbolic Stress-Strain Parameters for Nonlinear Finite Element Analyses of Stresses and Movements in Earth Masses. Univ. of California, Berkeley, Geotechnical Engineering Rept. TE 74-3, 1974.
6. Standard Specifications for Highway Bridges. AASHTO, Washington, DC, 1974.
7. Ontario Highway Bridge Design Code. Ministry of Transportation and Communications, Downsview, Ontario, 1979.

Publication of this paper sponsored by Committee on Subsurface Soil-Structure Interaction.

Correlation of ISO V-Block and Three-Edge Bearing Test Methods

A.P. MOSER

The objective of this study was to correlate crush strengths of various sizes and classes of rigid pipe as determined by two test methods: the three-edge bearing (wood-block) method and the International Standards Organization (ISO) V-block method. In addition, the crush strengths of the various pipe rings were determined by mathematical modeling and analytical solutions via computer programming. The experimentally determined crush strengths were in close agreement with those predicted by the analytical solutions. Crush strengths determined by the ISO V-block method are greater than those determined by the three-edge bearing method on similar pipe rings. That is, the ISO V-block method is less conservative, since it predicts that a pipe will withstand a greater crush load.

Traditionally, the crush load for rigid pipe has been determined by using the three-edge bearing wood-block method of testing. Other test methods have been used. It has long been recognized that the particular test method can have a substantial effect on the resulting crush strengths. The International Standards Organization (ISO) has proposed a so-called V-block method for testing.

The objective of this study was to determine the loads required to cause crush failure for pipe of various sizes and strengths. Asbestos cement pipes were used in the study because of the availability of a wide range of strengths. These crush loads were determined by using the two test methods referred to above. The data on strength variation due to test method were used to predict V-block strength from actual wood-block test data, and vice versa. The use of the data also permits one to calculate how changing from the wood-block test method to the V-block test method influences load factors that have previously been defined by using wood-block test data. Such an exercise is necessary since the load factor (LF) is defined as follows (1, p. 700; 2):

LF = crush failure load as determined by testing in soil in actual burial condition divided by crush load as determined by standard test method.

Obviously, if one changes the standard test method, a change in load factor will result.

ANALYTICAL SOLUTION TO EXTERNALLY LOADED PIPE RING

The problem of an externally loaded circular pipe ring can be considered a plane problem if variations along the pipe axis can be assumed negligible. For such a problem, the governing equation is (3) as follows:

$$\nabla^4\phi(r,\theta) = 0$$

The function $\phi(r,\theta)$ is a plane stress function that satisfies equilibrium if stresses are determined as follows:

$$\sigma_r = [(1/r)(\partial\phi/\partial r)] + [(1/r^2)(\partial^2\phi/\partial\phi^2)]$$

$$\tau_{r\theta} = -(\partial/\partial_r)[(1/r)(\partial\phi/\partial\theta)]$$

$$\sigma_\theta = \partial^2\phi/\partial r^2$$

The requirements for a solution are as follows:

1. $\phi(r,\theta)$ must satisfy $\nabla^4\phi = 0$, and
2. $\phi(r,\theta)$ must satisfy boundary conditions.

The following stress function satisfies $\nabla^4\phi = 0$:

$$\phi = A_0 \ell n r + C_0 r^2 + \sum_{n=2}^{\infty} (A_n r^n + b_n r^{n+2} + C_n r^{-n} + d_n r^{-n+2}) \cos n\theta \quad (1)$$

The constants A_0, C_0, A_n, b_n, C_n, and d_n can be determined in such a manner that the boundary conditions are satisfied. Thus, Equation 1 represents a solution that is exact with respect to initial assumptions. These assumptions are (a) circular ring, (b) no variations along pipe axis, and (c) symmetric loading.

Since the pipe ring geometry is symmetric and a symmetric stress function has been chosen (i.e., symmetric in θ), only half the pipe ring need be considered (Figure 1).

The inner boundary at r = a is traction free. Thus,

$$\left.\begin{aligned}\sigma_r &= 0\\ \tau_{r\theta} &= 0\end{aligned}\right\} \quad \text{at } r = a$$

The outer boundary at r = b is loaded as follows:

$$\text{Top of ring: } -(P/2) = \int_0^{\alpha/2} b\sigma_{r1}\cos\theta\, d\theta \quad (2)$$

$$\text{Bottom reaction: } -(P/2) = \int_{\gamma-\beta/2}^{\gamma+\beta/2} b\sigma_{r2}\cos\theta\, d\theta \quad (3)$$

Here σ_{r1} and σ_{r2} are radial stresses at the top and bottom, respectively. The integration of Equations 2 and 3 results in the following boundary stresses:

$$\sigma_{r1} = -P/(2b\sin\alpha/2) \quad (4)$$

$$\sigma_{r2} = P/2b[\sin(\gamma - \beta/2) - \sin(\gamma + \beta/2)] \quad (5)$$

These boundary stresses can be expressed in a Fourier series. A half-range expansion for a cosine series is as follows:

$$A_n = (2/\pi)\int_0^{\pi} (\sigma r)_{r=b}\cos\theta\, d\theta$$

$$= (2/\pi)\left[\int_0^{\alpha}\sigma_{r1}\cos n\theta\, d\theta + \int_{\pi-(\gamma+\beta/2)}^{\pi-(\gamma-\beta/2)}\sigma_{r2}\cos n\theta\, d\theta\right] \quad (6)$$

Integrating and substituting the expressions for σ_{r1} and σ_{r2} from the boundary conditions, one obtains

$$a_n = (P/n\pi b)\left(\left\{[\sin n(\pi - \gamma + \beta/2) - \sin n(\pi - \gamma - \beta/2)] \div [\sin(\gamma - \beta/2) - \sin(\gamma + \beta/2)]\right\} + [(\sin n\alpha/2)/(\sin\alpha/2)]\right) = Q_n \quad (7)$$

and

$$a_0 = (P/b\pi)\left\{\beta/[\sin(\gamma - \beta/2) - \sin(\gamma + \beta/2)] - \alpha/(2\sin\alpha/2)\right\} \quad (8)$$

The following two equations are used to solve for A_0 and C_0:

$$(A_0/b^2) + 2C_0 = a_0/2$$

$$(A_0/a^2) + 2C_0 = 0$$

Thus,

$$A_0 = a_0(ab)^2/2(a^2 - b^2) \qquad C_0 = -a_0 b^2/4(a^2 - b^2) \tag{9}$$

where a_0 is given in Equation 8 above. Four equations in four unknowns (a_n, b_n, c_n, d_n) may be written as follows:

$$a_n b^{n-2}(n - n^2) + b_n b^n(n - n^2 + 2) - c_n b^{-(n+2)}(n + n^2) - d_n b^{-n}(n + n^2 - 2) = Q_n$$

Figure 1. Schematic of test specimen that served as basis for mathematical model.

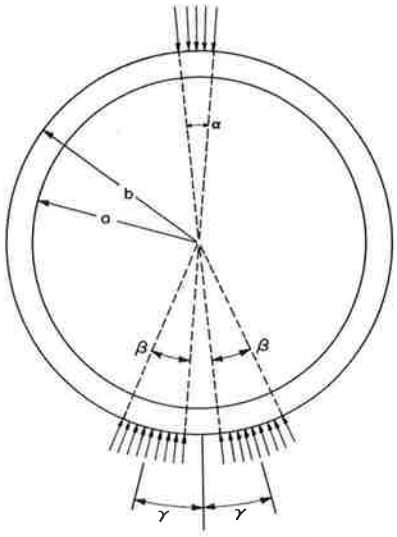

Figure 2. Three-edge bearing (wood-block) schematic.

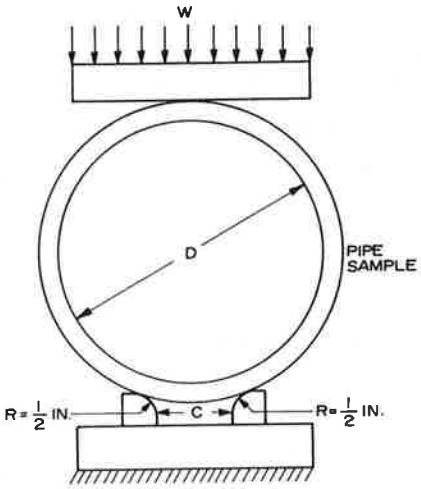

Figure 3. ISO V-block schematic.

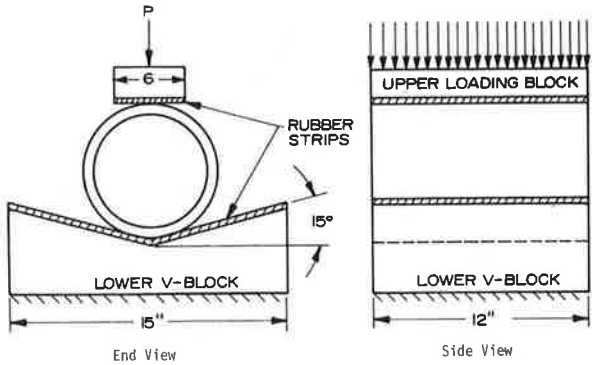

$$a_n a^{n-2}(n - n^2) + b_n a^n(n - n^2 + 2) - c_n a^{-(n-2)}(n - n^2) - d_n a^{-n}(n + n^2 - 2) = 0$$

$$a_n(n - 1)\,a^{n-2} + b_n(n + 1)\,a^n - c_n(n + 1)\,a^{-(n+2)} - d_n(n - 1)\,a^{-n} = 0$$

$$a_n(n - 1)\,b^{n-2} + b_n(n + 1)\,b^n - c_n(n + 1)\,b^{-(n+2)} - d_n(n - 1)\,b^{-n} = 0$$

The matrix form of these equations is as follows:

$$\begin{bmatrix} b^{n-2}(n - n^2) & b^n(n - n^2 + 2) & -b^{-(n+2)}(n + n^2) & -b^{-n}(n + n^2 - 2) \\ a^{n-2}(n - n^2) & a^n(n - n^2 + 2) & -a^{-(n+2)}(n + n^2) & -a^{-n}(n + n^2 - 2) \\ a^{n-2}(n - 1) & a^n(n + 1) & -a^{-(n+2)}(n + 1) & -a^{-n}(n - 1) \\ b^{n-2}(n - 1) & b^n(n + 1) & -b^{-(n+2)}(n + 1) & -b^{-n}(n - 1) \end{bmatrix} \begin{bmatrix} a_n \\ b_n \\ c_n \\ d_n \end{bmatrix} = \begin{bmatrix} Q_n \\ 0 \\ 0 \\ 0 \end{bmatrix}$$

A computer program was written that solves this system of equations for the constants a_n, b_n, c_n, and d_n and then calculates σ_θ for various loading angles and various diameter/thickness ratios.

EXPERIMENTAL PROCEDURES

Test Methods

The three-edge (wood-block) test method was conducted as described in ASTM C-500 (Figure 2). The ISO V-block test method consists of a V-shaped test block lined with rubber strips. The upper block also has a bonded rubber strip that comes in contact with the test pipe (Figure 3). In this method, the loading rate is constant and such that failure occurs in 15-30 s.

Sampling Protocol

The pipes to be tested had their pipe ends clearly marked either L (left) or R (right) to identify pipe orientation during manufacture. The pipes were then cut into 1-ft (305-mm) test sections as indicated in Figure 3. Each section was identified with a letter, starting with A on the left end of the pipe. The V's and the W's on the pipe section in Figure 4 stand for V-block and wood-block methods, respectively. That is, sections A, C, E, H, and J were tested by using the wood-block three-edge bearing method and sections B, D, G, W, and K were tested by using the V-block method.

The proposed ISO V-block test method recommends a sample length of 7.8 in (200 mm) for nominal diameters up to and including 11.8 in (300 mm) and a sample length of 11.8 in for nominal diameters above 13.8 in (350 mm). Tests were run on samples both 12 in and 8 in (203 mm) long to determine whether sample length in this range has a significant effect on the resulting crush load per unit length. Data from these tests show that resulting crush loads per unit length were essentially equal for the two sample lengths tested. Therefore, samples 1 ft in length (a common sample length in the United States) were used throughout this study.

RESULTS

Twenty-two pipe lengths of various classes and diameters were cut into samples following the procedure indicated in Figure 4. More than 100 V-block crush tests and 100 wood-block crush tests were run. Data are plotted graphically in Figures 5 and 6. Also shown in Figures 5 and 6 and in Table 1 are data from the analytical solution of the problem. Presentation of the data as in Figure 5 shows little scatter in the data. However, such a presentation hides some of the causes and effects. This can be clearly seen by plotting the same information on the (V - W)/W versus W axis (Figure 6).

Approximate mathematical models for the two test methods were determined and solutions obtained via computer programming. This was done by calculating the loading angle on the bottom of the test samples for the wood blocks. Of course, this angle varies with the outside diameter of the pipe and the wood-block spacing. Very narrow, almost line loadings were assumed. For the V-block test method the loading angle is always 15 degrees. Here the assumed loads were not applied along a line but were distributed about 10 degrees, 5 degrees each side of the contact point.

In both experimental and theoretical data, it appears that the change (V - W)/W x 100 approaches 7 percent as W gets very large. Why does a discrepancy exist between the experimental and the theoretical data? The answer is clear. The V-block method produces a higher apparent strength over the wood-block method for the following reasons:

1. The angle of loading at the bottom of the test specimen is different;
2. Due to the rubber pads, the loading has some distribution around the circumference (not a line load); and
3. Imperfections such as out-of-roundness, high spots, etc., are not so critical for the rubber-padded V-block. That is, point-load concentrations are much less likely to happen.

The mathematical model was approximate because item 3 could not be modeled even though items 1 and 2 were taken into account. Thus, the influence item 3 has on the resulting strength can be determined only experimentally. It is easily seen that statistically the experimental data points obtained from the V-block method are about 300 lbf higher than data points predicted from the theoretical solutions. This difference is due to item 3 above. The percentage influence of item 3 is relatively high for low-strength pipe, relatively low for high-strength pipe, and approaches zero for very-high-strength pipe. Thus, the experimental solution and the theoretical solution become asymptotic to the 7 percent line for very-high-strength pipes. The fact that the two solutions approach each other gives further verification that the experimental solution is correct and may be used to accurately predict V-block crush-load data from wood-block data, or vice versa. The equation correlating the two test methods is as follows (1 lbf = 0.004 kN):

$$F_V = 1.07F_W + 200\,(\text{lbf/ft}) \tag{10}$$

Figure 4. Sampling protocol: W-samples tested in three-edge bearing and V-samples tested in ISO V-block method.

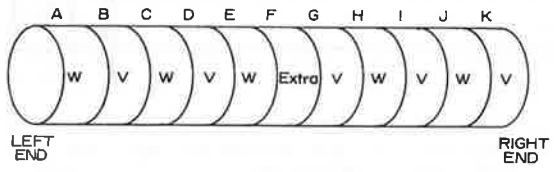

Figure 5. V-block versus wood-block strength.

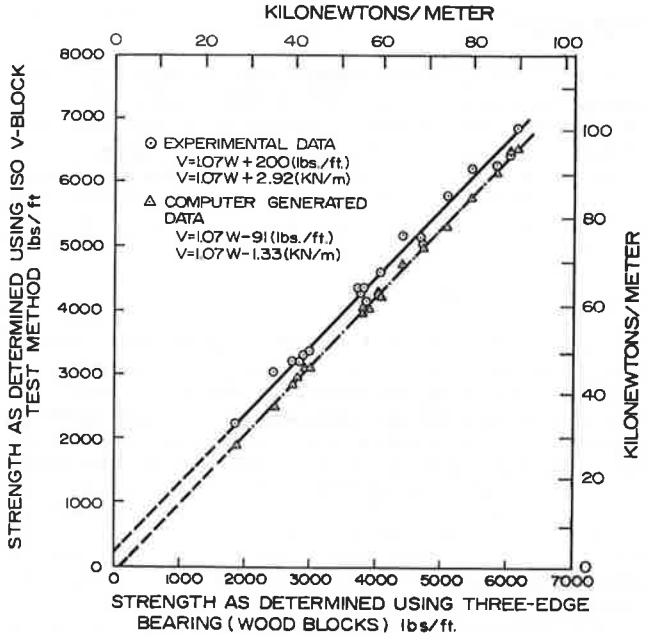

Figure 6. Apparent percentage increase in crush strength with ISO V-block test method.

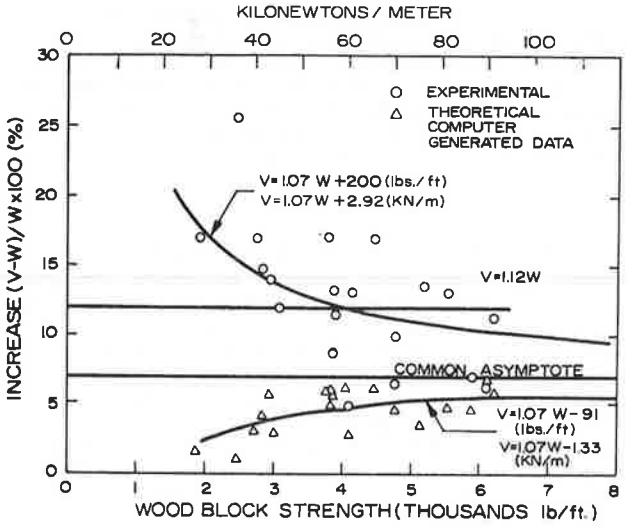

Table 1. Analytic solution for actual pipe samples tested.

Wood-Block Separation C	Diameter (in) and Class	D/t	Predicted Crush Load (lbf/ft) Wood Block	Predicted Crush Load (lbf/ft) ISO V-Block	Δ Percent
1-in spacing	4, 2400	9.9	2.454	2.479	1.0
	6, 1500	14.5	1.867	1.897	1.6
	6, 2400	12.7	4.103	4.214	2.7
	8, 1500	15.3	3.005	3.092	2.9
	8, 2400	15.8	2.736	2.815	2.9
	8, 3300	13.4	5.133	5.308	3.4
	10, 2400	16.6	2.929	3.093	5.6
	10, 3300	15.3	3.802	3.988	4.9
	12, 1500	18.7	2.822	2.941	4.2
	12, 2400	18.1	3.755	3.969	5.7
	12, 3300	14.9	3.840	4.044	5.3
	16, 3300	18.4	4.708	5.028	6.8
2-in spacing	18, 2400	17.7	4.748	4.962	4.5
	18, 3300	18.1	3.818	4.039	5.8
	18, 5000	16.3	5.501	5.754	4.6
	24, 2400	21.5	4.441	4.716	6.2
	24, 3300	20.3	4.064	4.316	6.2
	24, 5000	17.3	6.089	6.497	6.7
3-in spacing	30, TR-30	19.8	5.872	6.142	4.6
	30, 5000	19.8	6.191	6.544	5.7

Note: 1 in = 25 mm; 1 lbf = 0.004 kN.

Table 2. Load factors for asbestos cement pipe buried in either class C or class B bedding.

C-Bedding				B-Bedding	
Crush Load (lbf/ft)	Load Factor	Crush Load (lbf/ft)	Load Factor	Crush Load (lbf/ft)	Load Factor
3010	1.9	5580	1.43	2800	1.90
3500	1.32	2200	1.66	3400	1.51
5050	1.19	4900	1.24	4450	1.73
3410	1.74	2950	1.92	3800	1.77
3990	1.50	2700	1.60	5960	1.66
5580	1.28	2800	1.64	3970	1.64
4430	1.76	2800	1.74		
5910	1.24	2360	2.17		
5250	1.21	4700	1.16		
2990	1.31	6380	1.31		
2410	1.62	3900	1.54		
2500	1.60	2600	1.73		
5000	1.27	3400	1.50		
5050	1.24	3400	1.39		
5040	1.36	3350	1.50		
7000	1.07	2250	1.87		
6375	1.20	2200	2.03		
3130	1.75				
2525	1.67				

Note: 1 lbf = 0.004 kN.

Figure 7. Load factor as function of three-edge bearing crush strength.

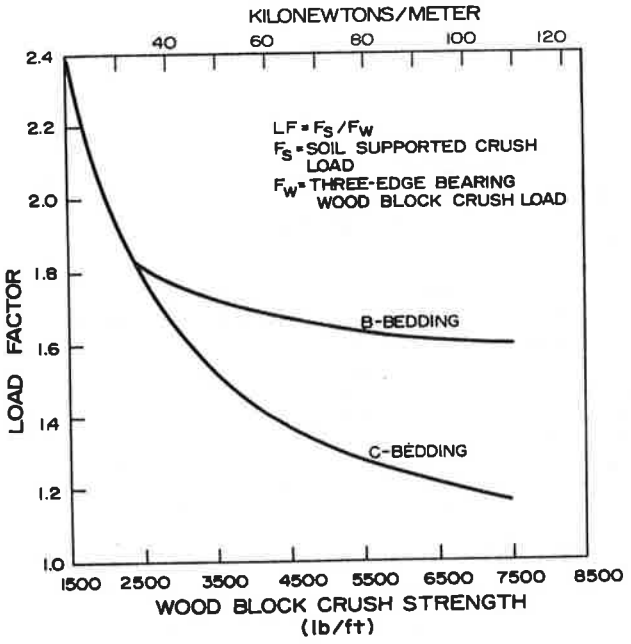

F_V represents crush load as determined by the V-block method. F_W represents the crush load as determined in the three-edge bearing (wood-block) method. This equation represents a least-squares fit to the experimental data shown graphically in Figure 5.

LOAD-FACTOR DATA FROM 1975 UTAH STATE UNIVERSITY REPORT

An experimental study was carried out at Utah State University in 1975 to determine load factors (4). In that study the load factors were determined by using the three-edge bearing (wood-block) method for determining the crush load (F_W). Similar samples were loaded in an embankment condition to determine the soil-supported crush load (F_s).

$$\text{Load factor} = LF = F_s/F_W \quad (11)$$

Data from this study are given in Table 2. Equations of the form $LF = \alpha/F_W + \beta$ were determined by using the least-squares method to determine α and β.

These equations are plotted in Figure 7. It is noted that B bedding gives little or no advantage over C bedding for low-strength pipes. It is assumed, for pipe crush strengths less than the intersection of the two curves, that the C curve applies to both C and B beddings. It is also noted that for high-strength pipes, the load factor for B bedding is about 30 percent higher than that for C bedding. The equations for the two curves that relate load factors $(LF)_W$ to wood-block bearing load (F_W) are as follows (1 lbf = 0.004 kN):

For C bedding,

$$(LF)_W = 2264/F_W + 0.87;\ F_W(\text{lbf/ft}) \quad (12)$$

For B bedding,

$$(LF)_W = 797/F_W + 1.49;\ F_W(\text{lbf/ft}) \quad (13)$$

V-BLOCK LOAD FACTORS

If the crush loads are to be determined by using the ISO V-block method, it is necessary to correct the load factors to a new base. Obviously, since V-block crush loads are larger than corresponding wood-block values, the load factors referred to the V-block base will be proportionally smaller. The load factors associated with the V-block and wood-block bases are as follows:

$$(LF)_V = F_s/F_V \quad (14)$$

$$(LF)_W = F_s/F_W \quad (15)$$

From Equation 15,

$$F_s = (LF)_W F_W \quad (16)$$

Upon the substitution of Equation 16 into Equation 14, one finds

$$(LF)_V = (LF)_W F_W/F_V \quad (17)$$

From Equation 10,

$$F_V = 1.07F_W + 200$$

Thus Equation 17 becomes

$$(LF)_V = (LF)_W F_W/(1.07F_W + 200) \quad (18)$$

From Equation 12 for C bedding, $(LF)_W = 2264/F_W + 0.87$. Thus, for C bedding, Equation 18 becomes

$$(LF)_V = (2264 + 0.87F_W)/(1.07F_W + 200) \quad (19)$$

From Equation 13 for B bedding, $(LF)_W = 797/F_W + 1.49$. Thus, for B bedding, Equation 18 becomes

$$(LF)_V = (797 + 1.49F_W)/(1.07F_W + 200) \quad (20)$$

One may use Equations 19 and 20 for calculating V-block load factors in terms of wood-block crush loads for C and B beddings, respectively.

In a similar manner, equations may be derived for calculating V-block load factors in terms of V-block crush loads. Equation 10 may be solved for F_W as follows (1 lbf = 0.004 kN):

$$F_W = (F_V - 200)/1.07\ (\text{lbf/ft}) \quad (21)$$

F_W from Equation 21 and $(LF)_W$ from Equation 12 may be substituted into Equation 17 to arrive at the following for C bedding (1 lbf = 0.004 kN):

$$(LF)_V = (2101/F_V) + 0.81; F_V(lbf/ft) \quad (22)$$

Similarly, F_W from Equation 21 and $(LF)_W$ from Equation 13 can be substituted into Equation 17. The result is the following equation for B bedding (1 lbf = 0.004 kN):

$$(LF)_V = (518/F_V) + 1.39; F_V(lbf/ft) \quad (23)$$

REFERENCES

1. M.G. Spangler and R.L. Handy. Soil Engineering, 3rd ed. Intext Educational Publishers, New York, 1973.
2. Design and Construction of Sanitary and Storm Sewers. In ASCE Manual and Report on Engineering Practice No. 37 (WPCF Manual of Practice No. 9), American Society of Civil Engineers and Water Pollution Control Federation, New York, 1973, pp. 210-211.
3. S.P. Timoshenko and J.N. Goodier. Theory of Elasticity, 3rd ed. McGraw-Hill, New York, 1970.
4. R.K. Watkins. A.P. Moser, and O.K. Shupe. Soil Supported Strength of Buried Asbestos Cement Pipe. Buried Structure Laboratory, Utah State Univ., Logan, 1976.

Publication of this paper sponsored by Committee on Culverts and Hydraulic Structures.

Rigid Pipe Prooftesting Under Excess Overfills with Varying Backfill Parameters

RAYMOND E. DAVIS AND FRANK M. SEMANS

Field testing and analyses of two culverts at Cross Canyon are described: a 96-in prestressed-concrete functioning culvert under 200 ft of overfill and an 84-in reinforced-concrete dummy culvert under a maximum 183-ft overfill in the same embankment. Eight instrumented and two noninstrumented zones in the dummy pipe and functional and unstressed control instrumented zones of the prestressed pipe were monitored during and after embankment construction to determine peripheral soil stresses, internal forces, and displacements. Correlations were established between quasi-theoretical and measured parameters (moments, thrusts, displacements, distress, etc.) with a programmed analysis. Some standard analytical tools (settlement ratio, finite element) were checked against observations, and relative costs of different construction modes were considered. Heger's recently developed criteria were checked against actual appearances of two of four distress modes. The programmed analysis was modified to predict these distress modes. Profiles of effective-density coefficients were established for various construction modes. The importance of designing for density distributions representative of contemplated construction modes is emphasized.

A comprehensive 15-year research program pertinent to structural behavior of culverts embedded in deep embankments (100+ ft) conducted by the California Department of Transportation (Caltrans) Structures Design Research Unit has been described (1-25). Eight papers (8,12,13,15-17,19,20) have discussed field tests of two reinforced-concrete pipe culverts at Mountainhouse Creek: a grossly underdesigned 1000D 84-in-diameter dummy culvert and (17) a functional 4000D 96-in-diameter pipe. Each pipe included six zones to be subjected to varying bedding and backfilling parameters. Buried under a 137-ft overfill (almost nine times the 16-ft maximum stipulated by current specifications), several zones of the dummy culvert responded encouragingly to specialized embedment techniques.

Tests of additional bedding and backfill parameters and pipe segments of varying strengths were conducted at Cross Canyon, near Sunland, California, to establish more realistic functional relationships between pipe strengths and allowable limiting overfills. Again, a functional culvert and a dummy pipe were tested.

Designed for 200 ft of overfill, the functional culvert is of 96-in diameter and 23.5-in wall thickness with two layers of closely spaced prestressing wires. Tests of one pipe segment (Zone 11) are described later.

The 84-in-diameter dummy culvert, its invert located 13 ft above the crown of the functional culvert at varying horizontal distances therefrom, was divided into 10 zones (Figure 1); pipe strengths and bedding and backfill parameters are as shown in Figures 2 and 3. Dummy pipe segments except those in Zones 5 (1750D), 6 (2500D), and 7 (3600D) were nominally classified as having a 1000D load rating; measured load ratings, based on tests of three pipe segments of each pipe strength, were Zones 1-4 and 8-10, 997D; Zone 5, 1910D; Zone 6, 2574D; and Zone 7, 3780D.

In all instrumented zones except Zone 1, at least one 8-ft-long pipe segment was placed on either side of the instrumented segment as a buffer segment where Method-A (ordinary embankment material) backfill was employed. Two segments were used in the zones (8, 9, and 10) with Method-B (low-modulus inclusion) backfill.

DESCRIPTION OF INSTRUMENTATION

Dummy culvert instrumentation design was influenced by observed behavior of culverts and instrumentation in earlier projects, briefly described as follows (Figures 4 and 5):

1. Symmetry of soil stress distribution has never been observed in Caltrans culvert research.
2. Integrated forces acting on pipe peripheries, based on measured soil stresses, have indicated vertical force unbalance often measured in tens of kips.
3. Failures of interface stress meters in sensitive locations or inconsistencies in measured stresses due to soil heterogeneity have often greatly decreased confidence in overall results.

F_W from Equation 21 and $(LF)_W$ from Equation 12 may be substituted into Equation 17 to arrive at the following for C bedding (1 lbf = 0.004 kN):

$$(LF)_V = (2101/F_V) + 0.81; F_V(lbf/ft) \quad (22)$$

Similarly, F_W from Equation 21 and $(LF)_W$ from Equation 13 can be substituted into Equation 17. The result is the following equation for B bedding (1 lbf = 0.004 kN):

$$(LF)_V = (518/F_V) + 1.39; F_V(lbf/ft) \quad (23)$$

REFERENCES

1. M.G. Spangler and R.L. Handy. Soil Engineering, 3rd ed. Intext Educational Publishers, New York, 1973.
2. Design and Construction of Sanitary and Storm Sewers. In ASCE Manual and Report on Engineering Practice No. 37 (WPCF Manual of Practice No. 9), American Society of Civil Engineers and Water Pollution Control Federation, New York, 1973, pp. 210-211.
3. S.P. Timoshenko and J.N. Goodier. Theory of Elasticity, 3rd ed. McGraw-Hill, New York, 1970.
4. R.K. Watkins. A.P. Moser, and O.K. Shupe. Soil Supported Strength of Buried Asbestos Cement Pipe. Buried Structure Laboratory, Utah State Univ., Logan, 1976.

Publication of this paper sponsored by Committee on Culverts and Hydraulic Structures.

Rigid Pipe Prooftesting Under Excess Overfills with Varying Backfill Parameters

RAYMOND E. DAVIS AND FRANK M. SEMANS

Field testing and analyses of two culverts at Cross Canyon are described: a 96-in prestressed-concrete functioning culvert under 200 ft of overfill and an 84-in reinforced-concrete dummy culvert under a maximum 183-ft overfill in the same embankment. Eight instrumented and two noninstrumented zones in the dummy pipe and functional and unstressed control instrumented zones of the prestressed pipe were monitored during and after embankment construction to determine peripheral soil stresses, internal forces, and displacements. Correlations were established between quasi-theoretical and measured parameters (moments, thrusts, displacements, distress, etc.) with a programmed analysis. Some standard analytical tools (settlement ratio, finite element) were checked against observations, and relative costs of different construction modes were considered. Heger's recently developed criteria were checked against actual appearances of two of four distress modes. The programmed analysis was modified to predict these distress modes. Profiles of effective-density coefficients were established for various construction modes. The importance of designing for density distributions representative of contemplated construction modes is emphasized.

A comprehensive 15-year research program pertinent to structural behavior of culverts embedded in deep embankments (100+ ft) conducted by the California Department of Transportation (Caltrans) Structures Design Research Unit has been described (1-25). Eight papers (8,12,13,15-17,19,20) have discussed field tests of two reinforced-concrete pipe culverts at Mountainhouse Creek: a grossly underdesigned 1000D 84-in-diameter dummy culvert and (17) a functional 4000D 96-in-diameter pipe. Each pipe included six zones to be subjected to varying bedding and backfilling parameters. Buried under a 137-ft overfill (almost nine times the 16-ft maximum stipulated by current specifications), several zones of the dummy culvert responded encouragingly to specialized embedment techniques.

Tests of additional bedding and backfill parameters and pipe segments of varying strengths were conducted at Cross Canyon, near Sunland, California, to establish more realistic functional relationships between pipe strengths and allowable limiting overfills. Again, a functional culvert and a dummy pipe were tested.

Designed for 200 ft of overfill, the functional culvert is of 96-in diameter and 23.5-in wall thickness with two layers of closely spaced prestressing wires. Tests of one pipe segment (Zone 11) are described later.

The 84-in-diameter dummy culvert, its invert located 13 ft above the crown of the functional culvert at varying horizontal distances therefrom, was divided into 10 zones (Figure 1); pipe strengths and bedding and backfill parameters are as shown in Figures 2 and 3. Dummy pipe segments except those in Zones 5 (1750D), 6 (2500D), and 7 (3600D) were nominally classified as having a 1000D load rating; measured load ratings, based on tests of three pipe segments of each pipe strength, were Zones 1-4 and 8-10, 997D; Zone 5, 1910D; Zone 6, 2574D; and Zone 7, 3780D.

In all instrumented zones except Zone 1, at least one 8-ft-long pipe segment was placed on either side of the instrumented segment as a buffer segment where Method-A (ordinary embankment material) backfill was employed. Two segments were used in the zones (8, 9, and 10) with Method-B (low-modulus inclusion) backfill.

DESCRIPTION OF INSTRUMENTATION

Dummy culvert instrumentation design was influenced by observed behavior of culverts and instrumentation in earlier projects, briefly described as follows (Figures 4 and 5):

1. Symmetry of soil stress distribution has never been observed in Caltrans culvert research.
2. Integrated forces acting on pipe peripheries, based on measured soil stresses, have indicated vertical force unbalance often measured in tens of kips.
3. Failures of interface stress meters in sensitive locations or inconsistencies in measured stresses due to soil heterogeneity have often greatly decreased confidence in overall results.

Figure 1. Longitudinal section of dummy culvert showing zone divisions and overfills.

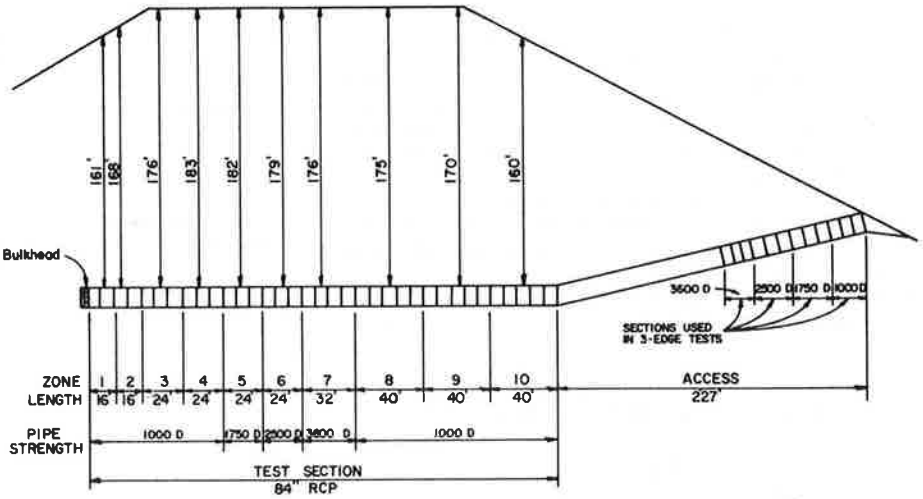

Figure 2. Bedding and backfilling parameters for Zones 1-7.

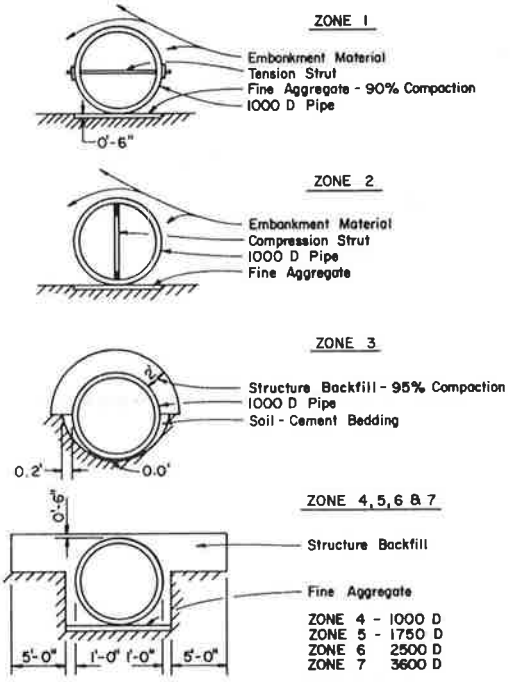

Figure 3. Bedding and backfilling parameters for Zones 8-11.

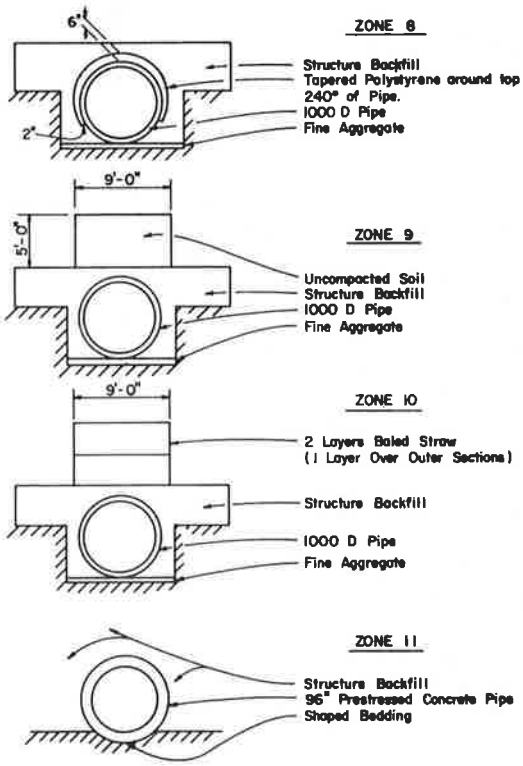

4. Lacking facility for measurement of tangential shear stresses acting at soil-concrete interfaces, researchers attributed deficiencies in static checks thereto.

Recently developed computer codes, Specifications of the American Association of State Highway and Transportation Officials (AASHTO) for effective-density distributions, and Marston-Spangler theories assume or produce soil stress distributions symmetrical about a conduit's vertical central plane. Observed asymmetrical loadings can produce significantly different structural behavior.

To detect asymmetry of loading and improve accuracy of force integrations, the researchers installed a heavy network of stress meters on both sides of the pipe (see Figure 5). Based on Hadala's recommendations (26), each zone was instrumented with three planes of stress meters at 3-ft spacing longitudinally, except Zones 1 and 9 (two planes) and Zones 2 and 7 (not instrumented).

Previous indications of static unbalance dictated need for a unique soil stress meter capable of measuring tangential forces. One complete plane of the three planes in each of Zones 4, 6, and 10 included 10 such Cambridge meters. [For comprehensive descriptions of soil stress meters, relative behavior, etc., see Caltrans report by Davis and others (24, Section 1, Vol. 1; Section 2, Vols. 1 and 2) and report by Jackura (27).]

Steel spheres affixed to the inner pipe wall at the octant points permitted measurements of shape changes. Fluid settlement platforms and Ormond and Kyowa stress meters were placed in the embankment at locations shown in Figure 6. Levels on monuments on

the pipe invert permitted assessment of pipe settlements and, in conjunction with fluid settlement platform measurements, of settlement ratios. Readings of an elevation rod placed on steel spheres near the springing lines indicated rigid body pipe rotations. Plate-and-rod settlement platforms were placed at outer surfaces of polystyrene planks at Zone 8 and at upper and lower surfaces of the uncompacted-soil and baled-straw layers in Zones 9 and 10. Differences in rod protrusions through holes cast in the pipe wall provided strain data for calculations of moduli of soft inclusions.

Figure 7 presents profiles of unadjusted soil stress increments for individual instrumented planes at Zone 3 at the 80-ft overfill based on a zero datum when the embankment was at crown level. Typically, some readings display wide divergence from those in similar locations in adjacent planes, but the majority exhibit reasonable comparisons.

Figure 4. Internal instrumentation of Cross Canyon culverts.

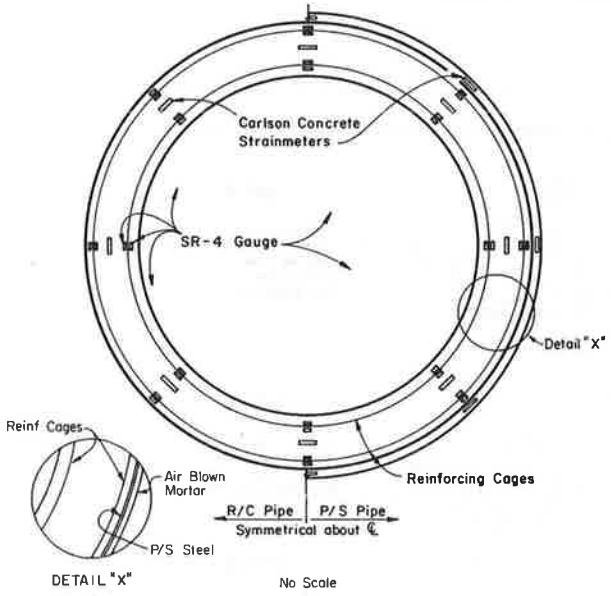

Figure 5. Soil stress-meter layout and instrumentation planes.

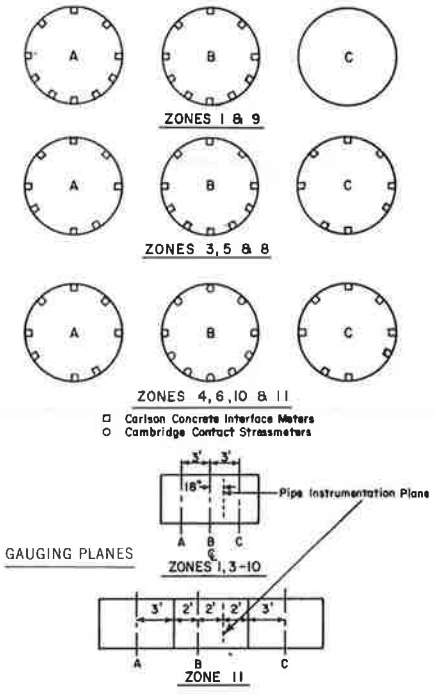

Figure 6. Locations of fluid settlement platforms, embankment soil stress meters, and plate-and-rod settlement platforms.

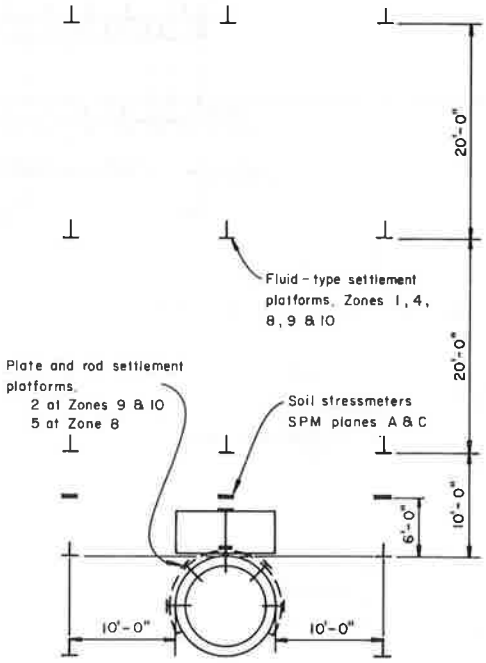

Figure 7. Profiles of unadjusted measured soil stresses at 80-ft overfill level, Zone 3.

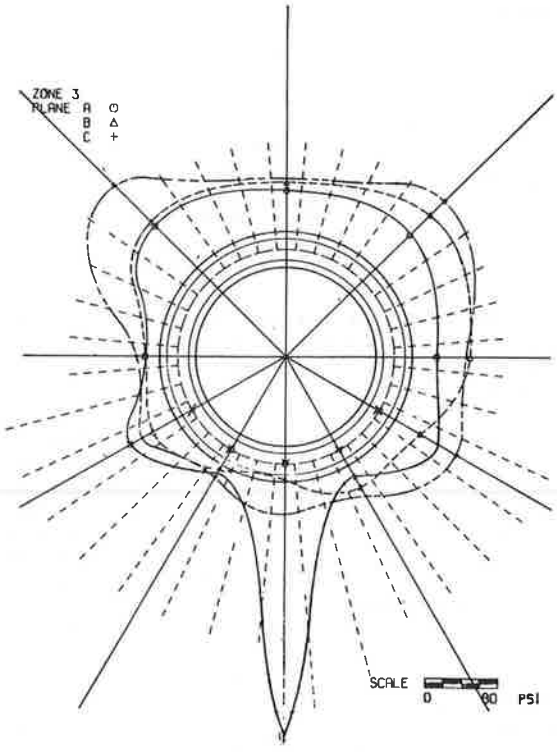

NEUTRAL-POINT ANALYSIS

Observed soil stress fields were used in conjunction with a programmed analysis based on the neutral-point method (24, Section 5, Vols. 1-12) to establish quasi-theoretical values of certain parameters for comparison with experimental values calculated from observed strain patterns, extensometer readings, visual observations, etc. Lacking static equilibrium in external forces, the analysis will produce large errors in calculated parameters.

The addition of Cambridge meters at Cross Canyon did not solve the problem of static unbalance, and it became necessary to induce static equilibrium artificially. Horizontal static unbalance was invariably small, and slight adjustments of normal forces produced equilibrium in this direction. Vertical static balance required synthesizing of tangential forces. Rotational equilibrium was first established for Zones 4, 6, and 10, where a set of interpolated tangential forces had been established from Cambridge-meter readings. These interpolated forces were altered by constant percentages to produce net zero summations of rotational forces and were then augmented or reduced as required to alleviate deficiencies in summed vertical force components.

For each remaining zone, tangential forces were synthesized that were symmetrical about the vertical diameter to ensure rotational equilibrium with magnitudes established to produce a total vertical force component equal in magnitude, but of opposite sign, to the unbalance in the summed vertical components of the normal forces. Each combination of adjusted normal and adjusted or synthesized shearing forces was then tested by the neutral-point analysis for compatibility with internal pipe wall forces based on stress-meter readings and readjusted as required.

Traditionally, Caltrans researchers have normalized normal tractions by converting them into effective densities, i.e., embankment densities required under hydrostatic conditions to produce given measured values of soil stress increments ΔP under given overfill increments ΔH. Thus,

$$\text{Effective density (pcf)} = 144\Delta P \text{ (psi)}/\Delta H \text{ (ft)}.$$

Interpolated effective densities for Zones 1 and 3, based on the adjusted normal tractions, are shown in Figures 8 and 9. Since functions of soil stress and overfill are nonlinear, effective-density profiles vary with overfill. Profiles have been included for 20-ft, 80-ft, and 160-ft overfills to illustrate typical distributions for relatively low, mid-height, and deep overfills (by California standards); for maximum overfills (where they differ appreciably from 160 ft); and for 24 months after achieving maximum overfills to illustrate time dependency.

Adjusted normal and tangential forces were used in conjunction with neutral-point analyses and experimental parameters to derive information about pipe structural behavior and relative effects of various bedding and backfilling parameters on that behavior.

Figure 10 depicts quasi-theoretical (i.e., based on measured soil stresses and theoretical analyses) wall bending moments with superimposed experimental moments based on measured strain data; Figure 11, quasi-theoretical wall displacements with superimposed displacements based on extensometer measurements, with a datum at the inner pipe invert; Figure 12, quasi-theoretical concrete extreme fiber stresses, all for Zone 3; and Figures 13, 14, and 15, changes in horizontal and vertical diameters as functions of overfill.

In the plots of inner and outer concrete extreme fiber stresses, a circular line was added at a tensile stress of 400 psi, assumed to be the limiting tensile working stress for concrete. The intersections of this curve with that for quasi-theoretical inner fiber tensile stresses suggest boundaries of observed cracking. These limits are designated Q-T (quasi-theoretical) and O (observed).

Pipe behavior was evaluated in part on the basis of observed distress, e.g., total lengths and maximum widths of cracking, delamination (i.e., shell separation in circumferential reinforcement planes), and diameter changes. Distress in all pipe segments was assessed separately, but the most significance, in comparisons of behavior, was attached to central segments in each zone, most distant from adjacent zones. Based on total length of cracking as the most significant criterion for comparison, the following information may be derived.

Zone 1 (high-strength steel tensile struts, full projection) exhibited a relatively small amount of cracking up to 70 ft but dropped into fifth place at fill completion. The high-strength rods provided lateral support at least as good as that provided by entrenchment throughout the entire course of embankment construction, and total diameter changes after rod removal were less than those at entrenched Zone 7 at Mountainhouse Creek.

This test could not assess behavior for low overfills for this parametric condition, since lateral support must be provided before and after rod removal. It had been hypothesized by the researchers that the deep overburden would compact soil on the sides of the pipe sufficiently to provide significant passive components of soil stress on rod removal to furnish required support. Ample evidence bears out this hypothesis, since the increase in horizontal diameter 24 months after fill completion (0.952 in) (see Figure 13) was less than the 1 5/8-in increase at entrenched Zone 7, Mountainhouse Creek, Part 1, under about half the overfill, and only 11 percent of the increase at positive-projecting Zone 9, Mountainhouse Creek, Part 1. The same degree of compaction would probably not have been obtained at much lower overfills, and rod removal prior to achievement of this compaction would almost certainly have produced the same pronounced distress observed at Zone 9, Mountainhouse Creek, Part 1.

Measured effective densities acting laterally on the pipe increased, while those at the crown and invert decreased after rod removal as a result of increases in the horizontal diameter and development of passive components of soil stress and local arching accompanying decreases in vertical diameter. [The augmentation of densities, shown at the ends of the horizontal diameter up to fill completion (but not thereafter), was determined by calculating the horizontal diameter changes (by the neutral-point analysis) for the unstrutted pipe under the observed soil stresses, calculating the horizontal forces required to produce the measured displacements, and treating these forces as additional soil stresses acting on two elements on each side.]

The first 0.01-in crack was observed in Zone 1 with the overfill at 67 ft.

Throughout the entire course of embankment construction and for 24 months following embankment completion, Zone 2 (timber compression struts, full projection) consistently exhibited the greatest total length of cracking. Since vertical timber struts do not provide the very important lateral support for the fully projecting pipe, this type of construction is not conducive to good pipe behavior.

Hundredth-inch cracks were first observed in Segment 202 at 51 ft of overfill and in Segment 203 at

57 ft. Delamination was observed for the first time at an overfill of 122 ft and compression spalling at the springing line at 137 ft. At higher overfills, extensive crushing of timber sills and wedges above the vertical struts was observed. Diameter changes were 2.5 times as large vertically and 3.3 times as large horizontally as those in entrenched Zone 4. The behavior of Zone 1, which had tension struts, was markedly better than that of Zone 2, which had compression struts.

Figure 8. Effective-density profiles, Zone 1.

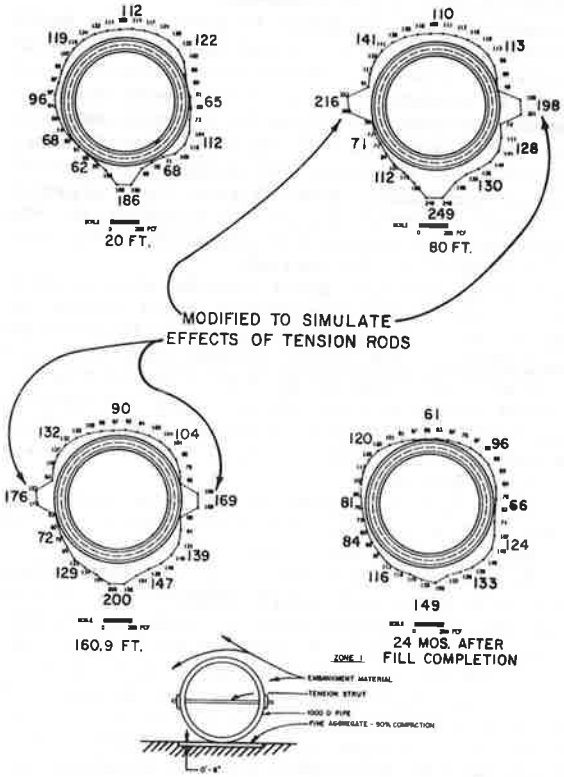

Figure 9. Effective-density profiles, Zone 3.

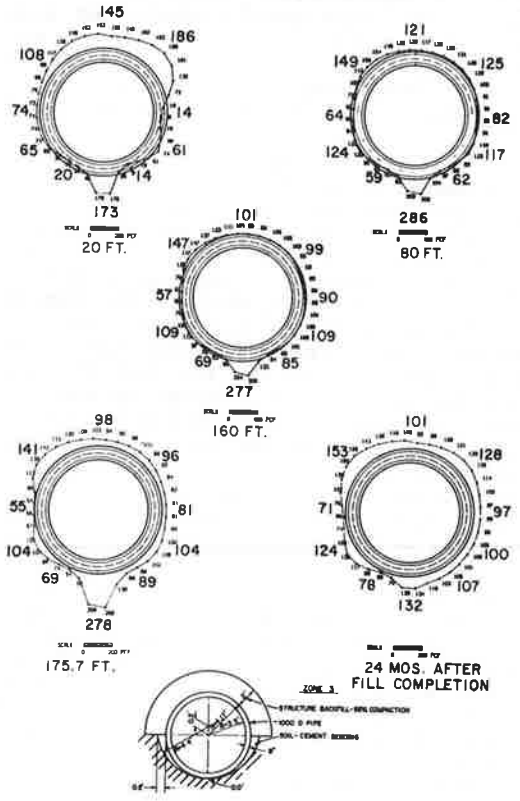

Figure 10. Quasi-theoretical bending moments with experimental moments, Zone 3.

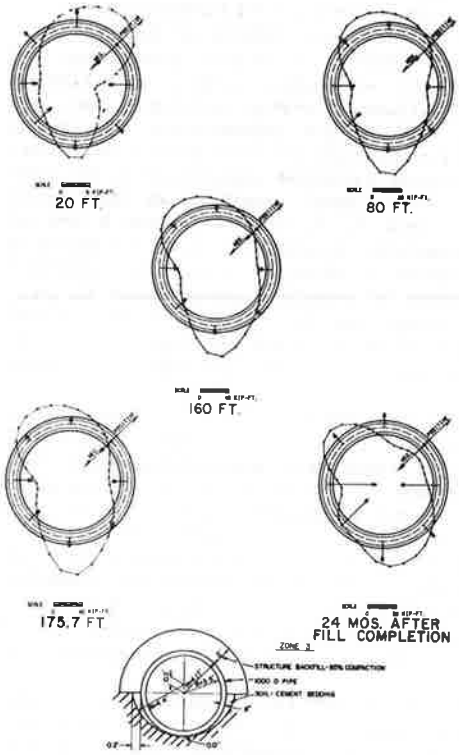

Figure 11. Quasi-theoretical pipe wall displacements with experimental displacements, Zone 3.

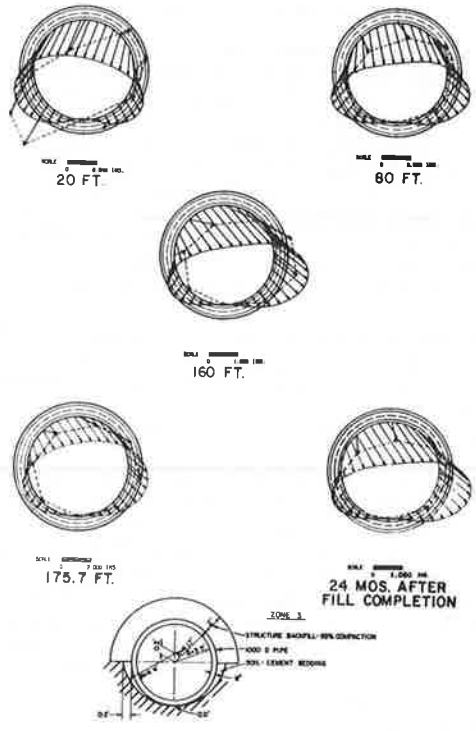

The Zone-3 construction method, extensively employed in the pipe industry, seems conducive to excellent structural behavior, since placement of the cement-soil slurry should eliminate irregularities of typical preshaped beddings and produce essentially uniform distributions of soil stress over the entire lower half of the pipe.

Surprisingly, then, Zone 3, from the viewpoint of total crack length, performed poorly by comparison with other zones, and performance of the lower half of the pipe was particularly bad. Throughout much of the embankment construction, at deeper overfills, this section ranked second only to Zone 2 in total crack length.

Initial input soil stress distributions, more or less uniform around the upper and lower halves of the pipe (the latter being of considerably less magnitude than the former), required inordinately large synthesized tangential forces to produce static equilibrium. Predicted cracking and other parameters output from neutral-point analyses did not agree with observations and corresponding experimental values, so input soil stresses were revised to give more weight to the large soil stress acting at the invert at Plane A (see Figure 7). The resulting correlations of quasi-theoretical and experimental parameters were thereby much improved (e.g., see Figures 10, 11, and 12), which suggests that the Plane-A invert soil stress could not safely be ignored and that the desired uniform distribution was not really obtained after all--this Plane-A invert stress had not actually been ignored previously, but a very tight stress gradient combined with an input scheme using stresses 5° on either side of the high stress with the averaging process including two low-gradient planes obscured it.

From the viewpoint of crack width rather than total length of cracking, this construction method did produce noticeable improvement in behavior. If the center segment only is considered representative, the 0.01-in crack was first observed at an overfill of 61 ft compared with 40 ft for adjoining Zone 4, which employed the unshaped fine-aggregate bedding. The 0.01-in crack for the 1000D pipe in Zone 3 thus appeared at the same overfill as that which may be considered representative for the entrenched 1750D (Zone 5) pipe with the fine-aggregate bedding (see Figure 33).

Diametral changes at comparable overfills in Zone 3 were of nearly the same magnitude as those in Zone

Figure 12. Quasi-theoretical concrete extreme fiber stresses, predicted zones of inner wall cracking, and limits of observed cracking, Zone 3.

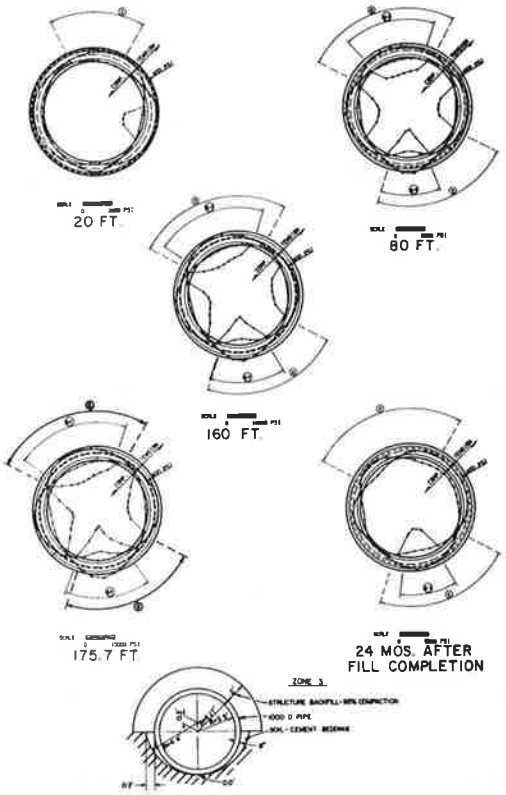

Figure 13. Changes in horizontal and vertical pipe diameters as function of overfill and time after embankment completion, Zone 1.

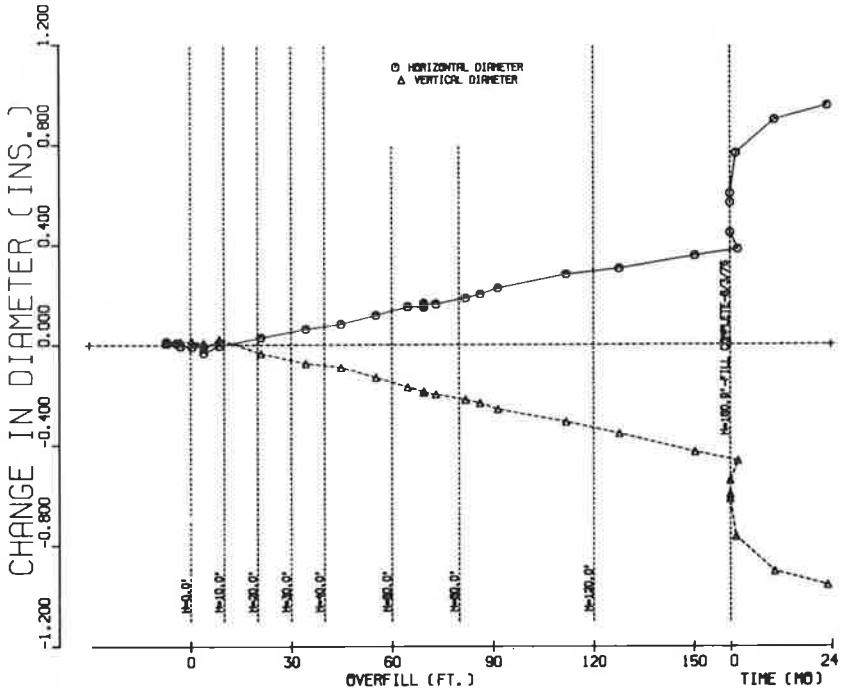

1 prior to removal of the steel rods, which proves that the lateral support provided by the trench and cement-treated slurry was almost as good as that provided by the tension struts. The soil stress distribution around the lower half of the pipe was better than at other zones in the centers of the lower quadrants, but a strong gradient of soil stress existed in the vicinity of the invert (see Figure 9). Behavior of the other zones will be described later.

OBSERVATIONS OF ENTRENCHED METHOD-A AND METHOD-B ZONES

Effective-density profiles are depicted for Zones 4, 5, 6, 8, 9, and 10 in Figures 16 through 21. These profiles exhibit a characteristic pattern: density maxima at upper quadrant midpoints and invert (1:30, 6:00, and 10:30 o'clock); density minima at the crown and lower quadrant midpoints (12:00, 4:30, and 7:30 o'clock). There were two exceptions: Zone 8 manifested a very uniform distribution about the upper 240° of the pipe periphery at and above the

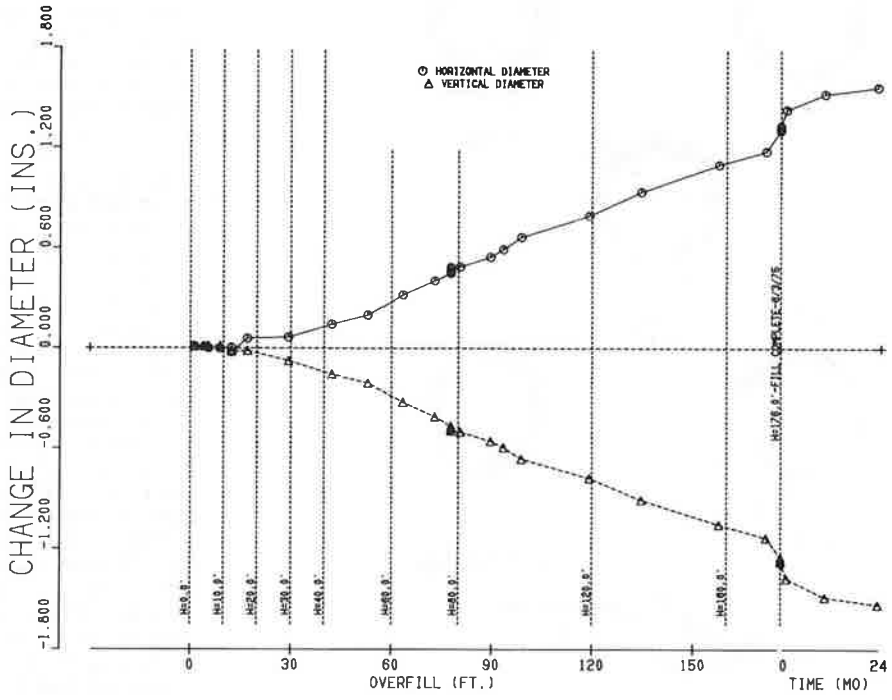

Figure 14. Changes in horizontal and vertical pipe diameters as function of overfill and time after embankment completion, Zone 2.

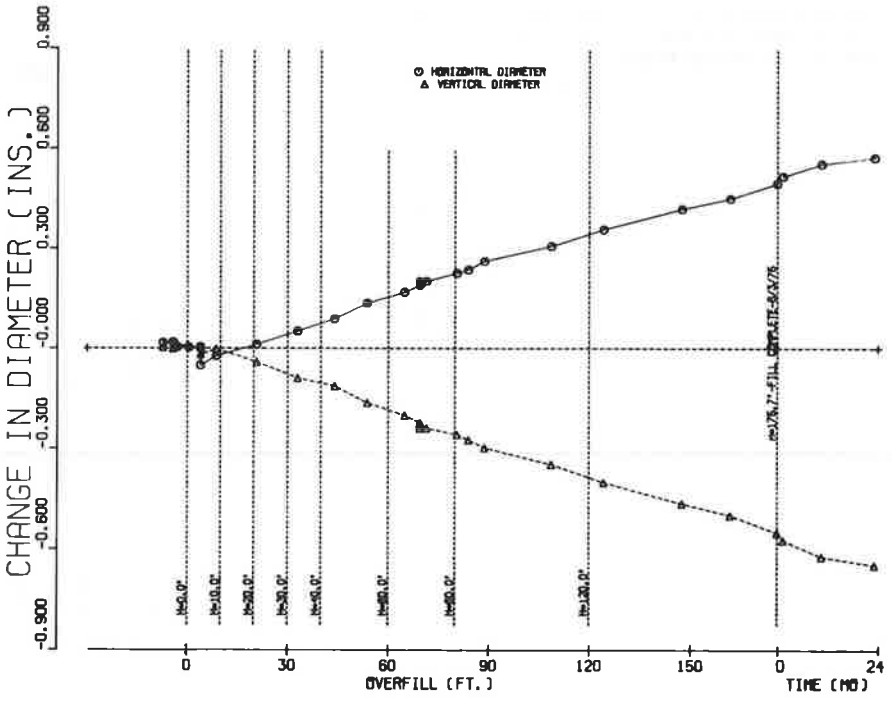

Figure 15. Changes in horizontal and vertical pipe diameters as function of overfill and time after embankment completion, Zone 3.

Figure 16. Effective-density profiles, Zone 4.

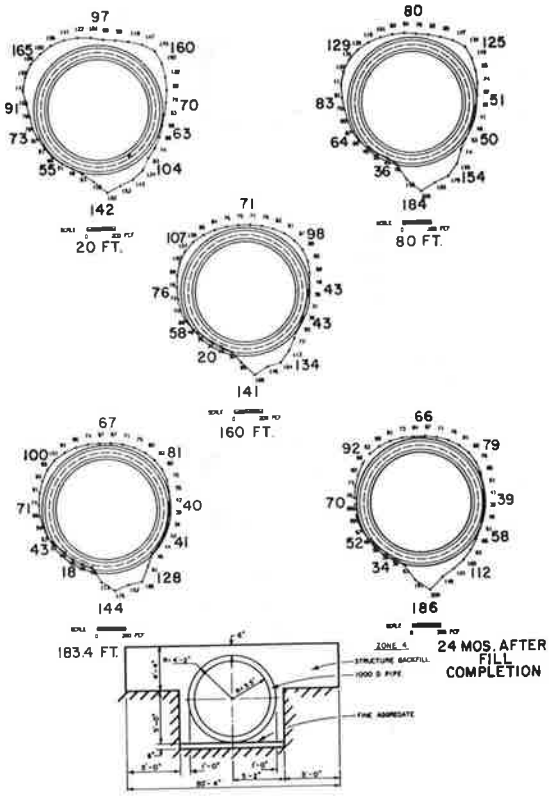

Figure 17. Effective-density profiles, Zone 5.

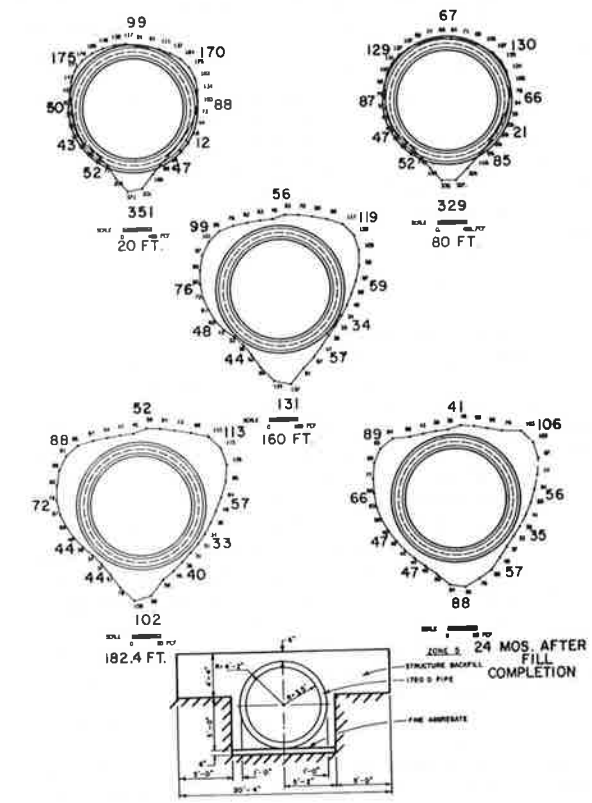

Figure 18. Effective-density profiles, Zone 6.

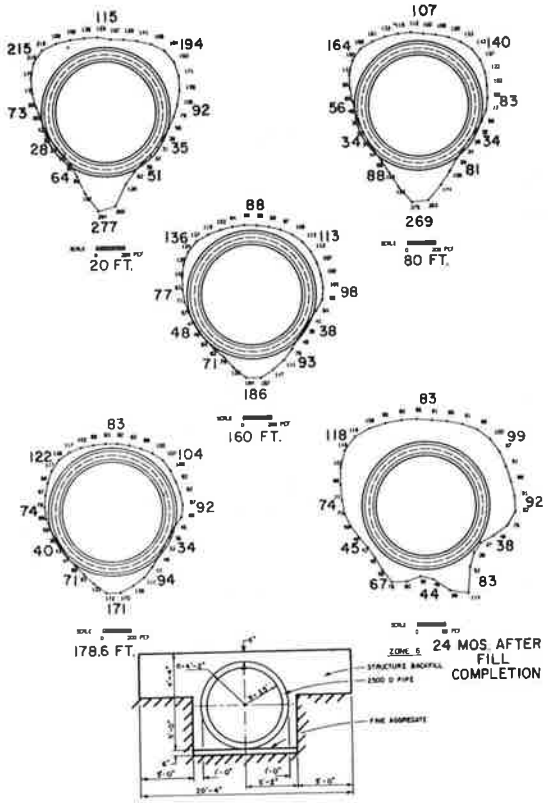

Figure 19. Effective-density profiles, Zone 8.

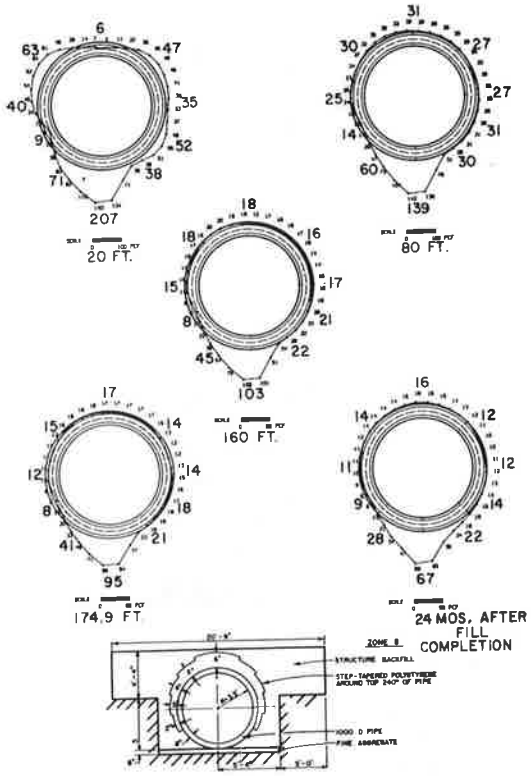

Figure 20. Effective-density profiles, Zone 9.

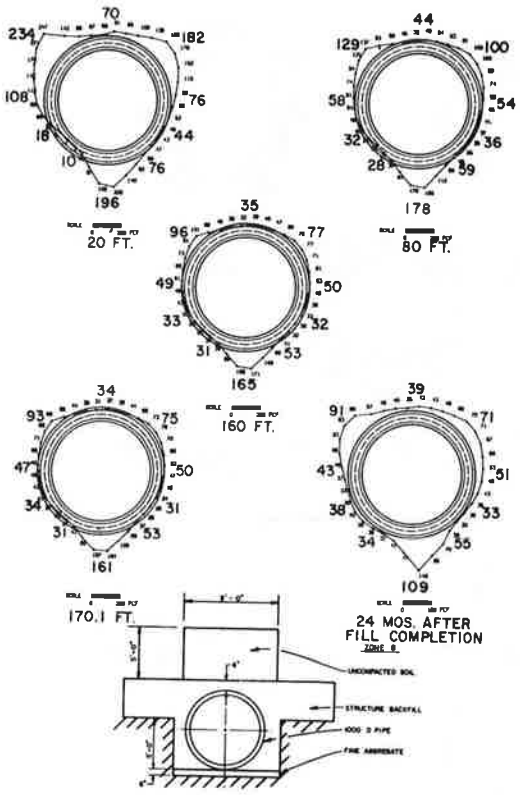

Figure 21. Effective-density profiles, Zone 10.

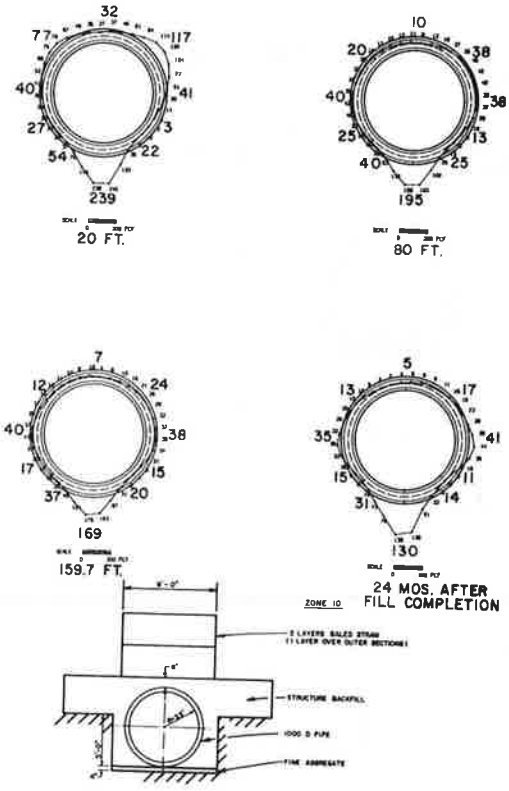

Figure 22. Quasi-theoretical pipe wall displacements compared with experimental displacement, Zone 4.

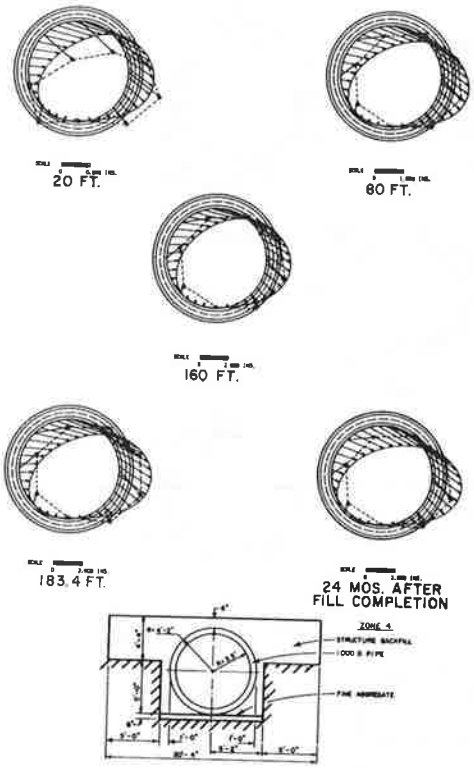

midlevel overfills and Zone-10 maxima moved from the upper quadrants to springing lines above midlevel overfills.

Nonlinear soil stress overfill functions produced general decreases in secant effective densities at the crown, upper quadrants, and invert, whereas lower quadrant densities tended to remain constant. Density maxima tended to decrease more rapidly than minima; there was a trend toward more uniform density distributions with increasing overfill.

Four zones (4, 5, 6, and 7) were placed in a stepped trench and bedded on a shallow layer of compacted fine aggregate (see Figure 2). Observations are described below.

Zone 4 (1000D Pipe)

Quasi-theoretical extreme fiber stress curves predicted limits of cracking with fair accuracy. Cracks appeared at lower overfills than at comparable Zone 8, Mountainhouse Creek, but did not develop to the same widths at higher overfills.

Measured wall displacements agreed favorably with quasi-theoretical ones (Figure 22), especially those based on Cambridge-meter stresses.

Diametral changes agreed closely with those in Zone 3 (cf. Figures 15 and 23), which demonstrates that 95 percent compacted structure backfill between pipe and trench can provide lateral support comparable with that of cement-treated backfill at the sides of the pipe. However, cement-treated backfill provides better support and more uniform soil stress gradients in lower quadrants (exclusive of the invert) where structure backfill is more difficult to consolidate by hand.

Diameter changes were much smaller at Zone 4 than at comparable Zone 8, Mountainhouse Creek (see Figure 23), even though installation procedures were supposed to be the same, which possibly indicates

differences in stringency of inspection, particularly in placement and compaction of structure backfill between the sides of the pipe and trench. Although this research will demonstrate feasibility of appreciable savings by use of lesser pipe strengths, it cannot be overemphasized that in order to take advantage of soil-structure interaction, suggested construction procedures must be performed under stringent inspection. For example, special consideration must be given to placement of backfill under lower pipe quadrants. California specifications recently increased the distance between pipe walls and sides of the trench from 1 ft to 2 ft to accommodate nuclear compaction testing equipment; this change will also help construction workers reach this relatively inaccessible area with hand-operated compaction tools.

Current California specifications prohibit placement of 1000D pipe in any highway embankment, and where this pipe strength is permitted, maximum allowable overfill is 16 ft. At Mountainhouse Creek, Part 1, entrenched 1000D pipe in Zones 7 and 8 did not exhibit hairline cracks until 44 ft of overfill had been placed. The plot in Figure 24 depicts overfills at which the 0.01-in crack appeared at Zone 8, Mountainhouse Creek, and either the 0.01-in crack or delamination for pipe segments comprising various pipe strengths installed at Cross Canyon (see also Table 1). Assuming that the same construction procedures as those used for an entrenched pipe with ordinary structure backfill are employed, with rigid inspection to assure compliance with construction specifications, the upper plotted line in Figure 24 provides suggested ultimate overfill

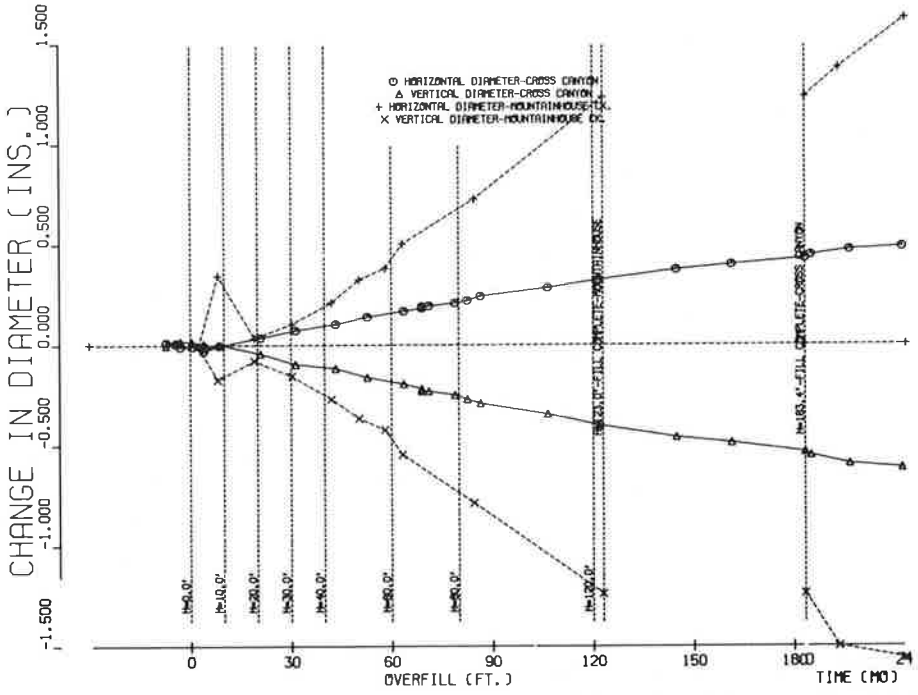

Figure 23. Comparison of diameter changes in Zone 4, Cross Canyon, with those in Zone 8, Mountainhouse Creek.

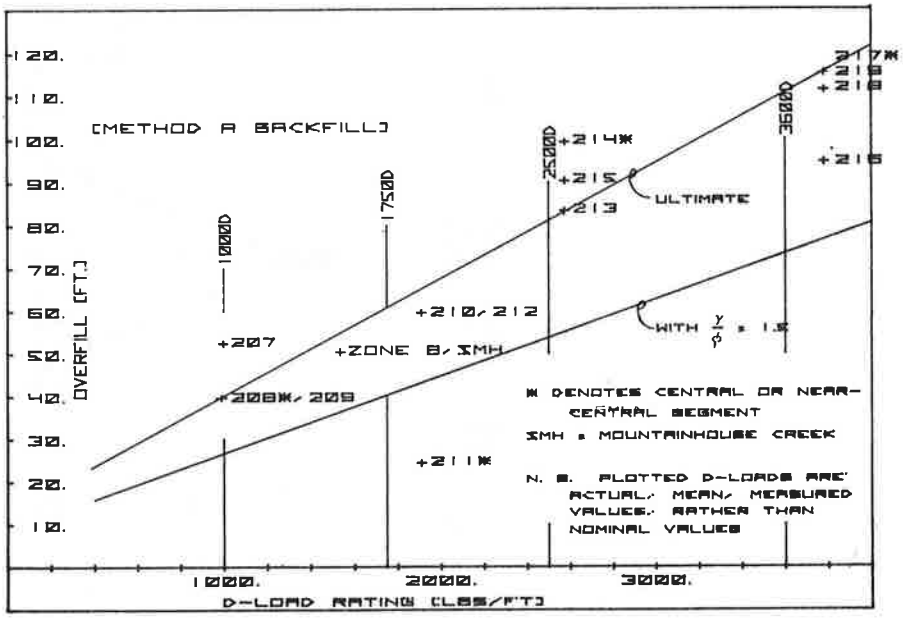

Figure 24. Plot of ultimate and recommended maximum overfills for various pipe strengths based on first appearance of 0.01-in crack or delamination.

limits for pipes of various strengths. A second line based on a safety factor (γ/ϕ) of 1.5 depicts recommended design overfills.

Zone 5 (1750D Pipe)

Much evidence favors the opinion that the central segment (211) in Zone 5 behaved in an anomalous manner. Toward the end of the project, it was learned quite by accident that the pipe manufacturer had used smooth, undeformed inner bars in Zone 5 only, which explains at least a portion of this zone's anomalous behavior for reasons to be noted later in this paper.

Although there was, in general, satisfactory agreement between quasi-theoretical and experimental parameters (e.g., bending moments and displacements), behavior of the central segment was quite different from that of two adjoining segments in this zone and also from that behavior which might have been expected from consideration of segments in other zones.

Central Segment 211 exhibited the 0.01-in crack at a lower overfill (24 ft) than did any of the other segments in any zone. Adjoining Segments 210 and 212, also in Zone 5, did not exhibit the 0.01-in crack until the overfill reached 60 ft.

Segments in this zone exhibited significant delamination above 80 ft of overfill--experimentally measured displacements typically begin to exceed

Table 1. Date and overfill at time of failure.

		Point of Failure[a]					Point of Failure[a]		
			Overfill					Overfill	
Zone	Segment	Date	Meters	Feet	Zone	Segment	Date	Meters	Feet
1	202	01/02/75	18.9	62.0	7	216	04/23/75	28.8	94.6 (delamination)
	201	01/09/75	20.6	67.4		217	05/02/75	35.1	115.2 (delamination)
2	202	12/10/74	15.4	50.6		218	05/01/75	33.9	111.3 (delamination)
	203	12/23/74	17.3	56.7		219	05/02/75	35.1	115.2 (delamination)
3	204	12/10/74	15.0	49.1	8	220	-	-	-
	205	01/02/75	18.7	61.2		221	-	-	-
	206	12/31/74	18.2	59.6		222	01/03/75	18.6	61.0
4	207	12/11/74	16.0	52.5		223	-	-	-
	208	12/05/74	12.1	39.6		224	01/03/75	18.6	61.0
	209	12/05/74	12.1	39.6	9	225			
5	210	01/02/75	18.2	59.6		226			
	211	11/21/74	7.4	24.4		227	DID NOT FAIL		
	212	01/02/75	18.2	59.6		228			
6	213	04/18/75	25.4	83.3 (delamination)		229			
	214	04/23/75	30.3	99.3 (delamination)	10	230	01/03/75	17.8	58.4
	215	04/21/75	27.5	90.3 (delamination)		231	12/03/74	11.4	37.4
						232	12/03/74	11.4	37.4
						233	12/10/74	12.9	42.3
						234	01/03/75	17.8	58.4

[a]Actually, first observation of 0.01-in crack or delamination.

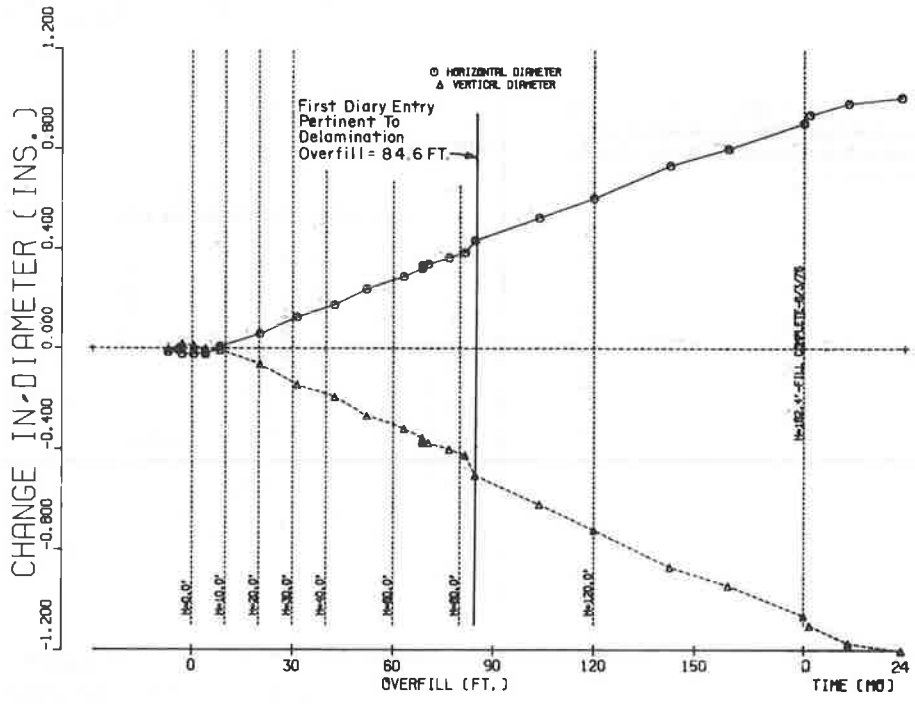

Figure 25. Changes in horizontal and vertical pipe diameters as function of overfill and time after embankment completion, Zone 5.

quasi-theoretical after delamination occurs and the pipe ceases to behave as a usable structure. Overfills at delamination are more accurately identifiable as discontinuities in slopes of the diameter-change curves (Figures 25, 26, and 27).

Diameter changes in the central segment were twice as large as those in Zone 4 (cf. Figures 23 and 25).

Zone 6 (2500D Pipe)

The 0.01-in crack appeared in Zone 6 for the first time in Segment 215 with an overfill of 99 ft. Delamination was observed at lower overfills: 83 ft in Segment 213; 99 ft in Segment 214; and 90 ft in Segment 215. These criteria have been used in the plot of overfills for acceptable behavior (Figure 24).

At any given overfill, effective densities acting on Zone 6 were significantly higher, in general, than those acting on Zones 4 and 5 (cf. Figures 16, 17, and 18).

Up to the 100-ft overfill, diameter changes were 33 percent greater than those in Zone 4 (cf. Figures

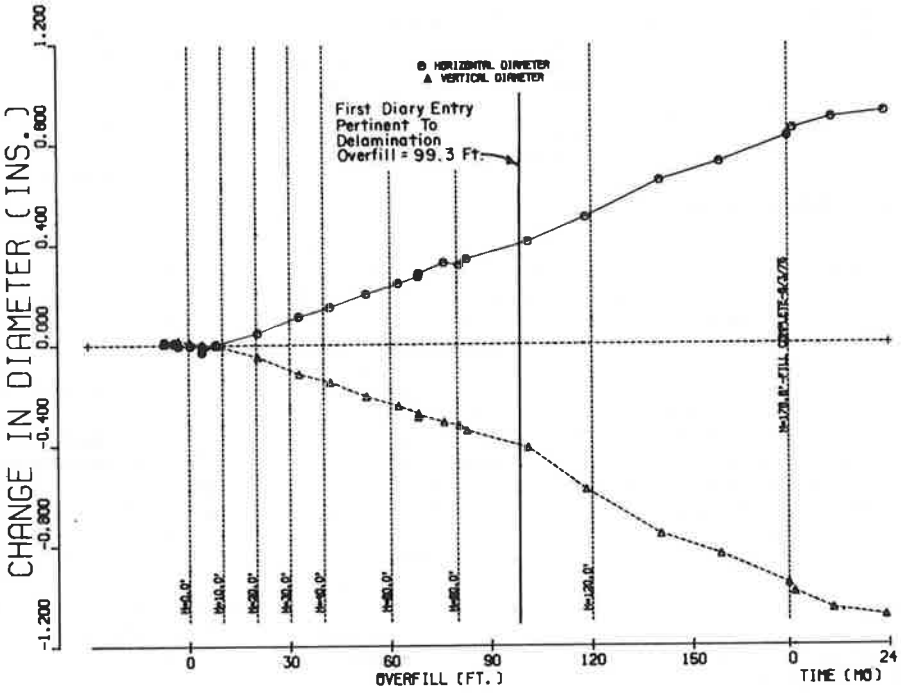

Fgiure 26. Changes in horizontal and vertical pipe diameters as function of overfill and time after embankment completion, Zone 6.

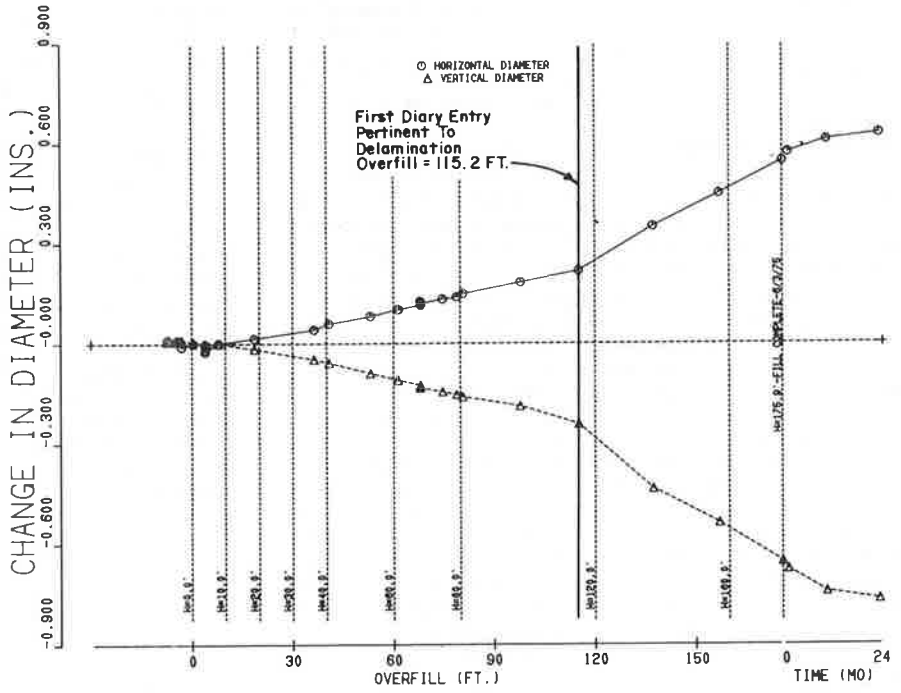

Figure 27. Changes in horizontal and vertical pipe diameters as function of overfill and time after embankment completion, Zone 7.

23 and 26). Above 100 ft, they were twice as great at Zone 6 as those at Zone 4. The Zone 6 pipe, being appreciably stiffer than that in Zones 4 and 5, drew greater load to itself than did the more flexible pipes.

Zone 7 (3600D Pipe)

The 0.01-in crack appeared for the first time in this zone with an overfill of 111 ft in Segment 216 and at an overfill of 115 ft in representative Segment 217 and in Segment 219. Segment 217 also began to delaminate under this overfill. Segment 216 began to delaminate at an overfill of 95 ft but is less representative because it adjoins the more flexible Zone 6.

Diameter changes in Segment 217 were about two-thirds as large as those in Zone 4 up to the 115-ft overfill (cf. Figures 23 and 27), at which point these functions exhibit significant discontinuities at the same time delamination was first observed in the zone. At fill completion, the Zone 7 diametral changes were 25 percent greater than those in Zone 4.

General Observations

A study of distress as manifested by total length of cracking in representative segments is of interest. At the lower overfills, the strongest pipe (Zone 7) exhibited, in general, the least cracking length and Zone 5, the greatest. The most flexible pipe (Zone 4) remained close to the middle-runner position among all zones throughout the entire course of fill construction. Conditions in the stiffer pipes deteriorated more rapidly, and two years after fill completion, based on total crack length, these zones were ranked in the following order: 4, 5, 6, and 7; the most flexible pipe cracked least and the stiffest pipe, the most.

The following are results of observations of three zones (8, 9, and 10) with low-modulus inclusions.

Zone 8 (1000D Pipe with Step-Tapered Polystyrene Plank Inclusion)

Uniaxial laboratory compression tests of small samples of the polystyrene plank demonstrated physical properties conducive to forming good low-modulus inclusions. In laterally confined and unconfined states, specimens were compressed for extended periods of time at varying levels of stress from 1.7 to 21 psi. At the latter level, the material suddenly collapsed.

In the field installation, normal soil stresses acting on the pipe increased gradually under the polystyrene until some point was reached between the 80- and 120-ft overfills when stresses were approximately 21 psi, after which there was no increase.

It is hypothesized that by the time the limiting stress capacity of the polystyrene had been reached, surrounding soil had become sufficiently compact to produce a soil arch so that the soil would not move into the collapsing polystyrene. As a result, this zone ultimately exhibited the most uniform distribution of low effective densities around the upper 240° of pipe periphery of all zones.

Two factors produced some cracking, however: (a) a large concentration of soil stress at the invert, which was characteristic of all zones, and (b) a large diminution of compressive thrust at the crown due to reduction of lateral soil stress by the polystyrene at the sides of the pipe (Figure 28). The tensile stresses at the crown due to heavy invert gradients in soil stresses could not be sufficiently reduced by the small compressive thrust stresses, and cracking occurred.

Diametral changes at Zone 8 were two-thirds as large as those in Zone 4 but seven times as great as those in Zone 9 (cf. Figures 23, 29, and 30); these differences must be attributed to relative lack of lateral support.

Zone 9 (1000D Pipe with Uncompacted Soil in Trench Surmounting Culvert)

The performance of Zone 9 proved superior to that of any other zone. While the observed distribution of soil stress appeared much less uniform, hence less favorable than that in Zone 8 (cf. Figures 19 and 20), the existence of more lateral support than in Zone 8 resulted in greater crown thrusts and hence less cracking (cf. Figures 23, 31, and 32).

Two years after fill completion, the maximum crack width in central Segment 227 was only 0.005 in, so the representative segment in this zone, unlike any other, never exhibited the 0.01-in crack.

Correlations between quasi-theoretical and observed cracking limits were satisfactory, although observed cracking limits were broader than quasi-theoretical. This phenomenon was very typical, which suggests that the 400-psi theoretical cracking stress chosen was too high.

Maximum diameter change was 0.05 in, much smaller than those in Zones 1 through 8 and about half that in Zone 10 (cf. Figures 30 and 33, noting difference in vertical scales).

Zone 10 (Baled-Straw Layer Surmounting Pipe)

Effective-density distributions (see Figure 21) in this zone exhibited sharp gradients in the upper and lower halves of the pipe. Such gradients were typical at the invert in all zones because of a large concentration of soil stress at the invert-bedding interface. At the crown, greatly reduced soil stresses under the straw combined with large stresses in the upper quadrants to produce large stress gradients that tended to dampen with increasing overfills.

Large bending moments in the pipe walls were the natural result of these stress gradients and produced significant early cracking. The 0.01-in crack was first observed under a relatively low overfill of 37 ft (see Table 1).

Above 60 ft of overfill, density gradients in the upper half of the pipe became small; a crown density 8 percent of embankment density transitioned smoothly to 0.3w at the springing line (see Figure 21).

Based on considerations of total crack length, and to some extent other factors, beneficial effects of low-modulus inclusions were more in evidence for deeper overfills. For overfills from 0 to 25 ft, Zones 6 and 7 (the 2500D and 3600D pipes) behaved better than Zone 9 (1000D with uncompacted soil); Zone 4 (the 1000D pipe) was better than Zones 8 and 10 (1000D with polystyrene plank and baled straw, respectively).

At 26 ft, Zone 9 had surpassed all zones but the very stiff Zone 7, but Zones 4 and 6 were still ahead of Zones 8 and 10.

At 66 ft, Zone 9 had surpassed Zone 7, and Zone 8 was below Zone 7 but better than Zones 4 and 6, which were still better than Zone 10.

From 130 ft to fill completion and 24 months beyond, Zones 9, 8, and 10, in that order, were in the best condition and crackwise were in about the same condition. Meanwhile, next in quality of behavior were Zones 4, 5, 6, and 7, in that order, which suggests the interesting anomaly that the degree of cracking distress was better for the more flexible pipes.

Based on considerations of diameter changes and cracking at Cross Canyon, Zone 9 was clearly better than any of the other zones. None of the low-modulus inclusion zones exhibited delamination.

Despite what might have been deemed inferior behavior of Zones 8 and 10 at the lower overfills, they demonstrated relatively small changes in distress beyond the 70-ft overfill, which suggests a potential for use of even higher fills with these construction methods. From 70 to 159 ft, a 127 percent increase in overfill, the total crack length in Zone 8 changed by only 5.5 ft (from 91.1 to 96.6 ft), or 6 percent; that in Zone 9, by 1.9 ft (from 93.1 to 95.0 ft), or 2 percent; and Zone 10, by 4.4 ft (from 92.6 to 97.0 ft), or 5 percent.

Comparison of behavior of Zones 8, 9, and 10 emphasizes the necessity for considering more than one factor in distress development. Large soil-stress gradients in Zone 9 should have been conducive to large bending moments and hence a high incidence of cracking. However, large lateral soil stresses produced large compressive crown thrusts, which reduced the tensile stresses and hence the cracking at the inner periphery of the pipe.

Figure 28. Quasi-theoretical thrusts, Zone 8.

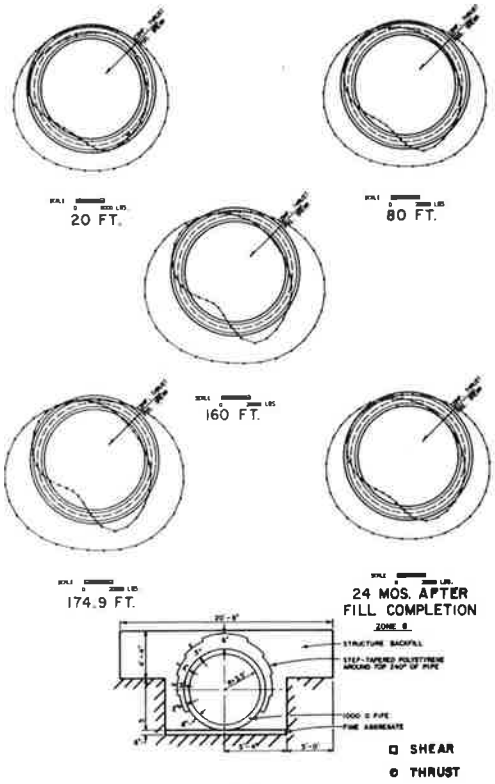

ANALYSIS OF PRESTRESSED PIPE

In order to establish a background of quasi-theoretical parameters for the functional prestressed pipe under 200 ft of earth fill for comparison with measured ones, a second neutral-point analysis was developed, patterned after theory found in Ameron's Prestressed Concrete Cylinder Pipe (28) with some modifications.

The researchers anticipated more difficulty interpreting measured internal strain data from the prestressed pipe walls than in the case of the reinforced-concrete pipe for several reasons: (a) early placement of pipe segments after casting superimposing creep and shrinkage strains due to prestressing on those due to earth loads and (b) the large ratio of wall thickness to pipe radius (approximately 1:2), which produced a nonlinear (hyperbolic) strain diagram.

Anticipating the first problem, the researchers placed a control segment of similar prestressed pipe in a comparable but essentially unstressed environment. The Zone-12 (control) segment was placed on end near the toe of the embankment and covered (outside only) to the level of its upper end. Thus, the segment was not completely unstressed; however,

Figure 29. Changes in horizontal and vertical pipe diameters as function of overfill and time after embankment completion, Zone 8.

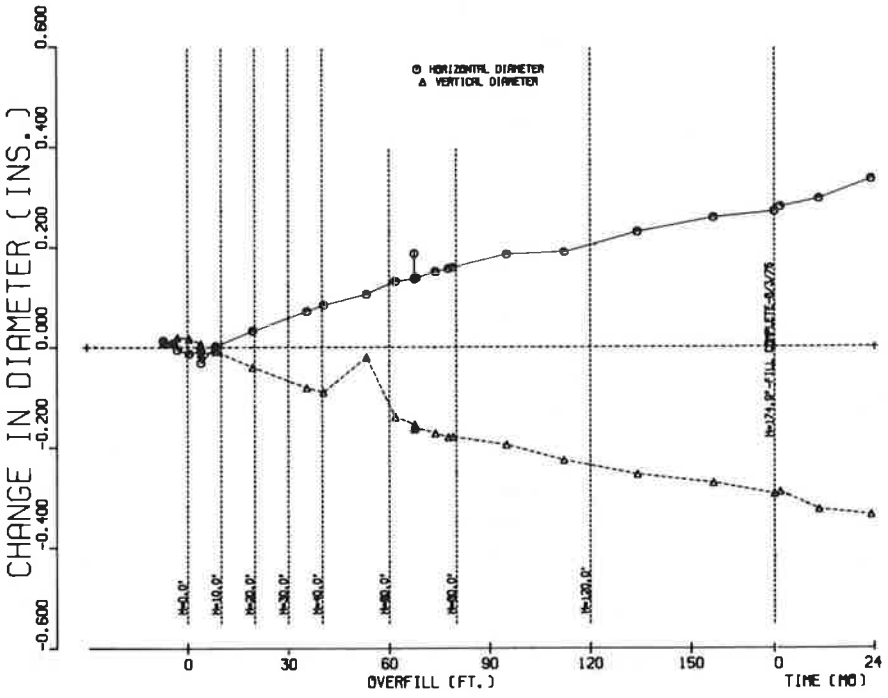

stresses due to the surrounding soil were very small compared with those due to the 200-ft overfill at Zone 11. More variations in ambient air temperature within the control segment might be expected than in Zone 11.

The Zone-12 strains were plotted as functions of time with a datum at June 18, 1974, the date of casting the Zone-12 segment (see Figures 34 and 35); the Zone-11 segment was cast on June 27, 1974. Most of this strain may be seen to have occurred during the first 110-120 days and may be attributed to normal creep and shrinkage.

Subsequent to this initial period, there was a prolonged, general gradual trend toward higher com-

Figure 30. Changes in horizontal and vertical pipe diameters as function of overfill and time after embankment completion, Zone 9.

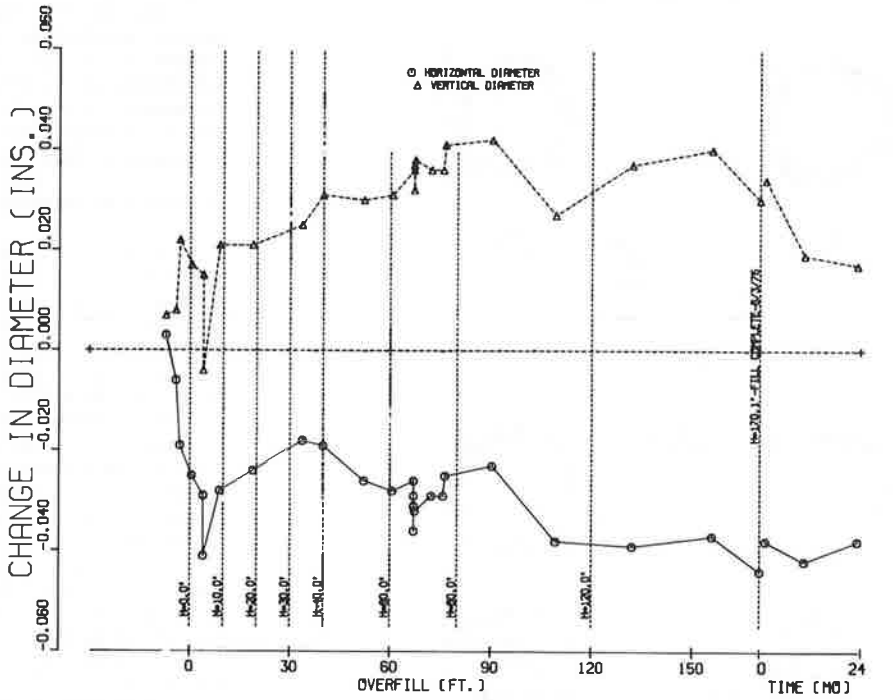

Figure 31. Quasi-theoretical thrusts, Zone 9.

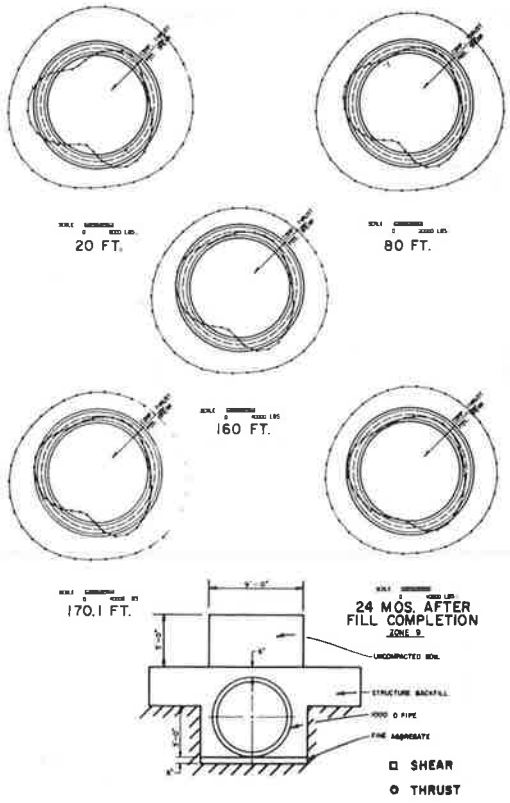

Figure 32. Quasi-theoretical thrusts, Zone 10.

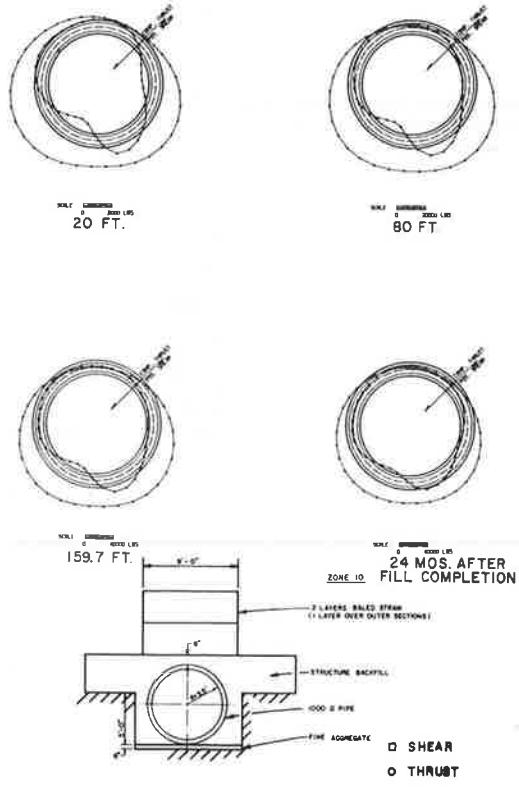

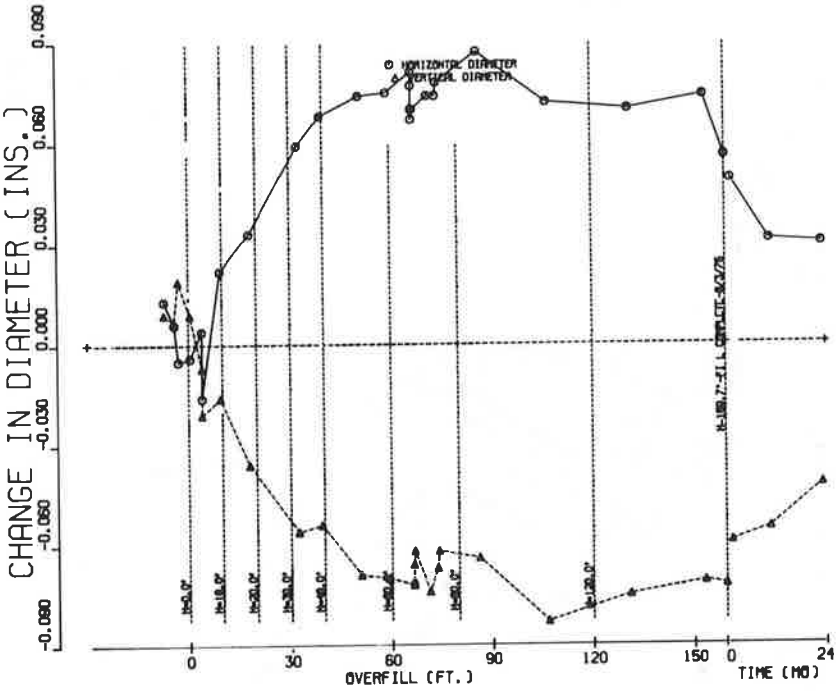

Figure 33. Changes in horizontal and vertical pipe diameters as function of overfill and time after embankment completion, Zone 10.

pressive strains with superimposed trends of shorter duration in a reversed, tensile direction. Such a trend is clearly visible between Days 110± and 350±, during which period the embankment was being constructed. Since this period encompassed the fall, winter, and spring seasons of 1974-1975, tensile trends may logically be attributed to absorption of moisture from the humid atmosphere or from embankment material.

There exists a very large amount of scatter in the readings from the Carlson strain meters embedded in the brush coats; they vary from roughly 130 to 320 microin/in (see Figure 34). The strain pattern shows a possibly significant localization; larger strains are in positions 1, 2, 7, and 8 on the top half of the segment, and smaller strains are in positions 3, 4, 5, and 6 on the bottom half. This phenomenon might have resulted from an increased loss of moisture due to insolation and consequent increased shrinkage during the postcuring storage period prior to pipe placement in the embankment; the top half of the pipe was placed on the sunny side and the bottom half in shadow. This large variation in strain by itself would have virtually precluded use of control Segment 12 for adjustment of Zone-11 strains.

The observed variation in strains in the midplane Carlson meters was much smaller (see Figure 35). Buried almost a foot from either pipe surface, this portion of the concrete was less susceptible to moisture variations and exhibited a strain range of 32-38 microin/in. The researchers elected to consider these Zone-12 midplane strains representative creep and shrinkage strains over the entire depth of the pipe wall. Only the computed thrust is affected.

A typical cross section of unadjusted strains measured at Zone 11 during embankment construction is given in Figure 36, which shows an incompatible strain pattern characteristic of all plots. Straight regression lines could not be fitted to strain readings. Parabolic regression curves could be plotted that closely approximated all strains except those in the brush coats, which were almost invariably on compressive sides of the parabolas. This phenomenon has a logical explanation. The rich gunite mixture air-blown around the surface of the hardened core should exhibit large shrinkage. As brush coats shrink against the restraint of the already shrunken core, extensive longitudinal cracking must develop. The relatively long Carlson minimeters may span a number of such cracks, and when cracks close under embankment loads, strain meters produce readings that are unrepresentative on the compressive side and incompatible with strain patterns in the core. The researchers elected to ignore brush-coat strains and approximate patterns of core strains by regression parabolas.

A new zero strain datum was plotted and coordinates were transformed to produce equal compressive and tensile areas between the parabolas and the new base lines. Thrust factors (T/E_C) were subsequently computed as products of the area of the transformed pipe cross section and differences in strains between old and new base lines; bending-moment factors (M/E_C) were computed as integrated products of the stress areas and lever arms about new x_0-axes.

The values of M/E_C and T/E_C were subsequently modified by a factor, E_C (= 3000 ksi), to produce experimental values of bending moments and thrusts in the pipe wall due to overburden for a number of significant overfills. Experimental values are compared with quasi-theoretical values of the same parameters from the neutral-point program and measured soil stresses for maximum overfill in Figures 37 and 38. Quasi-theoretical wall displacements are compared with extensometer measurements in Figure 39. The commensurate, observed distribution of effective densities about the pipe periphery, based only on Cambridge contact stress-meter readings, is plotted in Figure 40. Correlations between quasi-theoretical and measured parameters were extremely good.

ANALYSIS OF SETTLEMENTS

A method of analysis whereby earth loads acting on the crown of a buried conduit could be predicted

Figure 34. Zone 12, plane-1 (brush-coat) strains.

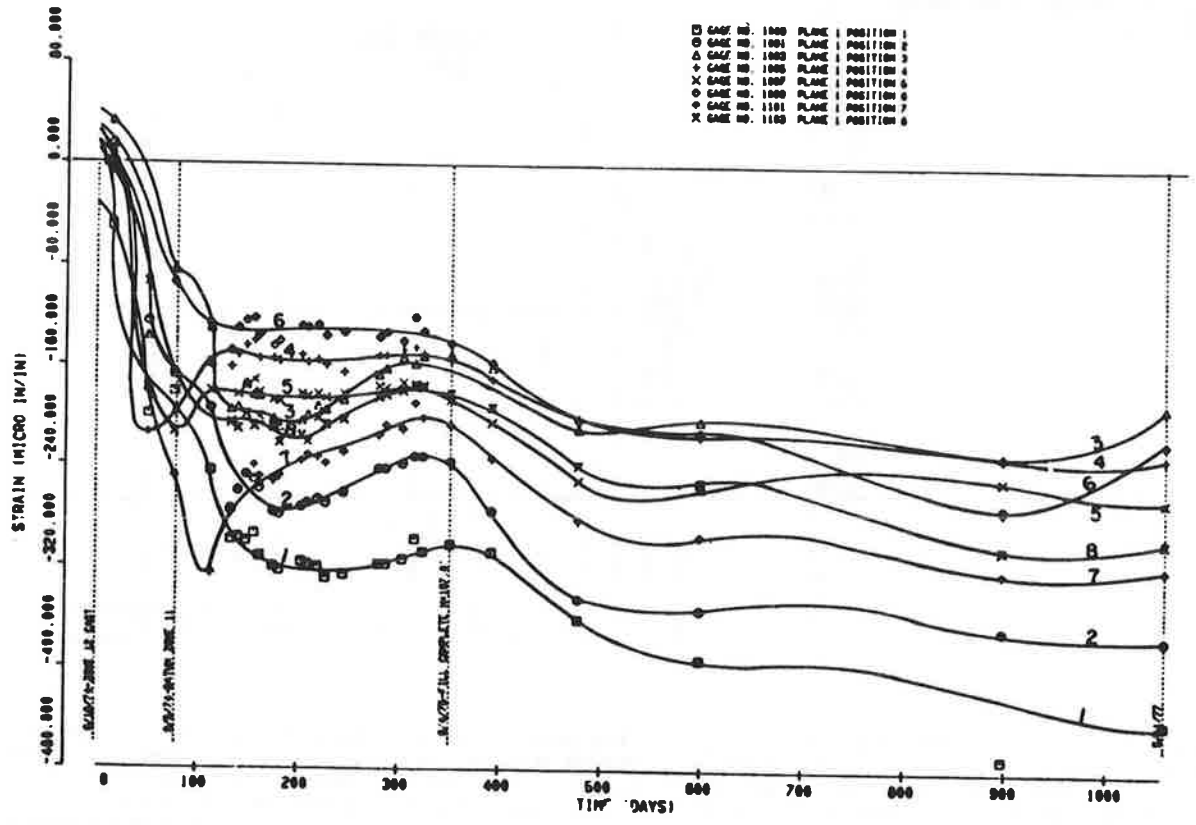

Figure 35. Zone 12, plane-2 (midplane) strains.

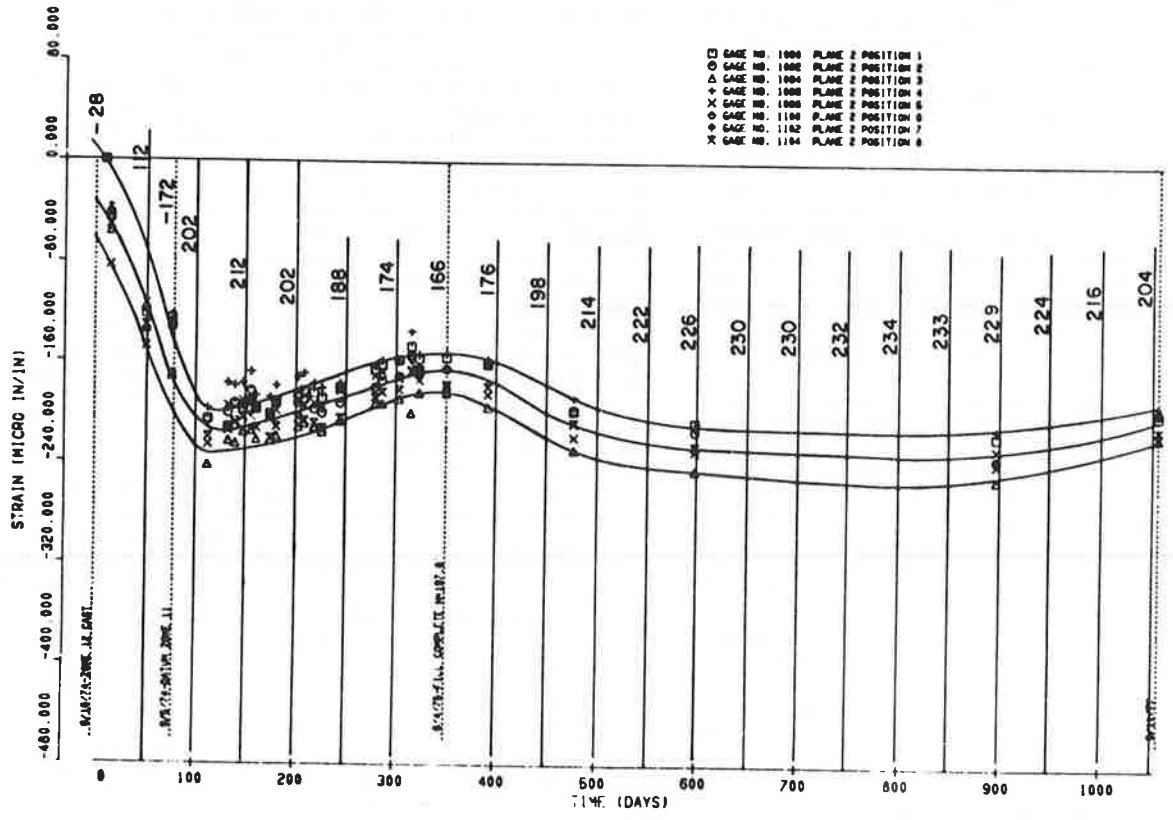

Figure 36. Typical strain cross section for prototype (Zone 11).

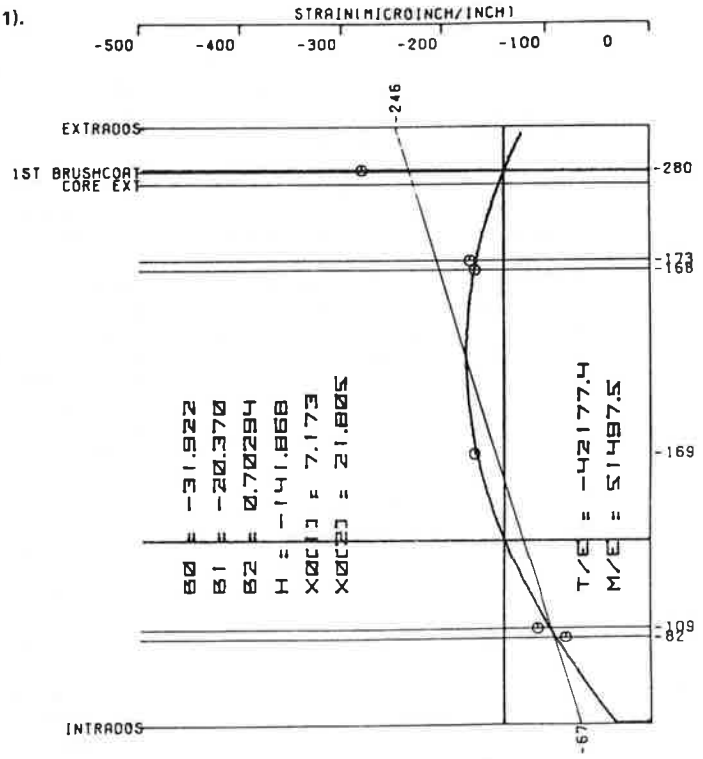

Figure 37. Quasi-theoretical versus experimental bending moments, maximum overfill.

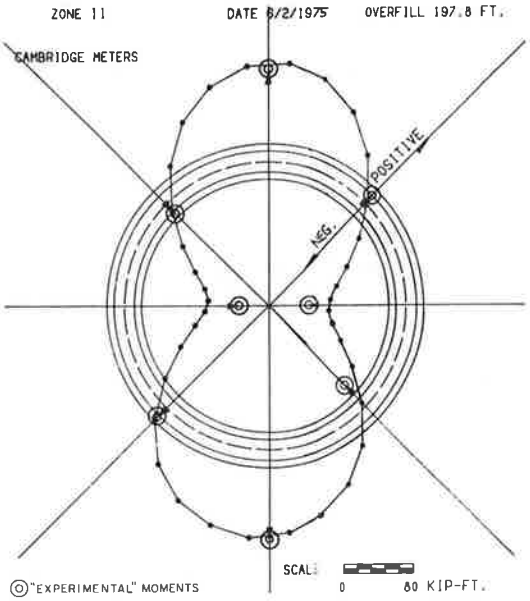

Figure 38. Quasi-theoretical versus experimental thrusts, maximum overfill.

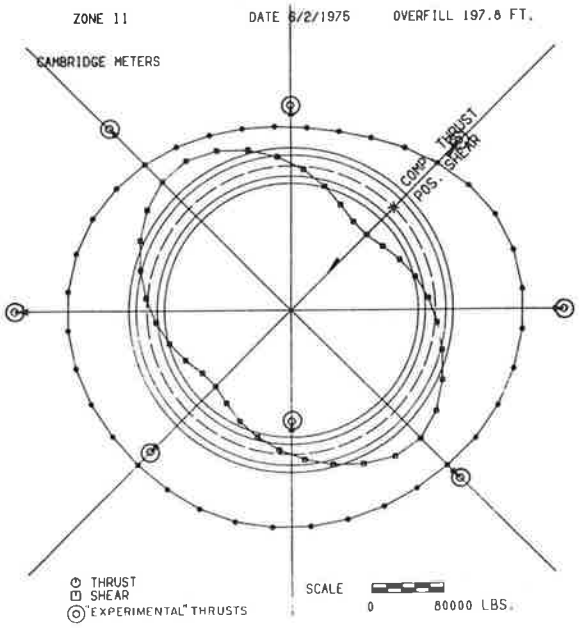

from assessment of differential settlements between the conduit centerline and the exterior prisms was developed by Marston, Spangler, Costes, and others (24, Section 6). For several decades this method, commonly described as settlement-ratio analysis, has been employed by engineers as a mainstay among design procedures for buried pipes.

At Cross Canyon, sophisticated measuring equipment produced a significant body of differential-settlement data for the embankment and pipe and strains in low-modulus inclusions. Comprehensive analyses of data have been made to compare experimentally measured crown loads with quasi-theoretical loads obtained from settlement ratios. Two solutions were examined in which (a) settlement ratios were determined from field measurements at Cross Canyon and (b) ratios recommended by Spangler on the basis of statistical studies of numerous field installations were used.

Figure 41, which is typical, provides comparisons

of calculated crown loads for various values of $r_{sd\rho}$ recommended by Spangler and for various quasi-theoretical values of $r_{sd\rho}$ based on field measurements; soil stresses are measured by stress meters at the crown and in the embankment above the crown for Zone 1. The plotted quasi-theoretical and recommended crown loads are, by comparison with measured ones, very high. Poor correlations were typical of all zones but Zone 9.

For induced-trench Zones 9 and 10, settlement ratios calculated from field data closely approximated the range of -0.3 to -0.5 recommended by Spangler. Encouraging correlations were obtained at Zone 9 between quasi-theoretical and measured crown loads by using Costes' approach, but Spangler's methods still produced very high crown loads compared with measured ones. For Zone 10, neither Spangler's nor Costes' approach produced valid results. Spangler's recommended values of r_{sd} failed to predict nonlinearity of observed functions of soil stress and overfill, especially for Method-B (low-modulus inclusion) installations.

In 1955, Costes modified Spangler's assumptions and presented a method by which an induced-trench culvert may be analyzed by using the same force diagram that Spangler used but taking into consideration differences in moduli of compaction of embankment and trench materials and the broad range of possibilities for the parameter $K\mu$. Implementation of Costes' method of analysis would be difficult unless extensive testing of fill and trench material were performed prior to design of a culvert. Closer predictions of crown stresses could be made if such testing could be performed economically. A less exact but more practical approach is to use average values for physical properties based on statistical analyses of similar materials; however, as was noted in analyses of Zones 9 and 10, this method is still not completely reliable.

Based on Cross Canyon studies, the settlement-ratio method of analysis is not reliable for predicting crown loads, and, especially for rigid conduits or deep embankments, the information it provides is not sufficient to make reasonable assessments of supporting strengths of culvert-soil systems.

Figure 39. Quasi-theoretical versus experimental wall displacements, maximum overfill.

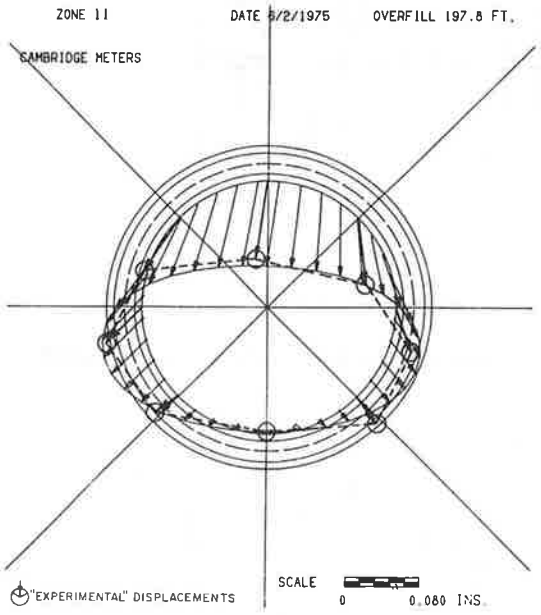

Figure 40. Observed effective-density profile, Zone 11, maximum overfill.

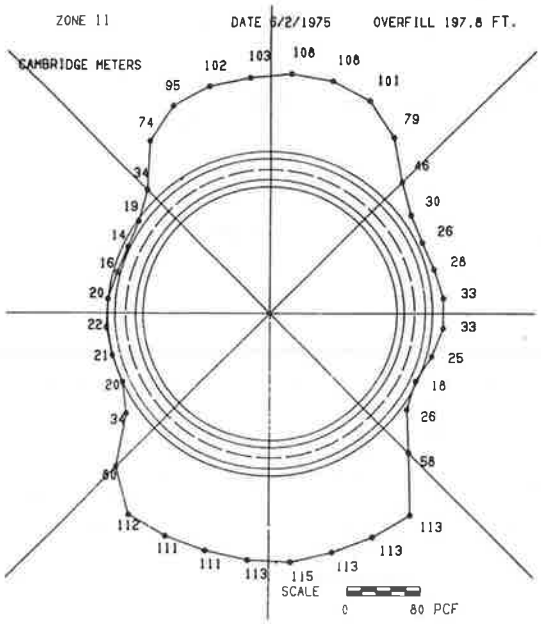

ANALYSIS OF COSTS

Costs per unit length of each test zone were calculated from bid prices to provide comparisons of relative economy of construction methods. Because of

Figure 41. Comparisons of measured soil stresses and those from settlement-ratio analysis, Zone 1.

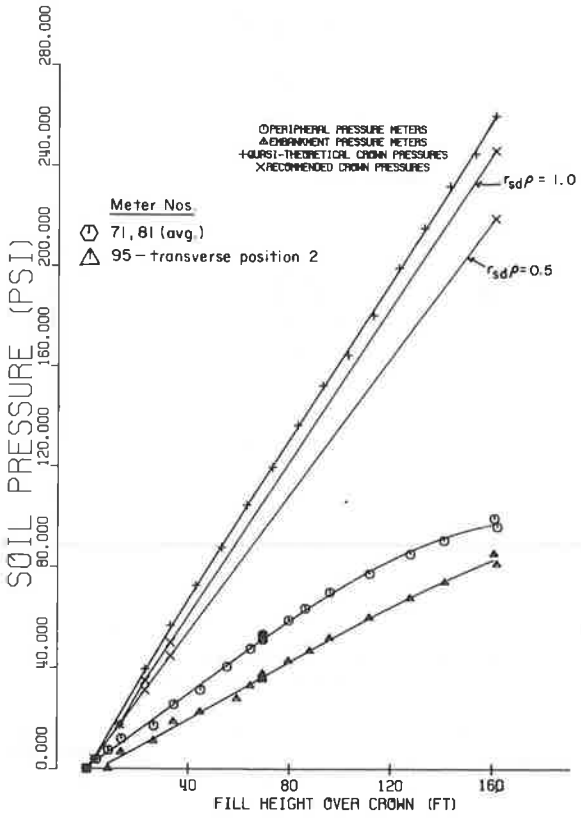

the highly specialized nature of the work, short zones, delays caused by instrumentation, etc., costs should be considered in a relative, not absolute, sense:

Zone	Cost ($) Per Linear Foot	Per Meter
2	152.08	498.81
4	163.42	536.02
1	164.88	540.79
3	168.29	551.99
9	171.75	563.35
5	173.42	586.82
8	184.44	604.95
6	188.42	618.02
10	193.01	633.07
7	209.28	686.43
11	493.16	1617.56

CORRELATIONS OF CROSS CANYON DATA WITH HEGER'S CRITERIA

Heger has published design equations for reinforced-concrete pipe distress as background criteria for a proposed design method. Four modes of distress are considered: crack control (appearance of the 0.01-in crack), radial tension, diagonal tension, and ultimate flexure. These criteria were developed from statistical analyses of data from a large number of three-edge bearing tests.

The 0.01-in crack is a particularly convenient criterion, primarily because it has traditionally been used as a significant point in the three-edge bearing test in the United States and Europe. This crack width is considered by many culvert designers as the limit beyond which corrosion of reinforcing steel poses a significant threat.

Delamination, or bowstringing, due to excessive radial tension is considered by the researchers to be a more important form of distress than cracking for several reasons:

1. Surface cracking is readily visible and may be repaired by patching with the expectation that structural integrity will not be significantly impaired.
2. Delamination may be observed only at the ends of pipe segments at open joints.
3. When delamination occurs, the inner or outer shells of the pipe wall and reinforcing cages cease to function structurally and the pipe loses a portion of its supporting capacity; this weakening is apparent from visible discontinuities in functions of diameter change and overfill and in deteriorations in correlations of quasi-theoretical and observed wall displacements.
4. Repairing delamination is difficult and offers little hope of restoring structural integrity.

Shear failure in pipe walls is more critical than delamination. The typical crack crosses the entire wall, and there may be radial wall displacement on one side of the crack relative to that on the other and resultant exposure of reinforcing cages.

Ultimate flexure may be observed in two phases, which involve yielding of the inner reinforcing bars at invert and crown and subsequent yielding of the outer bars at the springing lines to form four plastic hinges and possibly to induce pipe collapse.

Heger's equations may be used to predict these failure modes. We investigated their validity in the Cross Canyon installation.

The 0.01-in crack and delamination have been commonly observed during Caltrans pipe research, at least one shear failure has been observed, and ultimate flexure has also occurred. These distress modes do not occur in all instances in the same chronological sequence, and some modes may occur exclusively of others. At Cross Canyon, Zone 3, the first 0.01-in crack was observed at 61 ft of overfill, delamination at 175 ft. At Zone 5, the first 0.01-in crack was observed at 24 ft of overfill, delamination at 85 ft. Delamination and the 0.01-in crack were first observed at Zone 6 at about the same overfill (99 ft). Zones 4, 8, and 10 all exhibited the 0.01-in crack without delamination, whereas Zone 9 experienced neither failure mode.

At Mountainhouse Creek, Part 1, entrenched Zones 7 and 8 cracked, but for the almost fully positive-projecting Zone 9, the dominant mode of distress was pronounced "bowstringing." Zone 10, supported on any unyielding, 60° concrete bedding, failed in shear at one edge of the bedding, and one side of the wall moved inward 16 in relative to the other side. A shearing failure also occurred at Zone 11 as the pipe settled into a soft polystyrene bedding and encountered passive resistance from the soil outside the bedding. Positive-projecting Zones 9 through 12 at Mountainhouse Creek, Part 1, exhibited ultimate flexure by cracking of the invert and crown and crushing of the concrete at the springing lines. Cores taken from the entrenched 4000D Mountainhouse Creek, Part 2, exhibited incipient delamination but no surface cracking.

The equations furnished by Heger demonstrate that appearance of various failure modes depends on differing combinations of bending moment, thrust, and shear, which explains the aforementioned phenomena. For these reasons, much caution must be exercised in establishment of specified effective-density profiles for use in design. A profile that is not representative for a given construction condition may indicate stresses that are conservative for one failure mode and neglect to predict another mode.

In the establishment of such specifications, certain premises should be considered that seem sufficiently self-evident to be axiomatic; still, the researchers encountered sufficient inertia in their acceptance by other engineers to make them worth open discussion. The debatable premises are as follows:

1. In the general case of culverts embedded in deep embankments, the functions for soil stress and overfill will be nonlinear, although they may, under certain unique circumstances, be linear for embankments with or without low-modulus inclusions.
2. Typical effective-density profiles observed by Caltrans researchers for culvert installations with and without soft inclusions have been characterized by density minima at the crown and centers of lower quadrants (12:00, 4:30, and 7:30 o'clock) and density maxima at the invert and centers of the upper quadrants (1:30, 6:00, and 10:30 o'clock). Density gradients are more severe at low overfills but dampen toward more uniform distributions at higher overfills.
3. Because of items 1 and 2 above, it is unsafe to consider only the effective-density profile observed at time of fill completion to establish specifications. The embedded pipe culvert is statically indeterminate and must be checked at all construction levels for design safety.
4. A specified effective-density profile that envelopes all observed profiles for a given culvert does not necessarily produce a more conservative design than the encompassed profiles. The fact that observed density profiles fall essentially within certain bands of loading does not prove these latter to be safe for design specifications.
5. Because moments, thrusts, and shears in differing combinations produce different distress modes

and because of item 4 above, it is essential that specified density profiles be representative in the sense that they are of approximately the same configurations as might be expected for given construction conditions.

6. There is no justifiable reason for designing culverts with soft embankment inclusions for the same profiles as those without inclusions, or for very rigid and very flexible pipes, or for two similar pipes under similar construction modes at very different overfills. Culvert design specifications should differ for differing construction modes and for different ranges of overfill. A design for any given overfill should be checked at upper limits of lower overfill ranges by using appropriate density profiles for those ranges. Designs should be checked for all potential modes of distress at these levels. It is of little significance that a design does not suggest a shear failure under a deep overfill if irreparable delamination is indicated under more severe soil stress gradients characteristic of some lower overfill.

For very expensive culvert installations, where distress is not permissible, a finite-element analysis of the culvert and embankment may be useful. In addition to the expense and delays required by the analysis, the designer must consider the need for site surveys (to establish important boundary conditions); effects of clearing, grubbing, and stripping on such conditions; and the need for developing realistic embankment-material properties through soil classification or triaxial testing of samples from potential sources. If the installation does not warrant this expenditure of effort and money, the designer must use specified density profiles based on observations of past installations and weigh the risks involved in the possibility that construction conditions may produce very different soil-stress distributions.

In addition to making studies of finite-element programs such as REA, CANDE, and NUPIPE, we have advocated certain profiles of effective-density coefficients based largely on observed verified soil-stress distributions at Cross Canyon. The researchers suggest use of these coefficients in conjunction with anticipated embankment densities to establish effective-density profiles, to be converted in turn to soil-stress distributions for input to Caltrans' computerized neutral-point analysis. Output parameters would be evaluated on the basis of Heger's criteria for various possible distress modes.

Studies of Heger's criteria produced the following comparisons:

1. Crack control (f_s.01): Quasi-theoretical inner-reinforcing-bar and concrete stresses output from the neutral-point program were evaluated at overfills at which the 0.01-in crack first appeared, according to the field research coordinator's diary (see Table 2).

Smooth cold-drawn wire was used for inner bars at Zone 5 only. Heger's equations for this type of reinforcement use different coefficients than those for hot-drawn deformed bars, which explains at least part of the anomalous behavior of this zone, and its classification as 1750D is even questionable. It is of interest that calculated stresses exhibit encouraging agreement even when they are greater than the

Table 2. Comparisons of quasi-theoretical stresses at 0.01-in crack with those from Heger's criteria.

Zone	Inner-Reinforcing-Bar Stresses (psi)	
	Maximum Quasi-Theoretical	Heger's Criteria[a]
3	92 000	
4	60 000	
5	37 000	
6	56 000	
8	70 000[b]	
10	69 000	
Avg 1000D[c]	72 750	72 200
Avg 1750D[d]	37 000	36 700
Avg 2500D[e]	56 000	36 000

[a] f'_c = (6000 psi).
[b] See Figure 9.
[c] Zones 3, 4, 8, and 10.
[d] Zone 5.
[e] Zone 6.

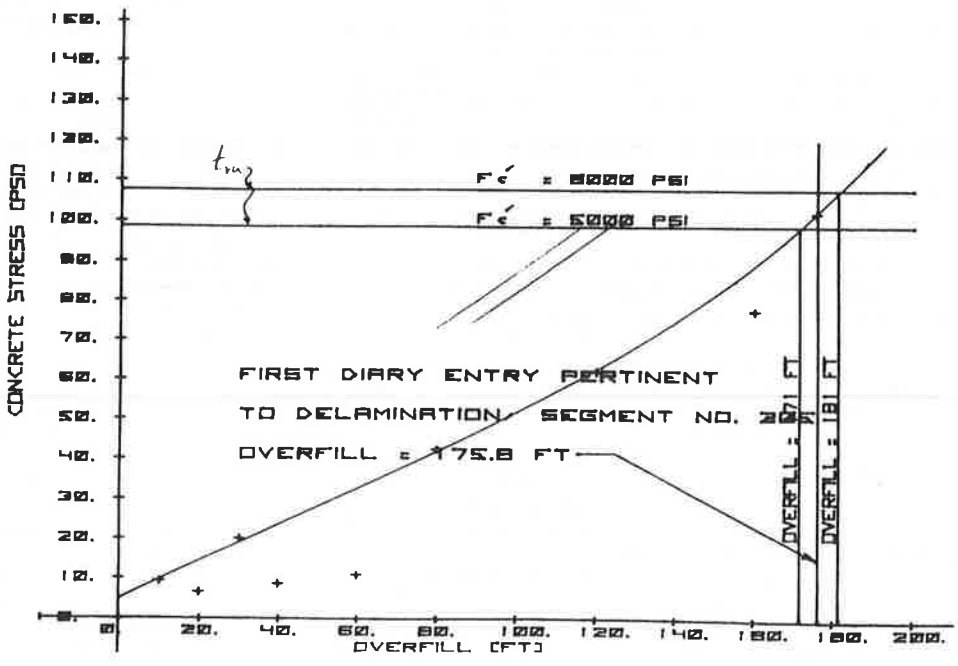

Figure 42. Radial tension stresses computed from Heger's criteria compared with 1.4fc', Zone 3.

f_y (=58 000 psi), which is an upper bound in the criterion.

2. Incipient delamination: Figures 42 and 43 show plots of radial tension stress (t_r) as functions of overfill for Zones 3 and 4 compared with t_{ru} $[=1.4(f_c')^{1/2}]$ for f_c' = 5000 and 6000 psi. Intersections of plots of t_r with t_{ru} should mark overfills at which delamination might be expected to begin. Plots for Zones 8, 9, and 10, for which no delamination was observed, showed curves of t_r not intersecting t_{ru}, whereas similar plots for Zones 5 and 6 closely predicted delamination overfills.

Also included is Figure 44, in which calculated values of t_r at the invert for a 140V:42H loading for various overfills have been compared with t_{ru}. A comparison of predicted overfills at which delamination would occur for this loading demonstrates that predictions would be highly unconservative for Zones 5 and 6, which delaminated at 85 and 99 ft, respectively, but would unjustly penalize the low-modulus inclusion Zones 8, 9, and 10, where no delamination was observed.

3. Diagonal tension and ultimate flexure: Although distress of these types was very evident at Mountainhouse Creek, Part 1, quantitative data that would allow application of Heger's criteria for these modes of failure are lacking. Either type of failure may have occurred at Zones 1, 2, and 4 at Cross Canyon in the late stages of the project, but they are not specifically mentioned in diaries and overfills at failure cannot be accurately specified.

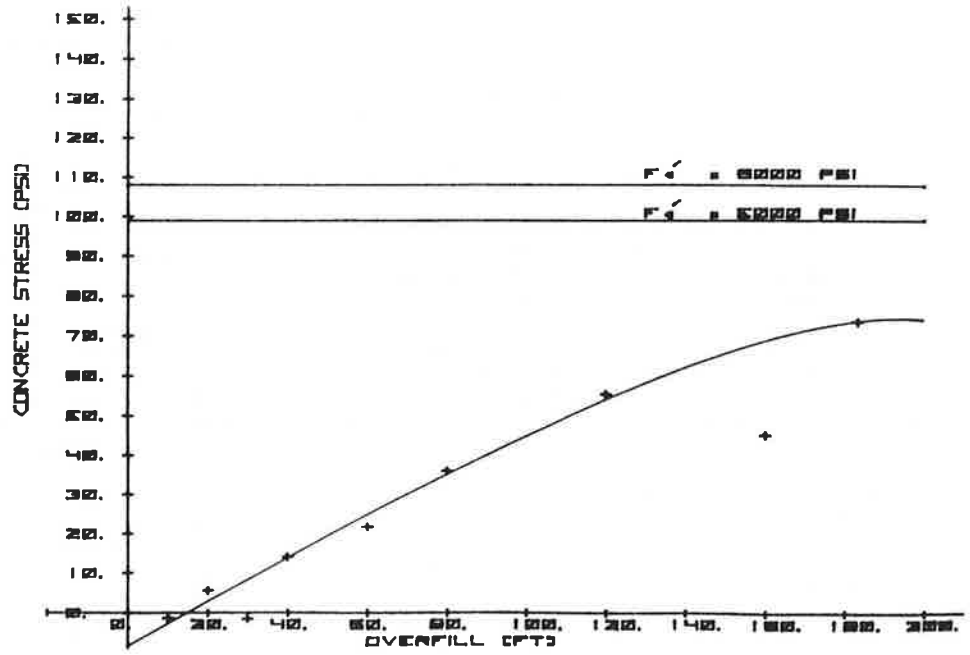

Figure 43. Radial tension stresses computed from Heger's criteria compared with 1.4fc', Zone 4.

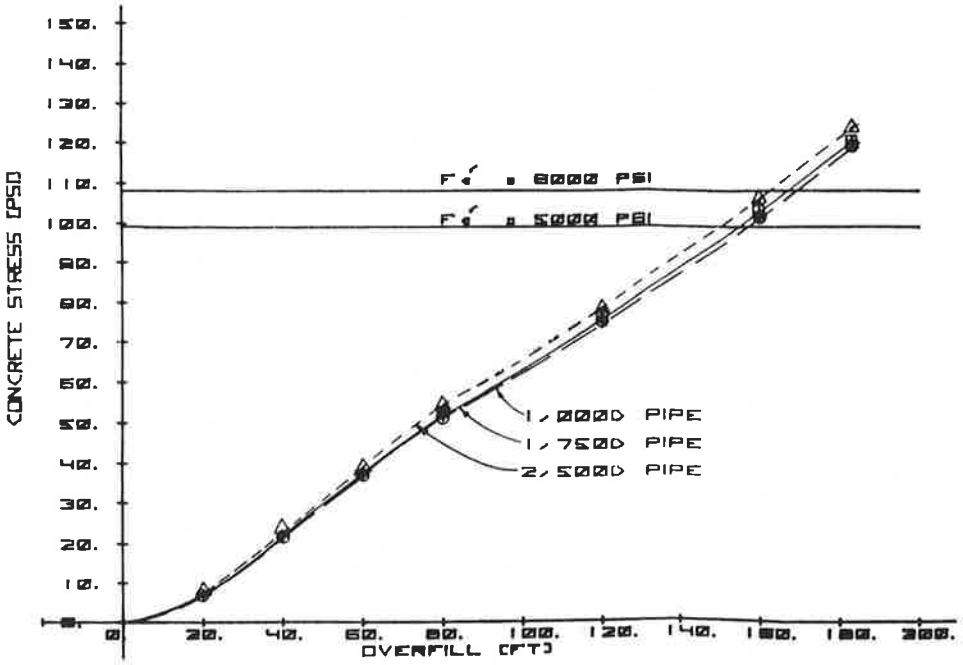

Figure 44. Radial tension stresses computed from Heger's criteria and neutral-point analysis moments and thrusts compared with 1.4fc', 140V:42H soil-stress distribution.

SUMMARY AND CONCLUSIONS

This paper has stressed the importance of using caution in establishment of design specifications for culverts; it should be ascertained that such specifications are representative of those that might occur for given, anticipated construction conditions in order that all possible modes of distress might be accurately evaluated. We caution against use of one or two bands of loading that may envelope all observed profiles and, in some instances, produce similar maximum stresses while failing to predict other, significant modes of failure.

ACKNOWLEDGMENT

Research described in this article was performed in conjunction with a project entitled Rigid Pipe Prooftesting Under Excess Overfills Using Varying Backfill Conditions by Caltrans in cooperation with the Federal Highway Administration, U.S. Department of Transportation.

Opinions, findings, and conclusions expressed in this article are ours and do not necessarily reflect official views or policies of Caltrans or the Federal Highway Administration. This paper does not constitute a standard, specification, or regulation.

REFERENCES

1. R.E. Davis. Structural Behavior of a Reinforced Concrete Arch Culvert. Bridge Department, California Division of Highways, Sacramento, Rept. SSR 9-66, 1966.
2. R.E. Davis and A.E. Bacher. California's Culvert Research Program--Description, Current Status, and Observed Peripheral Pressures. HRB, Highway Research Record 249, 1968, pp. 14-23.
3. R.E. Davis and A.E. Bacher. Forces on Rigid Culverts Under High Fills--Discussion. Journal of the Structural Division of ASCE, Vol. 93, Oct. 1967, p. 105.
4. R.E. Davis and L.R. Patterson. Structural Behavior of a Reinforced Concrete Arch Culvert, Phase 2: Posey Canyon. Bridge Department, California Division of Highways, Sacramento, Rept. SSR 2-68, 1968.
5. R.E. Davis. Structural Behavior of a Flexible Metal Culvert Under a Deep Earth Embankment Using Method B (Baled Straw) Backfill. Bridge Department, California Division of Highways, Sacramento, Rept. R&D 4-69, 1969.
6. R.E. Davis. Structural Behavior of Concrete Arch Culvert. Journal of the Structural Division of ASCE, Vol. 95, No. ST12, Dec. 1969, pp. 2665-2686.
7. R.E. Davis and A.E. Bacher. Structural Behavior of a Reinforced Concrete Arch Culvert, Phase 2: Posey Canyon (Supplemental). Bridge Department, California Division of Highways, Sacramento, Rept. R&D 6-70, 1970.
8. R.E. Davis, A.E. Bacher, and J.C. Obermuller. Structural Behavior of a Concrete Pipe Culvert--Mountainhouse Creek (Part 1). Bridge Department, California Division of Highways, Sacramento, Rept. R&D 4-71, 1971.
9. R.E. Davis. Structural Behavior of Concrete Arch Culvert: Closure and Errata. Journal of the Structural Division of ASCE, Vol. 97, No. ST4, April 1971.
10. R.E. Davis and A.E. Bacher. Concrete Arch Culvert Behavior--Phase 2. Journal of the Structural Division of ASCE, Vol. 98, No. ST11, Nov. 1972.
11. D.W. Spannagel, R.E. Davis, and A.E. Bacher. Structural Behavior of a Flexible Metal Culvert Under a Deep Earth Embankment Using Method A Backfill. Bridge Department, California Division of Highways, Sacramento, Rept. CA-HY-BD-624111-73-6, June 1973.
12. R.E. Davis, A.E. Bacher, and J.C. Obermuller. Concrete Pipe Culvert Behavior (Part 1). Journal of the Structural Division of ASCE, Vol. 100, No. ST3, March 1974, pp. 599-614.
13. R.E. Davis and A.E. Bacher. Concrete Pipe Culvert Behavior (Part 2). Journal of the Structural Division of ASCE, Vol. 100, No. ST 3, March 1974, pp. 615-630.
14. D.W. Spannagel, R.E. Davis, and A.E. Bacher. Effects of Method A and B Backfill on Flexible Culverts Under High Fills. TRB, Transportation Research Record 510, 1974, pp. 41-55.
15. R.E. Davis, A.E. Bacher, and J.C. Obermuller. Concrete Pipe Culvert Behavior (Part 1): Closure. Journal of the Structural Division of ASCE, Vol. 101, No. ST7, July 1975.
16. R.E. Davis and A.E. Bacher. Concrete Pipe Culvert Behavior (Part 2): Closure. Journal of the Structural Division of ASCE, Vol. 101, No. ST7, July 1975.
17. R.E. Davis, A.E. Bacher, and E.E. Evans. Structural Behavior of a Concrete Pipe Culvert--Mountainhouse Creek (Part 2). California Department of Transportation, Sacramento, Rept. CA-DOT-DS-4121-2-75-8, Sept. 1975.
18. R.E. Davis, H.D. Nix, and A.E. Bacher. Structural Behavior of a Reinforced Concrete Arch Culvert--Phase 3, Cedar Creek. California Department of Transportation, Sacramento, Rept. FHWA-CA-ST-4120-01 through FHWA-CA-ST-4120-11, 1977.
19. R.E. Davis and A.E. Bacher. Rigid Culvert Tests--Mountainhouse Creek, Part 1. Concrete Pipe News, American Concrete Pipe Association, Vienna, VA, Aug. 1978.
20. R.E. Davis and A.E. Bacher. Rigid Culvert Tests--Mountainhouse Creek, Part 2. Concrete Pipe News, American Concrete Pipe Association, Vienna, VA, Sept. 1978.
21. R.E. Davis and A.E. Bacher. Behavior of Buried Concrete Pipe: Discussion. Journal of Geotechnical Engineering Division of ASCE, Vol. 105, No. GT3, March 1979.
22. R.E. Davis, H.D. Nix, and A.E. Bacher. Arch Culvert Footing Movements. Journal of Structural Division of ASCE, Vol. 105, April 1979, pp. 729-738.
23. R.E. Davis, H.D. Nix, and A.E. Bacher. Arch Culvert Research--Phase 3. Journal of the Structural Division of ASCE, April 1979, pp. 739-743.
24. R.E. Davis, A.E. Bacher, and others. Rigid Pipe Prooftesting Under Excess Overfills with Varying Backfill Parameters (Sections 1-9). California Department of Transportation, Sacramento, 1978-1982.
25. R.E. Davis, H.D. Nix, and A.E. Bacher. Arch Culvert Footing Movements: Closure. Journal of the Structural Division of ASCE, Vol. 106, No. ST9, Sept. 1980.
26. P.F. Hadala. Effect of Placement Method on the Response of Soil Stress Gages. Proc., Soil Dynamics Conference, Albuquerque, NM, 1967.
27. K.A. Jackura. Instrument for Determining Stress Displacements in Soil. California Department of Transportation, Sacramento, Rept. FHWA/CA/TL-81/09, 1981.
28. Prestressed Concrete Cylinder Pipe. Ameron, Inc., Monterey Park, CA, July 1975.

Publication of this paper sponsored by Committee on Culverts and Hydraulic Structures.

Reinforced-Concrete Pipe Culverts: Design Summary and Implementation

ALFRED E. BACHER, ALBERT N. BANKE, AND DANIEL E. KIRKLAND

Research at Mountainhouse Creek and Cross Canyon on reinforced concrete pipe culverts has confirmed the following: (a) loadings 140V:140H and 140V:42H are acceptable for Method A; (b) there is no effective-density increase after fill completion; (c) Method B (baled straw, polystyrene, or uncompacted material) performed well; (d) fill height versus soil pressure is approximately linear for Method A and nonlinear for Method B; (e) there is good correlation between theoretical (soil pressure) and experimental (strain) moments and excellent correlation of the three instrumentation planes placed 3 ft apart; (f) there is asymmetry of loading and moderate success by using Cambridge meters, which measured normal and shear forces on the culvert periphery; (g) adjusted peripheral pressures based on normal and shear forces did not change essential validity of use of normal forces only; and (h) D-loads based on three-edge bearing tests provide valid allowable design overfills. Implementation of this research and future research considerations are discussed. Projected cost savings are $400 000 annually.

In 1963, the California Department of Transportation (Caltrans), in cooperation with the Federal Highway Administration, initiated a $3.5 million culvert research program to assess structural behavior of culverts embedded in deep embankments. Included in this extensive culvert research program were three reinforced-concrete (RC) pipes.

The research program on RC pipe was mandated by the following:

1. Significant distress was observed in RC pipe culverts under earth embankments that ranged up to 300 ft in depth on California highways. Such embankments were used as economical substitutes for long bridges and as convenient sites for excess material from deep cuts. For Method A (compacted structure backfill), requirements for bedding and backfill were restricted to pipes under the roadway only. In the case of long laterals, no controls were placed on bedding and backfill procedures, and subsequent severe distress was observed. For Method-B type installations (soft inclusion in the culvert backfill), unlimited overfills were permissible prior to 1963 based on Marston-Spangler design criteria; indiscriminate use of these criteria led to some of the observed problems.
2. There was conjecture that design criteria, previously employed for culverts with much lower overfills, could not be extrapolated safely.

Caltrans has recently completed the third and final phase of its RC pipe culvert research project at the third location. The three sites are described below:

Location	Culvert Size (in)	Overfill (ft)
Mountainhouse Creek, Part 1	84	136
Mountainhouse Creek, Part 2	84	136
Cross Canyon, RC pipe	84	188

MOUNTAINHOUSE CREEK

Research Summary

RC pipe culverts that Caltrans has tested are a grossly underdesigned 84-in RC pipe culvert (Part 1) and a functional 84-in RC pipe culvert (Part 2) in the same embankment under 136 ft of overfill at Mountainhouse Creek.

Mountainhouse Creek (Part 1) was a grossly underdesigned 1000D dummy pipe that terminated in the embankment at a timber bulkhead. All six test zones were positive projecting. The projection ratios were 0.4 in zones 7 and 8 and 1.0 in zones 9 through 12.

Mountainhouse Creek (Part 2) was a 4000D functional culvert. It was placed in a trench throughout its length and was surmounted by a layer of baled straw in all but one of its six test zones.

The research reports on the 1000D pipe (Part 1) and the 4000D pipe (Part 2) were published in April 1971 and September 1975, respectively (1-8).

Instrumentation consisted of soil-stress meters and displacement-measuring devices in Part 1 and soil-stress meters, strain gauges, and displacement-measuring devices in Part 2.

Design Summary and Applications

All effective-density plots in this paper are based on unadjusted meter readings. Effective density is the density of material, if hydrostatic conditions are assumed, required to produce measured soil stresses for a given overburden. The variations in loading about the periphery of RC pipes are somewhat similar to what was observed on the Caltrans RC arch culvert research. Method A-3 installations are zones 7-12 of Part 1 and zone 1 of Part 2. The plots at zones 7, 8, and 9 (Figures 1 and 2) indicate higher lateral effective densities falling approximately into the 140V:140H band of loading, whereas zone 1 more nearly approximates the 140V:42H band. These individual plots (Figures 1, 3, and 4) fall essentially within the two bands of loading now specified.

The effective density increases subsequent to fill completion were negligible. The total net increase would not justify an increased Beta Sub E for the design of RC pipes. Obviously, the 140V:42H band would be the more critical design value for a circular shape.

Method-B (baled straw) RC pipe tests compared zones 2-5 (Figures 4, 5, and 6) of Mountainhouse Creek, Part 2. This report was completed some four years after the Part 1 research report was completed. Before these Method-B zones are discussed, a further qualification is in order.

The absence of recorded effective densities on the periphery is indicative of the malfunction of soil-pressure meters at specific points on the culvert's periphery. At zone 3, for example, only 5 of the 12 meters on the periphery were functional. This does not, however, negate the research findings at these zones. In fact, there are at least five usable readings at each zone. Further, there was the initial presumption that because the readings were low, they were therefore invalid. However, the fact that five zones (zones 2-6) all shared these common low values attests to their validity. The results of Caltrans Method-B RC pipe research zones indicated a significant reduction in peripheral effective densities. As a consequence, however, the report was delayed several years. Because of this unfortunate experience with the soil-pressure meters, all Caltrans culvert research projects subsequent to Mountainhouse Creek mandated the use

Figure 1. Effective densities at Mountainhouse Creek, zones 7 and 8.

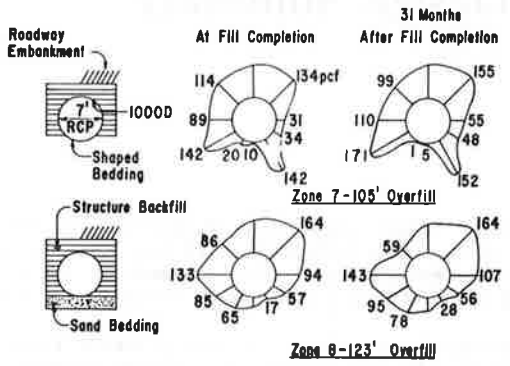

Figure 2. Effective densities at Mountainhouse Creek, zones 9 and 10.

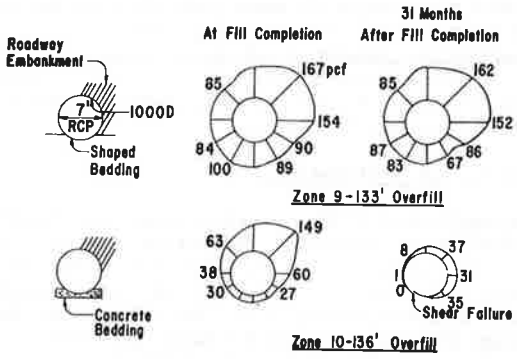

Figure 3. Effective densities at Mountainhouse Creek, zones 11 and 12.

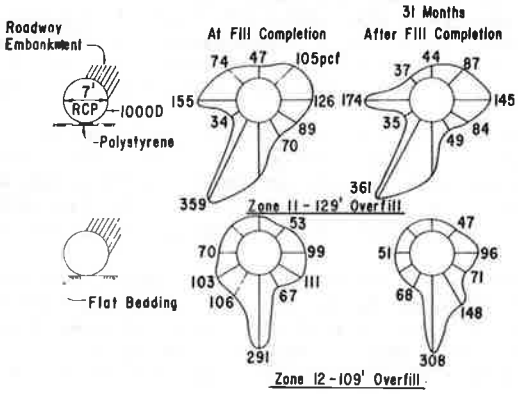

Figure 4. Effective densities at Mountainhouse Creek, zones 1 and 2.

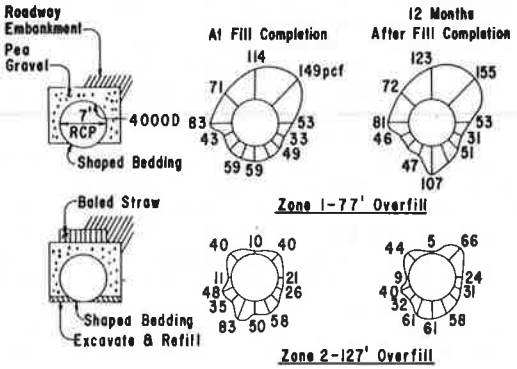

of the more reliable Carlson soil-pressure meters on the culvert periphery.

Caltrans has continued the use of Method B (baled straw) solely on RC pipe designs with the qualification that two layers of reinforcing steel be provided in the pipe. Caltrans has discontinued the application of Method B on the RC box, RC arch, and structural steel-plate pipe culverts based on experience and recent research on RC arch and structural steel-plate pipe.

There was approximate linearity of plots of soil stress versus fill height on RC pipe employing Method A. This is indicated on the plot for meter 12, zone 1 (Figure 7). Some meters in Method-B zones had distinct nonlinearity. Meter 11 at zone 4 (Figure 8) is an example. Initially, there was very little increase in the soil-pressure reading, but there was a significant increase after 65 ft of overfill up to 135 ft of overfill.

As in all other Caltrans culvert research projects, good correlation was established between theoretical moments based on the measured soil pressures and the experimental moments derived from the internal strains at zone 1 (Figure 9). The theoretical and experimental moments were derived from values averaged about the vertical diameter.

The pipes in all four positive projection zones (zones 9-12) exhibited significant distress. This was manifested by an appreciable flattening of the pipes and compression spalling at the sides. Deflections ranged as high as 18 percent.

The most favorable results were observed in the two partly entrenched pipes (zones 7 and 8). Diameter changes were less than 2 percent. Maximum permissible overfill for 1000D pipe was at one time assigned a value of 16 ft in Caltrans specifications. These two pipes developed first hairline cracks at 44 ft and remained serviceable at 140 ft of overfill, which demonstrated that one of the most

Figure 5. Effective densities at Mountainhouse Creek, zones 3 and 4.

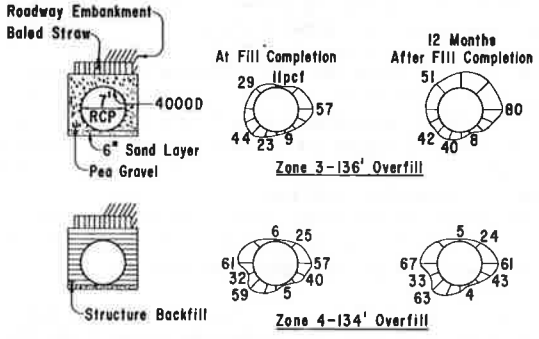

Figure 6. Effective densities at Mountainhouse Creek, zones 5 and 6.

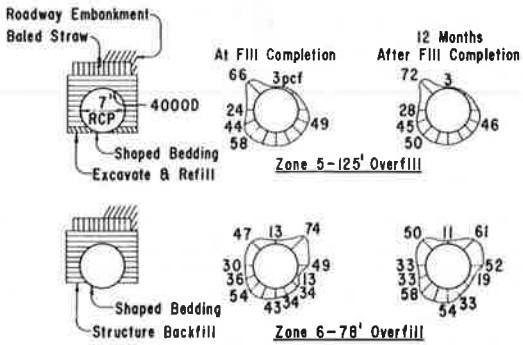

important factors in culvert design and construction is the provision of adequate lateral support. The research indicated no significant advantage in shaped bedding as compared with a flat sand bedding for Method A-3 installations only.

CROSS CANYON

Research Summary

As a consequence of the Mountainhouse Creek research, Parts 1 and 2, an additional RC research project was initiated at Cross Canyon Culvert. It consists of a grossly underdesigned 84-in dummy RC pipe under 188 ft of overfill (9).

The center pipe segment in each zone was instrumented with electric resistance strain gauges at each octant point. Rebar strains in the concrete pipe were measured and also strains in the concrete pipe core. There were two or three planes of instrumentation 3 ft apart at each zone, except for zones 2 and 7.

Soil-stress meters were imbedded in the surface of the concrete pipe in two or three planes at each zone and in the soil surrounding the concrete pipe. The upper half of the pipe contained meters at 45° intervals. The lower half had meters at 30° circumferential spacings. Strain gauges were placed in one plane at each zone.

A new specially designed Cambridge meter, obtained from Robertson Research Ltd., was installed in these culverts. This device measures both normal pressures and circumferential shears on the pipe wall. Displacement, settlement, rigid body rotation, and joint movement were measured manually.

The dummy pipe contains 10 zones. All zones are positive projecting. The projection ratios were 1.0 for zones 1 and 2 and approximately 0.5 for the other zones. Four pipe strength classes and five backfill conditions were employed. The four zones of different pipe strengths were installed to assess their relative structural capacities; Method B (imperfect trench conditions), which consisted of baled straw, loose soil, and polystyrene plank backpacking, comprised three more zones. One zone had soil cement backfill. Another zone had horizontal tension pipe struts, and one zone had vertical compression pipe struts.

Figure 7. Soil pressures at Mountainhouse Creek, zone 1.

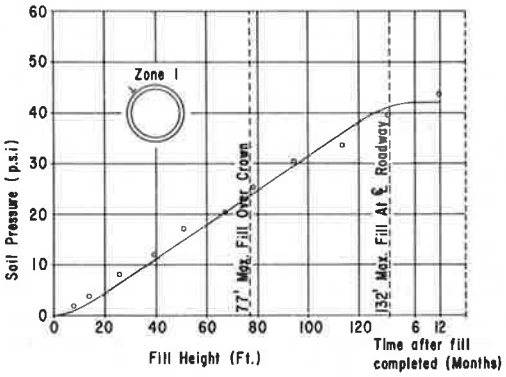

Figure 8. Soil pressures at Mountainhouse Creek, zone 4.

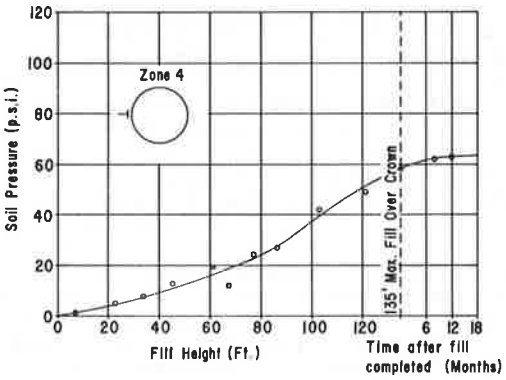

Figure 9. Theoretical and experimental moments at Mountainhouse Creek, zone 1.

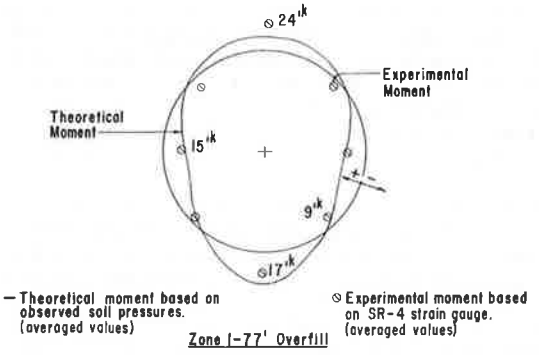

Design Summary and Applications

The plots of the unadjusted effective densities of the 10 zones of Cross Canyon are conclusive in the following respects.

The magnitude of the effective densities and the peripheral effective-density plot of Method A, zones 1, 3, 4, 5, and 6 (Figures 10-12), fall within the two bands previously projected for RC pipe design. This is in basic conformity with the Mountainhouse Creek research projects, Parts 1 and 2, Method A. Effective-density profiles indicated by the instrumentation verify that the two bands of loading are an acceptable, conservative design. The lesser pressure at the crown in zones 4, 5, and 6 may be attributed to the overzealous concern for the instrumentation by the contractor during backfill, which resulted in less compaction over the crown than that specified.

The effective-density increases subsequent to fill completion were negligible, which affirmed the use of a Beta Sub E factor of 1.0 for Method-A RC pipe design.

The three Method-B test zones (with soft inclusions in the backfill) all performed well--zone 8 (Figure 12), 2-6 in of polystyrene surrounding the upper 240° of the pipe; zone 9 (Figure 13), uncompacted material surmounting the RC pipe; and zone 10, baled straw surmounting the pipe. The uncompacted material gave the optimum results of the three types tested even though the uncompacted material had the largest soil gradients. The good performance of zone 9 can be attributed to the high compressive thrusts that resulted from the retention of large lateral soil stresses. The effective densities ranged between 27 and 96 pcf. The baled straw had effective densities that varied from 4 to 41 pcf around the periphery, except for the high invert effective density of 194 pcf. Excluding the invert, the effective densities were somewhat less than the average 50 pcf observed at five sections of research on Mountainhouse Creek RC pipe, Part 2. In effect, the low effective densities of baled-straw

Figure 10. Effective densities at Cross Canyon, zones 1 and 3.

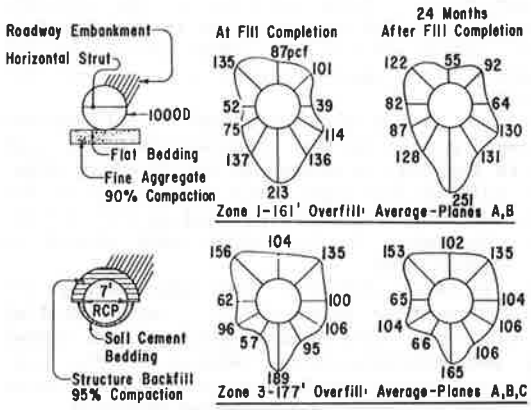

Figure 11. Effective densities at Cross Canyon, zones 4 and 5.

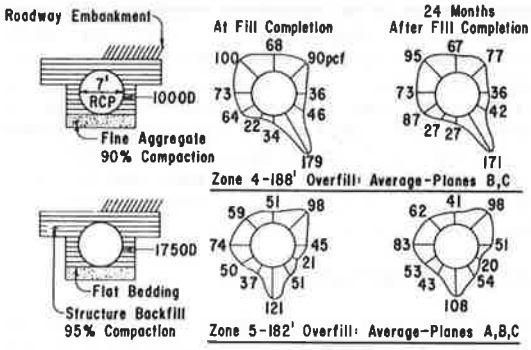

Figure 12. Effective densities at Cross Canyon, zones 6 and 8.

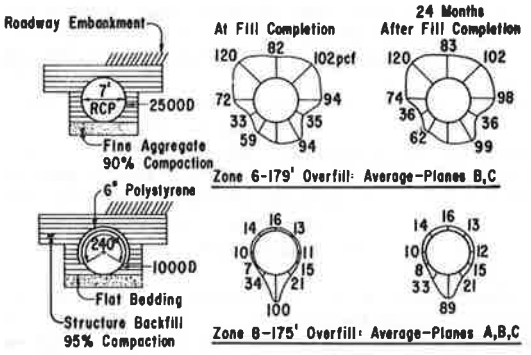

Figure 13. Effective densities at Cross Canyon, zones 9 and 10.

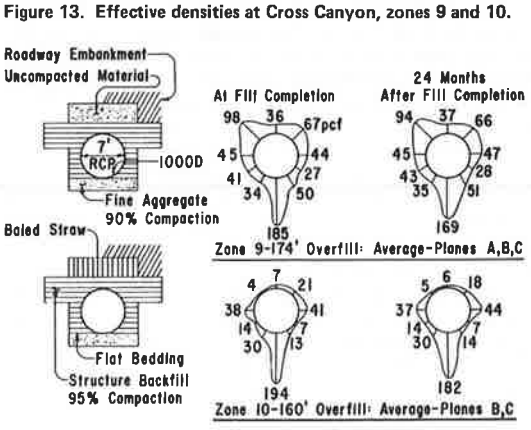

Method-B backfill observed in zones 2-6 at Mountainhouse Creek were affirmed by zone 9 Cross Canyon research, except for the invert effective density (meter 6). The beneficial effects of the 6-in polystyrene soft inclusion, with readings approximately 20 pcf at meters 1-5 and 7-10, were partly negated by the hard spot at meter 6 of 100 pcf on the bottom of the pipe.

In this research project, the effective densities for Method B (uncompacted material) were somewhat higher than for the other two Method-B alternatives. One further word of caution--the uncompacted earth can range between 70 and 95 percent relative compaction on individual projects. The introduction of the straw-backfill, Method-B alternative on Caltrans culverts was prompted by the inability to control the density of uncompacted earth during construction and the adverse reaction by contractors to the construction sequence required for its installation. The most recent specifications for Method-B RC pipe permit baled straw only.

There is approximate linearity on the plots of soil stress versus fill height of Method-A installations. Of the 50 individual plots of soil stress versus height, 34 were approximately linear; 80 percent of the readings were within 20 percent of a straight line. An example is zone 4 of Cross Canyon (Figure 14). This again correlates with the Mountainhouse Creek research, parts 1 and 2.

An attempt also has been made on this and all previous Caltrans culvert research to assess Spangler's settlement ratio. The results were unsatisfactory (Figure 14); the settlement ratio that predicts twice the crown pressure is actually observed at zone 4. However, there is a distinct nonlinearity on many of the meter readings of the Method-B backfill (zones 8, 9, and 10). A plot of meter 2, zone 9 (Figure 15), is indicative of this nonlinearity.

The external pressures and the internal strains had good correlation for moment and displacements. A comparison of the theoretical (soil-pressure) and experimental (strain) moments is shown for zone 4 (Figure 16).

Also of significance is the fact that where there were three planes of instrumentation, 75 percent of the sections (sections 1, 4, 6, 8, 9, and 10) had remarkably good correlation. For example, the plots shown on the three planes at zone 4 (Figure 17) of the observed peripheral pressures show virtually identical tracings. Experience in other culvert research projects has emphasized the fact that variations in the foundation, the side fill, and the embankment surmounting the culvert can occur along the length of any culvert installation; as a consequence, significant changes in the effective-density profiles have been observed. However, with a spacing of 3 ft between planes, there is assurance that these conditions did not change at this research site.

The asymmetry of effective-density profiles, common to all Caltrans rigid-culvert research projects thus far, was found in the Method-A test sections. Cambridge-meter circumferential shear readings were but one of the indications of the condition of asymmetrical loading. A considerable computational effort was exerted to establish rotational, horizontal, and vertical equilibrium at all zones.

A comparison has been made between an unadjusted effective-density profile and an effective-density profile based on the shear and normal soil stresses at zone 6 (Figure 18). It is of interest to note that the variations are generally less than 20 percent; all previous Caltrans culvert research conclusions are therefore valid despite the fact

Figure 14. Soil pressures at Cross Canyon, zone 4.

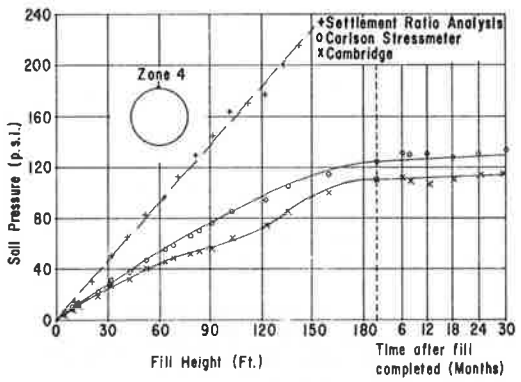

Figure 15. Soil pressures at Cross Canyon, zone 9.

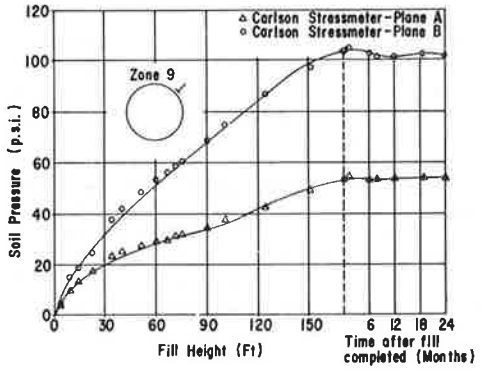

Figure 16. Theoretical and experimental moments, Cross Canyon, zone 4.

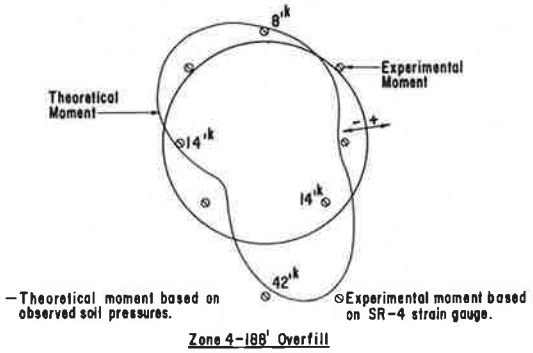

Figure 17. Soil stress meters at Cross Canyon, zone 4.

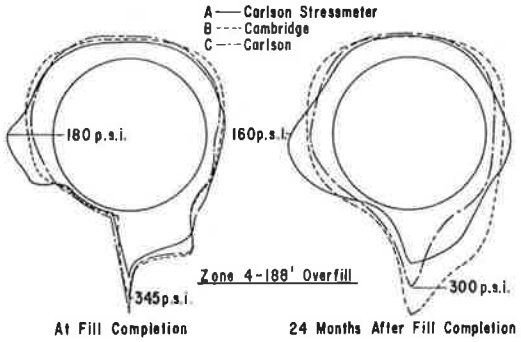

Figure 18. Effective densities at Cross Canyon, zone 6 (unadjusted, Cambridge-modified).

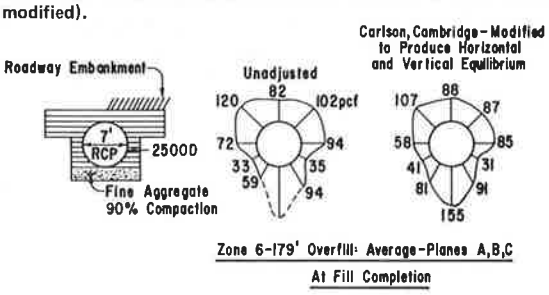

Figure 19. Limiting overfill: Method A-3 backfill.

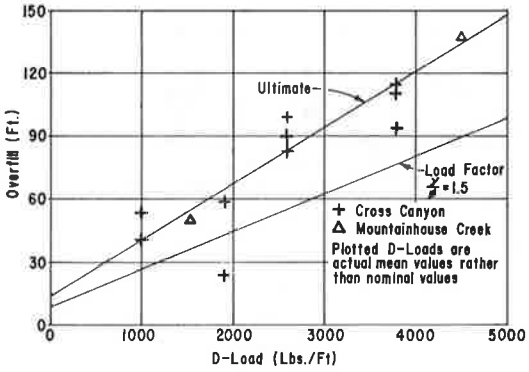

that no measurement of shear stresses was made.

The three-edge bearing test also was given a further assessment. Pipe strengths of 1000D, 1750D, 2500D, and 3600D were compared; all had approximately 180 ft of overfill. The results were rather surprising. Although the strength of pipe did not have a direct relationship with the D loading (i.e., the 3600D pipe does not support 3.6 times as much overfill as the 1000D), it did have remarkable validity with respect to allowable overfills used by Caltrans based empirically on the Mountainhouse Creek research. Method A-3 application of a load factor of 1.5 (Figure 19) provided confirmation of the current values used by Caltrans. Also of interest is the fact that values of allowable overfill based on the Design Manual of the American Concrete Pipe Association (ACPA) are 60 percent of the Cross Canyon D-load values.

A crack survey was made of the magnitude and frequency of cracking and the magnitude of the deformation in each zone, which are summarized as follows:

Zone	Maximum Crack Width (in)	Vertical Deformation (in)
1	0.05	0.9
3	0.05	0.6
4	0.07	0.6
5	0.05	1.2
6	0.03	1.1
7	0.02	0.8
8	0.01	0.3
9	0.02	0.0
10	0.03	0.1

Maximum cracks in all zones were less than 0.10 in. Maximum deformation for Method A was 1.4 percent; for Method B it was 0.4 percent and less.

Figure 20. Load factor design: RC pipe, Caltrans.

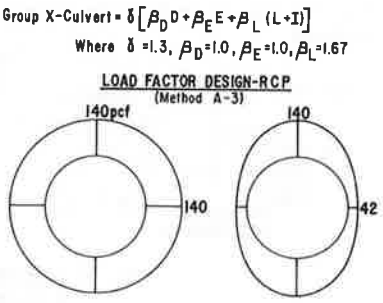

Figure 21. Portion of standard plan A62-D, excavation and backfill details, concrete and asbestos cement pipe culverts.

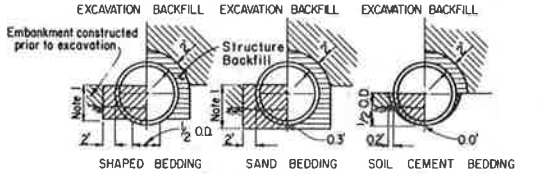

IN EMBANKMENT

MINIMUM ALLOWABLE CLASSES OF RCP FOR METHOD A-3

Cover (in feet)	Minimum Class & D-Load
Less than 26.0	Class II 1000D
26.0-31.9	Class III 1350D
32.0-37.9	Class III Special 1700D
38.0-44.9	Class IV 2000D
45.0-55.9	Class IV Special 2500D
56.0-67.9	Class V 3000D
68.0-80.0	Class V Special 3600D

Notes 7, 8 and 9

A62-D

Figure 22. Dimension ratio.

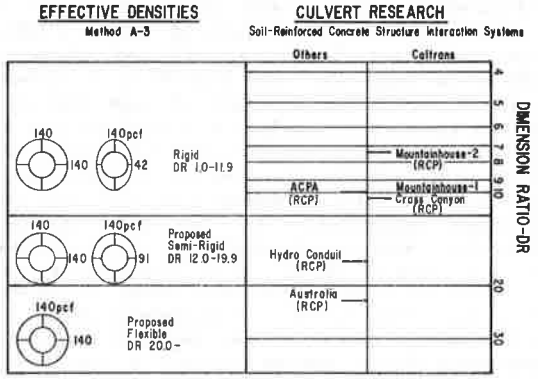

IMPLEMENTATION

Caltrans has implemented the following from this RC pipe research:

For Method A-3, two bands of loading (Figure 20) are now specified for RC pipe special designs--design loadings 140V:140H and 140V:42H. Allowable overfills are determined by D-loads based on the three-edge bearing tests. There is excellent correlation between the projected allowable overfills for Method 3 based on the Mountainhouse Creek research and the most recent RC pipe research at Cross Canyon. The soil-cement option for Method 3 (Figure 21) is specified as an alternative on Standard Plan A62. The maximum crack width observed at zone 3 was 0.05 in and there was a uniform soil gradient in the lower quadrants. The continued application of the soil-cement option is supported by the successful use of this option by contractors on recent Caltrans projects.

For Method B (baled straw surmounting the pipe), allowable overfills are specified by D-loads based on the three-edge bearing tests. Double cage reinforcement should be provided, and the bedding should be shaped.

The American Association of State Highway and Transportation Officials (AASHTO) has recently revised Article 1.2.2A (Loads on Culverts) to specify two loading conditions (120V:120H and 120V:30H). AASHTO specifications now include Section 1.15 (Soil-Reinforced Concrete Structure Interaction Systems) with input by Caltrans based on these three Caltrans RC pipe culvert research projects. AASHTO specifications also include Section 2.28 (Installation and Construction of Soil-Reinforced Concrete Structure Interaction Systems); active participation was provided by California in the development of these construction specifications.

FUTURE CONSIDERATIONS

Caltrans will introduce a new criterion, the dimension ratio (DR), for RC pipe design (Figure 22). DR is defined as the internal diameter in inches divided by the wall thickness in inches. Caltrans RC pipe research at Mountainhouse Creek and Cross Canyon and Caltrans special RC pipe designs have used pipes with dimension ratios that range between 3.7 and 10.5. ACPA has also conducted research on RC pipe in embankment and trench conditions with a DR of 10.0. Hydro Conduit Corporation has performed RC pipe research (10,11) on pipes with DRs that range between 14.9 and 19.2. Since 1962, the Australian Concrete Pipe Association has used RC pipe with DRs that range between 13.8 and 20.9 (Australian Standard CA-33-1962).

Phases of RC pipe load-factor design to be considered are as follows:

1. For Method A-3, develop load-factor design specifications: (a) rigid culvert design--DR 1.0-11.9, design loadings 140V:140H and 140V:42H; (b) semirigid culvert design--DR 12.0-19.9, design loadings 140V:140H and 140V:91H; and (c) flexible culvert design--DR 20.0-, design loading 140V:140H.
2. For Method B, develop load-factor design specifications. Consider application of earth effective-density profiles consistent with Mountainhouse Creek and Cross Canyon research projects.

AASHTO Bridge Specification 1.15.4, RC pipe, precast, has recently been approved. Caltrans is developing a standard plan based on the direct design method for RC precast pipe.

Caltrans is currently studying the applicability of the finite-element method to culvert design.

COST SAVINGS

A saving of $390 000 would have been realized at Cross Canyon had a 96-in RC pipe been used instead of the 96-in prestressed concrete pipe.

Savings projected for Caltrans RC pipe installations are as follows:

1. $100 000/year due to increased allowable overfills for conventionally designed RC pipes, and
2. $300 000/year due to use of concrete pipe with thinner walls.

The use of thinner-wall RC pipe will save material and result in more economical RC pipe designs.

ACKNOWLEDGMENT

The initiation of the RC pipe research of Mountain-

house Creek and Cross Canyon and the determination of design parameters were with the full cooperation and participation of the Caltrans Culvert Committee and the California Precast Concrete Pipe Association (CPCPA). It was a mutual involvement by both CPCPA and Caltrans.

Walt Creasmon of Ameron and Joe Zicaro of the Hydro Conduit Corporation contributed significantly to the Mountainhouse Creek research proposal and Ernie Rogers, managing engineer of the CPCPA, to the Cross Canyon research proposal. Tom Breitfuss of the Hydro Conduit Corporation and Bob Spickerman of the California Concrete Pipe Corporation have been particularly instrumental in the recent implementation aspects.

Discussion

R.E. Davis

As principal investigator on all Caltrans' major culvert research for 15 years, I believe that readers of this paper might misinterpret findings of the subject research.

The effective-density plots in Figures 1-4 do not resemble the two specified bands of loading. The phraseology "falling approximately into" and "fall essentially within" may lead the reader to believe (erroneously) that specified effective-density profiles that encompass all observed profiles will produce more conservative designs.

The use of Mountainhouse Creek soil stress data as a basis for important conclusions is questionable. At project inception, TRANSLAB purchased a bank of stress meters from two untried sources. Laboratory tests made of stress meters of the variety used in Mountainhouse Creek, Part 1, subsequent to project completion indicated 100 percent failure. Of 72 meters used in Mountainhouse Creek, Part 2, 15 failed at low overfills, no stress readings were reported for an additional 4, and 22, after producing small, finite stress readings, dipped to zero or negative stress ranges. Subsequent culvert tests have employed not only Carlson, but Kyowa, Ormond, and Cambridge stress meters.

Experimental moments shown in Figure 9 were averaged about the vertical diameter. Actual, omitted experimental moments departed significantly from the quasi-theoretical curve. High mortality rates for the stress meters and lack of valid correlations make all Mountainhouse soil-stress data suspect.

Promulgation of the baled-straw overlayer is polemic to many Cross Canyon observations, as follows:

1. Cost per foot: zone 9, $171.75; zone 8, $184.44; zone 10, $193.01, or 12 percent more than the uncompacted soil;
2. 0.01-in-crack overfill: zone 9, never reached; zone 8, 61 ft; zone 10, 37 ft;
3. Total length of cracking: zone 9 consistently one of the best;
4. Maximum vertical diameter change: zone 9, 0.041 in; zone 10, 0.080 in; zone 8, 0.326 in;
5. Material availability: uncompacted soil, always; baled straw, not always, and cost at time of testing was $27/ton; polystyrene plank is a petroleum derivative, cost $3/ft^3 at time of test;
6. Ease of construction: zone 9, embankment material handled three times, but all work by machines; zone 10, baled straw unloaded and placed by hand; zone 8, much work in hand placing, gluing, tacking, and winding ropes to prevent planks from being dislodged;
7. Theoretical assessment of behavior: zone 9, exhibited healthy compressive thrust at crown; zones 8 and 10, negligible thrust at crown conducive to cracking;
8. Uncompacted soil inorganic and not subject to decomposition, whereas baled straw is; and
9. Radial tension stress by Heger's criteria: zone 9, 65 psi; zone 8, 69 psi; zone 10, 82 psi.

Downgrading of the uncompacted-soil overlayer in the paper should be reconsidered.

The uppermost curve in Figure 14 is a hypothetical curve based on Marston-Spangler settlement ratio analysis and does not contain experimental data. If the ordinate scales in Figures 14 and 15 are matched, the uppermost curve in the latter correlates very well with experimental data from the lower curve on Figure 14, with a slight transposition of the origin; the authors' suggestion that one of these typical curves proves linearity while the other demonstrates "distinct nonlinearity" should be clarified. The argument is more than semantic. The mathematical definition of effective density is the slope of the secant joining the origin to points along the function of soil stress and overfill. For linear curves, the secants would degenerate into tangents, effective densities would be the same at all levels, and effective-density profiles at ultimate overfills could be considered representative of all levels. Typical effective-density maxima at 1:30, 6:00, and 10:30 o'clock dampen more rapidly with increasing overfill than minima at 12:00, 4:30, and 7:30 o'clock, which results in decreased soil-stress gradients. Use of the authors' ultimate-density profiles will produce unconservative designs for almost all construction methods at lower overfills where the soil-stress gradients are more severe.

Description of the Cross Canyon project as "an assessment of the three-edge bearing test" is questionable. The assertion that it verified with remarkable validity the results of the Mountainhouse Creek research is unclear. Zone 5 (the 1750D pipe) was a fluke (primarily because of the use of undeformed bars); the primary mode of failure at zones 6 (2500D) and 7 (3600D) and the 4000D pipe at Mountainhouse Creek was incipient delamination, not a three-edge bearing test criterion. The fact that an approximate linear function could be established between the various modes of failure and the D-strength of the pipe is only coincidental.

The table of maximum crack widths is invalid because it includes widths from all segments. Buffer segments were included on either side of each instrumented pipe (except in zones 1 and 2), and only "representative" center segments should be considered to eliminate the effects of longitudinal bridging between zones. Maximum crack widths (in inches) taken only from these segments are as follows: zone 1, 0.050; zone 2, 0.020; zone 4, 0.050+; zone 5, 0.035; zone 6, 0.040; zone 7, 0.015; zone 8, 0.020; zone 9, 0.005; zone 10, 0.020. The correct figures suggest superiority of uncompacted overfill at zone 9.

The authors suggest use of the 0.01-in crack as a failure criterion for Method 3 and a 0.05-in crack in zone 3 and also attach significance to the fact that all cracks were less than 0.1 in. Readers may fail to perceive the research project objective to assess relative structural behavior and economy of 10 construction modes.

It should be carefully noted that the suggestion concerning DR bears no relationship to Caltrans pipe

research. Excluding consideration of the prestressed pipe at Cross Canyon, the range of DRs studied by Caltrans is 7.3 to 10.5. The only valid data available pertinent to the low end of this range are from the noninstrumented zone 7 at Cross Canyon. All other pipe segments were of a single value of 10.5, yet structural behavior ranged from total failure to excellent. Since the DR does not consider the significant effects of soil-structure interaction, its value as a design criterion needs further explanation.

The recommendations for two bands of loading reflect the dangerous assumption described earlier. The 140V:140H uniform loading will produce zero moments and shears in a round pipe and can scarcely be critical. The 140V:42H loading may produce maximum stresses comparable with some of those observed at Cross Canyon but will produce designs that are unconservative for other failure modes, e.g., diagonal and radial tension failures. The authors' manifest philosophy that certain "bands of loading" that encompass all observed bands will produce conservative designs is incorrect. Stresses in the pipe result from moments, shears, and thrusts, which depend on soil-stress gradients rather than the absolute magnitudes of stress, and one profile may encompass another one completely and yet produce a much less conservative design.

Thus, the most serious deficiency in the paper is the fact that the recommended design profiles are not "representative" of anything observed in the field tests and particularly of the low-modulus inclusion installations. The recommended profiles will therefore produce unconservative designs for some significant failure modes.

Opinions, findings, and conclusions expressed in this discussion are mine and do not necessarily reflect the official views or policies of the California Department of Transportation or the Federal Highway Administration. This discussion does not constitute a standard, specification, or regulation.

CLOSURE

This closure by Bacher is in response to certain issues raised by R.E. Davis. Readers are urged to address further discussion directly to Bacher. Response to such discussion or inquiries relative to implementation of the research into Caltrans practice will be made directly by him. Davis' comments will be addressed in paragraph order.

PARAGRAPH 2

Davis essentially states that the two conditions of loading now specified will not provide a conservative RC pipe design. As background, in 1967 the Bridge Department Culvert Committee first specified that RC arch culverts be designed for two conditions of loading, applying a service load design of 120V:36H for overfills from 0 to 60 ft and 84V:84H for higher overfills. Subsequently, load-factor design was initiated and developed for all culverts. Similar rigid culvert loadings were implemented in 1967. Two conditions of loading are currently specified for Caltrans rigid culvert design, 140V:140H and 140V:42H. To my knowledge, there have been no RC pipe culvert failures attributable to underdesign since 1967.

PARAGRAPHS 3 AND 4

Davis refutes RC pipe research of record for Mountainhouse Creek research, which he coauthored. To date, there have been no published disclaimers by Davis of the Mountainhouse Creek research documents. These research documents have been widely disseminated and accepted by the design profession.

PARAGRAPH 5

The comparative costs of the three Method-B type installations are representative of the Cross Canyon research project only. The soil cement method used on a recent pipe contract was fully machine placed. Hand methods used on the Cross Canyon research are not representative of full-scale projects.

The retention of the baled-straw Method-B alternative is a decision shared by members of the Caltrans Culvert Committee. However, in the last three years, only 2 percent of the total RC pipes installed specified Method B. It is still made available as an option to designers where the overfill exceeds 50 ft.

PARAGRAPH 6

Davis has chosen to apply his own revised interpretation of effective density. The two research-project approaches used were as follows:

Mountainhouse Creek: $p\ (pcf) = [144 \times p\ (psi)]/h\ (ft)$.

Cross Canyon: $\Delta p\ (pcf) = [144 \times \Delta p\ (psi)/h\ (ft)$.

At Cross Canyon, emphasis has been placed on the incremental change in pressure reading with each corresponding incremental change in fill height. Considering the number of readings taken at Cross Canyon, Davis states that Method-A readings are not essentially linear. The fact is that by taking soil-pressure readings at increasing fill heights, there is approximate linearity; 80 percent of Method-A peripheral pressure plots have 80 percent of the interim soil pressures within 20 percent of a straight line between the origin and the maximum reading.

The issue is much more fundamental. Traditionally, there has been a basic belief of some engineers in the field of soil-structure interaction that soil arching takes place on Method-A installations. Caltrans RC arch culvert research, now completed, has reached the unequivocal conclusion that there is no observed soil arching on Method-A type installations.

The reality is that at 180 ft of overfill, there is approximately twice as much earth load acting on an underground structure as there is at 90 ft of overfill for Method-A installations.

The contention by Davis that the present specified effective-density profile (140V:140H, 140V:42H) will produce unconservative designs for rigid culverts is not supported by 15 years of experience. Davis further contends that during construction of RC pipes, severe soil-stress gradients can occur. The necessity of considering the possible handling and installation stresses for culverts has always been recognized in design practice. It is of such importance for flexible culverts (i.e., steel and aluminum corrugated-metal pipe) that a minimum flexibility factor is specified; in the case of long-span metal culverts, deflection controls are specified during construction and temporary internal strutting is frequently required. Similarly, a minimum pipe stiffness is specified for plastic pipe culverts in ASTM specifications. In the case of RC pipe, minimum wall thicknesses are specified in the materials specifications.

In the figures shown for zone 4 (Figures 23-28),

delineation has been made to emphasize that the current design for 1000D pipe permits only 26 ft of overfill. A neutral-point analysis has been applied with extrapolations to 188 ft of overfill. The specified 140V:42H for rigid culvert design has resulted in excellent correlation with the observed stresses. As stated previously, by using the three-edge bearing test, the 1000D pipe was considered adequate for a maximum of only 26 ft of overfill. The measured inner and outer steel reinforcing tensile stresses and the inner and outer concrete fiber tensile and compression stresses are approximately the same as the design specified, and during construction they did not exceed the minimum specified design stresses.

Finally, had Davis taken the opportunity to inspect the Cross Canyon research culvert four years after its completion, he would have observed the remarkably good condition of this grossly underdesigned RC pipe culvert.

PARAGRAPH 7

Davis was responsible for initiating the research of

Figure 23. Quasi-theoretical versus specification stresses: steel tensile stress, inner reinforcing bar, zone 4.

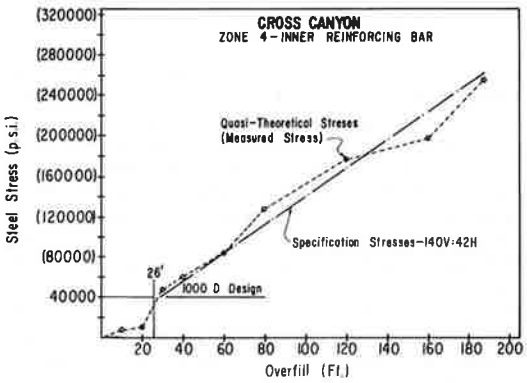

Figure 24. Quasi-theoretical versus specification stresses: steel tensile stress, outer reinforcing bar, zone 4.

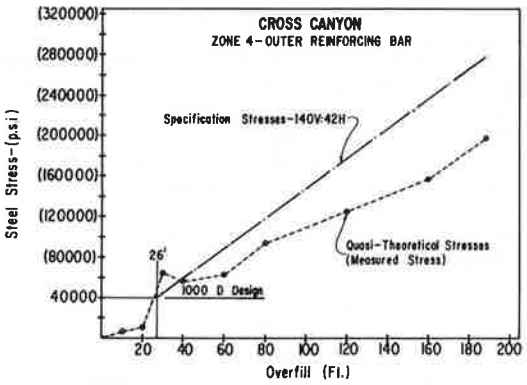

Figure 25. Quasi-theoretical versus specification stresses: concrete compressive stress, concrete inner fiber, zone 4.

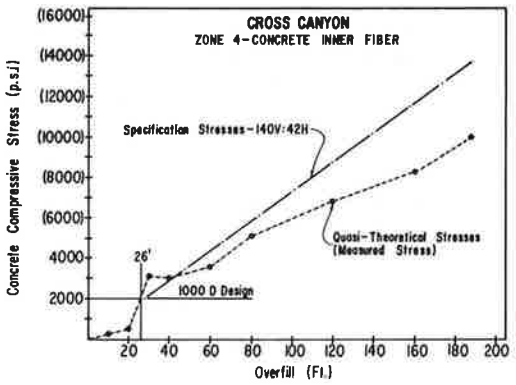

Figure 26. Quasi-theoretical versus specification stresses: concrete compressive stress, concrete outer fiber, zone 4.

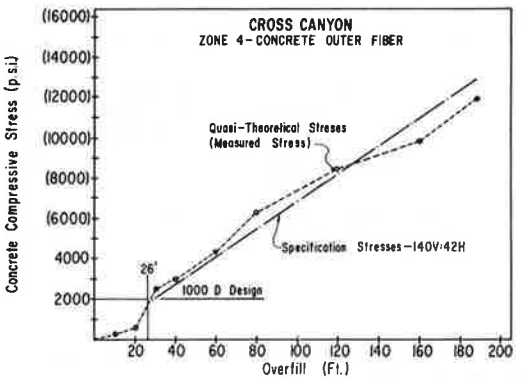

Figure 27. Quasi-theoretical versus specification stresses: concrete tensile stress, concrete inner fiber, zone 4.

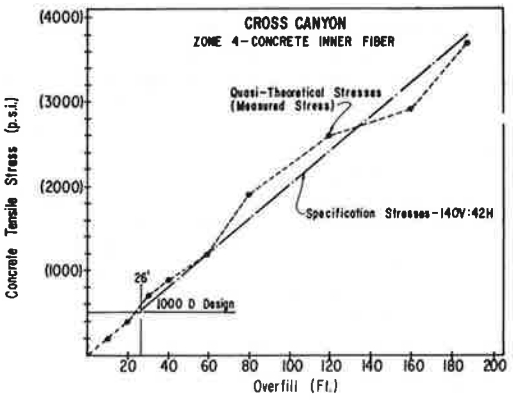

Figure 28. Quasi-theoretical versus specification stresses: concrete tensile stress, concrete outer fiber, zone 4.

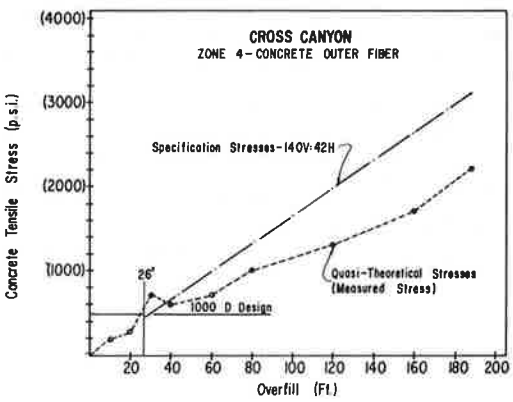

the 1000D, 1750D, 2500D, and 3600D specified D-load pipes at Cross Canyon. The 1000D and 4000D three-edge bearing test values witnessed on the Mountainhouse Creek research resulted in the interim allowable-overfill tables in the Caltrans Design Manual. The most recent research at Cross Canyon confirms these allowable-overfill tables.

PARAGRAPHS 8 AND 9

Apparently Davis is not familiar with the current Caltrans and AASHTO RC pipe construction specifications. In a corrosive environment, a 0.01-in crack is specified. However, from a structural standpoint, cracks of 0.10 in are considered acceptable in a noncorrosive environment.

It should be emphasized that the tentative AASHTO design specifications for RC pipe are based on a 0.01-in crack.

When the cracking reaches 0.10 in, the structure becomes hinged, which relieves the moment and creates a new interface condition that has thrust as the only significant design consideration. The structure continues to function, since the soil retains the peripheral shape of the pipe, similar to the stone arch construction dating back to the Roman era.

PARAGRAPH 10

Davis offers no alternative or constructive discussion to Bacher's proposed DR concept. The simple reality is that if an 84-in pipe with an 8-in wall can successfully support 180 ft of overfill, it is probable that a thinner-wall pipe can be used to support a 20-ft overfill. Initial design calculations based on the direct design criteria of AASHTO Section 1.15.4 (Reinforced Concrete Pipe, Precast) indicates that an 84-in RC pipe with a 5.25-in wall would safely support 20 ft of overfill.

Australia has successfully placed RC pipe with DRs ranging between 14 and 22 since 1962 (Australian Standard CA-33-1962); also, Hydro Conduit has performed research on pipes with DRs varying between 14.0 and 19.2. Finally, zones 3 and 4 of Cross Canyon research performed better than zones 5 and 6 (1750D and 2500D), which were more heavily reinforced. The fact that zones 3 and 4 were more flexible improved their structural performance; in effect, the moment considerations become less significant because there is moment relief under loading if the pipe is more flexible.

PARAGRAPHS 11 AND 12

The current AASHTO specification, Section 1.15 (Soil-Reinforced Concrete Structure Interaction System) in both Sections 1.15.2 (Service Load Design) and 1.15.3 (Load Factor Design) defines RC pipe as circular pipe, elliptical pipe, and arch pipe. It should be apparent to Davis that a vertical ellipse or pipe arch should be designed for the more critical 140V:140H loading.

The continued allegation by Davis that "two bands of loading reflect the dangerous assumption described earlier" is not supported by our experience.

Elementary logic tells one that a pipe designed for 180 ft of overfill will not suffer distress at 90 ft of overfill under conditions of interim loading with normal construction procedures and when reasonable care is taken by the contractor.

Application of the 140V:42H loading to a rigid culvert with a DR of 1-11.9 by using a neutral-point analysis has affirmed the validity of our current RC pipe design specifications. Application of the AASHTO and ACPA design method to semirigid RC pipe by using DRs of 12.0-19.9 will inevitably lead to future reduced wall thickness for RC pipe installations.

In conclusion, it is my opinion that, in dealing with the many variables of a soil-culvert interaction system, the establishment of a reasonable range of vertical and horizontal pressures for design consistent with variations in DRs and appropriate bedding and backfill parameters offers the most promising solution to safe, cost-effective RC pipe culvert installations.

REFERENCES

1. R.E. Davis and A.E. Bacher. California's Culvert Research Program--Description, Current Status, and Observed Peripheral Pressures. HRB, Highway Research Record 249, 1968, pp. 14-23.
2. R.E. Davis, A.E. Bacher, and J.C. Obermuller. Structural Behavior of a Concrete Pipe Culvert--Mountainhouse Creek (Part 1). Division of Highways, State of California, Business and Transportation Agency, Sacramento, Rept. 4-71, April 1971.
3. R.E. Davis, A.E. Bacher, and J.C. Obermuller. Concrete Pipe Culvert Behavior (Part 1). Journal of the Structural Division of ASCE, March 1974 (Proc. Paper 10404).
4. R.E. Davis and A.E. Bacher. Concrete Pipe Culvert Behavior (Part 2). Journal of the Structural Division of ASCE, March 1974 (Proc. Paper 10405).
5. R.E. Davis, A.E. Bacher, and E.E. Evans. Structural Behavior of a Concrete Pipe Culvert--Mountainhouse Creek (Part 2). Department of Transportation, State of California, Business and Transportation Agency, Sacramento, Rept. FHWA-CA-ST-4121-75-8, Sept. 1975.
6. R.E. Davis and A.E. Bacher. Rigid Culvert Tests--Mountainhouse Creek, Part 1. Concrete Pipe News, American Concrete Pipe Association, Vienna, VA, Aug. 1978.
7. R.E. Davis and A.E. Bacher. Rigid Culvert Tests--Mountainhouse Creek, Part 2. Concrete Pipe News, American Concrete Pipe Association, Vienna, VA, Oct. 1978.
8. A.E. Bacher and A.N. Banke. Rigid Culvert Tests--Mountainhouse Creek, Part 3. Concrete Pipe News, American Concrete Pipe Association, Vienna, VA, Dec. 1978.
9. R.E. Davis, A.E. Bacher, and others. Rigid Pipe Proof Testing Under Excess Overfills with Varying Backfill Parameters (Sections I-IX). California Department of Transportation, Sacramento, 1978-1982.
10. Composite Installed Pipe Tests. Hydro Conduit Corporation, Newport Beach, CA, Jan. 1977.
11. Suggested Specifications and Design Criteria for Composite Concrete Pipe. Hydro Conduit Corporation, Newport Beach, CA, March 1979.

Publication of this paper sponsored by Committee on Culverts and Hydraulic Structures.

Structural Design Method for Precast Reinforced-Concrete Pipe

FRANK. J. HEGER

A comprehensive direct structural design method for buried concrete pipe is presented that has been included in a new section (1.15.4—Reinforced Concrete Pipe, Precast) of the bridge specifications of the American Association of State Highway and Transportation Officials. The method is based on the ultimate-strength and crack-control behavior of reinforced-concrete pipe and other structures observed in various tests of pipe, box sections, slabs, and beams under known loading conditions that encompass both concentrated and distributed test loads. The new design method includes criteria for ultimate flexural strength based on both tensile yield of reinforcement and compressive strength of concrete, ultimate shear (diagonal tension) strength, and ultimate flexural strength as limited by radial tension in pipe without radial ties. Also included is a crack-control criterion. Additional design equations are provided for radial ties when radial tension or shear strength is inadequate without such reinforcement. In order to adequately predict the ultimate shear and radial tension strengths of buried concrete pipe, it was necessary to develop new relations between significant variables that go beyond or extensively modify existing design methods. These are based on an extensive evaluation of new and existing tests of pipe, box sections, slabs, beams, and frames without web reinforcement that failed in shear by tests of curved slabs that failed in radial tension without simultaneous application of shear and by pipe industry design practices derived from accumulated test data. Design relations proposed for crack control also differ significantly from crack-control criteria available in existing standards. They also have been based on extensive tests of pipe, box sections, and slabs. The design method may also be applied to pipe for three-edge bearing strength and for buried box sections.

During the past 10 years, the American Concrete Pipe Association (ACPA) has sponsored several long-range research projects to develop improved methods for determining earth loads and pressure distributions on buried concrete pipe. As a part of this research effort, Heger and McGrath developed an accurate method for determining the ultimate strength and crack-control characteristics of reinforced-concrete pipe under any load distribution (1). This work forms the basis of a direct design method that has recently been adopted by the Rigid Culvert Liaison Committee of the American Association of State Highway and Transportation Officials (AASHTO) for incorporation in a new Section 1.15.4 of the AASHTO bridge specifications (2) covering the design of concrete pipe. The new Section 1.15.4 (3) is entitled Reinforced Concrete Pipe, Precast. It includes two alternative design methods for buried concrete pipe:

1. Indirect method: Based on pipe strength in three-edge bearing tests and bedding factors that convert these test strengths to design earth loads for embankment and trench installations with various classes of bedding, and
2. Direct method: The pipe is analyzed for moments, thrusts, and shears produced at governing sections by the design earth load and pressure distribution. The pipe wall thickness and reinforcement are designed for adequate strength and crack control under the combined effects of the design moments, thrusts, and shears. Appropriate load and capacity-reduction factors are applied when designing for strength.

The purpose of this paper is to present and explain the new direct design method in Section 1.15.4. A comprehensive presentation of the test programs, analyses of test results, and comparisons of various test parameters with predicted results by using the design equations given below are found elsewhere (1).

The analyses of test results presented elsewhere (1) show that existing equations (2,4) for shear (diagonal tension) strength and crack control do not correlate with test strengths and would give erroneous and impractical pipe designs. In view of this, the equations for shear strength and crack control presented in this paper were developed to obtain improved correlations between predicted and test strengths. Also, an equation for radial-tension strength was developed to predict this potential mode of failure in a curved member. Equations for flexural strength were developed by using the same basic theory given (2,4) for ultimate strength of reinforced-concrete flexural members. Correlations of predicted strengths with test strengths for the above four criteria are given elsewhere (1) and are not presented here because of space limitations. Also, separate technical papers explaining the development and correlation of equations for shear strength, radial tension strength, and crack control will be presented elsewhere.

LOADS

With either the direct or the indirect design methods in Section 1.15.4, the total earth load is determined by an analysis that accounts for soil-structure interaction. The total earth load (W_E) is given by the following:

$$W_E = F_e w B_c H \quad (1)$$

where

W = unit weight of earth (psi),
B_c = outside horizontal projection of pipe (ft),
H = height of earth cover over crown of pipe (ft), and
F_e = soil-structure interaction factor.

F_e is greater than 1 for installations such as embankments, where earth adjacent to the pipe settles relative to earth supported on the pipe, and may be less than 1 in installations such as vertical wall trenches because the trench sides resist consolidation of earth over the pipe.

The determination of earth loads is not covered in detail here, since methods in current use are explained elsewhere (5). The following simplified relation is provided in Section 1.15.4 for determining F_e for an embankment or wide trench installation:

$$F_e = [1 + 0.2\,(H/B_c)] \quad (2)$$

A maximum F_e of 1.5 is specified when side fills are not compacted, whereas a maximum F_e of 1.2 is specified for compacted side fills. When trench widths are less than the transition width, F_e is reduced as described in Section 1.15.4. Transition width is defined as the trench width for which the calculated trench F_e equals the calculated embankment F_e. Graphs and equations for determining transition width are given elsewhere (3,5).

In addition to the earth load, a buried pipe is subject to its own weight (W_p). Also, live loads applied on the surface may increase the earth pressure on the pipe. These effects may be approxi-

mately taken into account by distributing live load through the earth cover over the pipe in accordance with AASHTO rules (2). In this approach, the equivalent surface live load at the crown of the pipe per foot of pipe length (W_L) is treated as additional total earth load to obtain a total equivalent external pressure load (W_T) for use in designing the pipe:

$$W_T = W_E + W_L \quad (3)$$

where

W_E = total weight of earth on unit length of buried structure (lbf/ft),
W_L = total live load on unit length of buried structure (lbf/ft), and
W_T = total live and earth load applied on pipe (lbf/ft).

DESIGN APPROACHES

The use of the traditional indirect design method avoids the need to estimate the earth pressure distribution and then to calculate moments, thrusts, and shears in the pipe because it provides empirically determined bedding factors that relate total earth load to the concentrated load and reactions applied in the three-edge test (5). This approach has the advantage of simplicity and a direct relationship to test strengths. However, it has obvious limitations since it cannot accurately reflect the many different conditions that may affect structural behavior of pipe in the ground.

The availability of more rigorous analytical soil-structure interaction theories based on finite-element computer methods and an improved understanding of the ultimate-strength and crack-control characteristics of reinforced-concrete members suggests that a more accurate procedure can be devised to achieve more economical designs for buried reinforced-concrete pipe. This approach has been under development by ACPA in several long-range research programs that have been sponsored and carefully monitored during the past 10 years.

At present, a practical computer program that determines total earth load and pressure distribution in many typical embankment and trench installations has been developed and partly tested and evaluated by comparison of calculations and a limited number of test results. The program, Soil-Pipe Interaction Design and Analysis (SPIDA), also contains subroutines for determining the moments, shears, and thrusts caused by the applied earth pressure and for designing the required circumferential reinforcement when a trial wall thickness is specified for circular pipe. In addition, pipe strength is checked for adequate resistance to failure in shear (diagonal tension), radial tension, and compression, and pipe reinforcement is checked for adequate crack control. Design is automatically modified, if necessary, to meet all of these criteria.

The first part of ACPA's computerized design system that determines earth load and pressure distribution based on soil-structure interaction analysis is still being evaluated and tested. Sufficient results are not yet available to provide improved procedures for determining total earth load and pressure distribution. Thus, in applying the direct design method at present, loads and pressure distributions must still be determined by previously available approximate methods. Total earth load is estimated by using the Marston-Spangler theory (5) or the soil-structure interaction factor (F_e) described above. Earth pressure distribution is estimated by using a method suggested by Olander (6) or by uniformly distributed vertical and lateral pressures (7). Such distributions are shown in Figure 1 for the traditionally defined (5) Embankment Class C bedding and in Figure 2 for Embankment Class B bedding. In Figure 1(a), the applied earth pressure is modified slightly from the assumptions proposed by Olander by limiting the lateral pressure to that provided when the pressure bulb extends 30 degrees below the springline. Different pressure distributions are appropriate for the Class B and Class C beddings shown in the ACPA design manual (5) for trench installations.

ANALYSIS OF LOAD EFFECTS

Moments, thrusts, and shears in the pipe are deter-

Figure 1. Earth pressure assumptions for Embankment Class C bedding.

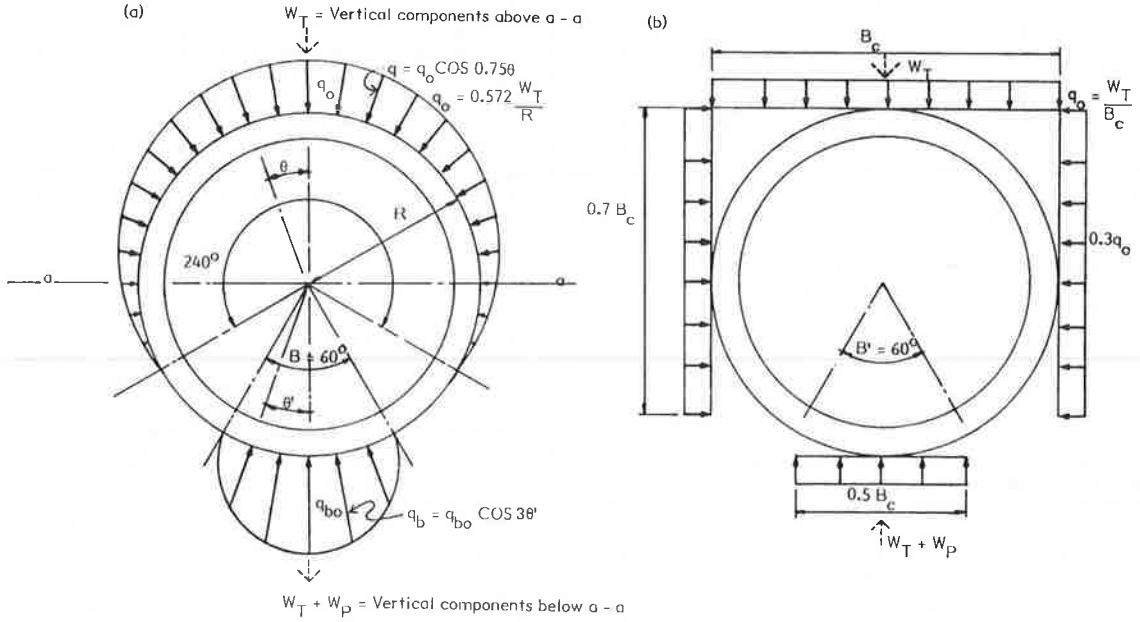

mined by elastic analysis of the pipe ring under the assumed earth pressure and pipe weight. The effect of cracking on pipe stiffness is taken into account in analyses performed with SPIDA but is usually neglected when pipe design is based on elastic analyses that use the estimated earth pressure distributions described above. This follows common structural engineering practice in design of other structures. The results of elastic analyses are given elsewhere (1,6) for several "bulb"-type distributions like the one shown in Figure 2(a) and in the paper by Paris (7) for uniformly distributed pressure assumptions like the ones shown in Figures 1(b) and 2(b).

DIRECT DESIGN METHOD

Once the moments, thrusts, and shears produced by earth load, surface load, and pipe weight are determined throughout the pipe structure, the pipe is designed by using an appropriate load factor (ultimate strength) design procedure for determining the required combination of wall thickness, concrete strength, and reinforcement characteristics at governing design sections. The conventional design approach for any reinforced-concrete structure is to select a geometry of structure, trial wall thickness, concrete strength, and reinforcement type and to calculate the required area of reinforcement at governing design sections based on factored values of the moments, thrusts, and shears obtained in the analysis.

Ultimate Flexural Strength Based on Tensile Reinforcement Yield

Usually, reinforcement area is first selected based on ultimate flexural strength. The required reinforcement is as follows:

$$A_s f_y = g\phi d - N_u - \left\{ g[g(\phi d)^2 - N_u(2\phi d - h) - 2M_u] \right\}^{1/2} \quad (4)$$

where

$g = 0.85bf'_c$;

A_s = tension reinforcement area on width b (in²);
b = width of section that resists M, N, V (in);
d = distance from compression face to centroid of tension reinforcement (in);
f'_c = design compressive strength of concrete (lbf/in²);
f_y = specified yield strength of reinforcement (lbf/in²);
h = overall thickness of member (wall thickness) (in);
M_u = ultimate moment acting on cross section of width b (in·lbf);
N_u = ultimate load axial thrust acting on cross section of width b (lbf); and
ϕ = capacity-reduction factor for variability in manufacture.

A form of the above design equation that is more familiar to many structural engineers is the following:

$$A_s f_y = \left\{ M_u - N_u[(h - a)/2] \right\} / (\phi d - a/2) \quad (5)$$

where $a = (f_y A_s + N_u)/g$.

The use of Equation 4 instead of Equation 5 avoids the trial calculations often needed to obtain the depth of the stress block (a) and thus is more appropriate for computerized solutions.

Load and Capacity-Reduction Factors

The ultimate bending moment (M_u) and compressive axial thrust (N_u) are obtained by multiplying the moment and thrust at governing sections as obtained in the above-described elastic analysis by an appropriate load factor. A load factor of 1.3 is provided in the AASHTO specifications (2, Table 1.2.22). This table is referenced in the new section (3).

Special provisions for capacity-reduction factors are given in the new section (3). A capacity-reduction factor ϕ no greater than 1.0 is proposed for flexure and no greater than 0.90 for shear. The 1.0 capacity-reduction factor is justified because of the good quality control achieved in plant-

Figure 2. Earth pressure assumptions for Embankment Class B bedding.

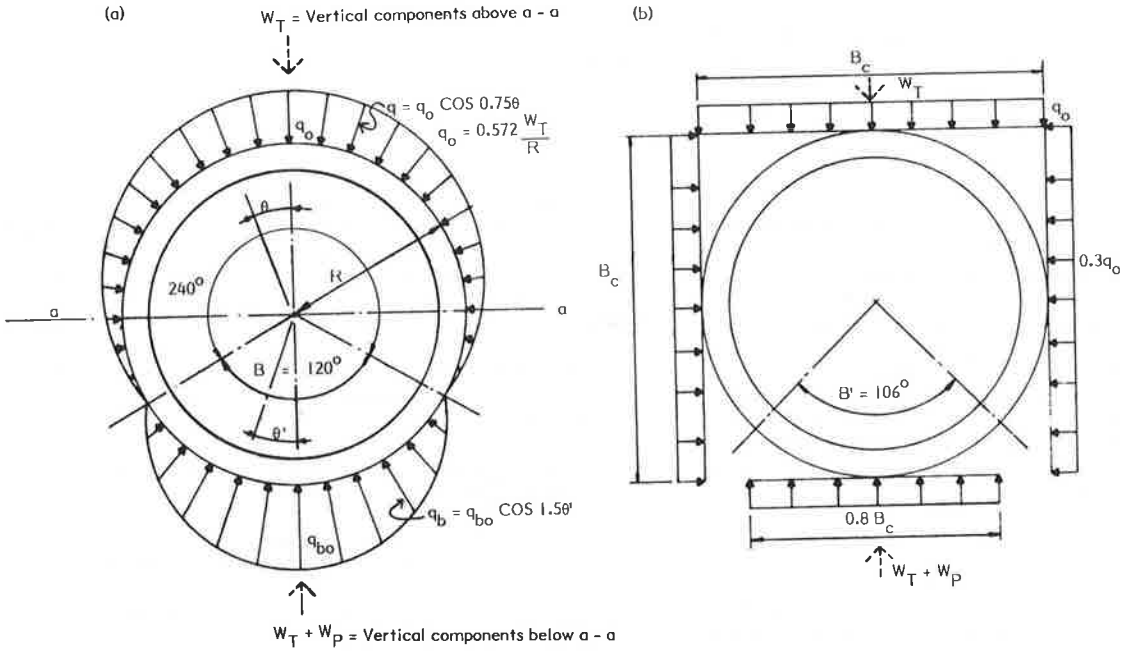

manufactured products such as pipe. Although philosophically ϕ should always be less than 1.0 (since it is impossible to assure perfect construction of any structure), the current provision of $\phi = 1.0$ for prestressed plank in the AASHTO bridge specifications (2) is cited as a precedent. I recommend that actual designs sometimes be based on ϕ-values less than 1.0 to reflect the tolerances in reinforcement placement and the reinforcement strength actually expected in manufacture. However, pipe made with some reinforcements, such as welded wire fabric, has ultimate flexural test strengths essentially equal to the ultimate strength of the reinforcement. This is substantially higher than the strength indicated by the yield strength of the reinforcement. Where such pipe has full-strength splices or splices located in regions of lower expected stress and properly controlled tolerances for reinforcement placement, the use of $\phi = 1.0$ combined with a maximum reinforcement strength of f_y or 65 000 psi, whichever is less, can be justified for determining reinforcement area based on ultimate flexural strength.

Minimum Reinforcement

In some practical cases involving shallow burial without surface loading, reinforcement areas obtained by using Equation 4 may be less than desirable minimum reinforcement areas for handling. Thus, the following relations for determining minimum reinforcement were recommended by the ACPA Technical Committee to provide adequate handling strength in reinforced-concrete pipe:

For inside face of pipe:

$$A_s = (S + h)^2/65\,000 \tag{6}$$

For outside face of pipe:

$$A_s = 0.75(S + h)^2/65\,000 \tag{7}$$

For elliptical reinforcement in circular pipe and for 33-in-diameter pipe and smaller with a single cage of reinforcement in the middle third of the pipe wall:

$$A_s = 2(S + h)^2/65\,000 \tag{8}$$

where S is the horizontal span between the inside of the walls in inches. In no case shall the minimum reinforcement be less than 0.07 in^2/linear ft. This is considered a lower limit of reinforcement areas that are practical for manufacturing.

Other Design Criteria

The above trial pipe design, based on requirements for ultimate flexural strength, is checked to determine whether other ultimate-strength or service-load criteria may require design modifications. Other ultimate-strength criteria include radial tension strength, flexural strength as limited by concrete compression strength instead of tensile yield of reinforcement, and shear (diagonal tension) strength. The primary service-load criterion is crack control. This is governed by the arrangement and type of reinforcement as well as by the reinforcement area, as described later.

Radial Tension

Bending moments that produce tension on the inside of a pipe also produce radial tension that is maximum in the concrete wall between the reinforcement and the neutral axis of the pipe ring. This radial tension may be envisioned as the distributed internal force that prevents the curved tension reinforcement from straightening. The nominal radial stress is as follows:

$$t_{ru} = (M_u - 0.45N_u d)/\phi b d r_s \tag{9}$$

where r_s is the radius to the inside reinforcement in inches.

Based on a limited number of special curved-slab tests and experience in three-edge bearing testing of concrete pipe (1,8), the nominal radial tension strength of concrete pipe, as determined by Equation 9, should be limited to the following (8):

$$t_{rc} = 1.2F_{pr}(f'_c)^{1/2} \tag{10}$$

The term F_{pr} is a factor used to reflect the variations that local materials and manufacturing processes can have on the tensile strength of concrete. Experience within the precast concrete pipe industry has shown that such variations are significant. F_{pr} may be determined from three-edge bearing test data:

$$F_{pr} = [(DL_{ut} + 9W_p/S)/1230r_s d(f'_c)^{1/2}]S(S + h) \tag{11}$$

where DL_{ut} is a statistically valid test strength obtained by using ASTM C655 and test pipe with inner reinforcement areas equal to or greater than A_s from Equation 12 below and W_p is the weight of a unit length of pipe.

Once determined, F_{pr} may be applied to other pipe built by the same process and with the same materials. If Equation 11 yields values of F_{pr} less than 1.0, a value of 1.0 may still be used if a review of test results shows that the failure mode was diagonal tension and not radial tension. $F_{pr} = 1.0$ gives predicted three-edge bearing strengths of about 0.9 times the highest strength classification (Class V in ASTM C76), which further justifies $F_{pr} = 1.0$ for use in design where specific tests for F_{pr} are not available.

The radial tension strength given by Equation 10 will exceed the radial tension stress given by Equation 9 if the maximum strength of reinforcement provided to resist M_u that produces tension on the inside of a pipe (Equations 4 or 5) is no greater than the following:

$$\max A_s f_y = 1.33 b r_s (f'_c)^{1/2} F_{pr} \tag{12}$$

For b = 12 in,

$$\max A_s f_y = 16 r_s (f'_c)^{1/2} F_{pr} \tag{13}$$

Also, max f'_c = 7000 psi, since neither test data nor sufficient experience is available for pipe with concrete strengths above this value.

When $A_s f_y$ obtained in Equation 4 (or Equation 5) exceeds $\max A_s f_y$ given by Equation 12, either radial ties must be used to preclude radial tension failure, as described later, or pipe wall thickness may be increased to reduce the ultimate tension force in the reinforcement for a given M_u required in the design.

Ultimate Flexural Strength Based on Concrete Compressive Strength

The ultimate strength of most conventional reinforced-concrete pipe is seldom limited by the ability of the pipe to resist concrete compressive failure prior to tensile yield of the reinforcement. However, in special designs for deep burial, flex-

ural compressive capacity may have to be investigated. Flexural compressive strength will not govern design of a pipe if the maximum reinforcement strength required by Equation 4 (or Equation 5) does not exceed the following:

$$\max A_s f_y = [(5.5 \times 10^4 g'\phi d)/(87\,000 + f_y)] - 0.75N_u \quad (14)$$

where

$$g' = bf_c'\{0.85 - 0.05[(f_c' - 4000)/1000]\}$$

$$g'_{max} = g = 0.85\,bf_c'$$

$$g'_{min} = 0.65bf_c'$$

The above equations reflect the provisions contained in the general reinforced-concrete design Section 1.5.32 (2) for compressive strength of reinforced-concrete flexural members.

If $A_s f_y$ obtained in Equation 4 exceeds $\max A_s f_y$ given by Equation 14, compression reinforcement and radial ties to support the compression reinforcement against buckling are required. This rarely occuring special case requires a design investigation based on provisions given by AASHTO (2) for design of flexural members with compression reinforcement. In cases where the axial compressive thrust (N_u) predominates over the bending moment (M_u), the pipe may have to be designed like a column subject to combined bending and axial load.

Shear (Diagonal Tension)

The shear design criteria given in Section 1.15.4 are based on an extensive new study of the shear strength of pipe, box sections, and slabs (1,9). The new shear tests of slabs as well as the extensive review of previous shear tests of pipe, box sections, slabs, and beams under both concentrated loads and uniformly distributed loads (1) show that the general provisions for shear strength (2,4) give excessively high strengths (unconservative) for certain flexural members under concentrated loads (particularly pipe in three-edge bearing) and excessively low strengths (too conservative) for flexural members with distributed loads (such as buried pipe and box sections).

New shear strength relations are given (1,9) that provide an accurate evaluation of shear strength for both of these load conditions. These new provisions are particularly applicable to pipe, box sections, slabs, and other flexural members without web reinforcement and with reinforcement ratios below about 0.015. Shear strength equations in existing design standards (2,4) give erroneous results for such members. Another new method (10) gives results that are more accurate than existing equations (2,4) for members with concentrated loads but much less accurate and too conservative for members with distributed loads.

The direct design method for determining shear strength of buried pipe given in Section 1.15.4 first locates the critical section for shear and then compares the shear strength of that section with the factored shear force at the same section as follows:

1. The critical section for shear strength is that in which the ratio $M_u/V_u\phi d$ is 3.0 (V_u is the ultimate shear force acting on a cross section of width b in pounds). For buried pipe with distributed bedding, this section is not the section of maximum shear stress resultant ($V_u$max). This section is located by calculating the $M_u/V_u\phi d$ ratio at several trial locations as determined from the shear and bending-moment diagrams for the earth pressure distribution used in the design analysis described previously. For most types of bedding, the critical section is usually located in a region between 10 and 20 degrees from the invert.

2. The calculated shear strength at the above critical section is the minimum shear strength of the pipe. This also applies to structures with straight flexural members such as box sections and slabs under high uniformly distributed loads. This minimum strength is termed the basic shear strength (V_b) and is given as follows:

$$\phi V_b = \phi bd(f_c')^{1/2}(1.1 + 63p)(F_d/F_cF_N)F_{pv} \quad (15)$$

where

V_b = basic shear strength of sections where $M_u/V_u\phi d \geq 3.0$,
p = $A_s/\phi bd$ (it is conservative to neglect the use of ϕ in this equation and in Equations 16 and 17 below),
p_{max} = 0.02,
$f_{c\,max}$ = 7000 psi, and
F_{pv} = process and material factor for radial tension strength that differs from theoretical strength.

The constants F_d, F_c, and F_N are modifying factors for crack depth, curvature, and axial thrust, respectively. Shear strength is reduced by flexural cracking. Wall thickness affects crack depth, and thinner walls, which have a smaller ratio of crack depth to crack spacing, can support a higher nominal shear stress than thicker walls. Curvature results in an increase in circumferential shear stress over the stress given by the conventional equation for nominal shear stress in prismatic members ($v = V/bd$) due to the additional relationship of change in thrust to change in bending moment in a curved member. Compressive axial thrust increases shear strength and tensile axial thrust reduces it relative to a flexural member without thrust. The following relations for the above modifying factors were determined semiempirically from derived relations and evaluations of conventional and special tests of pipe, slabs, and box sections, as described elsewhere (1):

$$F_d = 0.8 + (1.6/\phi d) \qquad F_{d\,max} = 1.25 \quad (16)$$

$$F_c = 1 \pm (\phi d/2r) \quad (17)$$

where r is the radius to the centerline of the pipe wall in inches and the plus indicates tension on the inside of the pipe and the minus, tension on the outside of the pipe.

For compressive thrust (N_u is +),

$$F_N = 1.0 - 0.12(N_u/V_u) \qquad F_{N\,min} = 0.75 \quad (18)$$

For tensile thrust (N_u is -),

$$F_N = 1.0 - 0.24(N_u/V_u) \qquad \text{up to } (N_u/V_u) = 1.0 \quad (19)$$

The term F_{pv} is a factor used to reflect the variations that local materials and manufacturing processes can have on the tensile strength of concrete. Experience within the precast concrete pipe industry has shown that such variations are significant. F_{pv} may be determined with Equation 20 below when a manufacturer has a sufficient amount of test data on pipe that fails in diagonal tension to determine a statistically valid test strength (DL_{ut}) by using the criteria given in ASTM C655.

$$F_{pv} = F_c(DL_{ut} + 11W_p/S)S/293F_d(1.1 + 63p)d(f_c')^{1/2} \quad (20)$$

Table 1. Methods of obtaining B_1 and C_1.

Type Reinforcement	B_1	C_1
1. Smooth wire or plain bars	$(0.5\,t_b^2\,s_\ell/n)^{1/3}$	1.0
2. Welded smooth wire fabric, 8-in maximum spacing of longitudinals	1.0	1.5
3. Welded deformed wire fabric, deformed wire, deformed bars, or any reinforcement with stirrups anchored thereto	$(0.5\,t_b^2\,s_\ell/n)^{1/3}$	1.9

Notes: Use n = 1 when the inner and the outer cages are each a single layer. Use n = 2 when the inner and the outer cages are each made from multiple layers. For type-2 reinforcement that has $(t_b^2\,s_\ell)/n > 3.0$, also check A_{scr} by using coefficients B_1 and C_1 for type-3 reinforcement and use larger value for A_{scr}.

Once determined, F_{pv} may be applied to other pipe built by the same process and with the same materials. $F_{pv} = 1.0$ gives predicted three-edge bearing test strengths in reasonably good agreement with pipe-industry experience, as reflected in the pipe designs for Class 4 strengths given in ASTM C76. Thus, it is appropriate to use $F_{pv} = 1.0$ for pipe manufactured by most combinations of process and local materials. Available three-edge bearing test data show minimum values of F_{pv} of about 0.9 for poor-quality materials and/or processes, as well as possible increases up to about 1.1 or more with some combinations of high-quality materials and manufacturing process.

Prior to making the above-described check for ultimate shear strength, the reinforcement area should be calculated based on both ultimate flexural strength (Equation 4) and the crack-control criteria described below. The larger of these required reinforcement areas should be used for the reinforcement ratio in Equation 15.

If the shear strength given by Equation 15 is less than the shear force (V_u) at the critical section for shear (where $M_u/V_u\phi d = 3.0$), increased shear strength may be obtained by increasing f_c' (but f_c' may not be taken greater than 7000 psi), by increasing A_s (but A_s may not be taken greater than 0.02bd), or by the use of radial ties (stirrups) as described later.

Shear strength at sections where $M_u/V_u\phi d < 3.0$ may be determined by using the following more general expression for shear strength:

$$\phi V_c = 4\phi V_b(M_u/V_u\phi d + 1) \qquad M_u/V_u\phi d \leq 3.0 \tag{21}$$

$$\max \phi V_c = 4.5\phi bd(f_c')^{1/2}/F_N \tag{22}$$

Design investigations have shown that the overall shear strength of buried pipe and box sections is governed by the section where $M_u/V_u\phi d = 3.0$ in a region where M_u produces tension on the inside of the pipe.

Crack Control

The proper service-load performance of reinforced-concrete pipe requires that the reinforcement area, spacing, and type be adequate to limit flexural cracking to acceptable widths. Reinforcements with a deformed surface or with welded cross wires at proper longitudinal spacing exhibit superior crack-control capability compared with smooth wire or bar reinforcements, primarily because they produce a greater number of more closely spaced cracks of smaller width than those that occur at the same stress with smooth reinforcements. The following semiempirical relationship, based in part on derived relations between variables and in part on analysis of pipe, box section, and slab flexural behavior in tests (1), provides a design procedure for limiting crack width in buried concrete pipe:

$$F_{cr} = (B_1/30\,000\,d\,A_s)\left[\left(\{M_s + N_s[d - (h/2)]\}/ij\right) - C_1 bh^2(f_c')^{1/2}\right] \tag{23}$$

where

$j \approx 0.74 + 0.1e/d \qquad j_{max} \approx 0.9$

$e = (M/N) + d - (h/2) \qquad i = 1/[1 - (jd/e)]$

and where

- B_1 = crack-control coefficient for effect of cover and spacing of reinforcement;
- C_1 = crack-control coefficient for type of reinforcement;
- e = thrust eccentricity, as given by Equation 23 (in);
- i = coefficient for effect of axial force at service load stress (f_s);
- j = coefficient for moment arm at service load stress;
- M_s = service load moment acting on cross section of width b (in·lbf); and
- N_s = service load axial thrust acting on cross section of width b (lbf).

(The approximations for j and i are only valid when e > 1.15d.)

B_1 and C_1 are obtained from Table 1 where n is number of layers of reinforcement in a cage (type 1 or 2); s_1 is the spacing (longitudinal) of circumferential wires or bars, in inches; and t_b is the clear cover distance from tension face of concrete to tension reinforcement, in inches.

The term F_{cr} is a crack-control index factor. When $F_{cr} = 1.0$, the reinforcement area (A_s) will produce an average maximum crack width = 0.01 in. If the value calculated for F_{cr} is too high, the designer may improve crack control by using a type of reinforcement with higher bond, a closer spacing of circumferential bars or wires (but not less than about 2 in), multiple layers of reinforcement, or a larger reinforcement area (A_s) than the minimum area required for ultimate flexural strength. Note that the maximum A_s limits given by Equations 12, 13, and 14 do not apply when A_s is increased for crack control.

If the designer wishes to tighten crack control, F_{cr} may be reduced somewhat but should probably not be taken less than about 0.7; for less stringent crack control, F_{cr} may be increased somewhat but probably not more than 1.5. This suggested range in F_{cr} reflects the fact that the data used to develop empirical constants in the above equations were from 0.01-in crack-strength tests of pipe, box sections, and slabs (1). If the designer wishes to account for variability in crack formation and control to minimize the occurrence of crack widths exceeding 0.01 in, $F_{cr} = 0.9$ may be used.

In tests, the use of radial ties (stirrups) improves the crack control provided by smooth reinforcements. Thus, the highest crack-control coefficients recommended for deformed reinforcements, B_1 and C_1, may also be used for pipe with any reinforcement type plus radial ties.

DESIGN OF RADIAL REINFORCEMENT

Occasionally, pipe subject to very heavy loads requires circumferential tensile reinforcement strengths that exceed the limits given previously for the radial tension (Equation 12), concrete compression (Equation 14), or shear (Equations 15 and 21) strengths of pipe without radial ties. In such cases, the circumferential tensile reinforcement

required for ultimate flexure (or crack control) may be provided together with radial ties. Since pipe walls generally are thin, ties are usually designed to be spaced at their maximum effective (allowable) circumferential spacing. Because these ties resist the combined effects of shear and radial tension, which makes the inclination of a potential diagonal crack flatter than the 45 degree angle assumed with prismatic members, their maximum allowable spacing is increased over the nominal 0.5d maximum stirrup spacing permitted for prismatic members by AASHTO (2). Thus, in typical pipe, the maximum allowable circumferential spacing is taken as follows:

$$\max s = 0.75\phi d \tag{24}$$

Longitudinal spacing of ties must coincide with longitudinal spacing of inside circumferential tensile reinforcement. When radial ties are needed to resist radial tension, each line of inside circumferential reinforcement must be restrained by radial ties anchored around the circumferential reinforcement and into the compression zone on the opposite side of the pipe wall. Anchorage strength must at least equal the effective ultimate tensile strength ($f_v A_v$) used to design the tie. In most practical cases, f_v is probably limited by the anchorage strength rather than the yield strength (f_{vy}) of the tie material. In this case, the anchorage strength of any specific type of tie should be proved by tests.

Ties may be designed for adequate radial tension strength and combined shear and radial tension strength as follows (8):

Radial tension ties,

$$A_{vr} f_v = 1.1s(M_u - 0.45N_u\phi d)/r_s\phi d \tag{25}$$

Shear and radial tension ties,

$$A_v f_v = (1.1s/\phi d)(V_u F_c - \phi V_c) + A_{vr} f_v \tag{26}$$

V_c is given by Equation 21, except that

$$\max \phi V_c = 2.0\phi b d(f'_c)^{1/2} \tag{27}$$

See the report by Heger and McGrath (1) for the derivation of the above equations for radial ties. The maximum contribution of concrete shear strength after diagonal cracking, V_c in Equation 26, is taken to be the same as concrete strength used in the design of web reinforcement for prismatic reinforced-concrete flexural members, as given by Equation 27 (2).

Equations 25 and 26 have been evaluated based on a very limited number of tests of pipe with ties in three-edge bearing and curved beams with ties, supported and loaded to simulate the invert region of a pipe in three-edge bearing. See the report by Heger and McGrath (1) for references and further discussion. Additional confirmation and experience would be desirable to validate the use of these equations for general design of highly loaded pipes. The user is especially cautioned to use a conservative value of f_v based on tie-anchorage strength unless limited by tie-material strength.

CONCLUSIONS

The design method presented in this paper was developed to represent the structural behavior of concrete pipe as accurately as possible and still be practical. The conventional ultimate flexural strength theory for under-reinforced sections was found to provide a practical basis for the design of reinforcement in most applications. The maximum allowable yield strength is increased to 65 000 psi for welded wire fabric reinforcement, and less allowance for capacity reduction due to construction variations often is acceptable since the ultimate tensile strength of cold-drawn wire reinforcement is reached in test pipe that fails in flexure.

Accurate representation of strength in shear requires extensive modification of existing shear-strength methods. The procedure suggested here, although somewhat more complex than methods in existing standards (2,4), predicts the lower shear strength of pipe under concentrated load (three-edge bearing test) as well as the much higher shear strength of pipe under distributed load (buried pipe) (9). The latter result occurs because the critical section for shear is found at a location where the $M_u/V_u\phi d$ ratio is 3.0. This is the location of both maximum shear and maximum moment in the three-edge bearing test. However, it is not the location of maximum shear for load distributions representative of buried concrete pipe.

Specific consideration of radial tension as a separate ultimate strength limit was suggested for the first time by Heger and McGrath (1,8) and is incorporated in the design method described here. It is shown that if the required tensile strength of reinforcement provided to resist flexural tension on the inside of a pipe at invert and crown does not exceed a specific radial tension limit, radial tension strength will not limit the flexural strength of the pipe.

Although usually only needed for special designs with concentrated bedding and/or very high fills, radial ties may be provided to increase the flexural strength of pipe beyond limits defined by radial tension, shear, or compressive strength. Design equations are provided to determine spacing and area of such reinforcement ties. Anchorage requirements for ties are also defined.

Extensive modifications in existing equations for crack control given elsewhere (2,4) are also necessary to predict accurately the crack-control behavior of buried pipe under service loads. New crack-control equations were developed applicable to the type and arrangement of reinforcements typically used in precast concrete pipe, and these indicate whether the reinforcement area required for ultimate strength needs to be increased for proper crack control. Equations are formulated to permit the design engineer to vary the basic crack-control criterion--average maximum crack width above or below an index value of 0.01 in--that has been widely used in three-edge bearing pipe tests.

Once the magnitude and distribution of earth pressure caused by earth and surface loads have been established with sufficient accuracy, the pipe may be analyzed by conventional methods of elastic stress analysis to obtain moments, thrust, and shears that act at all sections around the pipe. The design procedures presented in this paper may then be used to calculate the required wall thickness, concrete strength, and reinforcement area and strength or to evaluate accurately the expected minimum strength of an existing design. Furthermore, existing reinforced-concrete design methods, as available elsewhere (2,4), do not provide suitable procedures for the design of pipe structures. No provisions are included in these standards for determining radial tension strength, and the procedures for shear and crack control do not reflect the actual performance of buried pipe. Various arbitrary limits and design provisions are not appropriate for design of buried pipe.

The design methods presented here may also be used to design pipe for three-edge bearing strength

and to design prismatic structures such as buried box sections, slabs, or one-way spanning footings without web reinforcement.

FURTHER RESEARCH

I am currently directing the next phase of ACPA's long-range research program at Simpson Gumpertz & Heger Inc. (SGH), the development of a direct soil-structure interaction analysis for earth loads, earth pressure distributions, and moments, thrusts, and shears in a buried concrete pipe. This involves development of a finite-element representation of the soil and the pipe and a computerized analysis of the system as it is loaded incrementally by the soil and surface loads. Ernest Selig is consultant to SGH on the soil model and its properties. As mentioned previously, the computer program that results from this effort will be known as SPIDA and will provide a direct design for a buried pipe with specified earth cover, bedding, and pipe conditions.

ACKNOWLEDGMENT

As a part of their long-range research program, ACPA provided financial support to Simpson Gumpertz & Heger Inc., for the tests and investigations that led to the new approaches for shear and radial tension strength and crack control that form the basis of the proposed design method. The continued support and suggestions provided by the ACPA Technical Committee are acknowledged and appreciated. Main Committee Chairman Lee Stockton, Subcommittee Chairman Harry Peck, members Joseph Zicaro and Robert Spiekerman, ACPA Board Chairman Thomas Breitfuss, and Vice President Mike Bealey reviewed the research work and the design method and made valuable suggestions for its implementation. I also acknowledge the many valuable contributions of my associate, Timothy J. McGrath, who served as project manager for SGH, planning and evaluating the extensive test data and making numerous suggestions during development of the design method. Finally, thanks are due Chairman Adrianus Van Kampen and members of the AASHTO Rigid Culvert Liaison Committee, who reviewed the proposed design method and made further valuable suggestions for its implementation as Section 1.15.4 of the AASHTO bridge specifications.

REFERENCES

1. F.J. Heger and T.J. McGrath. Design Method for Reinforced Concrete Pipe and Box Sections. Simpson Gumpertz & Heger Inc., Cambridge, MA, Dec. 1980.
2. Interim Specifications: Bridges. AASHTO, Washington, DC, 1981.
3. Interim Specifications: Bridges. AASHTO, Washington, DC, 1982.
4. ACI Committee 318. ACI Standard Building Code Requirements for Reinforced Concrete (ACI 318-77). American Concrete Institute, Detroit, MI, 1977.
5. Concrete Pipe Design Manual. ACPA, Vienna, VA, 1980.
6. H.C. Olander. Stress Analysis of Concrete Pipe. U.S. Bureau of Reclamation, Denver, CO, Engineering Monograph 6, Oct. 1950.
7. J.M. Paris. Stress Coefficients for Large Horizontal Pipes. Engineering News Record, Vol. 87, No. 19, Nov. 10, 1921.
8. F.J. Heger and T.M. McGrath. Radial Tension Strength of Pipe and Curved Flexural Members. ACI Journal, Jan.-Feb. 1983.
9. F.J. Heger and T.J. McGrath. Shear Strength of Pipe, Box Sections, and Other One-Way Flexural Members. ACI Journal, Nov.-Dec. 1982.
10. ACI-ASCE Committee 426. Suggested Revisions to Shear Provisions for Building Codes (abstract). ACI Journal, Sept. 1977.

Publication of this paper sponsored by Committee on Culverts and Hydraulic Structures.

Abridgment

Behavior of Aluminum Structural Plate Culvert

DAVID B. BEAL

A corrugated aluminum culvert 17 ft 10 in high with a 28-ft 6-in span was instrumented to obtain measurements of strain and displacement during backfilling and under static live load. Values of circumferential bending moment and thrust at 16 locations spaced around the structure's circumference at midspan are reported for each 2 ft of backfill from the springline to 2 ft over the crown. Despite bending moments 70 percent of the fully plastic value and stresses exceeding the nominal yield point of the aluminum, it is concluded that the structural behavior is satisfactory. Discrepancies between measured values and design predictions are discussed.

Corrugated metal culverts can be economical replacements for short-span bridges and have been used for spans as long as 51 ft (1). Traditionally, culvert design has been largely empirical, but with the increasing demand for large-span structures the need for a rational analytical procedure has grown. The purpose of the research described here was to obtain strain and displacement measurements on a typical structure to provide data for comparison with analytical predictions. The work is described completely elsewhere (2). The structure is a 28.5-ft span pipe arch with a rise of 11 ft 9 in and a total height of 17 ft 10 in. The invert length is 140 ft. The structure was manufactured by Kaiser Aluminum and Chemical Sales, Inc., which contributed to this research.

The structure carries Van Campen Creek under State Route 275 in the town of Friendship, New York. With a filled invert, the culvert provides a clear opening of 346 ft². It is constructed of 0.175-in aluminum (5052-H141 alloy) structural plate with corrugations of 9-in pitch and 2.5-in depth. Bulb angle stiffening ribs (6061-T6 alloy) were bolted to the crown on 2-ft 3-in centers. Seven plates were assembled with 0.75-in diameter galvanized steel bolts on 9.75-in centers to form a complete circumference of the structure as shown in Figure 1. Circumferential seams are staggered.

and to design prismatic structures such as buried box sections, slabs, or one-way spanning footings without web reinforcement.

FURTHER RESEARCH

I am currently directing the next phase of ACPA's long-range research program at Simpson Gumpertz & Heger Inc. (SGH), the development of a direct soil-structure interaction analysis for earth loads, earth pressure distributions, and moments, thrusts, and shears in a buried concrete pipe. This involves development of a finite-element representation of the soil and the pipe and a computerized analysis of the system as it is loaded incrementally by the soil and surface loads. Ernest Selig is consultant to SGH on the soil model and its properties. As mentioned previously, the computer program that results from this effort will be known as SPIDA and will provide a direct design for a buried pipe with specified earth cover, bedding, and pipe conditions.

ACKNOWLEDGMENT

As a part of their long-range research program, ACPA provided financial support to Simpson Gumpertz & Heger Inc., for the tests and investigations that led to the new approaches for shear and radial tension strength and crack control that form the basis of the proposed design method. The continued support and suggestions provided by the ACPA Technical Committee are acknowledged and appreciated. Main Committee Chairman Lee Stockton, Subcommittee Chairman Harry Peck, members Joseph Zicaro and Robert Spiekerman, ACPA Board Chairman Thomas Breitfuss, and Vice President Mike Bealey reviewed the research work and the design method and made valuable suggestions for its implementation. I also acknowledge the many valuable contributions of my associate, Timothy J. McGrath, who served as project manager for SGH, planning and evaluating the extensive test data and making numerous suggestions during development of the design method. Finally, thanks are due Chairman Adrianus Van Kampen and members of the AASHTO Rigid Culvert Liaison Committee, who reviewed the proposed design method and made further valuable suggestions for its implementation as Section 1.15.4 of the AASHTO bridge specifications.

REFERENCES

1. F.J. Heger and T.J. McGrath. Design Method for Reinforced Concrete Pipe and Box Sections. Simpson Gumpertz & Heger Inc., Cambridge, MA, Dec. 1980.
2. Interim Specifications: Bridges. AASHTO, Washington, DC, 1981.
3. Interim Specifications: Bridges. AASHTO, Washington, DC, 1982.
4. ACI Committee 318. ACI Standard Building Code Requirements for Reinforced Concrete (ACI 318-77). American Concrete Institute, Detroit, MI, 1977.
5. Concrete Pipe Design Manual. ACPA, Vienna, VA, 1980.
6. H.C. Olander. Stress Analysis of Concrete Pipe. U.S. Bureau of Reclamation, Denver, CO, Engineering Monograph 6, Oct. 1950.
7. J.M. Paris. Stress Coefficients for Large Horizontal Pipes. Engineering News Record, Vol. 87, No. 19, Nov. 10, 1921.
8. F.J. Heger and T.M. McGrath. Radial Tension Strength of Pipe and Curved Flexural Members. ACI Journal, Jan.-Feb. 1983.
9. F.J. Heger and T.J. McGrath. Shear Strength of Pipe, Box Sections, and Other One-Way Flexural Members. ACI Journal, Nov.-Dec. 1982.
10. ACI-ASCE Committee 426. Suggested Revisions to Shear Provisions for Building Codes (abstract). ACI Journal, Sept. 1977.

Publication of this paper sponsored by Committee on Culverts and Hydraulic Structures.

Abridgment

Behavior of Aluminum Structural Plate Culvert

DAVID B. BEAL

A corrugated aluminum culvert 17 ft 10 in high with a 28-ft 6-in span was instrumented to obtain measurements of strain and displacement during backfilling and under static live load. Values of circumferential bending moment and thrust at 16 locations spaced around the structure's circumference at midspan are reported for each 2 ft of backfill from the springline to 2 ft over the crown. Despite bending moments 70 percent of the fully plastic value and stresses exceeding the nominal yield point of the aluminum, it is concluded that the structural behavior is satisfactory. Discrepancies between measured values and design predictions are discussed.

Corrugated metal culverts can be economical replacements for short-span bridges and have been used for spans as long as 51 ft (1). Traditionally, culvert design has been largely empirical, but with the increasing demand for large-span structures the need for a rational analytical procedure has grown. The purpose of the research described here was to obtain strain and displacement measurements on a typical structure to provide data for comparison with analytical predictions. The work is described completely elsewhere (2). The structure is a 28.5-ft span pipe arch with a rise of 11 ft 9 in and a total height of 17 ft 10 in. The invert length is 140 ft. The structure was manufactured by Kaiser Aluminum and Chemical Sales, Inc., which contributed to this research.

The structure carries Van Campen Creek under State Route 275 in the town of Friendship, New York. With a filled invert, the culvert provides a clear opening of 346 ft². It is constructed of 0.175-in aluminum (5052-H141 alloy) structural plate with corrugations of 9-in pitch and 2.5-in depth. Bulb angle stiffening ribs (6061-T6 alloy) were bolted to the crown on 2-ft 3-in centers. Seven plates were assembled with 0.75-in diameter galvanized steel bolts on 9.75-in centers to form a complete circumference of the structure as shown in Figure 1. Circumferential seams are staggered.

Immediately surrounding the structure, select granular backfill was placed to the limits indicated in Figure 1. Below the invert, 32 ft of a soft-to-firm grey clayey silt was left in place. The backfill was placed in 6-in lifts, and in accordance with construction specifications the difference in backfill elevation from one side of the structure to the other never exceeded 1 ft. Compaction was to 100 percent of the standard Proctor value and was checked after each 2 ft of backfill.

The major effort in this test was to monitor culvert behavior during backfilling. The structure's behavior under live load was also obtained from measurements taken with a single-axle dump truck statically positioned at several locations on the fill.

CULVERT INSTRUMENTATION

Changes in culvert shape were monitored by measuring the relative movement of four points around the culvert circumference with respect to points at the springline. This measurement was performed at the longitudinal centerline and at two sections 13 ft 6 in on either side of the centerline. Joint slip was monitored at each joint on a complete circumferential ring (seven joints) with linear potentiometers. These measurements were made to 0.001 in and are believed accurate to 0.005 in. Electrical-resistance strain gages were mounted on the inner surface of the structural plate in the circumferential and longitudinal directions at 16 sections around the culvert's centerline circumference (Figure 2). The stiffening rib was instrumented with T-rosette gages at 12 locations. Analysis of the strain-gage data permitted evaluation of the total moment and thrust at 16 circumferential locations. Temperatures were monitored with eight copper constantan thermocouples. Seven of these were mounted to the inner surface of the structural plate, and the remaining device monitored air temperature inside the pipe.

RESPONSE DURING BACKFILLING

The baseline for all measurements was taken with the fill at the springline. Strain, displacement, and temperature were monitored at 2-ft increments of backfill up to a fill depth of 10 ft. Increments from that level raised the fill depth successively to 11 ft 6 in, 13 ft 6 in, and 14 ft 2 in. Measurements were terminated at 14 ft 2 in because of a conflict between construction operations and the experiment.

Maximum stresses at all stages of backfilling occurred on the inner corrugation of the structural plate. The maximum tensile stress of 21 200 psi occurred at Section 10 with the backfill at the crown. Maximum compressive stress was -28 800 psi at Section 16 with full backfill depth. The average yield point of three samples taken from the structure's crown plate was 33 300 psi.

The experimentally determined moment distributions for 8 ft and 14 ft 2 in of fill are shown in Figure 3 as typical examples of the results obtained. In both cases shown and for all increments of backfill, the distribution of moments is regular; changes from positive to negative bending occur at the expected locations. The slight antisymmetry is a result of the backfilling sequence, which resulted in placement of the 6-in lifts on the north side first.

The maximum average crown moment of 5.3 kip•ft/ft occurred at maximum fill depth. Maximum quarter-point moment of 4.4 kip•ft/ft occurred on the north side with the fill at the crown.

Evaluation of thrust was less successful than for bending moment. This is believed to result from the small magnitude of thrust in this low-cover structure.

Interpretation of measured displacements was complicated by the increase in invert elevation. The upward displacement resulted because the large-radius invert plates were unable to resist the pressure from the soft native material underlying the structure. The maximum differential displacement between the crown and invert was 3.4 in. The maximum change in span was 1.6 in; this occurred at 10 ft of backfill.

The joint slip measurements are erratic and show no trend. Most readings were recorded as less than 0.002 in, which is less than the 0.005-in expected accuracy.

Live-load testing was performed by using a truck positioned on the backfill with the centerline of the 20-kip rear axle placed at a series of locations over the crown and quarter point of the structure. The maximum stress recorded on the inner corrugation was 2300 psi and occurred with the rear axle over the crown. At the crown, where the maximum backfill compressive stress was 28 500 psi, a maximum live-load compressive stress of 1700 psi was induced for a net compressive stress of 30 200 psi. This is the absolute maximum stress in the culvert. Live-load stress was always compressive at the quarter point, the location of the maximum dead-load tensile stress.

DISCUSSION OF RESULTS

Table 1 gives maximum values of moment and thrust with fill depth at the crown and at full backfill depth. It should be noted that the completed structure in service will have at least 2 ft of additional fill and asphalt paving. This additional load will decrease the magnitude of the reported bending moments. Thrusts will increase due to this additional load, and these values should be estimated to assess the reliability of the completed structure.

Figure 1. Limits of structural backfill.

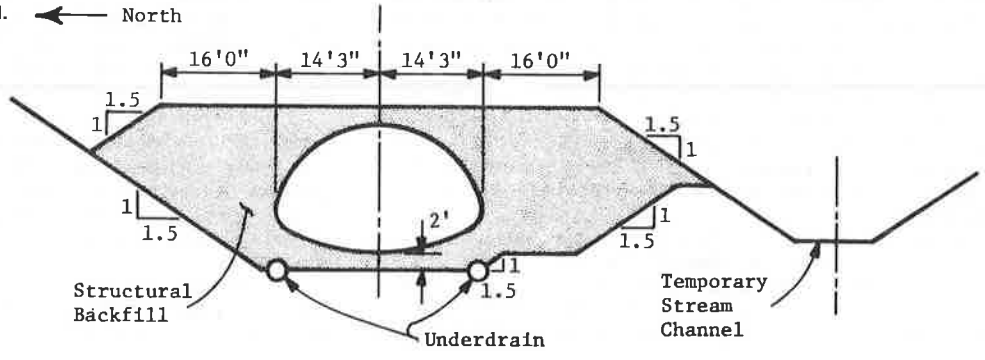

Figure 2. Locations of strain gages and thermocouples.

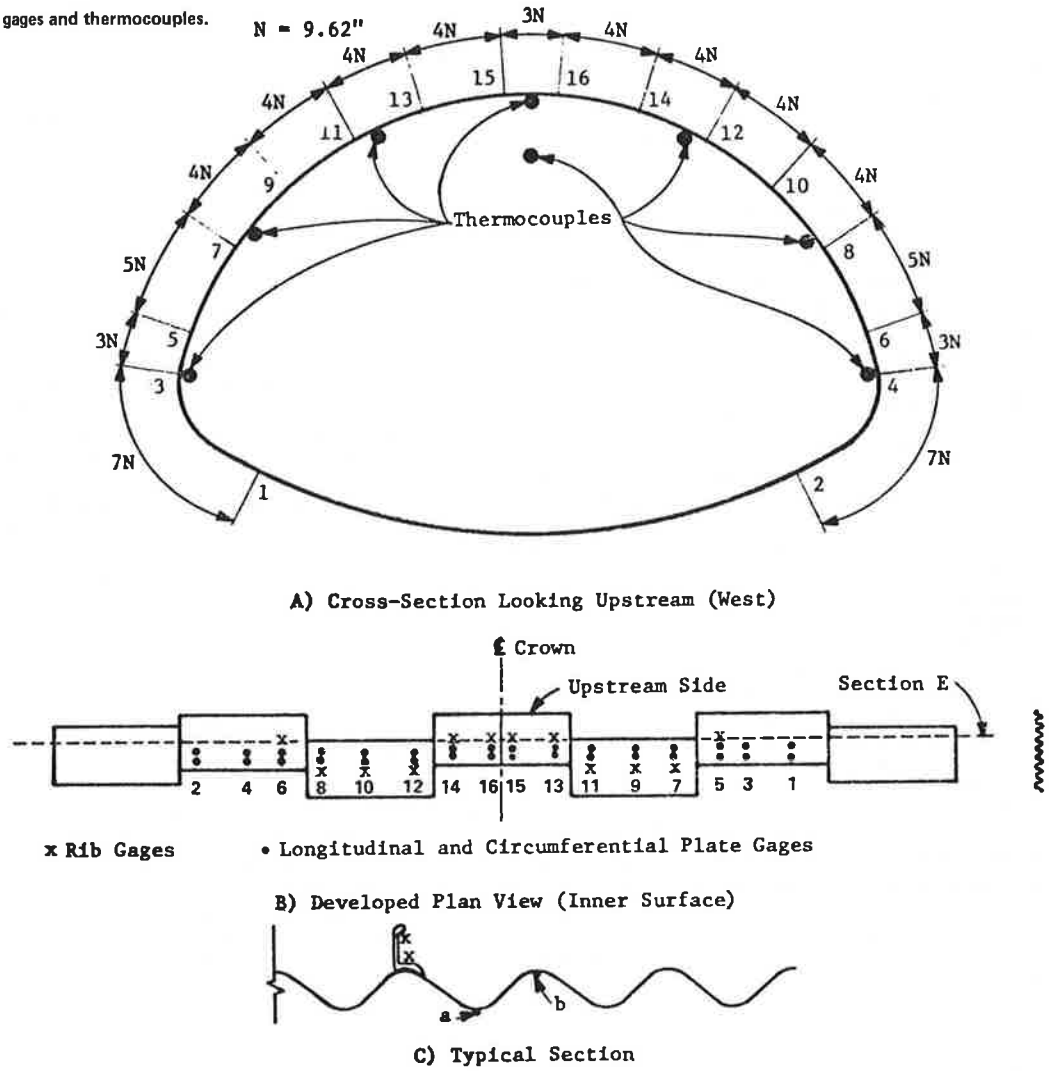

The fully plastic moment and thrust for this structure are 7.9 kip•ft/ft and 85.4 kips/ft, respectively. The maximum total measured thrust is 11 kips/ft, only 13 percent of the plastic value. By contrast, the maximum total moment is 70 percent of the plastic value. If we ignore thrust, the factor of safety against formation of a plastic hinge is 1.49 with 2 ft of cover and 1.44 with live load in place.

The high stresses observed are not unexpected but may alarm engineers accustomed to stress values less than 55 percent of the yield point. This concern is unfounded, however, because even at the stress levels observed, the structure is under no danger of collapse. Duncan (3,4) has suggested controlling the factor of safety against formation of a plastic hinge as a design requirement for flexible culverts with shallow fill and has given three reasons why structure collapse will not occur at this point: (a) multiple plastic hinges are required to form a collapse mechanism, (b) the soil will restrain deformations after formation of a mechanism, and (c) the design estimates are based on minimum values of yield stress.

Measured live-load bending moments were small. Nevertheless, based on design estimates (3), the bending moment induced by an HS 20 truck with 4-ft cover would be only 62 percent of those produced experimentally. Thus, despite the noted inaccuracies in the experimental force determination, it is unlikely that service loads will have a significant influence on culvert behavior.

CONCLUSIONS

From the test results presented, the following conclusions can be made about the behavior of this structural-plate culvert:

1. The backfill placement sequence resulted in distortion of culvert shape and increased positive bending moments on the north side of the structure;
2. The total change in height of the structure was less than the change in rise because of the upward movement of the invert;
3. Maximum compressive stresses at the crown exceeded the nominal yield point of the aluminum plate; the actual yield point was not exceeded;
4. The variation of dead-load moments around the circumference of the structure was consistent with intuitive expectation; the maximum moment was 70 percent of the fully plastic value;
5. The apparent irregularities in measured thrust values are greater than assumed measurement accuracies;
6. In-service bending moments due to backfilling will be less than the values reported due to the placement of an additional 2 ft of cover;

7. Live-load stresses were small with respect to dead-load stresses; and
8. Design estimates of thrust were greater than measured values and estimates of moment were less.

ACKNOWLEDGMENT

The work reported here was conducted in cooperation with the Federal Highway Administration, U.S. Department of Transportation.

Figure 3. Distribution of moment around circumference.

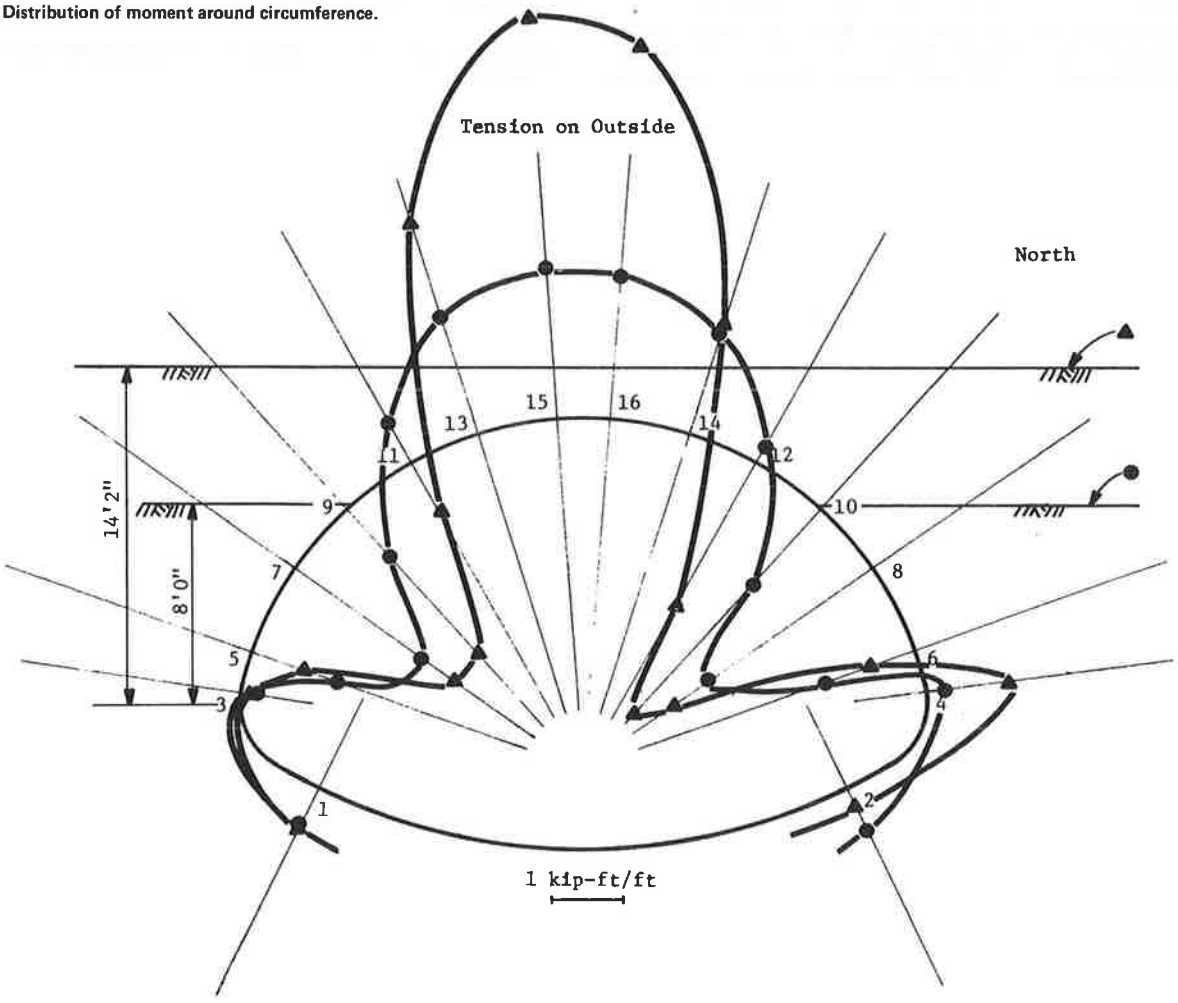

Table 1. Maximum experimental and calculated moment and thrust.

Location	Backfill				Live Load				Total			
	Moment (kip·ft/ft)		Thrust (kips/ft)		Moment (kip·ft/ft)		Thrust (kips/ft)		Moment (kip·ft/ft)		Thrust (kips/ft)	
	Experimental	Calculated	Experimental	Calculated	Experimental	Calculated[a]	Experimental	Calculated[a]	Experimental	Calculated	Experimental	Calculated
H = 0 ft												
Crown	-4.8	-2.6	0.8	-[b]	-	-	-	-	-4.8	-	0.8	-
Quarter point		2.6		8.9	-	-	-	-		2.6		8.9
North	4.4		2.5						4.4		2.5	
South	3.3		1.5						3.3		1.5	
Springline		-		9.3	-	-	-	-		-		9.3
North	-1.0		3.7						-1.0		3.7	
South	0.2		4.7						0.2		4.7	
H = 2 ft												
Crown	-5.3	-	3.0	-	-0.2	-	4.1	-	-5.5	-	7.1	-
Quarter point		1.9		14.1		1.4		2.8		3.3		16.9
North	4.0		6.4		0.0		1.6		4.0		8.0	
South	2.8		9.4		0.0		1.6		2.8		11.0	
Springline		-		14.9		-		2.9		-		17.8
North	-1.0		7.8		0.0		1.0		-1.1		8.9	
South	-0.2		8.1		0.0		1.0		0.2		9.1	

[a] Equivalent live load = 2.94 kips/ft. [b] Dash indicates that no value was available.

REFERENCES

1. E.T. Selig and others. Review of the Design and Construction of Long-Span Corrugated-Metal Buried Conduits. FHWA, Rept. RD-77-131, Aug. 1977.
2. D.B. Beal. Behavior of an Aluminum Structural Plate Culvert. Engineering Research and Development Bureau, New York State Department of Transportation, Albany, Res. Rept. 90, June 1981.
3. J.M. Duncan. Design Method for Flexible Metal Culverts and Long Span Super Plate Structures With and Without Vertical Tension Strutting During Backfill. Highway Products Division, Kaiser Aluminum and Chemical Sales, Inc., Oakland, CA, March 1978.
4. J.M. Duncan. Behavior and Design of Long-Span Metal Culverts. Journal of the Geotechnical Engineering Division of ASCE, Vol. 105, No. GT3, March 1979, pp. 399-418.

Publication of this paper sponsored by Committee on Culverts and Hydraulic Structures.